

*Microwave Electronics*

**DESIGN AND DEVELOPMENT OF COPLANAR STRIP  
FED PLANAR ANTENNAS**

*A thesis submitted by*

**SREEJITH M. NAIR**

*in partial fulfillment of the requirements for the degree of*

**DOCTOR OF PHILOSOPHY**

*Under the guidance of*

**Prof. P. MOHANAN**



**DEPARTMENT OF ELECTRONICS**

**FACULTY OF TECHNOLOGY**

**COCHIN UNIVERSITY OF SCIENCE AND TECHNOLOGY**

**KOCHI-22, INDIA**

*October2013*

# *“Design and Development of Coplanar Strip Fed Planar Antennas”*

*Ph.D. Thesis under the Faculty of Technology*

## *Author*

***Sreejith M. Nair***

*Research Scholar*

*Department of Electronics,*

*Cochin University of Science and Technology*

*Cochin-22*

*Email: sreejithnair@gmail.com*

*Assistant Professor,*

*Department of Electronics,*

*Government College Chittur,*

*Palakkad-678104*

*Mob: 9745682616*

## *Supervising Guide*

***Dr. P. Mohanan***

*Professor*

*Department of Electronics*

*Cochin University of Science and Technology*

*Kochi - 682022*

*Email: drmohan@gmail.com*

*Department of Electronics*

*Cochin University of Science and Technology*

*Kochi - 682022*

*7<sup>th</sup> October 2013*

*Dedicated to*

*Lord Chottanikkara Bhagavathy; My Amma, who  
made me what I am.....*





**DEPARTMENT OF ELECTRONICS  
COCHIN UNIVERSITY OF SCIENCE AND TECHNOLOGY,  
KOCHI, INDIA.**

---

**Dr. P. Mohanan**  
(Supervising guide)  
Professor  
Department of Electronics  
Cochin University of Science and Technology

---

## Certificate

*This is to certify that this thesis entitled “**DESIGN AND DEVELOPMENT OF COPLANAR STRIP FED PLANAR ANTENNAS**” is a bonafide record of the research work carried out by Mr. Sreejith M. Nair under my supervision in the Department of Electronics, Cochin University of Science and Technology. The results embodied in this thesis or parts of it have not been presented for any other degree.*

*I further certify that the corrections and modifications suggested by the audience during the pre-synopsis seminar and recommended by the Doctoral Committee of Mr. Sreejith M. Nair are incorporated in the thesis.*

Cochin-22  
7<sup>th</sup> October 2013

*Dr. P. Mohanan*



## *Declaration*

*I hereby declare that the work presented in this thesis entitled “**DESIGN AND DEVELOPMENT OF COPLANAR STRIP FED PLANAR ANTENNAS**” is a bonafide record of the research work done by me under the supervision of Dr. P. Mohanan, Professor, Department of Electronics, Cochin University of Science and Technology, India and that no part thereof has been presented for the award of any other degree.*

*Cochin-22  
7<sup>th</sup> October 2013*

***Sreejith. M. Nair**  
Part Time Research Scholar,  
Department of Electronics,  
CUSAT,  
Cochin-22.*





# Acknowledgement

*I remember with gratitude...*

*My supervising guide, Dr. P. Mohanan, Professor, Department of Electronics, Cochin University of Science and Technology, for his valuable guidance, advices and timely care extended to me throughout the research period.*

*Prof. K. Vasudevan, Department of Electronics, Cochin University of Science and Technology for his constant encouragement and concern. His dedication for research is always a leading source of energy.*

*Dr. C.K. Aanandan, Professor and Head Department of Electronics, Cochin University of Science and Technology for the advice, discussions and care rendered during these years.*

*Prof. K.T. Mathew, Prof. P.R.S. Pillai, Dr. Tessamma Thomas, Dr. James Kurian and Dr. M. H. Supria, Department of Electronics, Cochin University of Science and Technology for their support.*

*My friends at CREMA, especially my Sujithchettan, Sarinchettan, SreenathChettan, Shameenachechi, Nishachechi, Laila miss, Tony Sir, Dinesh., Nijas, Deepak, Rasheed, Roshna, Sajitha and Vineesh for their support.*

*My friends at Microwave Tomography and Material Research Laboratory, Centre for Ocean Electronics and Audio and Image Research Lab, CUSAT for their encouragement and help.*

*All non-teaching staff of Department of Electronics, CUSAT for their timely help.*

*My friends at Cochin College and Chittur College for their support, love and prayer throughout the Research life.*

*My chedathiesAnnieta Miss, Sindhu teacher, Supriya teacher, Sreevidya teacher, Premaja teacher, Geetha teachers, Reena teacher, Subhadhra teacher, Jaya teacher and Manjusha teacher for their support and advices.*

*My chettanReshi sir, Harikrishnan Sir, Jayesh sir, Rajagopal Sir and Dileep sir without the inspirations of them I cannot complete my work.*

*My Deepuchettan, for his kind heart and helps to complete my work,*

*My friends at Chottanikkara especially PresannaChechi, SijuChettan, Rajesh Chettan, ArunChottanikkara, Vishnu, Saroop and Umesh for their timely helps.*

*My students at Cochin College and at Chittur College for their support.*

*My Preethy teacher, one of my Amma for her great advices throughout my life and education.*

*My Achan, Amma and Sreethu for being there always as a constant source of energy. I am lucky to enjoy their deep love, care and patience to move on especially in hard times.*

*Above all my ChottanikkaraAmma whose lotus feet showers at me and gave me chances to become what me now*

***Sreejith. M. Nair***

## *ABSTRACT*

With the recent progress and rapid increase in the field of communication, the designs of antennas for small mobile terminals with enhanced radiation characteristics are acquiring great importance. Compactness, efficiency, high data rate capacity etc. are the major criteria for the new generation antennas. The challenging task of the microwave scientists and engineers is to design a compact printed radiating structure having broadband behavior along with good efficiency and enhanced gain. Printed antenna technology has received popularity among antenna scientists after the introduction of planar transmission lines in mid-seventies. When we view the antenna through a transmission line concept, the mechanism behind any electromagnetic radiator is quite simple and interesting. Any electromagnetic system with a discontinuity is radiating electromagnetic energy. The size, shape and orientation of the discontinuities control the radiation characteristics of the system such as radiation pattern, gain, polarization etc. It can be either resonant or non-resonant.

This thesis deals with antennas that are developed from a class of transmission lines known as coplanar strip-CPS, a planar analogy of parallel pair transmission line. The specialty of CPS is its symmetric structure compared to other transmission lines, which makes the antenna structures developed from CPS quite simple for design and fabrication. The structural modifications on either metallic strip of CPS results in different antennas. The first part of the thesis discusses a single band and dual band design derived from open ended slot lines which are very much suitable for 2.4 and 5.2 GHz WLAN applications. The second section of the study is vectored into the development of enhanced gain dipoles. A single band dipole and a wide band enhanced gain dipole suitable for 5.2/5.8 GHz band and imaging applications are developed and discussed. Last part of the thesis discusses the development of directional UWBs. Three different types of ultra-compact UWBs are developed and almost all the frequency domain and time domain analysis of the structures are discussed.



## Contents

<b>1. Introduction and Review of Literature. ....</b>	<b>1-38</b>
1.1. Introduction. ....	1
1.2. Important Milestones in Communication.....	2
1.3. Technologies and developments in the field of Planar Antennas.....	2
1.3.1. Microstrip Antennas. ....	6
1.3.2. Microstrip fed antennas with truncated ground plane. ....	8
1.3.3. Coplanar Waveguide fed Antennas.....	10
1.3.4. Photonic Band Gap structures.....	11
1.3.5. Metamaterial based antennas .....	12
1.3.6. Fractal Geometry Based antennas .....	12
1.3.7. Dielectric resonator based antennas.....	13
1.3.8. Ultra Wide Band antennas.....	14
1.3.9. LTCC based antennas.....	16
1.4. Motivation of the work.....	16
1.5. Organization of the thesis .....	18
References.....	20
<b>2. Design, Fabrication and Measurement Techniques of Antennas. ....</b>	<b>39-76</b>
2.1. Techniques for design and optimization of the antennas.....	39
2.1.1. High Frequency Structure Simulator. ....	40
2.2. Antenna fabrication. ....	44
2.2.1. Characteristics of Substrate material.....	44
2.2.2. Photo Lithography. ....	46
2.3. Antenna Measurement facilities.....	47
2.3.1. HP8510C Vector network Analyzer.....	47
2.3.2. E8362B Programmable Network Analyzer. ....	49

2.3.3. <i>Anechoic Chamber</i> .....	50
2.3.4. <i>Turn Table Assembly for Radiation Pattern Measurement</i> .....	51
2.4. <i>Experiments</i> .....	51
2.4.1. <i>Return loss, Resonant Frequency and Band Width</i> .....	52
2.4.2. <i>Radiation Pattern</i> .....	53
2.4.3. <i>Antenna Gain</i> .....	53
2.4.4. <i>Radiation Efficiency</i> .....	54
2.5. <i>Models/Techniques Used in Analysis of Antennas</i> .....	56
2.5.1. <i>Transmission Line Model</i> .....	56
2.5.2. <i>Cavity Model</i> .....	57
2.5.3. <i>Finite Element Method</i> .....	57
2.5.4. <i>Method of Moments</i> .....	57
2.5.5. <i>Finite difference Time Domain method</i> .....	58
2.6. <i>Wide Band Antenna Characteristics (Time Domain)</i> .....	58
2.6.1. <i>Description of UWB Antenna System</i> .....	59
2.6.2. <i>Group Delay</i> .....	61
2.6.3. <i>Choice of source pulse</i> .....	62
2.6.4. <i>Transfer Function</i> .....	65
2.6.5. <i>Impulse response</i> .....	65
2.6.6. <i>Received Signal Waveforms</i> .....	66
2.6.7. <i>Pulse distortion analysis-Fidelity Factor</i> .....	66
2.6.8. <i>Effective isotropic radiated power</i> .....	68
<i>References</i> .....	71
<b>3. <i>Coplanar strip fed Dual Band Antenna</i></b> .....	<b>77-148</b>
3.1. <i>Introduction to compact planar antennas</i> .....	77
3.2. <i>Planar Transmission Lines</i> .....	78
3.2.1. <i>The Microstrip Line</i> .....	78

3.2.2. The Coplanar Waveguide .....	79
3.2.3. The Slotline/Coplanar Strip (CPS).....	79
3.3. Open Ended Slotline.....	81
3.3.1. Reflection Characteristics of OES.....	82
3.3.2. Parametric Analysis .....	83
3.3.2.1. Variation in Reflection co-efficient with $L$ .....	83
3.3.2.2. Variation in Reflection co-efficient with $W$ .....	85
3.3.2.3. Variation in Reflection co-efficient with $h$ .....	86
3.3.2.4. Variation in Reflection co-efficient with $\epsilon_r$ .....	87
3.3.3. Radiation Characteristics of OES.....	88
3.3.4. Surface current analysis. ....	91
3.4. Single band dipole antenna from OES.....	94
3.4.1. Evolution. ....	94
3.4.2. Parametric Analysis. ....	96
3.4.2.1. Variation in Reflection co-efficient with $L_1$ .....	96
3.4.2.2. Variation in Reflection co-efficient with $W_1$ .....	97
3.4.2.3. Variation in Reflection co-efficient with $L_2$ .....	99
3.4.2.4. Variation in Reflection co-efficient with $W_2$ .....	100
3.4.2.5. Variation in Reflection co-efficient with $h$ .....	102
3.4.3. Design Equations.....	103
3.4.4. Coplanar Strip Fed Single band Antenna for 2.4 GHz WLAN Applications. ....	105
3.4.4.1. Structure of the antenna.....	105
3.4.4.2. Return Loss Characteristics.....	106
3.4.4.3. Radiation Characteristics.....	106
3.4.4.4. Surface current Analysis.....	108
3.4.4.5. Gain and Radiation Efficiency.....	109
3.4.5. BALUN-Microstrip to CPS transition.....	110
3.4.5.1. Structure and S Parameters .....	110

3.4.5.2. Surface current Analysis.....	112
3.4.5.3. Antenna characteristics with and without BALUN.....	112
3.5. Dual Band Dipole antenna.....	116
3.5.1. Evolution.....	116
3.5.2. Parametric Analysis.....	117
3.5.2.1. Variation in Reflection co-efficient with $L_1$ .....	118
3.5.2.2. Variation in Reflection co-efficient with $W_1$ .....	121
3.5.2.3. Variation in Reflection co-efficient with $L_2$ .....	122
3.5.2.4. Variation in Reflection co-efficient with $W_2$ .....	123
3.5.2.5. Variation in Reflection co-efficient with $L_3$ .....	125
3.5.2.6. Variation in Reflection co-efficient with $g_1$ .....	126
3.5.3. Design Equations for Dual Band antenna.....	128
3.5.4. Coplanar Strip Fed Dual Band antenna for 2.4/5.2 GHz WLAN.....	130
3.5.4.1. Structure of the antenna.....	130
3.5.4.2. Reflection Characteristics.....	131
3.5.4.3. Radiation Characteristics.....	131
3.5.4.4. Surface current Analysis.....	134
3.5.4.5. Gain of the antenna.....	136
3.5.4.6. Radiation Efficiency of the Antenna.....	137
3.6. FDTD Analysis.....	138
3.6.1. Open Ended Slotline.....	139
3.6.2. Coplanar Strip Fed Single band Antenna.....	141
3.6.3. Coplanar Strip Fed Dual Band antenna.....	142
3.7. Chapter Summary.....	145
<b>4. Coplanar strip fed High Gain Dipole Antennas.....</b>	<b>149-212</b>
4.1. High gain Dipole Antenna.....	149
4.1.1. Evolution.....	149
4.1.2. Parametric Analysis.....	152



4.1.2.1.	<i>Variation in Reflection co-efficient with <math>L</math>.....</i>	152
4.1.2.2.	<i>Variation in Reflection co-efficient with <math>W</math>.....</i>	154
4.1.2.3.	<i>Variation in Reflection co-efficient with <math>L_1</math>.....</i>	157
4.1.2.4.	<i>Variation in Reflection co-efficient with <math>W_1</math>.....</i>	158
4.1.2.5.	<i>Variation in Reflection co-efficient with <math>L_2</math>.....</i>	160
4.1.2.6.	<i>Variation in Reflection co-efficient with <math>W_2</math>.....</i>	162
4.1.2.7.	<i>Effect of <math>L_2</math> on Gain of the Antenna. ....</i>	163
4.1.2.8.	<i>Effect of <math>W</math> on Gain of the Antenna ....</i>	165
4.1.2.9.	<i>Effect of <math>L</math> on Gain of the Antenna.....</i>	167
4.1.3.	<i>Design Equations of High Gain Antenna.....</i>	168
4.1.4.	<i>Coplanar Strip fed High Gain Directive Dipole for 5.2/5.8 GHz Bands .....</i>	171
4.1.4.1.	<i>Structure of the antenna.....</i>	171
4.1.4.2.	<i>Return Loss Characteristics.....</i>	172
4.1.4.3.	<i>Radiation Characteristics.....</i>	172
4.1.4.4.	<i>Surface current Analysis.....</i>	176
4.1.4.5.	<i>Gain of the antenna.....</i>	177
4.1.4.6.	<i>Radiation Efficiency of the antenna.....</i>	177
4.2.	<i>Bandwidth Enhancement of High Gain antenna.....</i>	178
4.2.1.	<i>Evolution of the wide band antenna .....</i>	179
4.2.2.	<i>Parametric Analysis .....</i>	179
4.2.2.1.	<i>Variation in Reflection co-efficient with <math>L</math>.....</i>	180
4.2.2.2.	<i>Variation in Reflection co-efficient with <math>L_1</math>.....</i>	182
4.2.2.3.	<i>Variation in Reflection co-efficient with <math>L_2</math>.....</i>	183
4.2.2.4.	<i>Variation in Reflection co-efficient with <math>W_1</math>.....</i>	185
4.2.2.5.	<i>Variation in Reflection co-efficient with <math>L</math> and <math>L_2</math> by Keeping <math>L+L_2</math> Constant.....</i>	186
4.2.2.6.	<i>Effect of Variation in <math>h</math>.....</i>	187
4.2.2.7.	<i>Effect of <math>L_1</math> on Gain of the Antenna. ....</i>	188
4.2.2.8.	<i>Effect of <math>L_2</math> on Gain of the Antenna .....</i>	189

4.2.3. Design Equations.....	190
4.2.4. Coplanar Strip fed Directive dipole antenna for wide band applications. ....	192
4.2.4.1. Structure of the antenna.....	192
4.2.4.2. Return Loss Characteristics.....	193
4.2.4.3. Radiation Characteristics.....	194
4.2.4.4. Surface current Analysis. ....	200
4.2.4.5. Gain of the antenna.....	201
4.2.4.6. Radiation Efficiency of the antenna.....	202
4.3. FDTD Analysis.....	203
4.3.1. Coplanar strip fed High Gain Dipole antenna.....	203
4.3.2. Coplanar strip fed wide band directive dipole antenna.....	205
4.4. Chapter Summary. ....	210
<b>5. Coplanar strip fed Ultra Wide Band Antennas. ....</b>	<b>213-274</b>
5.1. Coplanar strip fed V groove UWB Antenna.....	213
5.1.1. Parametric Analysis. ....	215
5.1.1.1. Variation in Reflection co-efficient with $L$ .....	215
5.1.1.2. Variation in Reflection co-efficient with $W$ .....	216
5.1.1.3. Variation in Reflection co-efficient with $L_{off}$ .....	217
5.1.1.4. Variation in Reflection co-efficient with $W_{off}$ .....	218
5.1.1.5. Variation in Reflection co-efficient with $h$ .....	219
5.1.2. Design Equations.....	220
5.1.3. Optimized Structure of V Groove UWB Antenna .....	222
5.1.4. Reflection Characteristics.....	223
5.1.5. Radiation Characteristics.....	223
5.1.6. Surface Current Analysis.....	228
5.1.7. Gain and Efficiency.....	230
5.2. Coplanar strip fed Ultra compact semi circular slot UWB Antenna.....	231

5.2.1. Parametric Analysis.....	232
5.2.1.1. Variation in Reflection co-efficient with $L$ .....	233
5.2.1.2. Variation in Reflection co-efficient with $W$ .....	234
5.2.1.3. Variation in Reflection co-efficient with $R$ .....	234
5.2.1.4. Variation in Reflection co-efficient with $h$ .....	235
5.2.2. Design Equations.....	236
5.2.3. Optimized Structure of semi circular slot $UWB$ Antenna.....	238
5.2.4. Reflection Characteristics.....	239
5.2.5. Radiation Characteristics.....	240
5.2.6. Surface Current Analysis.....	245
5.2.7. Gain and Efficiency.....	247
5.3. Coplanar strip fed Enhanced Gain Semi circular $UWB$ Antenna.....	247
5.3.1. Parametric Analysis.....	248
5.3.1.1. Variation in Reflection co-efficient with $R$ .....	248
5.3.1.2. Variation in Reflection co-efficient with $L$ .....	249
5.3.1.3. Variation in Reflection co-efficient with $h$ .....	250
5.3.2. Design Equations.....	251
5.3.3. Optimized Structure of semi circular $UWB$ Antenna.....	253
5.3.4. Reflection Characteristics.....	254
5.3.5. Radiation Characteristics.....	255
5.3.6. Surface Current Analysis.....	260
5.3.7. Gain and Efficiency.....	262
5.4. Time Domain Analysis.....	263
5.4.1. Group Delay.....	263
5.4.2. Transfer Function.....	264
5.4.3. Impulse Response.....	267
5.4.4. Received signal Waveforms.....	268
5.4.5. Fidelity Factor.....	270

5.4.6. <i>Effective Isotropic Radiated Power</i> .....	271
5.5. <i>Chapter Summary</i> . ....	271
<b>6. <i>Conclusion and Future Perspectives</i>. ....</b>	<b>275-280</b>
6.1. <i>Thesis Summary and Conclusions</i> . ....	275
6.2. <i>Suggestions for future work</i> , .....	279
<i>Appendix-1 Extraction of Distributed RLC Parameters</i> .....	281-290
<i>Appendix-2 FDTD Analysis</i> .....	291-309

## INTRODUCTION AND REVIEW OF LITERATURE



*This chapter provides a brief overview of the field of antennas. A brief history of the contributions by various eminent scientists to the field of microwaves and antennas is depicted. This is followed by the discussion of various techniques and state of art innovations in the field of planar antennas with related literatures. The chapter also presents the motivation of the thesis and its organization.*

### 1.1 Introduction

Antennas – The electronic eye and ear of all communication systems are unavoidable and inseparable part of modern communication gadgets. The IEEE defines the antenna or aerial as “a means for radiating or receiving radio waves”. In general, an antenna is a *transition device or a transducer, which convert guided wave into free space wave/photons OR it is an impedance matching device which matches the impedance of a transmission line with that of free space OR it is a device which convert electrical current in a particular frequency into electromagnetic wave in the same frequency and vice versa*. The wide range of application of antennas is available in various regions of electromagnetic spectrum. The type and property of antenna depends on the frequency region at which it operates. The electrical and mechanical

characteristics together with operating cost and operating environment will determine the design criterion for a particular antenna. Antennas are not only utilized for communication and broadcasting but also for the fascinating field of radio astronomy, biomedicine, defence, radar, remote sensing, collision avoidance, air traffic control, GPS, WLAN's etc. This wide range of application makes the field of antenna as an interesting area of research.

## **1.2 Important Milestones in Communication**

Major developments in the field of electromagnetics, microwaves and antennas - all started with the arguments about the electromagnetic nature of light. The initial foundations on this field were laid by James Clark Maxwell who unified the theories of electricity and magnetism in 1873 [1] and eloquently represented the relations through a set of equations which are known as “*Maxwell's Equations*”. He showed that light is electromagnetic in nature and both light and electromagnetic waves travel with the same velocity. Maxwell's theories were supported and proved by the experiments carried out by Heinrich Hertz in 1888 [2, 3].

Guglielmo Marconi was the first scientist who commercially used “Air waves” for practical communication in 1897 [4]. He started the first commercial transatlantic wireless communication using radio waves with the help of the large antennas constructed by him in 1901.

Jagdish Chandra Bose a talented Indian Scientist started studies in millimeter waves in the same period. He used waveguides, horn antennas, dielectric lenses, various polarizers and even semiconductors for his studies. He is considered as the inventor of horn antenna. It is interesting to note that a 1.3 mm multi-beam receiver now in use in the NRAO 12 Meter Telescope,

Arizona, U.S.A. incorporates his concepts 100 years back! [5-7]. Now J. C. Bose is considered as the first man who use wireless communication system.

Karl Jansky who is known as the “father of astronomy” discovered extraterrestrial radio waves using huge antennas designed by him. He belongs to Bell Laboratories [8].

These experiments were followed by numerous inventions by scientists and engineers from different parts of the world. The Yagi – Uda antenna is one of the remarkable findings of that period [9].

At the period of Second World War there is a tremendous push to field of antenna and radar research. Many of the work remained classified as those were associated with military and defense. Huge reflector antennas were built for communications, radar, and radio astronomy. The technology for phased arrays and satellite antennas were refined and realized in several versions. The study of array effects was greatly advanced, and the fundamental ideas of adaptive arrays were put into practice. [10 -12]

A turning point in the field of antenna was the introduction of microstrip antennas by Deschamps in 1953[13]. But it took around twenty years for the practical and large scale development of these antennas.

The twentieth century witnessed remarkable progress in antenna technology from the large transceivers used by Marconi to the sub wavelength antennas with dimensions of the order of fraction of wavelength. Another remarkable development during this period is the birth of smart and active arrays [14 -17].

Table 1.1 shows the important mile stones in the field of communication as a quick reference.

**Table 1.1** Milestones in Communication

Year	Importance
1837	Morse demonstration of telegraph
1865	Prediction of electromagnetic wave propagation by Maxwell
1876	Alexander Graham Bell invented the Telephone
1887	The existence of ElectroMagnetic waves is verified by Heinrich Rudolph Hertz.
1894	Wireless telegraphy by Marconi
1895	Jagadish Chandra Bose gave his first public demonstration of electromagnetic waves.
1901	First wireless transmission by Guglielmo Marconi with his transatlantic transmission.
1906	Lee de Forest's Radio Telephone company sold the first radio
1915	Direct telephone communications opened for service.
1921	Radio dispatch service initiated for police cars in Detroit, Michigan
1924	Directive Yagi-Uda antenna developed by Prof.Hidetsugu Yagi
1927	First television transmission.
1929	Microwave communication established by Andre G. Clavier
1933	Demonstration of Frequency Modulation by Armstrong
1934	AM(Amplitude Modulation)mobile communications systems used by state and municipal forces in the U.S
1935	RADAR by Watson Watt, Radio astronomy by Janskey
1943	The first telephone line from Calcutta, India to Kunming, China.
1944	Telephone cable laid across the English channel
1946	Radiotelephone connections made to PSTN(Public-switched telephone network),3.7-4.2 LOS link by AT&T
1947	First Mobile phone demonstration
1953	Deep space communication proposed by John Pierce.
1957	Soviet Union launches Sputnik, humanity's first artificial satellite.
1958	Invention of Integrated Circuit
1968	Development of the cellular telephony concept at Bell Laboratories.
1979	A 62,000 mile telecommunications system is implemented in Saudi Arabia
1980	1G first generation - only mobile voice service
1981	Beginning of first commercial cellular mobile communication
1982	Two way video teleconferencing service started
1986	Integrated Service Digital Network deployed
1990	2G-Second generation digital cellular deployed throughout the world.
1995	CDMA is introduced
2000	3G Standard is proposed.
2008	ITU-R organization specified the IMT-Advanced (International Mobile Telecommunications Advanced) requirements for 4G standards., Skin-tenna
2010	Solar funnel antenna and sea water antenna
2011	Slit time lens
2012	Better invisibility cloak.



### 1.3 Technologies and Development in the field of Planar Antennas

This thesis concentrates on the design and development of compact coplanar strip fed uniplanar antennas. So a brief account of the various planar antenna designs and their methodology is outlined in this section.

The frequency range allotted for different band designation together with their usage is listed in the table.1.2. This table covers not only the mobile communication but from VHF to Ka band (3 KHz-40 GHz). [18-21]

**Table 1.2** Frequency range allotment for different communication [18-21]

Band Designation		Frequency range	Usage
VLF		3-30KHz	Long distance telegraphy and navigation
LF		30-300 KHz	Aeronautical navigation services, Radio broadcasting, Long distance communication,
MF		300-3000	Regional broadcasting, AM radio
HF		3-30MHz	Communications, broadcasting, surveillance, CB radio
VHF		30-300 MHz	Surveillance, TV broadcasting, FM radio
UHF		30-1000MHz	Cellular communications
Old	New		
L	D	1-2 GHz	Long range surveillance, remote sensing
S	E,F	2-4 GHz	Weather detection, Long range tracking
C	G,H	4-8 GHz	Weather detection, long-range tracking
X	I,J	8-12 GHz	Satellite communications, missile guidance, mapping
Ku	J	12-18 GHz	Satellite communications, altimetry, high resolution mapping
K	J	18-26 GHz	Very high resolution mapping
Ka	K	26-40 GHz	Air port surveillance

Table 1.3 shows the commonly used communication bands based on FCC and ITU regulations [22, 23]. The succeeding section gives a brief account

of different kinds of planar antennas. The antennas designed and discussed in this thesis is mainly working on the bands specified in Table. 1.3.

**Table 1.3** Commonly used communication frequency bands

Name	Service	Allocated Band
RFID	Radio Frequency identification	865 - 868 MHz, 2.446 -2.454 GHz
DVB-H	Digital video Broadcasting - Handheld	470 MHz – 702 MHz
GSM 900	Global system for mobile	890 MHz -960 MHz
DCS 1800	Digital communication system	1710 MHz-1880 MHz
GPS 1200 GPS 1575	Global Positioning System	1227-1575 MHz 1565-1585 MHz
PCS 1900	Personal Communication System	1850-1990 MHz
3G IMT-2000	International Mobile Telecommunication-2000	1885-2200 MHz
UMTS 2000	Universal Mobile Telecommunications Systems	1920-2170 MHz
ISM 2.4 ISM 5.2 ISM 5.8	Industrial, scientific, medical	2400-2484 MHz 5150-5350 MHz 5725-5825 MHz
UWB	Ultra wide band communication	3.1 -10.6 GHz

### 1.3.1 Microstrip Antennas

The first microstrip antenna was practically realized in 1970 which gave a kick to planar antenna research owing excellent characteristics and low profile of the antenna. The typical geometry of a Microstrip antenna consists of a radiating metallic patch and a larger ground plane etched on either sides of a substrate having a fixed dielectric constant and thickness as shown in Fig.1.1.

The length of the patch is normally about one half of the dielectric wavelength corresponding to the operating frequency of the antenna [24, 25].

The substrate material has large influence in determining the size and bandwidth of an antenna. By increasing the dielectric constant of the substrate we can reduce the size of the antenna but lowers the bandwidth and efficiency. While decreasing the dielectric constant, the bandwidth increases with an increase in size of the antenna.

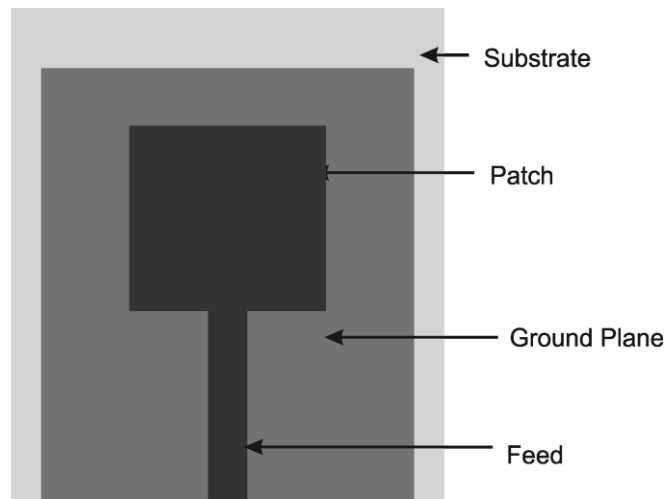


**Fig. 1.1** Microstrip Patch antenna

The major advantages of the microstrip antennas are their low profile, light weight, compatibility to planar and non planar structures and ease of fabrication [26, 27]. The ease of integration of MMICs and other active elements is also an added advantage. Main disadvantages of microstrip antennas are its high Q and resulting narrow band width. This may be reduced by increasing the thickness of the dielectric substrate which results in decrease in efficiency due to increase in surface waves [28, 29]. Another disadvantage is its unipolar radiation characteristic [30-31]. This bars its use in Omni directional radiation applications but can used in directional application.

Many studies have been performed to reduce the disadvantages of microstrip antennas. The surface waves which deteriorate the performance in microstrip antennas can be reduced by using cavities as proposed by Mailloux [32].

There are many bandwidth enhancement techniques like Stacking [33], Aperture coupling [34], Proximity coupling [35], Slot coupling [36], addition of parasitic elements [37], use of different feed geometries and slots [38-42] etc which can be implemented in microstrip antennas.

The advantage of exciting multiple bands using a single antenna increases the need of development of dual and multi band microstrip antennas. There exists many techniques to excite dual and multiple bands in microstrip antenna. They include the insertion of shorting pins [43], slots [44] etc. Many designs for producing circularly polarized radiation have also been proposed [45].

Even with these modifications the achieved bandwidth of these antennas is still low and they still exhibit unipolar radiation. These defects can be mitigated by the use of truncated ground plane structures [46]. This is discussed in the next section.

### **1.3.2 Microstrip fed antennas with Truncated ground plane**

Truncated ground plane microstrip antennas are the planar realizations of conventional vertical monopoles. Truncated microstrip configurations are designed by removing a part of the ground plane at the far end of the feed region along the length of the patch as shown in Fig.1.2. The signal strip extends beyond the length of the ground plane and the configuration acts similarly as a monopole above a ground plane. The resulting structure is a quarter wavelength radiator and thus it is very much

compact than above said microstrip antennas. This configuration reduces the Q factor of the structure.

The main attractions of truncated ground plane structures are apple shaped radiation pattern, large band width and ease of fabrication. The bandwidth of these antennas can be further increased by loading an arbitrary shape on the monopole. The band widths of these antennas are large, capable of easily covering the conventional communication bands [47, 48].

It is very interesting that by properly truncating the ground plane width, an additional resonance near the fundamental mode can be excited in the antenna which can be merged with the fundamental mode to yield more band width [49].

Many interesting dual band and multi band designs have also been developed using truncated microstrip configurations [50 – 54].

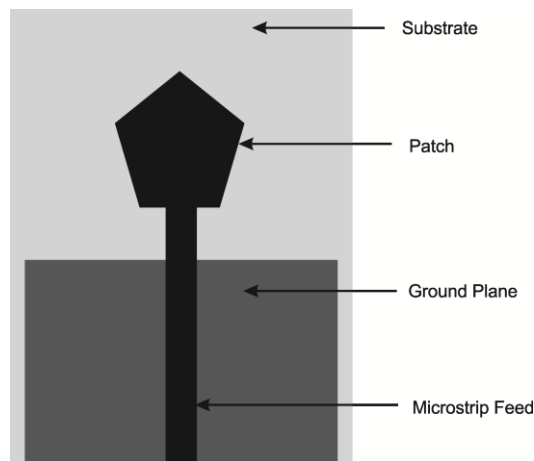


**Fig.1.2** A pentagon patch loaded on a monopole fed by a microstrip with a truncated ground plane

The truncated ground plane structure due to its large band width makes the design and development of the ultra wide band antennas very simple. Many interesting UWB designs using this method have been reported [55-58].

The design of the ground plane and the radiating patch needs ultimate care in this structure. Since the structure is integrated on both sides of the substrate, usually vias or shorting pins are required for the integration of active devices and MMICs. This has created a greater interest for the design of uniplanar antennas. Uniplanar antennas can be conveniently designed on the single side of a substrate, which makes fabrication of the structure and integration of active devices in to the structure very easy. The most widely used uniplanar antennas are the coplanar wave guide fed and coplanar strip/slotline fed designs.

### 1.3.3 Coplanar Waveguide fed (CPW) Antennas

The coplanar wave guide consists of a central signal strip with lateral ground strips separated by a small gap on either sides. The entire coplanar wave guide structure can be printed on the single side of a substrate. A typical pentagon patch monopole fed by the CPW feed is given in Fig.1.3.

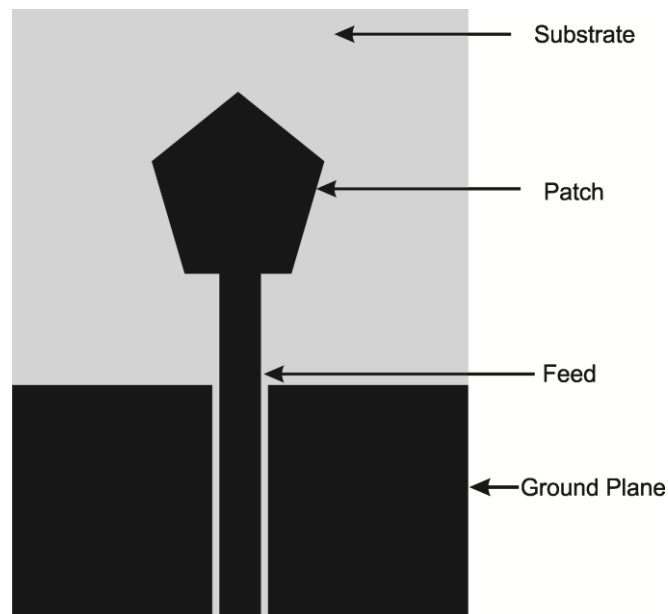


**Fig.1.3** Coplanar wave guide fed pentagon shaped antenna

Different types of CPW fed designs for single band [59, 60] and multi band [61] antennas have already been reported in literature.

The microstrip line and the coplanar wave guide are the commonly used transmission lines to guide power from the source to the antenna. Based on the challenges and constraints before the designer various interesting modified designs of these transmission lines have been proposed. They include the slotline/Coplanar strips, Asymmetric coplanar waveguide etc [62].

All the above mentioned antennas are with a size of the order of half wavelength or quarter wavelength. The insertion of these antennas into modern communication devices requires them to be more compact. Various techniques have been proposed to achieve this compactness. The use of Photonic Band gap (PBG) structures, metamaterials and fractal based geometries are most common to attain this compactness.

### **1.3.4 Photonic Band Gap (PBG) structures**

The "Photonic Band Gap" (PBG) structures present a very useful and interesting feature; they attenuate the propagation of electromagnetic wave in a frequency range for certain space directions [63, 64].

To enhance the bandwidth in microstrip based structures, methods like increasing the height of the substrate have been proposed. But this method will leads to increased surface waves which will absorb the power from direct radiation and results in degrading the pattern shape and stability and the efficiency of the antenna. In order to avoid this effect due to surface waves, a PBG structure can be utilized. The PBG backed microstrip antennas exhibits improved antenna efficiency, low side lobe level and high antenna gain by reducing the surface wave propagation.

Photonic band gap structures are also used to increase the gain or bandwidth of compact planar antenna designs. Various designs of PBG Structures for enhancing the bandwidth, reducing the size, suppression of unwanted harmonics, reduction of cross polarization etc can be found in many literature [65-68].

### **1.3.5 Metamaterial based antennas designs**

Another innovation that is bringing tremendous changes in the field of electromagnetics is the introduction of metamaterials. The first metamaterials were developed in the 1940s, but wide research in the field of metamaterials started only in the 1990s. V.G Veselago proposed materials with simultaneous negative permittivity and permeability and possess a negative index of refraction [69]. He termed these as Left-Handed Media (LHM), because here the vectors E, H, and k form a left-handed triplet instead of a right-handed triplet, as is the case in conventional, Right-Handed Media (RHM).

Recently, novel electromagnetic metamaterials have been successfully demonstrated with the permittivity and permeability functions simultaneously negative using an array of resonant cells consisting of thin wire strips and Split-Ring Resonators (SRRs) [70,71].

Materials with such characteristics could enable the miniaturization in size of antenna, filters and other passive devices [72 -74].

### **1.3.6 Fractal geometry based antenna designs**

The term fractal means broken fragments. Fractals are complex geometric designs that are formed by repeated addition of small sized similar structures. Their statistical properties on many scales, and are thus “self similar.” The self similarity properties of fractals make them especially suitable



for designing multiband antennas. Some fractals have complex, highly convoluted and complex shapes that can enhance radiation when used as antennas. Fractals can improve the performance of antenna or antenna arrays. In antenna design, the use of fractal shapes makes the frequency of operation of an antenna, independent of its size. This means that a fractal antenna can be constructed in small sizes, yet possessing a broad frequency range with enhancement in bandwidth and gain [75, 76].

Fractals geometries like such as Koch curves, Minkowski fractals and Sierpinski triangles etc, have been used to design compact antennas and arrays for multiband, broadband and ultra wide band applications [77 - 84].

### **1.3.7 Dielectric Resonator based designs**

A solid volume or a piece of a dielectric material will acts as a resonator of microwave frequency in which the guided wavelength is very small when compared to free space. The dielectric resonators have been in existence for almost 30 years, and over that time a wide deal of research has been performed in this field. The most attractive feature of dielectric resonators are their low loss behaviour due to the absence of conducting materials which eliminate ohmic losses [85]. Dielectric resonators are useful in communication devices like filters, low noise oscillators, and other circuits [86].

Dielectric resonator antennas (DRAs) are miniaturized antennas of ceramics or another dielectric medium for microwave frequencies. Their radiation characteristics are a function of the mode of operation excited in the DRA. The mode is generally chosen based upon the operational requirement. The main advantages of DRAs are small size, high radiation efficiency and simplified coupling schemes for various transmission lines. The bandwidth can be controlled over a wide range by properly choosing the dielectric constant,

and the geometric parameters of the resonator. The dielectric resonator antennas can be fed by a typical microstrip line or by a co planar wave guide. A typical dielectric loaded monopole antenna is shown in Fig. 1.4.

Designs for increased bandwidth, circular polarization, varying radiation patterns, and for use in arrays have all been demonstrated [87 – 91]. Due to these attracting characteristics, gigantic antennas like standard whip, helical and other upright antennas can be replaced by DRAs.

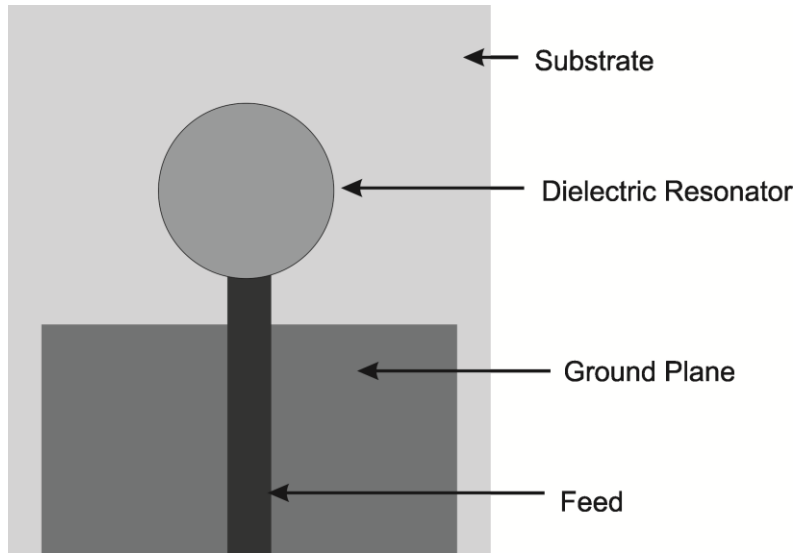


**Fig.1.4** Dielectric loaded microstrip fed monopole antenna

### **1.3.8 Ultra wide band antennas**

UWB antennas are considered as the shining star among the antennas because of their various superior qualities [92-94]. According to the definition of the FCC, a UWB device has a fractional bandwidth that is greater than 0.2, or occupies 500 MHz or more of the frequency spectrum, regardless of the fractional bandwidth. For commercial microwave UWB applications, the FCC prescribed a band width in the range of 3.1GHz –10.6 GHz [95]. Many

researchers are contributed for the development of microwave ultra wideband (UWB) technology for communications, imaging, radar, and localization applications. Many studies have been performed in the design, development and measurement of UWB antennas [96-100].

The great field of ultra wide band antenna designs may be broadly divided as travelling wave structures like Vivaldi antenna [101,102], Frequency independent structures like the biconical antenna or the bowtie Antenna [103,104], complementary antennas that are characterized by a self-complementary metallization like the fractal antennas and logarithmic spiral antennas [105-107], combinations of the above like the log periodic antenna [108-110] and the electrically small antennas whose size is very small when compared to the wave length which includes the modified monopoles [111-119]. New designs with frequency notch in the existing WLAN bands in the 5-6 GHz range have also been reported [120-123]. A few typical UWB monopole designs are given in fig.1.5.

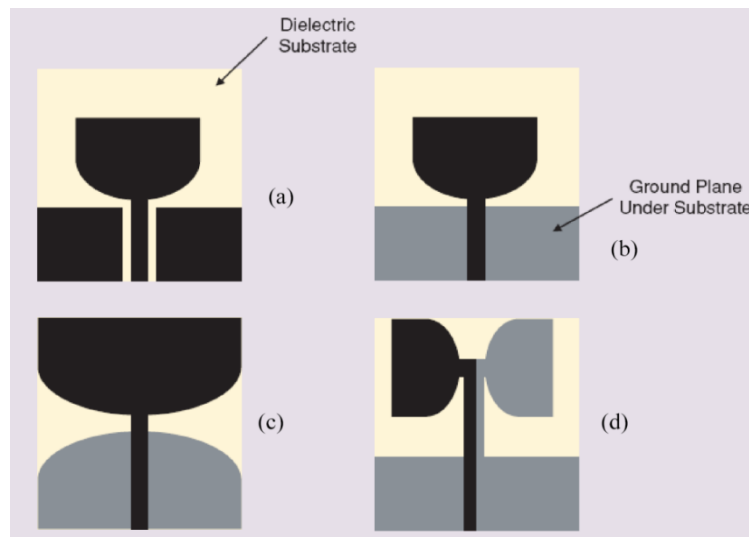


**Fig.1.5** Various monopole configuration for ultra wide band applications

A number of literatures are available in the field of directional UWBs also. They are mainly used in medical imaging applications and directional applications like GPRS and other positioning applications and secure high data rate communications. The main design idea of these antennas includes exponential tapering and Vivaldi like structures. However, these antennas are of large size with poor pattern stability in the entire band of operation [124-129]

### **1.3.9 LTCC based antenna designs**

Low-temperature Co-fired Ceramics (LTCC) is a modular technology which is capable to reduce the volume of a circuit drastically when compared to individual integrated circuit (IC) mounting. This is achieved by stacking several ceramic substrates each of only several micro meter thickness and building-in passive components like resistors, capacitors, inductors etc. LTCC makes it possible to pack the filters and other components used in a mobile phone into a package having dimensions of only a few mm<sup>3</sup> [130].

LTCC technology is based on integration of multi-layered thick-film sheets of thickness in the range of 50-250  $\mu\text{m}$  or so-called green tapes, which are screen-printed with thick-film pastes of conductors, resistors, etc. Many ultra compact antenna designs have been reported using LTCC technology proving it as viable alternative to the conventional miniaturization techniques [131-134].

## **1.4 Motivation of the work**

Antenna is considered as the un avoidable part of the communication system. All most all the human beings are the stake holders of the antenna by knowing or not knowing about it. Thus the study about the antenna is very much interesting.

An antenna can be constructed from a normal transmission line by creating a discontinuity or by a bending or a curve in it. But in case of transmission line like slotline/ coplanar strip (CPS), an open ended slotline can be acts as a radiator with upper edge acts a half wave long dipole. As the length of the slotline/CPS wave guide increases, the efficiency of the radiator is found to be very low and the matching is very poor. Thus the conclusion is that the CPS is not an ideal waveguide for transfer power from one point into other, but can be a good and ideal feed for the radiators.

It is very interesting that, the modification in CPS can result in very efficient radiators with enhanced gain and excellent radiating characteristics. Several Compact multi band, dual band, wide band and ultra wide band designs also can be generated using this principle.

Another interesting characteristics of the CPS is its inherent directionality. The open ended slotline itself acts as a directional structure. This property can be effectively utilized to generate several high gain directional antennas. From the literature review it can be noted that only few efforts are taken for the analysis of slotline fed designs [135-137].

Due to the above mentioned reasons, I am very interested in effectively transform the CPS into a good radiator. The transformation is done through selective removal of metallic parts from either strips of the slotline. For simplicity of the structure, the removal is carried out symmetrically in either strips of the slotline which results in laterally symmetric antennas. Excellent radiators are obtained from this study with compact size and good directional properties.

## **1.5 Organisation of the Thesis**

The Thesis is organized into six chapters.

Chapter 1 gives a brief introduction about the evolution of planar antennas. Various antenna designs for specific applications have been briefly reviewed along with the motivation of the present work.

Chapter 2 gives an account of the various techniques used for the design fabrication and measurement of antennas. Basic concepts and measurement methodology is briefly outlined in this chapter. Since one of the chapters in this thesis deals with ultra wideband antennas, time domain analysis techniques are also thoroughly discussed in this chapter.

Chapter 3 gives a detailed study of coplanar strip fed Dual band antenna. The chapter starts by introductory analysis of various planar transmission lines and then goes to detailed analysis of CPS and Open Ended Slotline. Then an effort to convert CPS into single band antenna is discussed. The developed single band antenna is analyzed thoroughly. Since the structure is a balanced one, a comparative analysis of the performance of the antenna with and without BALUN is performed and discussed in this chapter. Then the study is vectored into the development of dual band antenna from the single band dipole and the developed structure is analyzed thoroughly. FDTD analysis of the structures discussed in this chapter are performed and included as the last part of the chapter.

Chapter 4 gives the development of a high gain dipole antenna derived from an open ended CPS transmission line. The antenna offers an enhanced directivity without the help of any parasitic directors and reflector elements. As a next step of chapter 4 the study is pointed towards the development of an

enhanced gain antenna from the successor which is very much suitable for wide band applications. Here also the FDTD analysis is performed and included.

Chapter 5 deals with the discussion about the development of CPS fed Ultra Wide Band antennas with directional properties. As the part of the study, a V groove antenna, an ultra compact semi circular cut UWB antenna and a high gain semicircular UWB antenna are developed and analyzed thoroughly. All the frequency domain and time domain analysis of the UWBs are performed and discussed.

Chapter 6 serves as a conclusion of the thesis with thesis highlights and ending with many directions for future study and development in the field of slotline fed antennas.

Since Chapter 3 and 4 discusses about the distributed RLC parameters of the antenna, the extraction of these parameters from reflection characteristics cannot be excluded. It is given as Appendix-1.

Detailed analysis techniques used in FDTD is included as Appendix-2.

## **References**

- [1] Maxwell, "A Treatise on Electricity and Magnetism". Macmillan and Co., Oxford University, 1873.
- [2] J.D. Kraus, Ronald J. Marhefka, Antennas for all applications, Tata McGraw-Hill , 3rd Edition, pp. 785-788
- [3] Carter, P.S.; Beverage, H.H, "Early History of the Antennas and Propagation Field until the End of World War I, Part I – Antennas" Proceedings of the IRE ,Volume 50, Issue 5, pp 679 – 682, May 1962
- [4] John D. Kraus, "Antennas since Hertz and Marconi", IEEE Trans. Antennas and Propagat. vol.33, no.2, pp 131-136, February 1985.
- [5] G.L. Pearson, and W.H. Brattain, "History of Semiconductor Research," Proc. IRE, 43, pp.1794-1806, 1955
- [6] John F. Ramsay, "Microwave Antenna and Waveguide Techniques before 1900," Proc. IRE., Vol.46, No.2, pp. 405-415, February 1958.
- [7] Tapan K. Sarkar and Dipak L. Sengupta., "An Appreciation of J. C. Bose's Pioneering Work in Millimeter Waves" IEEE Antennas and Propagation Magazine, Vol. 39, No. 5, pp.55-63, October 1997.
- [8] Jansky, K.G "Electrical disturbances apparently of extraterrestrial origin" in Proc. IRE in 1933 (Reprinted in Proc. IEEE, vol. 86, no. 7, pp. 1510-1515, July 1998.
- [9] S. Uda, Wireless Beam of short electric waves, J. IEE (Japan), pp. 273-282, March 1926



- [10] Skolnik, M, Radar: from Hertz to the 21st century, Antennas and Propagation Society International Symposium, 1988. AP-S. Digest,6-10 Pp:929 vol.3, June 1988
- [11] Schell,A.C, “Antenna developments of the 1950s to the 1980s”, Antennas and Propagation Society International Symposium, IEEE Vol. 1, Pp 30 – 33, July 2001
- [12] W. A. Imbriale, “Evolution of the Large Deep Space Network Antennas,” IEEE Antennas and Propagation Magazine, Vol. 33, No. 6. pp. 7- 19, Dec. 1991.
- [13] Deschamps G. A, “Microstrip Microwave Antennas”, III rd USAF symposium on Antennas, 1953.
- [14] Yongxi Qian and Tatsuo Itoh, “ Progress in Active Integrated Antennas and Their Applications”, IEEE Transactions on Microwave Theory and Techniques, vol. 46, no. 11, Pp 1891 – 1900,November 1998
- [15] Edvardsson. O, “Recent advances in handset antennas for satellite communication”; IEEE Antennas and Propagation Society International Symposium,Volume 4, Pp 553 - 556, July 2001
- [16] Heberling, D, “Modern trends in the development of small and handy antennas” Proceedings of the 2001 SBMO/IEEE MTT-S International, Volume 2, Pp 59 - 64 vol.2,Aug. 2001 .
- [17] Guha,D, “Microstrip and printed antennas -recent trends and developments”,. TELSIXS 2003. 6th International Conference on Volume 1, Page (s):39 - 44 vol.1, Oct. 2003.
- [18] John D Kraus and Ronald J Marhefka, Antennas and Wave propagation, Tata McGraw hill,2010

- [19] Mridula S, “Investigations on a microstrip excited rectangular dielectric resonator antenna”, Ph.D thesis, Cochin University of science and Technology.
- [20] Binu Paul, “Development and Analysis of microstrip antennas for dual band microwave communication” Ph.D thesis, Cochin University of science and Technology.
- [21] Tapan K Sarkar, “History of Wireless” , John Wiley and Sons
- [22] <http://www.itu.int/>
- [23] <http://www.fcc.gov/>
- [24] Constantine A Balanis "Antenna theory analysis and design" John Wiley and Sons II nd edition
- [25] Pozar, D.M, “Microstrip antennas”, Proceedings of the IEEE Volume 80, Issue 1, Pp 79 – 91,Jan. 1992
- [26] Pozar D.M., “The Analysis and Design of Microstrip Antennas and Arrays”, IEEE press, New York, 1995.
- [27] Fonseca, S.D.A. Giarola, A. “Microstrip disk antennas, Part I: Efficiency of space wave launching”, IEEE Trans. Antennas and Propagat. vol.32, no.6, pp 561- 567, June 1984
- [28] Fonseca, S.D.A. Giarola, A. “Microstrip disk antennas, Part II: Efficiency of space wave launching”, IEEE Trans. Antennas and Propagat. vol.32, no.6, pp 568- 573, June 1984
- [29] J. Huang, “The Finite Ground Plane Effect on the Microstrip Antenna Radiation Patterns,” IEEE Trans. Antennas Propagat. Vol. AP-31,pp 978-984, July 1983

- [30] C A Balanis, "Advanced Engineering Electromagnetics", John Wiley & sons, New York 1989.
- [31] Ramesh Garg, Prakash Bhartia and Inder Bahl, "Microstrip Antenna Design Handbook", 1st ed. MA Artech House, 2001.
- [32] R.J. Mailloux, "On the use of metallized cavities in printed slot arrays with dielectric Substrates" IEEE Trans. Antennas Propagat. Vol. AP-35, pp 477-487, May 1987.
- [33] S.A Long and M.D. Walton, "A Dual-frequency Stacked circular Disc antenna", IEEE Trans. Antennas Propagat. Vol. AP-27, No.2, pp 270-273, May 1987.
- [34] C H Tsao, Y M Hwang, F Kilburg and F. Dietrich, "Aperture Coupled patch antennas with wide bandwidth and Dual Polarisation capabilities", IEEE Antennas and Propagation symposium dig. pp 1220-1223, 1989.
- [35] D M Pozar and B Kaufman, "Increasing the bandwidth of microstrip antennas by Proximity coupling," IEE Electronics Lett. Vol.23 pp 1070 – 1072, September 1987.
- [36] A. Ittipiboon, B Clarke, and M Cuhaci, "Slot Coupled Stacked microstrip antennas", IEEE Antennas and Propagation symposium dig. pp 63-66, 1983.
- [37] C. K. Aanandan, P. Mohanan and K. G. Nair, "Broad band gap coupled microstrip antenna", IEEE Transactions on Antennas and Propagat., Vo. 38, No. 10, pp. 1581-1586, Oct. 1990.
- [38] S. Mridula, Sreedevi K. Menon, B. Lethakumary, Binu Paul, C. K. Aanandan, P. Mohanan, "Planar L-strip fed broadband microstrip

- antenna”, Microwave and optical technology letters, Vol. 34, Issue 2 , pp. 115 – 117,Jun 2002,.
- [39] J. George, K. Vasudevan, P. Mohanan and K.G. Nair, “Dual frequency miniature microstrip antenna”, Electronics Letters Vol. 34 No. 12, pp. 1168-1170, June 1998
- [40] B. Lethakumary, Sreedevi K. Menon, C. K. Aanandan, P. Mohanan, “A wideband rectangular microstrip antenna using an asymmetric T-shaped feed”, Microwave and optical technology letters, Vol. 37, Issue 1 , pp. 31 – 32, Feb 2003.
- [41] Binu Paul, S. Mridula, C. K. Aanandan, P. Mohanan, “A new microstrip patch antenna for mobile communications and bluetooth applications”, Microwave and Optical Technology Letters Volume 33, Issue 4, Pages: 285-286, May 2002.
- [42] Manju Paulson, Sona O. Kundukulam, C. K. Aanandan, P. Mohanan, K. Vasudevan, “Compact microstrip slot antenna for broadband operation”, Microwave and optical technology letters, Vol. 37, Issue 4, pp. 248 – 250, March 2003.
- [43] Latif, S.I.; Shafai, L.; Sharma, S.K, “Bandwidth enhancement and size reduction of microstrip slot antennas”.; IEEE Transactions on Antennas and Propagat., Volume 53, Issue 3, Pp 994 – 1003, March 2005
- [44] Sona O. Kundukulam, Manju Paulson, C. K. Aanandan, P. Mohanan, “Slot-loaded compact microstrip antenna for dual-frequency operation”, Microwave and optical technology letters, Vol. 31, Issue 5 , Oct 2001, pp. 379 – 381

- [45] Nasimuddin, Esselle, Verma, A. K, “Wideband Circularly Polarized Stacked Microstrip Antennas”, IEEE Antennas and Wireless Propogat. Lett.,Vol.6,pp 21 – 24, 2007
- [46] Zhi Ning Chen; Ammann, M.J.; Xianming Qing; Xuan Hui Wu; See, T.S.P, “ Planar Antennas”, IEEE Antennas and Propagation magazine,Vol.7,No.6,pp 59 – 61, December 2006
- [47] Ammann, M.J and John, M, “Optimum design of the printed strip monopole”,IEEE Antennas and Propagation magazine, Vol.47, No.6, pp 59 – 61, 2005
- [48] M. N. Suma, Rohith K. Raj, Manoj Joseph, P. C. Bybi, and P. Mohanan, “A Compact Dual Band Planar Branched Monopole Antenna for DCS/2.4-GHz WLAN Applications”, IEEE Microwave and Wireless Components Letters, Vol. 16, No. 5, pp. 275-277, May 2006.
- [49] Suma M.N, Bybi P.C and P.Mohanan, “A wide Band Printed Monopole antenna for 2.4GHz WLAN Applications” Microwave and Optical Technology Lett. Vol.48, No.5, May 2006. pp 871-873.
- [50] Yuehe Ge, Karu P. Esselle and Trevor S. Bird, “A Spiral-Shaped Printed Monopole Antenna for Mobile Communications”, IEEE Antennas and Propagation Society International Symposium Pp 3681 - 3684 July 2006.
- [51] J.-S. Rowand S.-W.Wu, “Monopolar square patch antennas with wideband operation”, IEE Electron. Lett., vol. 42, no. 3, pp. 139–140, Feb.2006

- [52] Joon II Kim and Yong Jee, “Design of Ultra wide band Coplanar wave guide fed LI- shape planar monopole antennas”, IEEE Antennas and Wireless propagation let., Pp 383-387, vol. 6, 2007.
- [53] Y.-L. Kuo and K.-L. Wong, “Printed Double – T monopole for 2.4/5.2 GHz dual-band Operations”, IEEE Trans. Antennas and Propagat., vol. 51, pp. 2187–2192, Sep. 2003.
- [54] Raj, R.K., Joseph, M., Aanandan, C.K.; Vasudevan, K.; Mohanan, P., A New Compact Microstrip-Fed Dual-Band Coplanar Antenna for WLAN Applications, IEEE Transactions on Antennas and Propagat, Volume 54, Issue 12, Pp :3755 – 3762, Dec. 2006
- [55] Manoj Joseph, Rohith K.Raj, Suma M.N, C.K.Aanandan, K.Vasudevan And P.Mohanan, “Microstrip-fed dual band folded dipole antenna for DCS/PCS/2.4GHz WLAN applications” International Journal On Wireless and Optical Communications, Volume.4, No.1, pp 43-51, 2007.
- [56] D. C. Chang, M. Y. Lin, and C. H. Lin, "A CPW-fed U type Monopole Antenna for UWB Applications," in Proc. IEEE Antennas and Propagation Society Int. Symposium., vol.5A, pp512-515, July 2005.
- [57] W. S. Lee, D. Z. Kim, K. J. Kim, and J. W. Yu, "Wideband Planar Monopole Antennas with Dual Band-Notched Characteristics," IEEE Transactions on Microwave Theory Tech., vol.54, no.6, pp2800-2806, June 2006.
- [58] W. C. Liu and C.-F. Hsu, “Dual-band CPW-fed Y-shaped monopole antenna for PCS/WLAN application”, IEE Electron lett.Vol.No.41,no.7, pp. 390–391, Mar. 2005.

- [59] K. F. Jacob, M. N. Suma, R. K. Raj, M. Joseph and P. Mohanan, “Planar Branched Monopole Antenna for UWB Applications,” *Microwave and optical technology letters*, vol.49, no.1, pp45-47, Jan. 2007
- [60] Horng-Dean Chen and Hong-Twu Chen, “A CPW-Fed Dual-Frequency Monopole Antenna”, *IEEE Transactions on Antennas and Propagat*, Vol.52, No.4, pp 978 – 982, April 2004.
- [61] W.-C. Liu and H.-J. Liu, “Compact Triple band slotted monopole antenna with asymmetrical grounds”, *IET Electronics lett.*, Vol. 42 No. 15, pp 78 -79, July 2006
- [62] R. Garg, P. Bhartia, and I. Bahl, *Microstrip Antenna Design Hand book*, 1st ed. Boston, MA: Artech House, 2001, pp. 790–795.
- [63] Inrik Chang and Bomson Lec, “Design of Defected Ground Structures for Harmonic Control of Active Microstrip Antenna”, *Antennas and Propagation Society International Symposium*, 2002. *IEEE Volume 2*, Pp: 852 – 855, June 2002 .
- [64] Radisic, V.; Qian, Y.; Coccioli, R.; Itoh, T, Novel 2-D photonic bandgap structure for microstrip lines *Microwave and Guided Wave Letters*, *IEEE* ,Volume 8, Issue 2, Pp :69 – 71, Feb. 1998
- [65] P. Salonen, M. Keskilammi, L. Sydanheimo, “A low-cost 2.45 Ghz photonic band-gap patch antenna for wearable systems”, *IEEE Intemational Conference on Antennas and Propagation*, 77-20 April 2001
- [66] Y. J. Sung and Y.-S. Kim, “An Improved Design of Microstrip Patch Antennas using photonic Band Gap structures”, *IEEE Transactions on Antennas and Propagat*, Vol.53, No.5, pp 1799 – 1802, May 2005.

- [67] Haiwen Liu, Zhengfan Li, Xiaowei Sun, and Junfa Mao, " Harmonic Suppression With Photonic Bandgap and Defected Ground Structure" IEEE Microwave and wireless components lett., vol. 15, no. 2, Pp 55-56, february 2005
- [68] Debatosh Guha, Manotosh Biswas, and Yahia M. M. Antar, "Microstrip Patch Antenna With Defected Ground Structure for Cross Polarization Suppression", IEEE antennas and wireless propagation letters, vol. 4, pp 455-458, 2005.
- [69] V. G. Veselago, "The electrodynamics of substances with simultaneously negative values of  $\epsilon$  and  $\mu$ ," Sov. Phys., vol. 10, no. 4, pp. 509-514, Jan.-Feb.1968.
- [70] J. B. Pendry, A. J. Holden, D. J. Robins, W. J. Stewart, "Magnetism from conductors and enhanced nonlinear phenomena," IEEE Trans. on Microwave Theory and Tech., vol. 47, no. 11, pp. 2075-2084, Nov. 1999.
- [71] D. R. Smith, W. J. Padilla, D. C. Vier, S. C. Nemat-Nasser, S. Schultz, "Composite medium with simultaneously negative permeability and permittivity," Phys. Rev. Lett., vol. 84, no. 18, pp. 4184-4187, May 2000.
- [72] Special issue on Metamaterials, IEEE Trans. On Antennas Propagat., 2003, Vol. 51
- [73] Filiberto Bilotti, Andrea Alú, Membe, and Lucio Vegni, Design of Miniaturized Metamaterial Patch Antennas With  $\mu$ -Negative Loading, IEEE Trans on Antennas and Propagat., Vo. 56, No. 6, pp. 1640-1586, June 2008.



- [74] Werner, D.H.; Ganguly, S, “An overview of fractal antenna engineering research”, *Antennas and Propagation Magazine, IEEE* Volume 45, Issue 1, Pp38 – 57, Feb. 2003.
- [75] J. Kim, C.S. Cho and J.W. Lee “5.2 GHz notched ultra-wideband antenna using slot-type SRR”, *IEE Electron Lett.*vol.42,Pp 42-43, No.6,June 2006.
- [76] D. H. Wemer, R. 1. Haupt, and P. L. Wemer, “Fractal Antenna Engineering: The Theory and Design of Fractal Antenna Arrays *IEEE Antennas and Propagation Magazine*, 41, No.5, pp. 37-59.October 1999.
- [77] J.P. Gianviffwb and Y. Rahmat-Samii, “Fractal antennas: A novel antenna miniaturization technique, and applications”, *Antennas Propagation Magazine* 44 (2002), 20–36.
- [78] C. Puente, J. Romeu, and R. Pous., “Small but long Koch fractal monopole,” *IEE Electron. Lett.*, vol. 34, no. 1, pp. 9–10, 1998.
- [79] Min Ding, Ronghong Jin, Junping Geng, and Qi Wu., “ Design Of A Cpw-Fed Ultrawideband Fractal Antenna”, *Microwave And Optical Technology Letters* , Vol. 49, No. 1, January 2007
- [80] H. A. Ghali and T. A. Moselhy, “Broad-band and circularly polarized space-filling-based slot antenna,” *IEEE Trans. Microw. Theory Tech.*, vol. 53, no. 6, pp. 1946–1950, Jun. 2005.
- [81] C. Puente, J. Romeu, and R. Pous, “On the behavior of the Sierpinski multiband fractal antenna,” *IEEE Trans. Antennas Propag.*, vol. 46, no. 4, pp. 517–524, Apr. 1998.
- [82] K. J. Vinoy, Jose K. Abraham, and Vijay K. Varadan, “On the Relationship Between Fractal Dimension and the Performance of Multi-

- Resonant Dipole Antennas Using Koch Curves” IEEE Trans On Antennas And Propagat., Vol. 51, No. 9, September 2003.pp 2296-2303.
- [83] K.J. Vinoy, K.A. Jose, V.K. Varadan, and V.V. Varadan, “Hilbert curve fractal antenna: A small resonant antenna for VHF/UHF applications,” Microwave and Optical Technology Letters., vol. 29, pp. 2 15-2 19, 2000.
- [84] Long, S.A., Oapos, Connor, E.M., “The History of the Development of the Dielectric Resonator Antenna”, International Conference on Electromagnetics in Advanced Applications, 2007. ICEAA 2007, Issue, 17-21, Pp:872 – 875, Sept. 2007.
- [85] P. W. Tang and P. F. Wahid “Hexagonal Fractal Multiband Antenna”, IEEE Antennas and Wireless Propagation Letters, Vol. 3, 2004.pp.111-112.
- [86] Okaya and I. F. Barash ,, “The Dielectric microwave Resonator”, Proceedings of IRE, Vol. 58, No.6, Pp. 922- 923,June 1970.
- [87] S.A. Long, M.W. McAllister and L.C. Shen,"The Resonant Cylindrical Dielectric Cavity Antenna," IEEE Trans. Antennas Propagat.,vol. AP-31, pp. 406-412, May 1983.
- [88] J. T. H. St. Martin, Y. M. M. Antar, A. A. Kishk, A. Ittipiboon, and M. Cuhaci, "Dielectric resonator antenna using aperture coupling," Electron. Lett., vol. 26, pp. 2015-2016, Nov. 1990.
- [89] G. Drossos, Z. Wu, and L. E. Davis, "Theoretical and experimental investigation of cylindrical dielectric resonator antennas," Microwave and optical technology letters vol. 13, pp. 119-123, Oct. 1996.

- [90] Ittipiboon, R. K. Mongia, Y. M. M. Antar, P. Bhartia, and M. Cuhaci, "Aperture fed rectangular and triangular dielectric resonators for use as magnetic dipole antennas," *Electron. Lett.*, vol. 29, pp. 2001-2002, Nov. 1993.
- [91] Guha, D.; Antar, Y.M.M, " New Half-Hemispherical Dielectric Resonator Antenna for Broadband Monopole-Type Radiation", *IEEE Transactions on Antennas and Propagation*, Volume 54, Issue 12, Pp 3621 – 3628, Dec. 2006 .
- [92] Hans Gregory Schantz ,A brief History of UWB Antennas ,*IEEE A & E systems magazine* Pp 23-26, April 2004
- [93] Wiesbeck, W.; Adamiuk, G.; Sturm, C.; "Basic Properties and Design Principles of UWB Antennas", *Proceedings of the IEEE*, Volume 97, Issue 2, Pp:372 – 385, Feb. 2009
- [94] F. Sabath, E. L. Mokole, and S. N. Samaddar, "Definition and Classification of Ultra-Wideband Signals and Devices", *Radio Science bulletin*, No.313, Pp 12-26, June 2005.
- [95] Commission of the European Communities, B Commission decision on allowing the use of the radio spectrum for equipment using ultra-wideband technology in a harmonised manner in the community, *Official J. Eur. Union*, Feb. 21, 2007
- [96] Yiqong Shi; Aditya, S.; Law, C.L.; "Time Domain Responses of Printed UWB Antennas", *Fifth International Conference on Information, Communications and Signal Processing*, Pp:153 – 156, 2005

- [97] Shlivinski, E. Heyman, and R. Kastner, Antenna characterization in the time domain, *IEEE Trans. Antennas Propag.*, vol. 45, pp. 1140–1149, Jul. 1997.
- [98] Levitas, B, “UWB Time Domain Measurements”, European Conference on Antennas and Propagation ,EuCAP 2007,11-16, Pp:1 – 8,Nov. 2007
- [99] Debalina Ghosh, Arijit De, Sarkar,C. Wicks and Eric L. Mokole “Transmission and Reception by Ultra-Wideband (UWB) Antennas”, *IEEE Antennas and Propagation Magazine*, Vol. 48, No. 5, pp 67-99,October 2006
- [100] Duroc, Y.; Ghiotto, A.; Vuong, T.P.; Tedjini, S, “UWB Antennas: Systems With Transfer Function and Impulse Response”, *IEEE Trans. Antennas Propagat.*, Vol. 55, No. 5, Pp 1449 – 1451,May 2007
- [101] Hood, A.Z.; Karacolak, T.; Topsakal, E, “A Small Antipodal Vivaldi Antenna for Ultrawide-Band Applications,; *Antennas and Wireless Propagation Lett.*, IEEE ,Volume 7, Pp:656 – 660,2008
- [102] Li Ying; Chen Ai-xin; “Design and application of Vivaldi antenna array Antennas”, *Propagation and EM Theory*, 2008. ISAPE 2008. 8th International Symposium Pp:267 – 270, Nov. 2008
- [103] Kiminami, K.; Hirata, A.; Shiozawa, T, “Double-sided printed bow-tie antenna for UWB communications”, *IEEE Antennas and wireless Propagation Lett.*, Vol. 3, No. 1, Pp 152 – 153,2004.
- [104] Ito, Y., Ameya, M.; Yamamoto, M.; Nojima, “Unidirectional uwb array antenna using leaf-shaped bowtie elements and flat reflector”, *IEE Electron Lett.*,Volume 44, Issue 1, Page(s):9 – 11,January 2008

- [105] Naghshvarian-Jahromi, M. “Novel Wideband Planar Fractal Monopole Antenna”, *IEEE Transactions on Antennas and Propagat.*, Volume 56, Issue 12, Pp:3844 – 3849, Dec. 2008
- [106] Karlsson, M.; Shaofang Gong, “An integrated spiral antenna system for UWB”, *Microwave Conference, 2005 European*, Volume 3, 4-6 Oct. 2005.
- [107] Shih-Yuan Chen; Po-Hsiang Wang; Hsu, P, “Uniplanar Log-Periodic Slot Antenna Fed by a CPW for UWB Applications”, *Antennas and Wireless Propagation Lett.*, *IEEE* Volume 5, Issue 1, Pp:256 - 259, Dec. 2006
- [108] J. Dyson, B “The equiangular spiral antenna”, *IEEE Trans. Antennas Propag.*, vol. AP-7 pp. 181–187, Apr. 1959
- [109] Calmon, A.; Pacheco, G.; Terada, M, “A novel reconfigurable UWB log-periodic antenna”, *Antennas and Propagation Society International Symposium 2006, IEEE*, Pp:213 - 216 July 2006
- [110] R. Pantoja, A. Sapienza, and F. M. Filho A microwave printed planar log-periodic dipole array antenna, *IEEE Trans. Antennas Propag* vol. AP-35, pp. 1176–1178, Oct. 1987
- [111] Valderas, D.; Alvarez, R.; Melendez, J.; Gurutzeaga, I.; Legarda, J.; Sancho, J.I.; “UWB Staircase-Profile Printed Monopole Design”, *IEEE Antennas and Wireless Propagation Lett.* Volume 7, Pp:255 - 259, 2008
- [112] D. Schaubert, E. Kollberg, T. Korzeniowski, T. Thungren, J. Johansson, and K. Yngvesson, Endfire tapered slot antennas on dielectric substrates, *IEEE Trans. Antennas Propagat .*, vol. AP-33, pp. 1392–1400, Dec. 1985.

- [113] Yang, G.M.; Jin, R.H.; Xiao, G.B.; Vittoria, C.; Harris, V.G.; Sun, N.X, “Ultrawideband (UWB) Antennas With Multiresonant Split-Ring Loops”,. IEEE Transactions on Antennas and Propagation, Pp 256 – 260, on Volume 57, Issue 1, Jan. 2009
- [114] N. Behdad and K. Sarabandi, A compact antenna for ultrawide-band applications IEEE Trans. Antennas Propag., vol. 53, pp. 2185–2192, Jul. 2005
- [115] Wiesbeck, W.; Adamiuk, G.; Sturm, C, “Basic Properties and Design Principles of UWB Antennas”, Proceedings of the IEEE Volume 97, Issue 2, Pp.372 – 385 Feb. 2009
- [116] C.-C Lin, Y.-C. Kan, L.-C. Kuo, H.-R. Chuang A planar triangular monopole antenna for UWB communication IEEE Microw. Compon. Lett., vol. 15, pp. 624–626 Oct. 2005.
- [117] Jia-Yi Sze; Hsu, C.-I.G.; Jen-Yi Shiu, “Small CPW-Fed Band-Notched Ultrawideband Rectangular Aperture Antenna”, Antennas and Wireless Propagation Lett., IEEE Volume 7, Pp:513 – 516, 2008
- [118] Valderas, D.; Alvarez, R.; Melendez, J.; Gurutzeaga, I.; Legarda, J.; Sancho, J.I, “UWB Staircase-Profile Printed Monopole Design” Antennas and Wireless Propagation Lett., IEEE Volume 7,Pp 255 – 259, 2008.
- [119] Qing-Xin Chu; Ying-Ying Yang, “A Compact Ultrawideband Antenna With 3.4/5.5 GHz Dual Band-Notched Characteristics” IEEE Trans on Antennas and Propagat., Volume 56, Issue 12, Dec. 2008 Page(s):3637 – 3644

- [120] Marchais, C.; Le Ray, G.; Sharaiha, A.; “Stripline Slot Antenna for UWB Communications”, *IEEE Antennas and Wireless Propagation Lett.*, Volume 5, Issue 1, Pp:319 – 322, Dec. 2006
- [121] A. M. Abbosh “Miniaturized Microstrip fed tapered slot antenna with ultrawideband performance”, *IEEE. Antenna Wirel.Propag.Lett.*,2009, 8,pp.690-692
- [122] Gopikrishna, M.; Krishna, D.D.; Aanandan, C.K.; Mohanan, P.; Vasudevan, K, Compact linear tapered slot antenna for UWB applications, *IEE Electron Lett.*, Volume 44, Issue 20, Pp 1174 – 1175, September 2008
- [123] Shameena.V.A, Suma M.N, Rohith.K.Raj, Bybi P.C and P Mohanan “Compact Ultra wide Band Planar Serrated Antenna with Notch band ON/OFF Control” *IEE Electron Letters*. Volume 42, Issue 23, Pp : 1323 – 1324, November 2006
- [124] Chow-Yen-Desmond Sim, Wen-Tsan Chung, Ching-Her Lee, “ A circular-disc monopole antenna with band-rejection function for ultrawideband application”, *Microwave and Optical Technology Letters*, Volume 51, Issue 6, Date:, Pp: 1607-1613, June 2009
- [125] J. Y siddiqui, Y. M. M.Anthar, E.C.Smith ”Design of an ultrawideband antipodal tapered slot antenna using elliptical strip conductors” *IEEE.Antenna Wirel.Propag.Lett.*,2011,10,pp.251-254
- [126] A. Z. Hood, T. Karacolak “A small antipodal Vivaldi Antenna for ultrawideband applications” *IEEE Antenna Wirel.Propag.Lett.*,2008, 7,pp.656-660

- [127] C. R. Mederios, Jorge R Costa “Compact tapered slot UWB antenna with WLAN band rejection”, *IEEE. Antenna Wirel.Propag.Lett.*, 2009, 8,pp.661-664
- [128] T. Ghuang Ma and S Kang Jeng “A printed dipole antenna with tapered slot feed for ultra wideband application” *IEEE Trans.Antennas Propag.*, vol. 53.no.11, pp.3833–3836.Nov. 2005.
- [129] S. Nikolaou, George E. P “Conformal double exponentially tapered slot antenna on lcp for UWB applications”*IEEE Trans. Antennas Propag.*, vol.54, no.6, pp.1663-1669,JUNE.2006.
- [130] Jantunen H, Rautioaho R, Uusimäki A & Leppävuori S, “ Preparing low loss LTCC material without glass addition”, *Journal of American Ceramic Society*, Vol. 83, No. 11, (2000), pp. 2855-2857.
- [131] X. Chen, J. Liang, S. Wang, Z. Wang and C. Parini “Small ultra wideband antennas for medical imaging” 2008 Loughborough Antennas & Propagation Conference, Loughborough, UK
- [132] Gautier, W.; Schoenlinner, B.; Ziegler, V.; Prechtel, U.; Menzel, W, “LTCC Patch Array for RF-MEMS based Phased Array Antenna at 35GHz”, 38th European Microwave Conference,. 27-31, Pp:151 – 154, Oct. 2008
- [133] Brzezina, G.; Roy, L.; MacEachern, L, “Planar antennas in LTCC technology with transceiver integration capability for ultra-wideband applications” *IEEE Trans. on Microwave Theory and Tech*, Volume 54, Issue 6, Part 2, Pp:2830 - 2839June 2006
- [134] RongLin Li; DeJean, G.; Moonkyun Maeng; Kyutae Lim; Pinel, S.; Tentzeris, M.M.; Laskar, J , “Design of compact stacked-patch antennas



- in LTCC multilayer packaging modules for wireless application”; IEEE Transactions on Advanced Packaging, Volume 27, Issue 4, Page(s):581 – 589,Nov. 2004
- [135] Son Xuat Ta; Byoungchul Kim; Hosung Choo; Ikmo Park; “Slot-line-fed quasi-Yagi antenna “ Antennas Propagation and EM Theory ISAPE, 2010 9th International Symposium on Digital Object Identifier: 10.1109/ISAPE.2010.5696461 Publication Year: 2010 , Page(s): 307 - 310
- [136] V. Deepu, S. Mridula, R. Sujith and P. Mohanan. “Slot line FED dipole antenna for wide band applications”Microwave and Optical Technology Letters Volume 51, Issue 3, March 2009, Pages: 826–830.
- [137] V. Deepu, K.R. Rohith, J. Manoj, M.N. Suma, K. Vasudevan, C.K. Aanandan, and P. Mohanan, Compact uniplanar antenna for WLAN applications, IEE Electron Lett 43 (2007).



## Chapter 2

# DESIGN, FABRICATION AND MEASUREMENT TECHNIQUES OF ANTENNAS



*The chapter deals with the techniques used for the design, fabrication and measurement of antennas. The design and simulations are performed using the FEM based Ansoft High Frequency Structure Simulator (HFSS). The antennas are fabricated using photolithographic method. Vector Network Analyzer HP8510C and Agilent Performance Network Analyzer 8362B are used for the measurement of antenna characteristics such as Return loss, Radiation pattern, Gain, Efficiency etc. Various methods and measurements specially used for the analysis of the performance of wide band antennas are also discussed at the end of this chapter.*

### 2.1 Techniques for the Design and Optimization of Antennas

The design and optimization studies of the antennas presented in this thesis are performed using the commercial software Ansoft High Frequency Structure Simulator (HFSS). HFSS is a high-performance full-wave electromagnetic (EM) field simulator for arbitrary 3D volumetric device modeling and analysis.

### **2.1.1 High Frequency Structure Simulator (HFSS)**

Ansoft HFSS utilizes the 3D full-wave Finite Element Method (FEM) with adaptive meshing to compute the electrical behavior of high-frequency and high-speed components[1]. The basic mesh element is a tetrahedron. This allows solving any arbitrary 3D geometry, especially those with complex curves and shapes, in minimum time. Ansoft HFSS can be used to calculate antenna parameters such as S Parameters, radiation pattern, gain, current distributions, fields, efficiency etc. HFSS integrates simulation, modeling, visualization and automation in a user friendly environment. With adaptive meshing and brilliant graphics HFSS gives an unparalleled performance and complete insight to the actual radiation phenomenon in the antenna. With HFSS one can extract the parameters such as Scattering ( $S_{11}$ ,  $S_{12}$ ,  $S_{21}$  and  $S_{22}$ ) , admittance ( $Y_{11}$ ,  $Y_{12}$ ,  $Y_{21}$  and  $Y_{22}$ ) and impedance ( $Z_{11}$ ,  $Z_{12}$ ,  $Z_{21}$  and  $Z_{22}$ ), visualize 3D electromagnetic fields (near-field and far-field), and optimize design performance. An important and useful feature of this simulation engine is the availability of different kinds of port schemes. It provides lumped port, wave port, incident wave scheme etc. The accurate simulation of coplanar and microstrip lines can be done using the port schemes. The parametric set up available with HFSS is highly suitable for an antenna engineer to optimize the desired dimensions.

The first step in simulating a structure in HFSS is to define the geometry of the structure by giving the material properties and boundaries for 3D or 2D elements available in HFSS window. The next step is to draw the intended architecture using the drawing tools available in the software. The designed structure is excited using the suitable port excitation schemes. The next step is the assigning of boundary scheme. A radiation boundary filled with air or

vacuum is commonly used for radiating structures. It is important that the size of air column is taken to be equal to a quarter of the free space wavelength of the lowest frequency of operation otherwise there may be chances of mismatch between simulated and experimental results. Now, the simulation engine can be invoked by giving the proper frequency of operation and the number of frequency points. Finally the simulation results such as scattering parameters, current distributions and far field radiation pattern can be displayed. The vector as well as scalar representation of E, H and J values of the device under simulation gives a good insight into the various parameters of the structure under analysis.

As mentioned above HFSS make use of the FEM technique for the calculation of different parameters. The Finite Element Method is well-established and widely used for the time-harmonic solution of Maxwell's equations. The unstructured nature of the time domain version of FEM gives a clear advantage over numerical computational methods in modeling complex antenna geometries. The main concept of the finite element method is based on subdividing the geometrical domain of a boundary-value problem into smaller sub-domains, called finite elements, and expressing the governing differential equation along with the associated boundary conditions as a set of linear equations that can be solved computationally using linear algebra techniques.

FEM has enjoyed a strong interest for electromagnetic analysis. In fact, over the past 10 years, the greatest progress in computational electromagnetics is based on the development and application of partial differential equation (PDE) methods such as the finite difference-time domain (FDTD), finite element (FEM) and methods including hybridizations of these with integral equations and high frequency techniques. The major reasons for the increasing reliance on PDE

methods stem from their inherent geometrical adaptability, low memory demand and their capability to model heterogeneous (isotropic or anisotropic) geometries. These attributes are essential in developing general-purpose codes for electromagnetic analysis/design, including antennas and their characterization.

FEM is a mature method and is the workhorse of standard analysis and design packages in Mechanical Engineering and Applied Mechanics. In this approach Resistive/material and impedance boundary conditions are readily implemented in a modular fashion. Established hybridizations of the FEM with moment methods and ray methods provide an added advantage by delivering the most adaptable and efficient code when compared to other approaches [2].

The main idea behind the FEM [3,4] is to solve Boundary Value Problems (BVP)s governed by a differential equation and a set of boundary conditions. The representation of the domain is split into smaller sub-domains called the finite elements. The distribution of the primary unknown quantity inside an element is interpolated based on the values at the nodes, provided nodal elements are used, or the values at the edges, in case vector elements are used. The interpolation or shape functions must be a complete set of polynomials.

The accuracy of the solution depends, among other factors, on the order of these polynomials, which may be linear, quadratic, or higher order. The numerical solution corresponds to the values of the primary unknown quantity at the nodes or the edges of the discretized domain. The solution is obtained after solving a system of linear equations. To form such a linear system of equations, the governing differential equation and associated boundary conditions must first be converted to an integro-differential formulation either by minimizing a functional or using a weighted residual method such as the

Galerkin approach. This integro-differential formulation is applied to a single element and with the use of proper weight and interpolation functions the respective element equations are obtained. The assembly of all elements results in a global matrix system that represents the entire domain of the BVP.

There are two methods that are widely used to obtain the finite element equations: the variational method and the weighted-residual method.

The variational approach requires construction of a functional which represents the energy associated with the BVP at hand. A functional is a function expressed in an integral form and has arguments that are functions themselves. Many engineers and scientists refer to a functional as being a function of functions. A stable or stationary solution to a BVP can be obtained by minimizing or maximizing the governing functional. Such a solution corresponds to either a minimum point, a maximum point, or a saddle point. In the vicinity of such a point, the numerical solution is stable (insensitive to small variations of dependent parameters). This translates to a smaller numerical error compared to a solution that corresponds to any other point.

The second method is a weighted-residual method widely known as the Galerkin method. This method begins by forming a residual directly from the partial differential equation that is associated with the BVP under study. Simply stated, this method does not require the use of a functional. The residual is formed by transferring all terms of the partial differential equation on one side. This residual is then multiplied by a weight function and integrated over the domain of a single element. This is the reason why the method is termed as weighted-residual method. The Galerkin approach is simple and starts directly from the governing differential equation.

## **2.2 Antenna fabrication**

The antennas studied in the thesis are fabricated using the photolithographic technique. This is a chemical etching process by which the unwanted metal regions of the metallic layer on the substrate are removed so that the intended design is obtained. Depending upon the design of the antenna as biplanar or uniplanar, dual or single side substrates is used. The selection of a proper substrate material is an important part in antenna design.

### **2.2.1 Characteristics of substrate materials**

Recent developments in the microelectronic industry demand high performance microwave materials for substrate and packaging applications. Materials for such applications should have low relative permittivity and low dielectric loss to reduce the propagation delay and to increase the speed of the signal. In addition to these properties, the materials should have high thermal conductivity for dissipating heat. Other important substrate characteristics include the thickness, isotropicity, homogeneity, and dimensional strength of the substrate [5 - 9].

The selection of dielectric constant of the substrate depends on the application of the antenna and the required radiation characteristics. High dielectric constant substrates will result in surface wave excitation and low bandwidth performance. Also as the frequency of operation increases, the loss tangent of the material used for substrates slightly increases, which in turn adversely affects the efficiency of the antenna. Also increasing the thickness of the substrate increases the band width of the antennas at the expense of efficiency owing to increase in surface waves.



Various methods have been already established to accurately measure the dielectric properties of substrates[10 -11].

The microwave dielectric properties of the sample were measured by the cavity perturbation technique using a vector Network Analyzer. This technique is widely used for the determination of the dielectric characteristics of thin samples of low and medium dielectric loss.

A rectangular S-band or X-band slotted wave-guide cavity with optimum iris coupling is used for the measurement of dielectric properties of the samples. The resonant frequency and quality factor of the empty cavity were determined for different cavity modes. Then the extremely thin sample having known dimensions is inserted and positioned at the E-field antinode in the cavity. The new resonant frequency and Q of the sample were again measured. The complex dielectric constant of the sample was calculated using the following equations.

$$\epsilon_r' = 1 + \left( \frac{V_c (f_0 - f_s)}{2V_s f_s} \right)$$

$$\epsilon_r'' = \frac{V_c (Q_0 - Q_s)}{4V_s Q_0 C_s}$$

$$\tan \delta = \frac{\epsilon_r''}{\epsilon_r'}$$

where  $f_0$  = resonant frequency of the cavity

$f_s$  = resonant frequency of the samples

$V_c$  = Volume of the cavity

$V_s$  = Volume of the sample

$Q_0$  = Quality factor of the empty cavity

$Q_s$  = Quality factor of the sample loaded cavity

### **2.2.2 Photo Lithography**

After the proper selection of the substrate material, a computer aided design of the geometry is initially made and a negative mask of the geometry to be generated is printed on a transparent or semi transparent sheet. A single or double sided substrate with copper metallization of suitable dimension is properly cleaned using acetone to free from impurities and tarnish.

A thin layer of negative photo resist solution (1:1 mix of negative photoresist solution and thinner) is coated over the substrate using spinning technique and is dried. The mask is placed above the photo resist and exposed to UV light. After the proper UV exposure, the substrate is dipped in developer to harden the photoresist in the exposed portion and to remove the photoresist in masked portions.

The sample is then dipped in dye ink solution in order to clearly view the hardened photo resist portions on the copper coating. The board is then washed in water. After developing phase the unwanted copper portions are etched off using Ferric Chloride ( $\text{FeCl}_3$ ) solution to get the required antenna geometry on the substrate. The etched board is rinsed in running water to remove any etchant.  $\text{FeCl}_3$  dissolves all the copper parts except underneath the hardened photo resist layer after few minutes. The laminate is then cleaned carefully to remove the hardened photo resist using acetone solution. The various steps involved in the fabrication process are illustrated in Fig.2.1

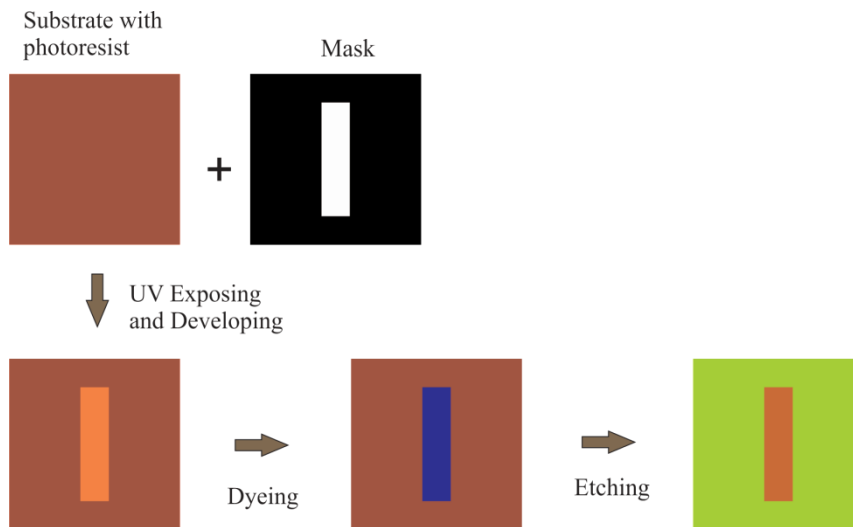


Fig.2.1 Photolithographic technique for antenna fabrication

## 2.3 Antenna Measurement Facilities

An overview of the equipments and facilities used for extracting the antenna reflection and radiation characteristics is presented in this section with details of the measurement procedure. The measurement of radiation characteristics of the antennas were carried out using Network analyzers HP 8510C VNA and Agilent 8362B PNA.

### 2.3.1 HP 8510C Vector Network analyzer (VNA)

HP8510C is sophisticated equipment capable of making rapid and accurate measurements in both frequency and time domain [12]. The NWA can measure the magnitude and phase of the Scattering parameters. The NWA system is based on the 32 bit microcontroller MC68000 and capable of measuring two port network parameters such as  $S_{11}$ ,  $S_{12}$ ,  $S_{22}$ ,  $S_{21}$  and it's built in signal processor analyses the transmit and receive data and displays the results in many plot formats. The NWA consists of a source, S parameter test set, a signal processor and a display unit. The synthesized sweep generator *HP*

83651B uses an open loop YIG tuned element to generate the RF stimulus. It can synthesize a wide range of frequencies from 10 MHz to 50 GHz. The frequencies can be set in step mode or ramp mode depending on the required measurement accuracy. The antenna under test is connected to the two port S parameter test set unit, HP8514B and incident and reflected wave at the port are then down converted to an intermediate frequency (IF) of 20MHz and fed to the detector. These signals are suitably processed to display the magnitude and phase information in the required format. These constituent modules are interconnected through HPIB system bus. An in-house developed MATLAB based data acquisition system coordinates the measurements and saves the data in the CSV format. Schematic diagram of HP8510C NWA and setup for reflection and transmission characteristic measurement is shown in Fig.2.2

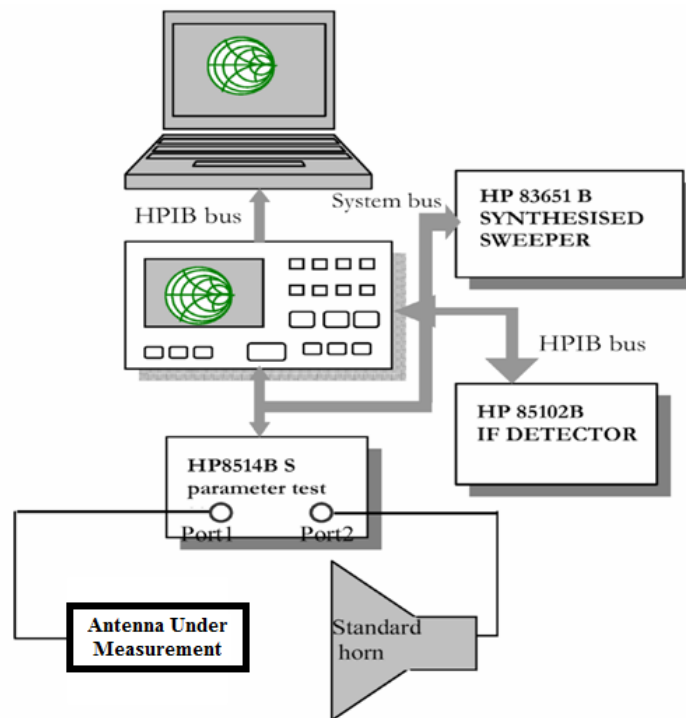


**Fig.2.2** Setup for measuring reflection and transmission characteristic using HP 8510C VNA

The Antenna characteristics such as return loss, radiation pattern and gain are measured using the HP8510C and associated setup. The indigenously developed CREMA SOFT is used for the automatic measurement of the radiation properties using HP 8510C Network analyzer. The important systems used for the antenna characterization are Vector network Analyzer, Anechoic Chamber, Automated turn table etc.

The antenna under test (AUT) is connected to the port of the S-parameter test set HP8514B and the forward and reflected power at the measurement point is separated and down converted to 20MHz using frequency down converter. It is again down converted to lower frequency and processed in the HP8510C processing unit. All the systems discussed above are interconnected using GPIB bus. A computer interfaced to the system is used for coordinating the whole operation remotely. Measurement data can be saved on a storage medium.

### **2.3.2E8362B Programmable Network Analyzer (PNA)**

The Agilent E8362B Vector Network Analyzer is a member of the PNA Series Network Analyzer platform and provides the combination of speed and precision for high frequency measurements [13]. The operation range is from 10 MHz to 20 GHz. For antenna measurements it provides exceptional results with more points and faster measurement speed. It has 16,001 points per channel with  $< 26 \mu\text{sec/point}$  measurement speed and 32 independent measurement channels. Windows operating system and user interface input device (mouse) makes measurement procedure much easier. Embedded help system with full manual, extensive measurement tutorials, and complete programming guide helps to carry out accurate measurement of antenna characteristics using this.

### **2.3.3 Anechoic Chamber**

The anechoic chamber provides a quiet zone, free from all types of EM distortions for antenna measurements. All the antenna characterizations are done in an Anechoic chamber to avoid reflections from nearby objects.

It is a very big room consisting of microwave absorbers fixed on the walls, roof and the floor to avoid the electromagnetic energy reflections. A photograph of the anechoic chamber associated with our laboratory is shown in Fig. 2.3 below.

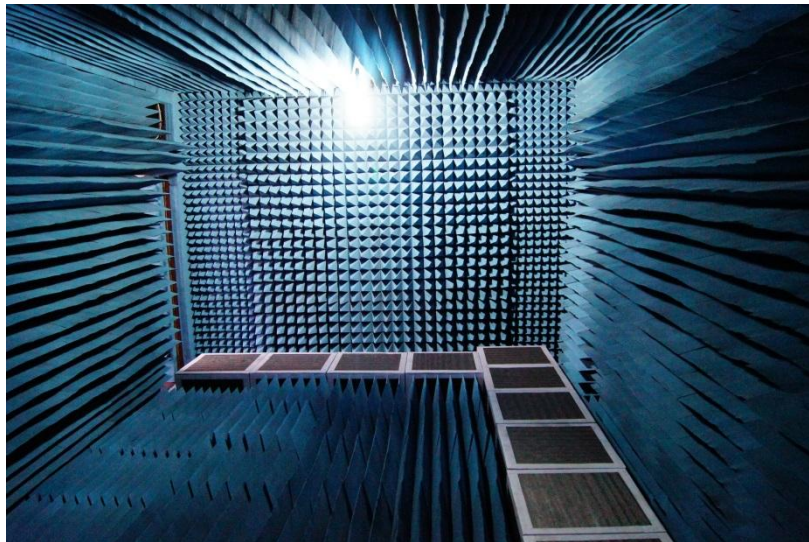


**Fig.2.3** Photograph of the anechoic chamber used for the antenna measurements

The absorbers fixed on the walls are highly lossy at microwave frequencies. They have tapered pyramidal shapes to achieve good absorption for the microwave power incident on it. The chamber is made free from the surrounding EM interferences by covering all the walls and the roof with an aluminium sheet.

### **2.3.4 Turn table assembly for far field radiation pattern measurement**

The turn table assembly consists of a stepper motor driven rotating platform for mounting the Antenna Under Test (AUT). The in-house developed microcontroller based antenna positioner STIC 310C is used for radiation pattern measurement. The beam maxima tracking for gain measurement and radiation pattern measurement is done using this setup. A standard wideband horn (1-18GHz) is used as receiving antenna for radiation pattern measurements. The in-house developed automation software '*Crema Soft*' (Developed at the Centre for Research in Electromagnetics and Antennas, CUSAT ,INDIA ) coordinates all the measurements.

## **2.4 Experiments**

The experimental procedures followed to determine the antenna characteristics are discussed in the following sections. Power is fed to the antenna from the S parameter test set of the analyzer through cables and connectors. The connectors and cables tend to be lossy at higher microwave bands. Hence the instrument should be calibrated with known standards of open, short and matched loads to get accurate scattering parameters. There are many calibration procedures available in the network analyzer. Single port and full two port calibration methods are usually used. Return loss, VSWR and input impedance can be characterized using single port calibration method.

The fabricated antennas are tested to study the various characteristics. Since all the antennas have very compact dimensions of the order of a quarter of the wavelength various factors have to be considered for efficient and accurate measurements.

Ideally, antennas would be measured without any perturbation from measurement cables and connectors. However for cost and speed reasons, most handset and WLAN antennas are measured using a coaxial cable to connect the antenna under test (AUT) to the transceiver. This feed cable couples to the currents on the AUT and can affect both the antenna match and also the radiation performance. Various techniques have been reported in literature to nullify this effect. A new method of suppressing spurious measurement cable currents has been developed in [14]. This relies on computer simulation to predict the low electric field regions where the measurement cable can be safely attached, and upon comparison between simulation and measurement results the measurement cable spurious surface currents can be accounted. Another common practice is the use of ferrite beads and quarter wave sleeve balm (“bazookas”) to be used to suppress the current on the feed cable. But even with all these methods the effects cannot be completely negated [15].

#### **2.4.1 Return loss, Resonant frequency and Bandwidth**

The calibration of the port is done for the frequency range of interest using the standard open, short and matched load. The calibrated instrument including the port cable is now connected to the device under test. The return loss characteristic of the antenna is obtained by connecting the antenna to any one of the network analyzer port and operating the VNA in  $s_{11}/s_{22}$  mode. The frequency vs reflection parameter ( $s_{11}/s_{22}$ ) is then stored on a computer using the ‘Crema Soft’ automation software.

The frequency for which the return loss value is the minimum is taken as resonant frequency of the antenna. The range of frequencies for which the return loss value is within the -10dB points is usually treated as the bandwidth of the antenna. The -10 dB points corresponding to the frequency at which 90 % of the fed power is transmitted and only 10 % power reflected back.



The antenna bandwidth is usually expressed as percentage of bandwidth, which is defined as

$$\% \text{Bandwidth} = \frac{f_2 - f_1}{f_c} \times 100$$

Where  $f_2$  denotes the higher -10 dB point,  $f_1$  the lower -10 dB point and  $f_c$  the centre frequency having the minimum return loss value. At -10dB points the VSWR is  $\sim 2$ . The above bandwidth is sometimes referred to as 2:1 VSWR bandwidth.

### **2.4.2 Radiation pattern measurement**

The measurement of far field radiation pattern is conducted in an anechoic chamber. The AUT is placed in the quiet zone of the chamber on a turn table and connected to one port of the network analyzer. The network analyzer is kept to measure transmission coefficient mode with the frequency range within the -10dB return loss bandwidth. The number of frequency points is set according to convenience. The start angle, stop angle and step angle of the motor is also configured with the help of '*Crema Soft*'. The antenna positioner is bore sighted manually. Now the THRU calibration is performed for the frequency band specified and saved in the CAL set. Suitable gate parameters are provided in the time domain to avoid spurious radiations if any. The *Crema Soft* automatically performs the radiation pattern measurement and stores it as a CSV file. This is used to plot the 2-D radiation pattern at the required frequency.

### **2.4.3 Antenna Gain**

The gain of the antenna under test is measured in the bore sight direction. The gain transfer method using a standard gain antenna is employed to determine

the absolute gain of the AUT [16-18]. The experimental setup is similar to the radiation pattern measurement setup. An antenna with known gain is first placed in the antenna positioner and the THRU calibration is done for the frequency range of interest. Standard antenna is then replaced by the AUT and the change in  $S_{21}$  is noted. Note that the AUT should be aligned so that the gain in the main beam direction is measured. This is the relative gain of the antenna with respect to the reference antenna. The absolute gain of the antenna is obtained by adding this relative gain to the original gain of the standard antenna.

#### 2.4.4 Radiation Efficiency

One of the main figures of merit of an antenna is its radiation efficiency. It is very important to know about how effectively or efficiently a radiator will radiate electromagnetic energy which is fed into it. Here this session will explain a technique to measure the radiation efficiency of an antenna.

Conventional antenna radiation efficiency measurement technique is Wheeler cap method and are well suited for resonant antennas [19,20]. In this method we requires only two input resistance of the antenna in two different conditions, one with a conducting cap enclosing the antenna and one without the conducting cap. For the Wheeler cap, a conducting cylindrical cavity is used whose radius is radian sphere of the antenna and which completely encloses the test antenna. Input impedance of the test antenna is measured with and without the cap using E8362B PNA. The efficiency is calculated by the following expression:

$$\text{Efficiency, } \eta = \frac{R_{no\_cap} - R_{cap}}{R_{no\_cap}}$$

Where,  $R_{no\_cap}$  denotes the input resistance without the cap and  $R_{cap}$  the resistance with the cap.

The above cited method is well suited for narrow band applications and this thesis also deals with wideband antenna an alternate Wheeler cap method to measure the efficiency of wideband and UWB antennas. This method is a modification of the Wheeler Cap method which is already discussed [21]. Rather than inhibiting radiation efficiency from the antenna to a radiation sphere with radius  $r = \lambda/2\pi$  as in the narrow band approach, UWB Wheeler Cap method allows the antenna to radiate freely and then receive its own transmitted power reflected signal from a metallic boundary.

The power budget for a transmit antenna may be expressed in terms of three power fractions. They are dissipation losses ( $l = P_{\text{loss}}/P_{\text{in}}$ ), reflection losses due to mismatch ( $m = P_{\text{refl}}/P_{\text{in}}$ ), and a radiation fraction ( $\eta = P_{\text{rad}}/P_{\text{in}}$ ). According to conservation of energy,

$$l + m + \eta = 1$$

In this method, we use a spherical shell surrounding the AUT which enforces approximately near ideal time reversal of the transmitted signal. Thus the antenna receives the reflected signal with negligible structural scattering, and the antenna mode scattering term will be the mismatch fraction ( $m = |S_{11} - F_s|^2$ ). The receive efficiency and transmit efficiency ( $\eta$ ) are identical by reciprocity. The scattering coefficient inside the spherical shell becomes:

$$\begin{aligned} |S_{11} - F_s|^2 &= m + \eta^2 + \eta^2 m^2 + \eta^2 m^2 + \eta^2 m^2 \dots\dots\dots \\ &= |S_{11} - F_s|^2 + \eta^2 \sum_{n=0} |S_{11} - F_s|^{2n} \\ &= |S_{11} - F_s|^2 + \eta^2 \frac{1}{1 - |S_{11} - F_s|^2} \end{aligned}$$

$$\eta = \sqrt{(1 - |S_{11} - F_s|^2) \left( (|S_{11} - W_c|^2) - |S_{11} - F_s|^2 \right)}$$

For measurements, an oblate metallic chamber with diameter 70cm is used. First, the AUT is placed in free space and the return loss  $S_{11}-F_s$  is measured. It is then placed at the center of the closed metallic chamber and the  $S_{11}-W_c$  is measured. Finally, the above given equation is employed to calculate the radiation efficiency.

## **2.5 Models/Techniques used in the analysis of antennas**

Different methods are available in the literature for the analysis of antennas. For antennas having different geometrical shapes, analytical techniques like cavity model and transmission line model can be applied. For geometries which can be readily divided into few regular geometrical shapes, these analytical techniques could be applied along with segmentation technique. These techniques are suitable in the case of arbitrary shaped patches. Here numerical techniques like Finite Element Method (FEM), Finite Difference Time Domain method (FDTD), etc., could be used. Some important techniques used for the analysis of antennas are described briefly in the following sections.

### **2.5.1 Transmission line model**

This model was proposed by Munson [22] and Derneryd [23]. Here the microstrip resonator is represented by two radiating slots (corresponding to the two radiating edges) separated and connected by an approximately half wavelength ideal transmission line. The input impedance is determined as a function of the distance from the edge of the patch to the feed point. The different radiation characteristics are determined by assuming that the fields vary along the length of the patch and remain constant across the width. The main shortcoming of this model is that, it is applicable only to rectangular or square patch geometries.

### **2.5.2 Cavity model**

Here, the microstrip geometry is considered as a cavity bounded by electric wall at its top and bottom by magnetic walls on its side. The magnetic current flowing on the cavity side walls radiate at the resonant frequencies of the cavity, which is assumed to be surrounded by free space. This model is suitable for geometries in which the Helmholtz equation possesses an analytical solution such as disks, rectangles, triangles, ellipses etc.

### **2.5.3 Finite element method (FEM)**

The finite element method is also an important computer aided mathematical technique for obtaining approximate numerical solutions for the abstract equations of calculus that predicts the response of physical systems subjected to external influences such as electric and magnetic fields. In the case of antennas, the fields associated to the antenna can be determined by this method. Here the region of which the field to be calculated is subdivided into small areas or volumes depending upon the dimensions of the region. Usually these small regions are polygons such as triangles and rectangles for two dimensional problems and tetrahedral elements for three dimensional problems. The interior electric field, satisfying the inhomogeneous wave equation along with an impedance boundary condition on the perimeter walls, is solved for each of the elements subdividing the region of interest. This method is applicable to arbitrary shaped patches also.

### **2.5.4 Method of moments**

Method of Moments (MoM) is an important numerical method used in antenna analysis. In method of moments, the electric surface currents flowing over the metallization planes are evaluated by using the Richmond's reaction

method [24]. The reaction integral equation is solved using the boundary conditions and method of moments. Now using suitable expansion functions for electric surface currents, the integral equations are reduced to algebraic equations. These equations are then solved for the unknown coefficients using any of the known numerical techniques. This technique is analytically simple and versatile, but it requires large amounts of computation. The limitation of this technique is usually the speed and storage capacity of the computer.

### **2.5.5 Finite Difference Time Domain (FDTD) method**

This is a method which can be applied to all kinds of antennas for all types of feeds [25]. This method consists of a discretisation and a solution of the Maxwell's curl equations directly in the time domain. In FDTD, antennas are treated in the time domain for the analysis. The frequency dependence of the different parameters is determined from the Fourier transform of the transient current. However, this method becomes computationally costly and requires large amounts of memory when the structure becomes complex. The calculations used here are time consuming also. FDTD technique is used in this thesis to analyze the performance of the antenna. Detailed discussion on FDTD is included as appendix-2.

### **2.6 Wide band Antenna Characteristics Analysis (Time Domain Analysis)**

Since the thesis also handle with wide band and ultra wide band antennas, it is necessary to analyze various wide band antenna characteristics in time domain. Wide Band and UWB systems employs short pulses to deliver information the bandwidth is occupied is very large. Thus the ability of the antenna on preserving transmitted signal shape is a vital issue. Ideally, the

received UWB signal should maintain exactly the same shape as the source pulse. Practically, the signal waveforms reaching the receiver usually do not resemble the input pulse at the transmitter. The received signals normally are distorted in shape and sometimes present a long tail termed the “ringing effect”. The antenna, therefore, should be carefully designed to avoid unwanted distortions and a time domain study of UWB and wideband antennas is unavoidable.

### 2.6.1 Description of UWB Antenna System

Consider a typical transmitting / receiving antenna system in UWB radio systems [26], as shown in figure 2.2.

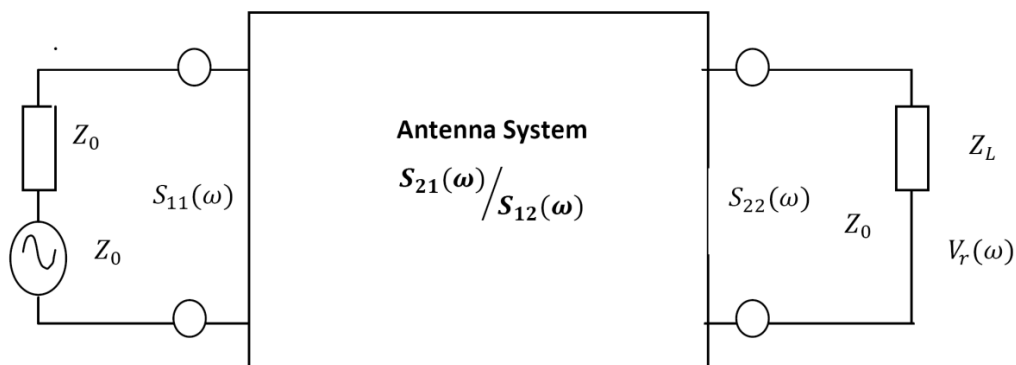


Fig. 2.4 Schematic diagram of UWB antenna system

The Friis transmission equation relates the received power to the transmitted power between two antennas [26], are given in equation 2.6.1.

$$\frac{P_r}{P_t} = (1 - |\tau_t|^2)(1 - |\tau_r|^2) G_r G_t |P_t^{\wedge} P_r^{\wedge}|^2 \left( \frac{\lambda}{4\pi d} \right)^2 |P_t^{\wedge} P_r^{\wedge}|^2 \quad (2.6.1)$$

where  $P_t$  and  $P_r$  are the time average input power of the transmitting antenna and time average output power of the receiving antenna respectively.  $G_t$  and  $G_r$  are the

gains of the transmitting and the receiving antenna respectively,  $\lambda$  is the operating wavelength and  $d$  is the distance between the two antennas.

Normally a wideband system operates over a range of frequency and all of the parameters in equation 2.6.1 are frequency-dependent. Then the formula can be rewritten as follows

$$\frac{P_r(\omega)}{P_t(\omega)} = (1 - |\tau_t(\omega)|^2)(1 - |\tau_r(\omega)|^2) G_t(\omega) G_r(\omega) |P_t(\omega) P_r(\omega)|^2 \left( \frac{\lambda}{4\pi d} \right)^2 \quad (2.6.2)$$

For reflection and polarization matched antennas aligned for maximum directional radiation and reception, equation 2.6.2 reduces to:

$$\frac{P_r(\omega)}{P_t(\omega)} = \left( \frac{\lambda}{4\pi d} \right)^2 G_r(\omega) G_t(\omega) \quad (2.6.3)$$

The transfer function of the system  $S_{21}$ , is defined to describe the relation between the input and the output signal. According to Fig. 2.4

$$\frac{V_t^2(\omega)}{2} = P_t(\omega) Z_0$$

$$\frac{V_r^2(\omega)}{2} = P_r(\omega) Z_0$$

Then  $S_{21}$  can be written as

$$\begin{aligned} S_{21}(\omega) &= \frac{V_r(\omega)}{V_t(\omega)} = \sqrt{\frac{P_r(\omega) Z_L}{P_t(\omega) 4Z_L}} e^{-j\varphi(\omega)} \\ &= |S_{21}(\omega)| e^{-j\varphi(\omega)} \\ \varphi(\omega) &= \varphi_t(\omega) + \varphi_r(\omega) + \frac{\omega d}{c} \end{aligned} \quad (2.6.4)$$



Where  $c$  is the velocity of light,  $\varphi_t(\omega)$  and  $\varphi_r(\omega)$  are the phase variation related to the transmitting and receiving antenna respectively.

It is evident from equation 2.6.2 and equation 2.6.4 that the transfer function is determined by the characteristics of both transmitting and receiving antennas, such as impedance match, gain, polarization match and the spacing between the two antennas.  $S_{21}$  also integrates all of the important system performance, such as path loss and phase delay. Thus, it can be used to assess the behavior of antenna systems.

### **2.6.2 Group Delay**

Group delay is defined as the negative derivative of the signal phase with respect to frequency. When a signal passes through a device or medium, it experiences both amplitude and phase distortion. The amount of distortion depends on the characteristics of the device/medium. A waveform incident at the input of a device may have several frequency components. The group delay gives a measure of average time delay of input signal at each frequency OR it gives a measure of the dispersive nature of the device.

Mathematically, the device response and group delay are given by:

$$H(f) = A(\omega)e^{j\theta(\omega)} \quad (2.6.5)$$

and

$$\tau_g = \frac{-d\theta(\omega)}{d(\omega)}$$

If the device has a non-linear phase response, the group delay will vary with frequency ie. the input signal will have different delays at different frequencies. As a result, the output waveform will be distorted. For a filter to be

linear phase (have constant group delay), its phase response must satisfy one of the following relationships:

$$\theta(\omega) = -\alpha\omega \text{ OR } \theta(\omega) = \beta - \alpha\omega. \quad (2.6.6)$$

From [28] it is clear that to satisfy either one of the above conditions of linear phase, the impulse response of an FIR filter must have positive or negative symmetry. The antenna can be viewed as a band pass filter with some magnitude and phase response. By representing the Rx/Tx antenna system as a filter, we can determine its phase linearity within the required frequency band by analysis of its group delay. The phase response and group delay are related to the antenna magnitude (gain) response.

The group delay plot is very efficient to analyze any nonlinearity that is present in the phase. The pulse input to the antenna system has an extremely large bandwidth and hence, any variation in group delay across the pass band of the transmitted pulse is likely to distort the pulse. To characterize the antenna, the peak to- peak variations of the gain and group delay within the 10dB bandwidth of the input pulse is determined.

For this the two antennas are oriented in two extreme cases. They are face to face and side by side and their corresponding group delays are determined.

### **2.6.3 Choice of Source Pulse**

For the time domain analysis it is very important to select a narrow pulse which contains all the spectral components of the required band. If the pulse width is very narrow, typically in nanoseconds, which will satisfies the spectral mask regulatory requirements. Several non-damped waveforms have been proposed in the literature for UWB systems, such as Gaussian pulse, Rayleigh pulse, Laplacian pulse, cubic and modified Hermitian monocycles.

In all these waveforms, the main goals are nearly flat frequency domain spectrum over the bandwidth of the pulse and absence of DC component [29]. In principle, all the impulses with the spectra wider than 500MHz, stipulated by the FCC, can be used as signals for UWB systems. However, the choice of the pulse shape is a key design decision in UWB systems because of the critical transmission power limitations, SNR considerations and efficient utilization of the bandwidth and power allowed by the FCC masks [30].

A Gaussian pulse is a suitable candidate for UWB radar and communication systems [31]. However, its PSD has a direct current offset and hence will not radiate effectively. In addition, it does not fit in to the emission mask for any value of the pulse width.

One approach to the design of digital pulse shapers that agrees with the FCC spectral masks is to employ prolate spheroidal wave functions to generate pulses from the eigen vectors of a channel matrix that is constructed by sampling the spectral mask [32-34]. The pulses generated from different eigenvectors are mutually orthogonal, but require a high sampling rate that could lead to implementation difficulties and huge memory requirements.

Another possible solution for this is to shift the center frequency and adjust the bandwidth so as to satisfy the requirements. This could be done by modulating the signal with a sinusoid to shift the center frequency and by varying the pulse width. Since the impulse radio being a carrier less system, modulation will increase the cost and complexity.

Other pulse shaping methods include changing the properties of Hermite orthogonal polynomials [35], and fine-tuning higher-order derivatives of the Gaussian pulse [36].

Owing to unique temporal and spectral properties, a family of differentiated Gaussian pulses which resemble sinusoids modulated by a Gaussian envelope,  $V_n(t)$ , is widely used as the source pulses in the UWB systems.

$$V_n(t) = \frac{d^n}{dt^n} \left[ e^{-2\pi \left(\frac{t}{\tau}\right)^2} \right] \quad (2.6.7)$$

Where the pulse parameter  $\sigma$  stands for the time in radians when  $v_0(\sigma) = e^{-1}$  as shown in Fig.2.5(a) and  $n$  is the order of differentiation. Some of the higher order derivative of Gaussian pulses can match the UWB band directly, such as the fourth-order Rayleigh pulses as shown in Fig.2.5(b), with the  $\sigma$  chosen such that the pulse spectrum peaks at 5.5GHz. This is the waveform template chosen for pulse distortion analysis in this thesis. Note that the waveforms are shifted in X-axis for clearer distinction in Fig.2.5(a).

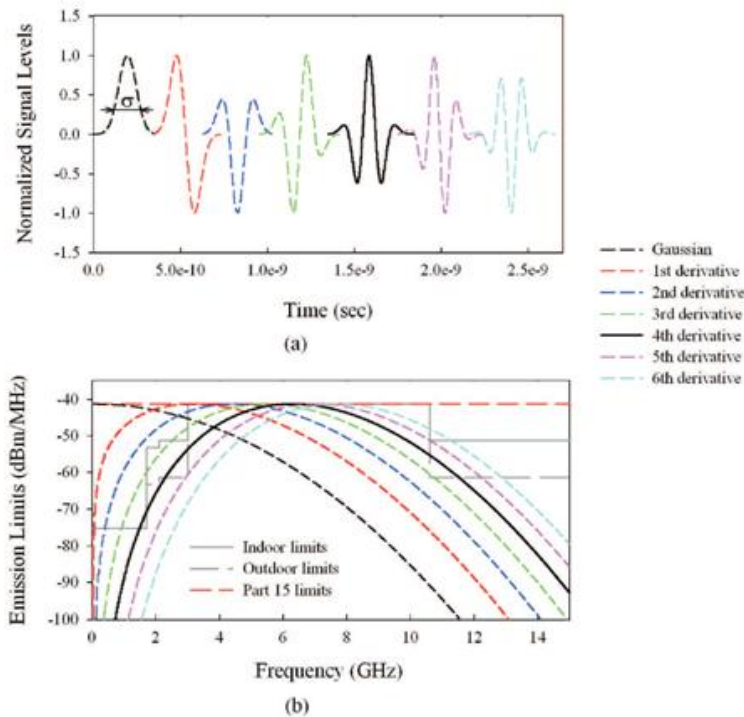


**Fig.2.5** Gaussian pulse and its derivatives (a) waveforms in the time domain and (b) their power spectral densities

#### **2.6.4 Transfer function determination**

The transfer function of the antennas is determined from the measured values of  $S_{21}$  in the frequency domain. Using two identical antennas oriented along various angles, the  $S_{21}$  is measured and using the following relation the transfer function is calculated.

$$H(\omega) = \sqrt{(2\pi R c S_{21}(\omega) e^{j\omega R/c}) / j\omega}$$

Where  $H(\omega)$  is the transfer function,  $c$  is the free space velocity and  $R$  is the distance between the two antennas. The measured transfer function is first transformed to time domain  $[h(t)]$  by performing the inverse Fourier transform to find out the impulse response.

#### **2.6.5 Impulse Response**

The impulse responses are deduced from the measured transfer functions by taking their inverse fast Fourier transforms (IFFT) but with certain precautions. The measured data used in this thesis is over a frequency range 3 to 12GHz. The data is complemented by zero padding for 0 to 3GHz and 12GHz to  $f_{\max}$ . It is assumed that the antenna's response is so poor out of band that the data obtained is clearly dominated by noise and it might be advantageous to blank or zero data in those frequency ranges [37]. To correspond to the spectrum of a real signal, the conjugate of the zero-padded data is taken and reflected to the negative frequencies resulting in a spectrum which is symmetric around DC. The IFFT of the resulting measured data in frequency domain gives a real impulse waveform.

### **2.6.6 Received Signal Waveforms**

For a UWB system, the received signal should resemble the source pulse with minimum distortions. The received waveform is determined by both the source pulse and the system transfer function which has already considered the effects from the entire system including the transmitting and receiving antennas.

The transfer function measured by the vector network analyzer is a frequency response of the system. However, the frequency domain information can be transformed to the time domain. Here, Hermitian processing is used for the data conversion [38]. Firstly, the pass-band signal is obtained with zero padding from the lowest frequency down to DC (Direct Current). Then, the conjugate of the signal is taken and reflected to the negative frequencies. The resulting double-sided spectrum corresponds to a real signal, i.e. the system impulse response. It is then transformed to the time domain using Inverse Fast Fourier Transform (IFFT). Finally, the system impulse response is convolved with the input signal to obtain the received pulse.

### **2.6.7 Pulse Distortion Analysis: Fidelity Factor**

Ideally, an impulse antenna should faithfully replicate the transmitted pulse on reception. But the changes in the phase center position and radiation characteristics alter the properties of the transmitted pulses. The non-linearity in the antenna phase response leads to pulse dispersion. In addition, its radiation characteristics also have a significant impact on its performance. Any distortion of the signal in the frequency domain will cause distortions of the transmitted pulse shape, therefore increases the complexity of the detection mechanism at the receiver.

The antenna gain should be smooth across the frequency band in order to avoid frequency selective distortion of the transmitted pulse. Since the antenna gain typically appears different from different angles, the shape of received pulse show spatial dependence [39].

From the spatio-temporal antenna impulse responses, we are able to calculate the pulse distortions introduced by the antenna along different orientations. These distortions are often quantized as the fidelity factor which is a measure of the faithfulness with which an antenna reproduces the time shape of the input signal. For UWB systems, the commonly used receivers are based on the pulse energy detection or correlation with the template waveform. Therefore we need to examine the pulse distortions by calculating the fidelity factor [40].

Fidelity factor F is defined by

$$F = \max_{\tau} \frac{\int x(t) \cdot \int y(t - \tau) dt}{\sqrt{\int |x(t)|^2 dt \cdot \int |y(t)|^2 dt}}$$

where  $\tau$  is the delay which is varied to maximize the numerator. The fidelity parameter F, is the maximum of the cross-correlation function and compares only shape of the waveforms not the amplitudes. It is deduced from the measured and simulated data for different RX antenna orientations, with  $y(t)$  as the incident and  $x(t)$  as the received waveform [41].

To assess antenna performance as a system, we have considered a pair of the designed planar antennas. One antenna is assumed to be transmitting and the other receiving. The distance between the transmitting and the receiving antennas is 120cms of free space, which is more than 12 wavelengths at the

lowest frequency of the considered band of operation i.e. the antennas are in the far field of each other.

### 2.6.8 Effective Isotropic Radiated Power (EIRP)

The ultimate goal of an indoor UWB communication system is to transmit and receive high speed data via a wireless link. This makes the study of antennas an inevitable part of the system design. FCC spectral mask constrains the effective isotropic radiated power (EIRP) of the antenna rather than PSD of pulses before transmission. This requires some further study of the antenna effects on UWB pulses.

For an isotropic antenna the gain is identical in all directions, so that

$$G_T(f, \theta, \phi) = G_T(f)$$

where  $G_T$  is the transmit antenna gain, where  $\Phi$  is the elevation angle and  $\theta$  is the azimuth angle in the spherical coordinate system. The radiation power density is

$$\rho(f) = \frac{P_T(f)G_T(f)}{4\pi d^2}$$

over a sphere of radius  $d$ .  $IRP(f)$  is the transmitted power density.

The radiated power of an isotropic antenna at a reference distance  $d_{ref}$  is

$$IRP(f) = d_{ref}^2 \int_0^{2\pi} \int_0^\pi \frac{P_T(f)G_T(f) \sin \theta d\theta d\phi}{4\pi d_{ref}^2}$$

For an arbitrary antenna, not necessarily isotropic, the FCC requires that on any point of the sphere at  $d_{ref}$ , the radiated power should not exceed that of an isotropic antenna, hence the term EIRP.



$$\begin{aligned} IRP(f) &= \max_{\phi, \theta} P_T(f) G_T(f, \phi, \theta) \\ &= P_T(f) G_T(f, \phi_0, \theta_0) \end{aligned} \quad (2.6.8)$$

where  $(\phi_0, \theta_0)$  represents the direction of maximal gain.

For simplicity we will write  $G_T(f)$  for the maximal gain of frequency  $f$  for any direction, hence

$$EIRP(f) = P_T(f) G_T(f)$$

A general procedure for determining the EIRP per unit bandwidth is the use of the Friis power transmission formula in its simple form where antennas are assumed to be both impedance and polarization matched [42]

$$EIRP(f) = P_T(f) G_R(f) \left( \frac{c}{4\pi df} \right)^2 \quad (2.6.9)$$

where  $P_T(f)$  is the received / transmitted power density,  $G_R(f)$  is the receive antenna gain,  $c$  is the speed of propagation of wave,  $d$  is the far field radial distance between the transmitter and the receiver and  $f$  is the frequency of operation. Equation (2.6.9) is valid for  $r$  larger than  $2D_{\max}^2 / \lambda$ , where  $D_{\max}$  is the maximum dimension of the transmit antenna and  $\lambda$  is the free space wavelength. When  $D_{\max}$  is much greater than the wavelength, the far field criterion becomes very large and the field strength that must be measured at the far field location is less than the receiver noise floor. In such cases, the near field measurement techniques should be used for EIRP determination [43]. The dimensions of antenna and the maximum frequency of interest (10 GHz) in our case result in a reasonable far field distance where (2.6.9) is still valid. To obtain the EIRP, we use similar transmit (Tx) and receive (Rx) antennas and measure, using a network analyzer, the total frequency response of system,

$$H_{CH}(f) = \frac{P_R(f)}{P_T(f)}$$

This channel response,  $H_{CH}$ , includes free space propagation and transmit and receive antennas responses. The orientations of antennas are carefully adjusted so that they see each other with the same angle. Thus, for similar transmit and receive antennas (identical models),  $G(f) = G_T(f) = G_R(f)$  and from (2.6.8) and (2.6.9) we have

$$H_{CH}(f) = \frac{P_R(f)}{P_T(f)}$$
$$EIRP(f) = \sqrt{H_{CH}(f)} \left( \frac{4\pi df}{c} \right) \quad (2.6.10)$$

Under the assumption no multipath reflections in the Friis formula. This condition can be created experimentally by attenuating the major reflections by placing RF absorbers around the antennas during  $H_{CH}$ -measurement; all remaining multipath reflections are easily removed by truncating the channel impulse response. The truncated impulse response is then Fourier transformed and used in (2.6.10) for the EIRP calculation.

## **References**

- [1] Ansoft HFSS, <http://www.ansoft.com/products/hf/hfss/>
- [2] Volakis, J.L, Hybrid finite element methods for conformal antenna simulations, Antennas and Propagation Society International Symposium, 1997. IEEE., 1997 Digest Volume 2 ,Page(s):1318 - 1321, July 1997 .
- [3] Anastasis C. Polycarpous, Introduction to the Finite Element Method in Electromagnetics, Morgan & Claypool, USA, 2006.
- [4] Joao pedro a. Bastos and Nelson Sadowski , “Electromagnetic modeling by finite element methods”, Marcel Dekker, 2003
- [5] J. Youngs, G. C. Stevens and A. S. Voughan, “Trends in dielectric research: an international review from 1980 to 2004,” J. Phys. D: Appl. Phys. 39 1267-76 (2006).
- [6] M. G. Pecht, G, R. Agarwal, P. McCluskey, T. Dishongh, S. Javadpour and R. Mahajan, “Electronic Packaging Materials and there Properties,” CRC Press, London, (1999).
- [7] T. Hu, J. Juuti, H. Jantunen, and T. Vilkmán, “Dielectric properties of BST/polymer composite,” J. Eur. Ceram.Soc., 27, 3997-4001 (2007).
- [8] D. D. L. Chung, “Materials for Electronic Packaging,” Butterworth Heinemann, Washington, (1995).
- [9] M. T. Sebastian, “Dielectric materials for wireless communications,” Elsevier publishers UK., (2008).
- [10] Rao Y, Qu J, Marinis T, Wong C P, “ A precise numerical prediction of effective dielectric constant for polymer ceramic composites based on

effective medium theory” IEEE Trans. Compon. Packag. Tech Pp 680-683, 2000

- [11] Prakash A, Vaid J K Mansingh A, “Measurement of dielectric parameters at microwave frequencies by cavity perturbation technique”, IEEE Trans. Microwave Theory and Tech.,vol.27:Pp 791-795, 1979
- [12] HP8510C Network Analyzer operating and programming manual, Hewlett Packard, 1988.
- [13] <http://www.home.agilent.com>
- [14] Massey, P.J.; Boyle, K.R, “Controlling the effects of feed cable in small antenna measurements”, Twelfth International Conference on Antennas and Propagation, Volume 2, 31 Pp:561 - 564 vol.2 April 2003
- [15] Kin Seong Leong; MunLeng Ng; Cole, P.H, “Investigation of RF cable effect on RFID tag antenna impedance measurement” Antennas and Propagation International Symposium, 2007 IEEE, Page(s):573 – 576, 9-15 June 2007
- [16] C. A. Balanis, Antenna Theory: Analysis and Design, Second Edition, John Wiley & Sons Inc. 1982
- [17] John D. Kraus, Antennas Mc. Graw Hill International, second edition, 1988
- [18] JaumeAnguera, Alfonso Sanz, Young-JikKo, Carmen Borja ,Carles Puente and JordiSoler, “Theoretical and practical experiments for a single antenna gain testing method: Application to wireless communication devices”, Microwave and optical technology letters Vol. 49, No. 8,Pp 1781 – 1786, August 2007

- [19] H.A Wheeler, “The Radiansphere around a small antenna”, in Proc. IRE, August 1959, pp 1325-1331.
- [20] HosungChoo; Rogers, R.; Hao Ling; “On the Wheeler cap measurement of the efficiency of microstrip antennas”, IEEE Transactions on Antennas and Propagat., Volume 53, Issue 7, Pp:2328 – 2332,July 2005.
- [21] H. G. Schantz. Radiation Efficiency of UWB Antennas. Proceedings of the 2002 IEEE UWBST Conference, 2002.
- [22] R.E Munson, Conformal Microstrip Antennas and Phased Arrays, IEEE Trans. Antennas.& Propagation,Ap-22, pp. 74-77, 1974.
- [23] A.G Derneryd, Linear Microstrip Antenna, Chalmer Univ. Technology, Report, Goteborge, Sweden, 1975.
- [24] J.R Mosig and F.E Fred Gardiol, A Dynamic Radiation Model for Microstrip Structures, Advances in Electronics and Electron Physics, Vol. 59, 1982,pp. 139-234.
- [25] K.S Yee, Numerical Solution of Initial Boundary Value Problems Involving Maxwell’s Equations in Isotropic Media, IEEE Transactions on Antennas and Propagation, Vol-14, 1966, pp. 302-307.
- [26] L. Guo, J. Liang, C.C. Parini and X. Chen, “A time domain study of CPW-Fed disk monopole for UWB applications”, Asia-Pacific Microwave Conference 2005, 4-7 December 2005, Suzhou, China.
- [27] Y. Cho, K. Kim, D. Choi, S. Lee and S. Park, “A Miniature UWB Planar Monopole Antenna With 5-GHz Band-Rejection Filter and the Time-Domain Characteristics”, IEEE Transactions on Antennas and Propagation, vol. 54, no. 5, May 2006, pp. 1453-1460.

- [28] E. C. Ifeachor, B.W. Jervis, *Digital Signal Processing, A practical Approach*, Addison-Wesley, 1993.
- [29] M. Ghavami, L. B. Michael and R. Kohno. Generation of ultra wideband waveforms. In *Ultra Wideband Signals and Systems in Communication Engineering*. John Wiley and Sons, Inc., 2004.
- [30] Z. N. Chen, X. H. Wu, H. F. Li, N. Yang and M. Y. W. Chia. Considerations for source pulses and antennas in UWB radio systems. *IEEE Trans. Antennas Propag.*, vol. 52, no. 7, pages 1739–1748, 2004.
- [31] J. D. Taylor. *Introduction to ultrawideband radar systems*. CRC Press, 1995.
- [32] R. S. Dilmaghani, M. Ghavami, B. Allen and H. Aghvami. Novel UWB pulse shaping using prolate spheroidal wave functions. *Proc. IEEE Int. Symp. on Personal, Indoor and Mobile Radio Communications*, Beijing, vol. 1, pages 602–606, 2003.
- [33] B. Parr, B. Cho, K. Wallace and Z. Ding. A novel ultra-wideband pulse design algorithm. *IEEE Communications Letters*, vol. 7, no. 5, pages 219–221, 2003.
- [34] H. Zhang and R. Kohno. SSA realization in UWB multiple access systems based on prolate spheroidal wave functions. *Proc. IEEE Wireless Communications and Networking Conf.*, pages 1794–1799, 2004.
- [35] M. Ghavami, L. B. Michael and R. Kohno. Hermite function based orthogonal pulses for UWB communication. *Proc. Int. Symp. on Wireless Personal Multimedia Communications*, pages 437–440, 2001.

- [36] H. Sheng, P. Orlik, A. M. Haimovich, L. J. Cimini and J. Zhang. On the spectral and power requirements for ultra-wideband transmission. Proc. IEEE Int. Conf. on Communications, pages 738–742, 2003.
- [37] J. S. McLean and R. Sutton. Considerations for source pulses and antennas in UWB radio systems. Proc. IEEE Int. Conf. on Ultrawideband, vol. 2, pages 113–116, 2008.
- [38] J. Liang, L. Guo, C.C. Chiau and X. Chen, “Time domain characteristics of UWB disc monopole antennas”, 35th European Microwave Conference, 3-7 October, 2005, Paris, France.
- [39] N. Fortino, J.-Y. Dauvignac, G. Kossiavas and R. Staraj. Design optimization of UWB printed antennas for omnidirectional pulse radiation. IEEE Trans. on Antennas and Propagat., vol. 56, no. 7, pages 1875–1881, 2008.
- [40] D. Lamensdorf and L. Susman. Baseband-pulse-antenna techniques. IEEE Antennas and Propagation Magazine, vol. 36, no. 1, pages 20–30, 1994.
- [41] M. Klemm, I. Z. Koves, G. F. Pederson and G. Troster. Novel small-size directional antenna for UWB WBAN/WPAN applications. IEEE Trans. on Antennas and Propagat., vol. 53, no. 12, pages 3884–3896, 2005.
- [42] D. Pozar, "Microwave engineering," John Wiley & Sons, 3rd Ed, 2005.
- [43] J. D. Brunett, R. M. Ringler, V. V. Liepa, "On measurements for EIRP compliance of UWB devices," *IEEE Electromagnetic Compatibility*, vol. 2, pp. 473-476, Aug. 2005.





**COPLANAR STRIP FED DUAL BAND ANTENNA**

*The chapter deals with the design development and analysis of a compact Coplanar strip Fed Dual Band Dipole Antenna suitable for IEEE 2.4 GHz and 5.2 GHz WLAN applications. The chapter starts with a brief introduction of different types of feeding mechanisms for planar antennas. From the various kinds of feeds described, the symmetric Slotline/CPS feed is found to be the best suited for compact antennas. A detailed analysis of Open Ended Slotline (OES) is also performed. Since the connector used is asymmetric one, a BALUN is also introduced for the study. Reflection, Radiation, Gain, and Efficiency Characteristics of the antenna are discussed in detail. FDTD analysis of the structures discussed in this chapter are also included.*

**3.1 Introduction to Compact Planar Antennas**

The main characteristic of an antenna is to radiate energy which is launched into its input end (feed). According to maximum power transfer theorem, the design of a matched feed is important for transferring maximum power from the source to the radiating antenna. This implies that the feed will play an important role in the design of compact antennas.

This chapter starts with a brief discussion about different feeding mechanisms used for planar antennas. Then the design and development of compact antennas with optimum feed is presented. A dual band antenna is developed with this idea. Exhaustive experimental and simulation studies of the above antenna are also presented and discussed.

### 3.2 Planar Transmission Lines

In this section different types of antenna feeds are briefly presented. Since the thesis is about the study of planar antennas, emphasis is given to planar transmission lines. The widely used planar transmission lines like microstrip line (dual layer structure) and the coplanar wave guide (uniplanar structure) etc are discussed in the following sessions.

#### 3.2.1 The Microstrip line

The Micro Strip Line (MSL) consists of a narrow Perfect Electric Conductor (PEC) signal strip on an infinite ground plane separated by a low loss dielectric. The cross section of a typical MSL is shown in fig.3.1. The characteristic impedance of the line depends on the width ( $w$ ) of the signal strip, the height ( $h$ ) and the dielectric constant ( $\epsilon_r$ ) of the substrate [1]. This is a biplanar structure.

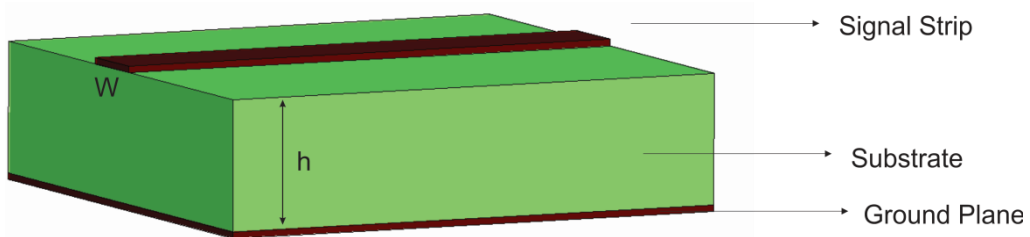


**Fig. 3.1** Microstrip transmission line

Integrating passive and active components along the biplanar structure is very difficult and uniplanar or co planar structures are used to mitigate that problem. The members of this category include the CoPlanar Wave guide (CPW), the SlotLine (SL)/CoPlanar Strip (CPS)etc [2].

### **3.2.2 The Coplanar Wave guide**

The coplanar wave guide consists of a central signal strip bounded by twin lateral ground strips separated by a small gap (Fig.3.2.). The characteristic impedance is determined by the width of the signal strip ( $w$ ), the gap between the signal strip and the lateral ground strips ( $s$ ) for fixed substrate height ( $h$ ) and dielectric constant ( $\epsilon_r$ ) [2]. In these lines, the passive and active components are easily integrated in between the central strip and the lateral ground plane without any via holes.

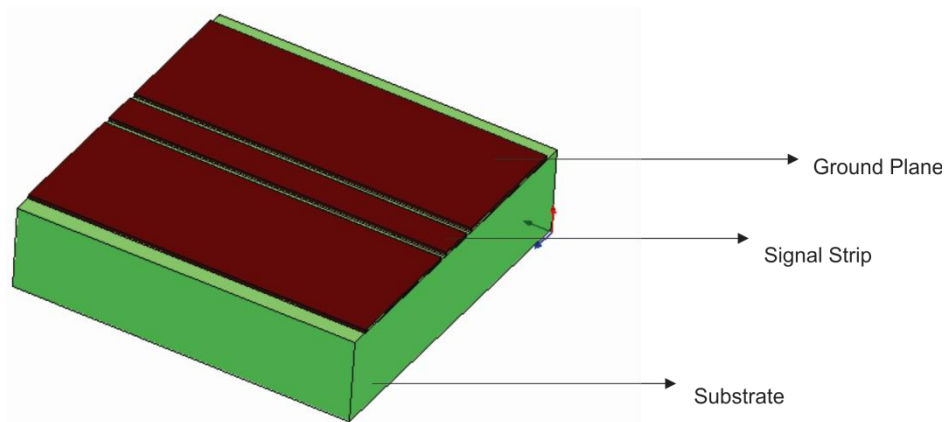


**Fig.3.2** The CPW transmission line

### **3.2.3 The Slotline/ Co-Planar Strip (CPS)**

The slotline may be considered as a complementary to the CPW. Coplanar Strip is a general term used for slotlines in which the conductor strip widths are finite and same. The main advantage of this transmission line is the

ease of mounting active and passive circuits into these lines. The structure of a typical slotline/CPS is given in Fig.3.3. It consists of two metallic strips separated by a slot of width 'g' ie it is a planar analogy of parallel pair transmission line. One of either strip is used as signal strip and the other one is ground plane. Since both strips are of same surface area, the surface current densities on both the strips are same. So CPS is considered as a balanced transmission line. According to [2] slotline on low  $\epsilon_r$  substrates have interesting applications in antennas.

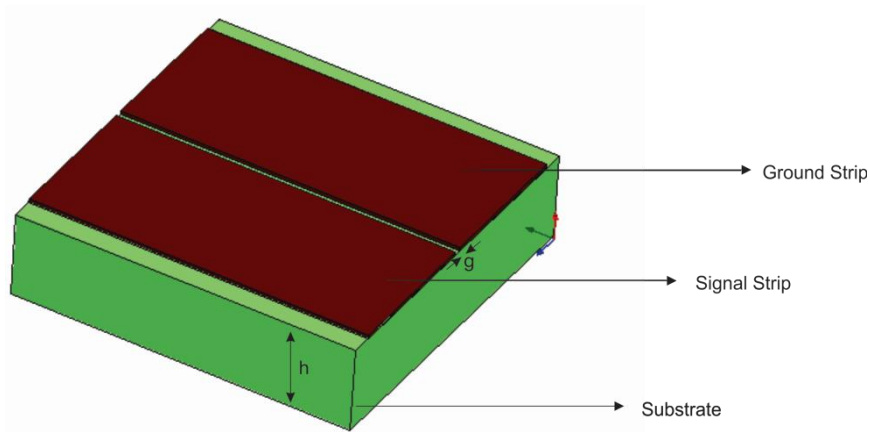


**Fig.3.3** Geometry of a Slotline/Coplanar strip

The characteristic impedance of the slotline is a function of slot width 'g' and dielectric constant ' $\epsilon_r$ '. The characteristic impedance is obtained in [3] by curve-fitting the numerical results obtained from Galerkin's method in Fourier transform domain.

For  $0.0015 < g/\lambda_0 < 0.075$  and  $3.8 < \epsilon_r < 9.8$  the characteristic impedance of the slotline is given by the following equation.

$$\begin{aligned}
 Z_0 = & 73.76 - 2.15\epsilon_r + (638.9 - 31.37\epsilon_r) \left(\frac{g}{\lambda_0}\right)^{0.6} \\
 & + \left(36.23\sqrt{\epsilon_r^2 + 41} - 225\right) \frac{\frac{g}{h}}{\frac{g}{h} + 0.876\epsilon_r - 2} \\
 & + 0.51(\epsilon_r + 2.12) \left(\frac{g}{h}\right) \ln\left(\frac{100h}{\lambda_0}\right) - 0.753\epsilon_r(h/\lambda_0)/\sqrt{g/\lambda_0}
 \end{aligned}
 \tag{3.1}$$

This equation has an average error of 1.58% and a maximum error of 5.4%.

### 3.3 Open Ended Slotline (OES)

Since the study is based on coplanar strip fed antennas, a detailed analysis of open ended slotline is necessary and unavoidable. A miniaturized OES and its dimensions are shown in Fig.3.4.

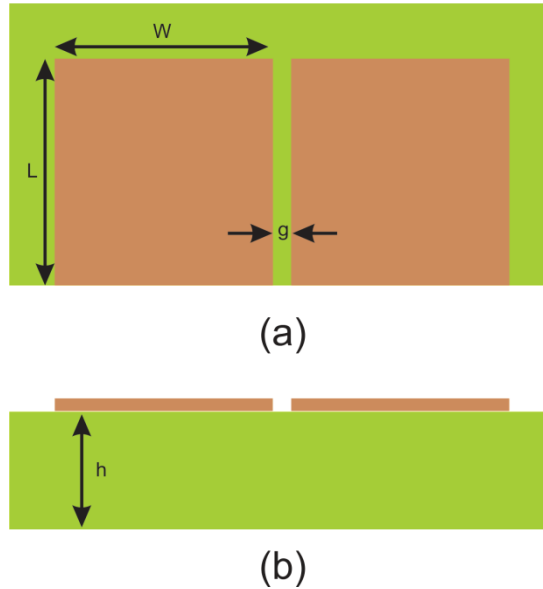


**Fig.3.4** An Open Ended Slotline (OES) (a). Top view. (b). Side view(L=10mm, W=14.85mm,g=0.3mm, h=1.6mm, ε=4.4)

The structure is fabricated on a commercially available FR4 Epoxy substrate with relative dielectric constant  $\epsilon_r=4.4$  and loss tangent  $\tan \delta=0.02$ . The dimensions of proposed OES are arbitrarily selected and are  $L=10\text{mm}$ ,  $W=14.85\text{mm}$  and  $g=0.3\text{mm}$ . The  $W$  is selected as  $14.85\text{ mm}$  to reduce the overall dimension of the structure to  $10\times 30\times 1.6\text{ mm}^3$ .

### 3.3.1 Reflection characteristics of OES

The measured and simulated reflection characteristics of the OES with dimensions  $L=10\text{mm}$ ,  $W=14.85\text{mm}$ ,  $g=0.3\text{mm}$ ,  $h=1.6\text{mm}$  and  $\epsilon=4.4$  are given in Fig.3.5. The OES resonate at  $4.28\text{ GHz}$  and offers a band width of  $1.4\text{ GHz}$  from  $3.74\text{ GHz}$  to  $5.14\text{ GHz}$ .

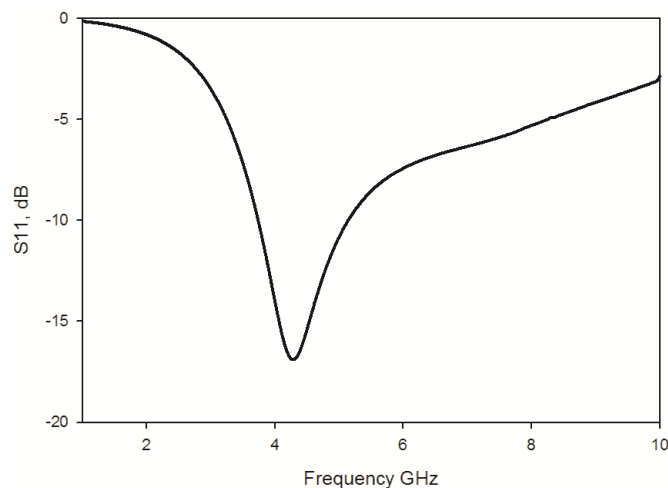


**Fig.3.5** Reflection co-efficient of an Open Ended Slotline (OES) ( $L=10\text{mm}$ ,  $W=14.85\text{mm}$ ,  $g=0.3\text{mm}$ ,  $h=1.6\text{mm}$ ,  $\epsilon=4.4$ )

From the figure it is clear that an OES with small length act as an antenna with a resonant frequency corresponding to a wavelength which is approximately four times the width of any one of the strip of a symmetric OES.

### **3.3.2 Parametric analysis**

To get further insight of how the radiation is occurring and to know the performance of the OES with dimensional factors, we have to analyze the effect of various dimensional parameters in detail. These are discussed in the following sessions.

#### **3.3.2.1 Variation in reflection co-efficient with L**

The variation in reflection characteristics with the small values of length of the slotline is shown in Fig.3.6. From the figure it is clear that the slotline length has no major impact on the resonant frequency. Only a slight variation is present in the resonant frequency with the slotline length. The interesting factor is that the resonant frequency shows a higher shift with increase in L. As the length of the slotline increases, the fringing field tends to confine near the slot and at the far ends of the conducting planes the surface current density is nearly zero. Thus in an OES with higher length, the resonance current will tends to maximize near the field maxima points ie at the vicinity of slot which results in reduction of length of resonant current path and thus increasing resonant frequency. This can be verified from the surface current distributions of OESs with different lengths which are given in Fig. 3.15.

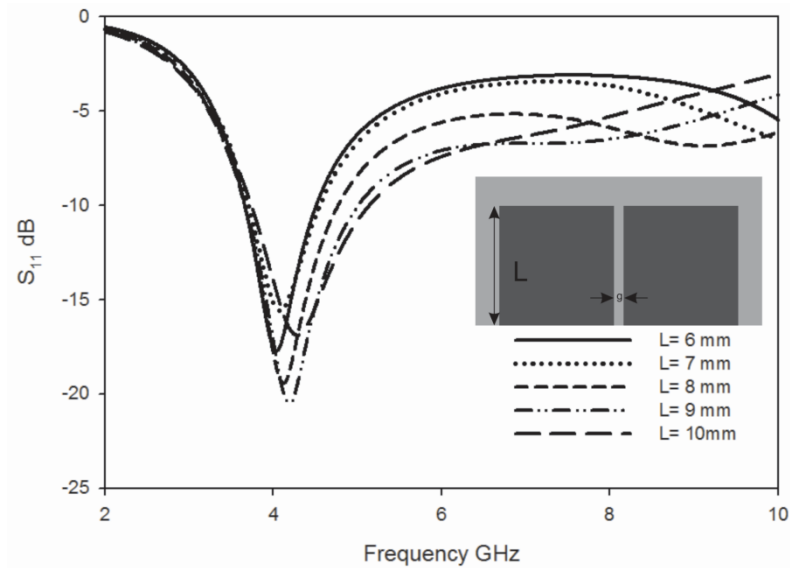


**Fig.3.6** Variation in reflection co-efficient with small values of L of an Open Ended Slotline (OES) ( $W=14.85\text{mm}, g=0.3\text{mm}, h=1.6\text{mm}, \epsilon=4.4$ )

From Fig.3.6 it is clear that the impedance matching and the band width of the resonator are affected by the length of the OES. For further analysis of the effects on these parameters, it is necessary to vary the length for higher values. The variation of reflection co efficient of the antenna for higher values of length is shown in Fig. 3.7. It is evident from the figure that as the length of the slotline increases and approaches  $W$ , the matching deteriorates. This is due to the impedance transformation of an open ended transmission line. As the  $L$  increases and approaches to  $W$ , the length of the slotline become quarter length corresponding to the resonant frequency. The input impedance of an open ended quarter wave transmission line will be zero ie at the resonant frequency, the input impedance of the slotline become very small when  $L$  tends to reach the value of  $W$ . This will drastically change the impedance matching of the OES at resonant frequency.



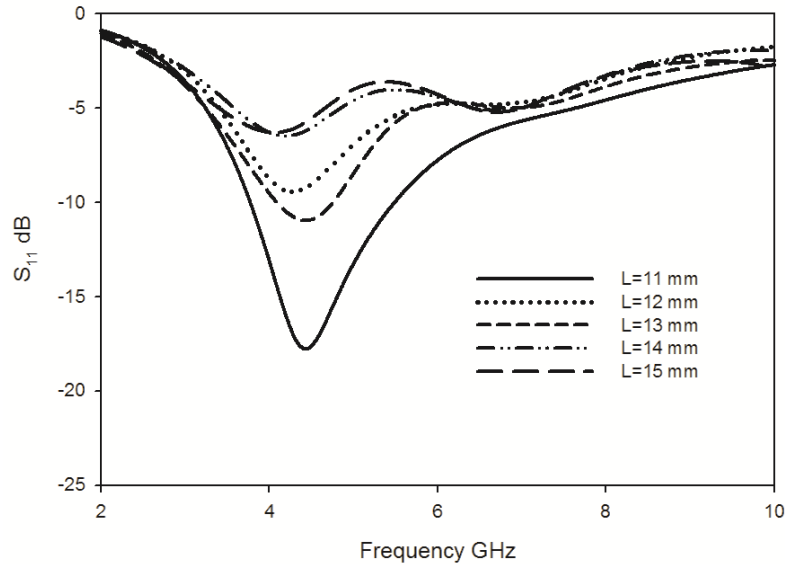


**Fig.3.7** Variation of reflection co-efficient with large value of L of an Open Ended Slotline (OES) ( $W=14.85\text{mm}, g=0.3\text{mm}, h=1.6\text{mm}, \epsilon=4.4$ )

Band width of the antenna is strongly affected with the length of the slotline. This is due to the change in Q factor with the length. In any planar structure, the distributed capacitance is a function of parallel edge length. Thus in an OES, as the length increases, the distributed capacitance increases and therefore the Q decreases (since antenna is a series resonant circuit). The reduction in Q factor will results in poor selectivity and higher bandwidth. It is also to be noted that for very small values of L, the OES is simply a dipole antenna with high selectivity and Q. As the length increases, it acts as a mismatched transmission line with abrupt termination.

### 3.3.2.2 Variation in reflection co-efficient with W

The variation of reflection co-efficient of the antenna with width of the metallic strip of a slotline is shown in Fig.3.8. The strip width W strongly affects the resonant frequency of an OES. As the W increases the resonant frequency decreases. This is due to the increase in resonant current path length with W. This

can be verified from the surface current distribution of the OES shown in Fig.3.14. Thus the strip width of the OES is the frequency determining factor. The bandwidth remains unchanged with the strip width. The matching is found to be varying with  $W$ . this is due to the change in input impedance at resonant frequency. As the parameter  $L$  is constant and  $W$  varies, the resonant frequency varies which results in variation of open ended transmission line length in terms of guided resonant wavelength. This will results in a change in input impedance and corresponding change in impedance matching.

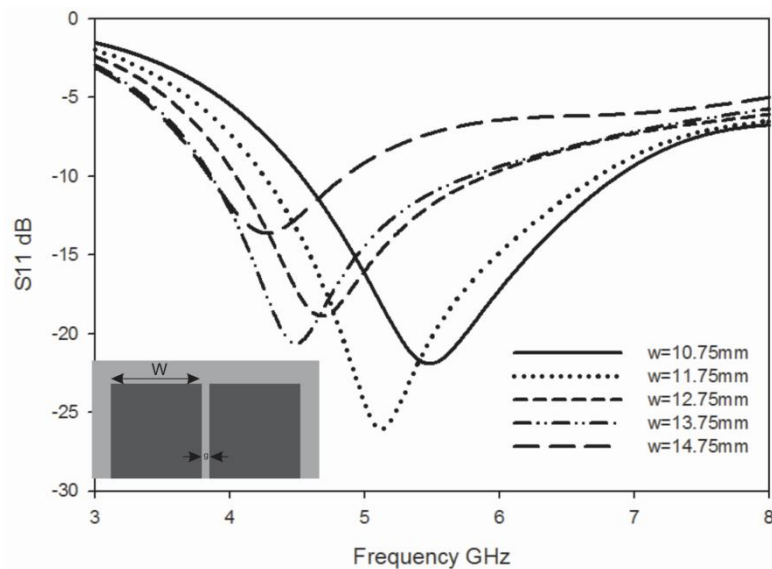


**Fig.3.8** Variation in reflection co-efficient with  $W$  of an Open Ended Slotline (OES) ( $L=10\text{mm}$ ,  $g=0.3\text{mm}$ ,  $h=1.6\text{mm}$ ,  $\epsilon=4.4$ )

### 3.3.2.3 Variation in reflection co-efficient with $h$

The variation of reflection co-efficient of the OES with different substrate heights are shown in Fig. 3.9. The resonant frequency is found to be unaffected by the substrate height  $h$ . The impedance matching is found to be better for thick substrates. According to equation 3.1 the characteristic impedance slightly varies

with height of the substrate. The variation in impedance matching of the OES with  $h$  is due to the change in input impedance.

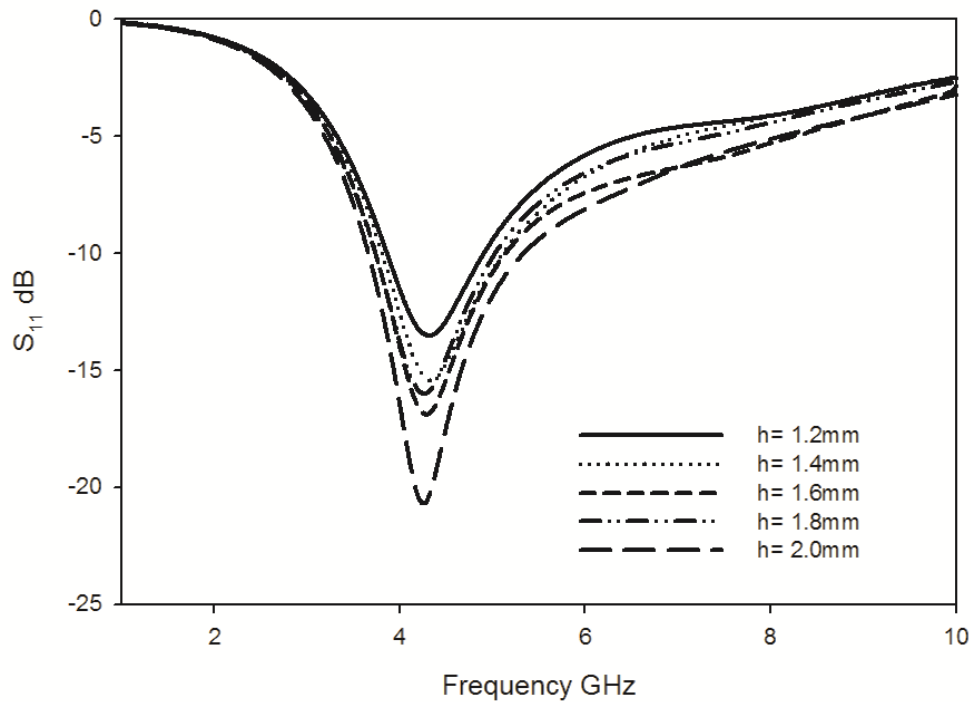


**Fig.3.9** Variation in reflection co-efficient with  $h$  of an Open Ended Slotline (OES) ( $L=10\text{mm}, W=14.85\text{mm}, g=0.3\text{mm}$  and  $\epsilon=4.4$ )

### 3.3.2.4 Variation in reflection co-efficient with $\epsilon_r$

To study the effect of dielectric constant of the substrate on the reflection co-efficient of the OES, four OES are studied in different substrates. The slot width  $g$  is calculated as per equation 3.1 and the parameters  $L$  and  $W$  remains constant. The simulated reflection co-efficient of the developed OES in different substrates are shown in Fig. 3.10. As the dielectric constant increases, the resonant frequency shows a shift towards the lower side. This is due to the lowering of guided wavelength with increase in  $\epsilon$  of the substrate. The impedance matching remains nearly same for all the substrate materials.

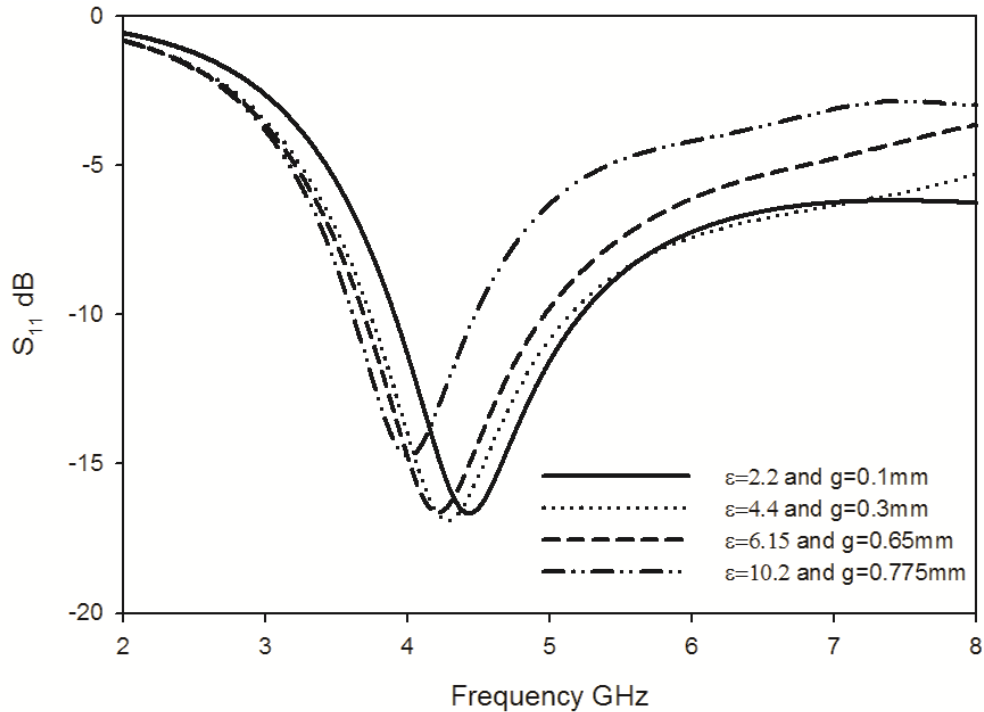


**Fig.3.10** Reflection co-efficient of an Open Ended Slotline (OES) developed on different substrates ( $L=10\text{mm}, W=14.85\text{mm}, h=1.6\text{mm}$ )

### 3.3.3 Radiation Characteristics of OES

The measured co polarized radiated power from the OES picked by a standard horn antenna arranged along the bore sight direction at a distance of 25 cm is shown in Fig. 3.11. The plot proves that at resonant frequency, the OES acts as a good radiator of electromagnetic energy. Nearly 20 dB difference in power is present between the operating band and other frequencies. This confirms that the structure is radiating effectively.

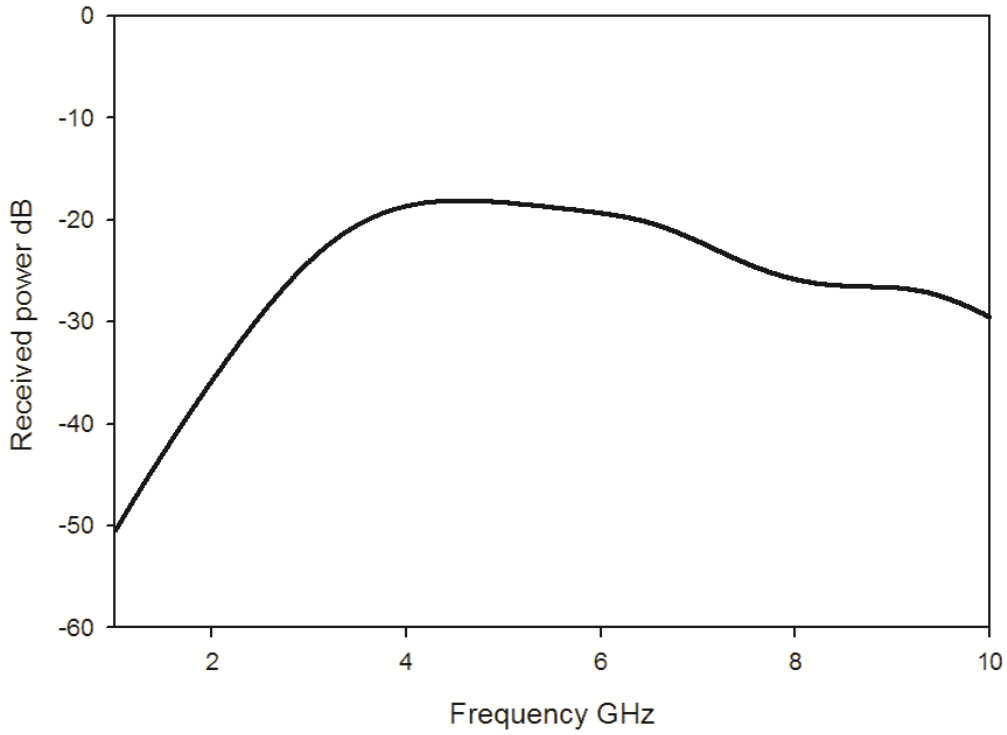


**Fig.3.11** Radiated power from an Open Ended Slotline picked by a standard horn antenna (L=10mm,W=14.85mm,h=1.6mm and  $\epsilon=4.4$ )

The simulated three dimensional radiation patterns of the OES at the resonant frequency are given in Fig.3.12. The OES offer an eight shaped radiation pattern along E plane and almost uniform radiation pattern with a slight enhancement in power towards Y direction along the H plane. From the radiation pattern it is clear that the OES is an antenna with polarization oriented along X direction and with a radiation maximum pointing towards the open end ie towards positive Y direction.

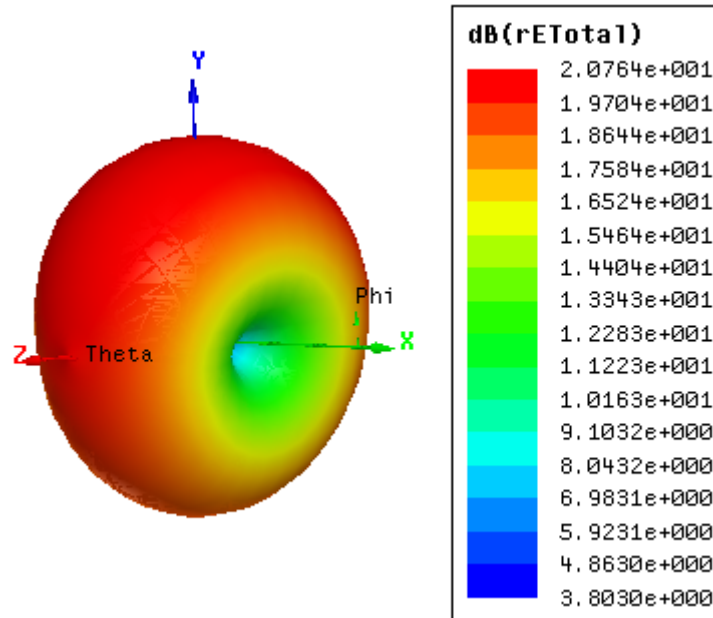


**Fig.3.12** Three dimensional Radiation Pattern of an Open Ended Slotline (OES) at 4.28 GHz  
( $L=10\text{mm}$ ,  $W=14.85\text{mm}$ ,  $g=0.5\text{mm}$ ,  $h=1.6\text{mm}$ ,  $\epsilon=4.4$ )

Measured two dimensional radiation patterns of the antenna at the resonant frequency along the two principal planes are shown in Fig. 3.13. From the figure it is clear that the open ended slotline act as antenna with a small directive behavior. From the E plane pattern it is found that the antenna has a front to back ratio of nearly 5 dB. A large cross polar purity of nearly 30 dB is present along the E plane pattern. The H plane radiation pattern also shows a small directive property with a front to back ratio of nearly 3 dB. The cross polar level difference in the H plane pattern is nearly 50 dB.

From the study of the radiation pattern of the Open Ended Slotline, it is clear that without any additional technology or parasitic elements, the structure offer a slight directive behavior. The directionality is an inherent property of slotline/CPS feed. The principle behind this directionality is also similar to that of an open ended wave guides. The open edges of the antenna contribute to

radiation and all other parts of the structure will contribute to the forward pushing of the electromagnetic energy.

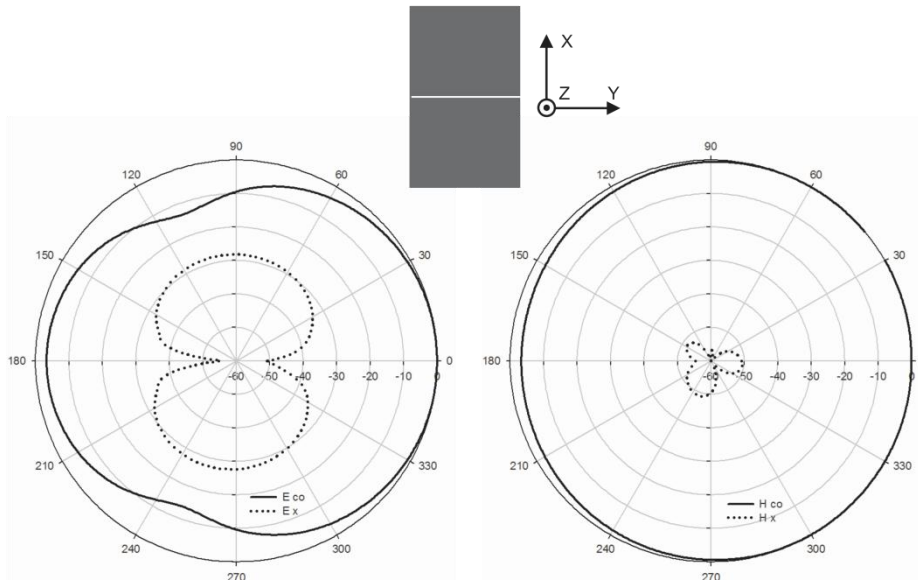


**Fig.3.13** Two dimensional Radiation Pattern of an Open Ended Slotline (OES) at 4.28 GHz ( $L=10\text{mm}$ ,  $W=14.85\text{mm}$ ,  $g=0.3\text{mm}$ ,  $h=1.6\text{mm}$ ,  $\epsilon=4.4$ )

### 3.3.4 Surface Current Analysis

The simulated surface current distribution of the OES at 4.28 GHz is shown in Fig.3.14. The figure says that at the lower part of the OES (input end OR Transmission line part) the field intensities are same but oriented in antiparallel direction which are destructive in nature and doesn't contribute to radiation. But at the upper edge ie at the open end there is a half wavelength variation of surface current through the OES. This variation of surface current have same intensity and direction and thus are additive in nature and contributes to the radiative behavior of the structure. From the figure it is inferred that the top edge of an OES act as a half wave dipole with polarization lies along X direction. As the length of the transmission line decreases, the OES become perfectly a half wave dipole.

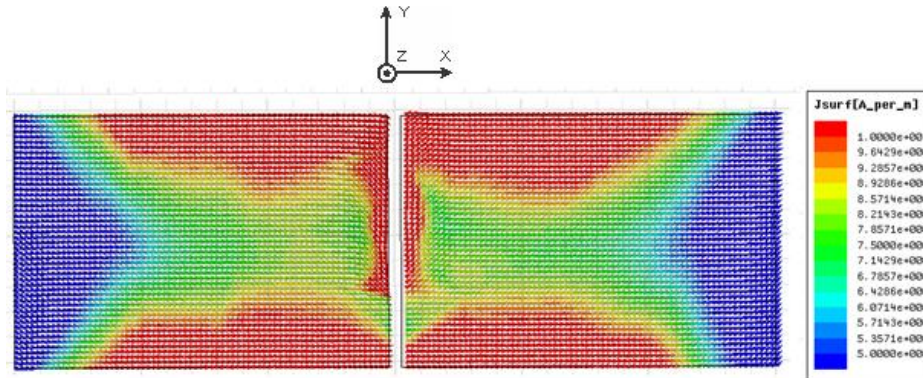


**Fig.3.14** Simulated surface current distribution of an Open Ended Slotline (OES) at 4.28 GHz ( $L=10\text{mm}$ ,  $W=14.85\text{mm}$ ,  $g=0.3\text{mm}$ ,  $h=1.6\text{mm}$ ,  $\epsilon=4.4$ )

The parametric analysis discussed in session 3.3.2.1, noticed an abnormal variation for resonant frequency with  $L$ . Normally the resonant frequency shows a lower shift with increase in dimension. But in the case of OES, the resonant frequency is found to be increasing with increase in  $L$ . This abnormal phenomenon is due to the fringing field concentration near the slot of the OES. To substantiate this, the simulated surface current of OESs with different  $L$  at their resonant frequencies are analyzed and is discussed here.

The simulated surface current distributions of different OESs with different lengths at their resonant frequency are shown in Fig.3.15. From the current patterns it is inferred that, at lower lengths, the surface current peaks not only at the vicinity of slot but also at the conducting parts of the OES. As the length increases, the current maximum is tends to concentrate more nearer to the slot. It is also to be noted from the current distribution that, the far ends of the slot line has almost zero current densities at higher lengths.

This will clearly substantiate beyond doubt that the increase in length of the OES will result in fringing field concentration near the slot which will in turn reduce the effective length and create a higher shift in resonant frequency.



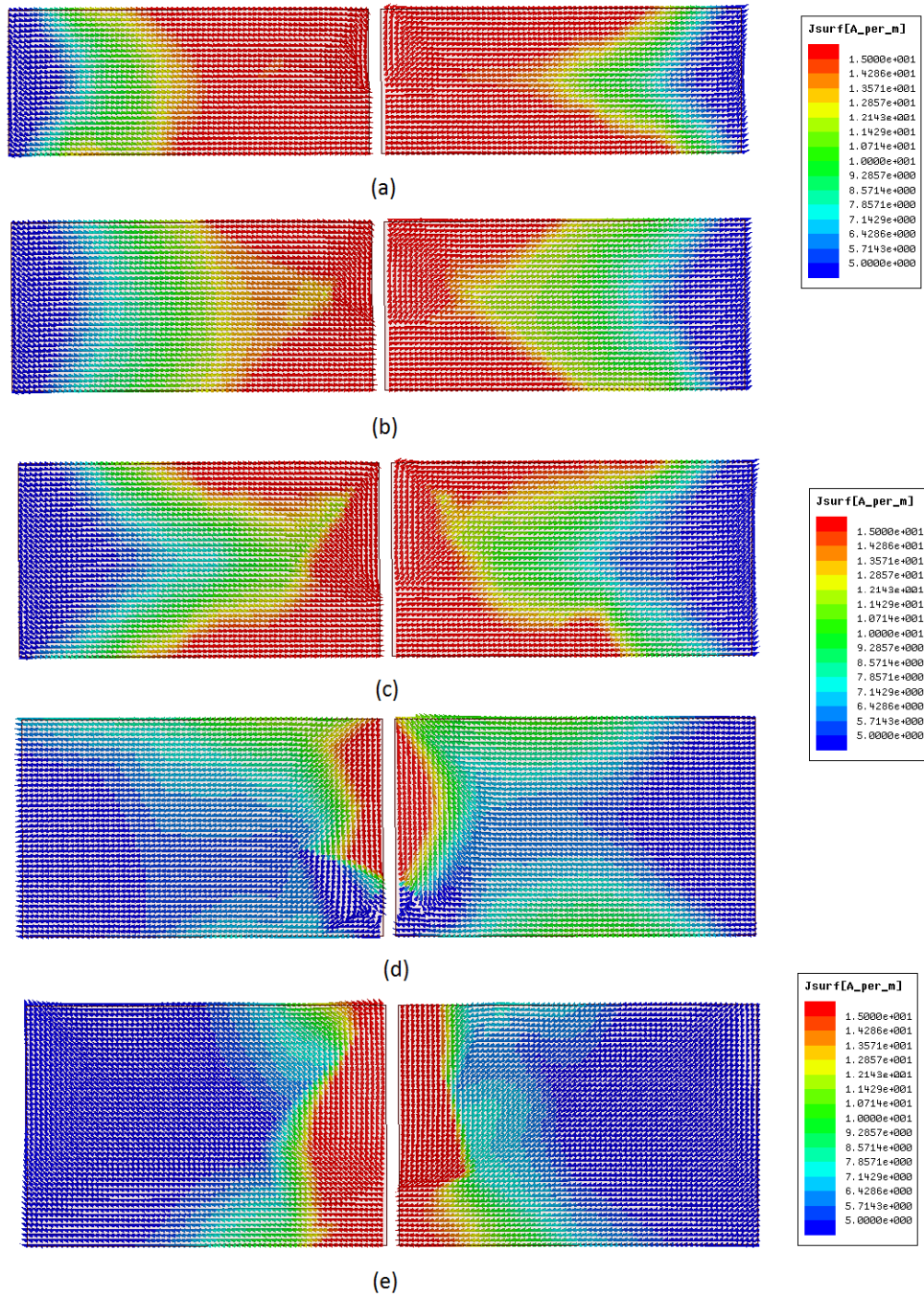


**Fig.3.15** Simulated surface current distribution of Open Ended Slotlines (a)  $L=5\text{mm}$  at  $4.03\text{ GHz}$  (b)  $L=6\text{mm}$  at  $4.07\text{ GHz}$  (c)  $L=7\text{mm}$  at  $4.13\text{ GHz}$  (d)  $L=8\text{mm}$  at  $4.18\text{ GHz}$  (e)  $L=9\text{mm}$  at  $4.21\text{ GHz}$  ( $W=14.85\text{mm}$ ,  $g=0.3\text{mm}$ ,  $h=1.6\text{mm}$ ,  $\epsilon=4.4$ )

From the above discussed analyses it can be found that the slotline/coplanar strip cannot be used as an effective transmission line for the energy transfer applications but it has tremendous application in antenna feeding mechanism. It can be easily converted into antennas with good efficiency and directivity by geometrical modifications. The transformations of OES into antennas for different applications are discussed in the following sessions.

### 3.4. Single band Dipole Antenna from an OES

Development of a single band compact dipole antenna is performed as the next stage of the study. It is interesting that by cutting off a rectangular piece from both the strips of the OES results in a dipole antenna with a resonating frequency much lower than that of the initial OES ie without compromising the compactness of the structure it is able to develop an antenna with lower resonant frequency. This session of the chapter deals with the study and analysis of the single band dipole developed from the OES.

#### 3.4.1 Evolution of Single band dipole

Evolution of a single band dipole antenna from an OES is shown in Fig. 3.16. The dipole is obtained from an OES by removing a rectangular area of dimension  $L_1 \times W_1$  from both the finite metallic strips of the slotline. Selective removal of these rectangles creates two symmetric L shaped arms as shown in figure.

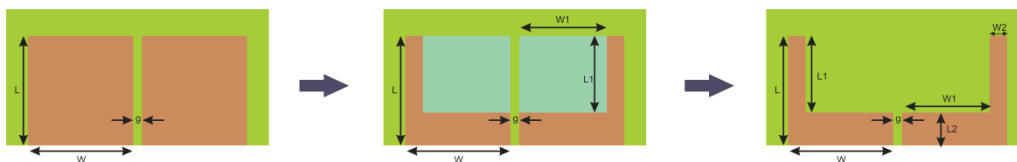


**Fig.3.16** Evolution of Compact Single Band Antenna from OES

The simulated reflection co-efficient of a single band dipole derived from an OES of dimensions  $L=15\text{mm}$ ,  $W=14.85\text{mm}$  and  $g=0.3\text{mm}$  by removing an arbitrary rectangle of dimensions  $L_1=8\text{mm}$  and  $W_1=9\text{mm}$  along with that of the parental OES are shown in Fig.3.17. The derived antenna resonates at 2.86 GHz with a bandwidth of 600 MHz. The antenna is well matched and the system is highly selective. At the same time the OES with same dimension is resonating at 4.06 GHz. It can be noted that the OES is not matched also. From the figure it is clear that cutting off a rectangle piece symmetrically from two metallic strip of an OES will results in a compact single band dipole antenna whose resonating frequency is much more lower than that the parental OES. The impedance matching and Q are also increased by removing the rectangular parts from the slotline.

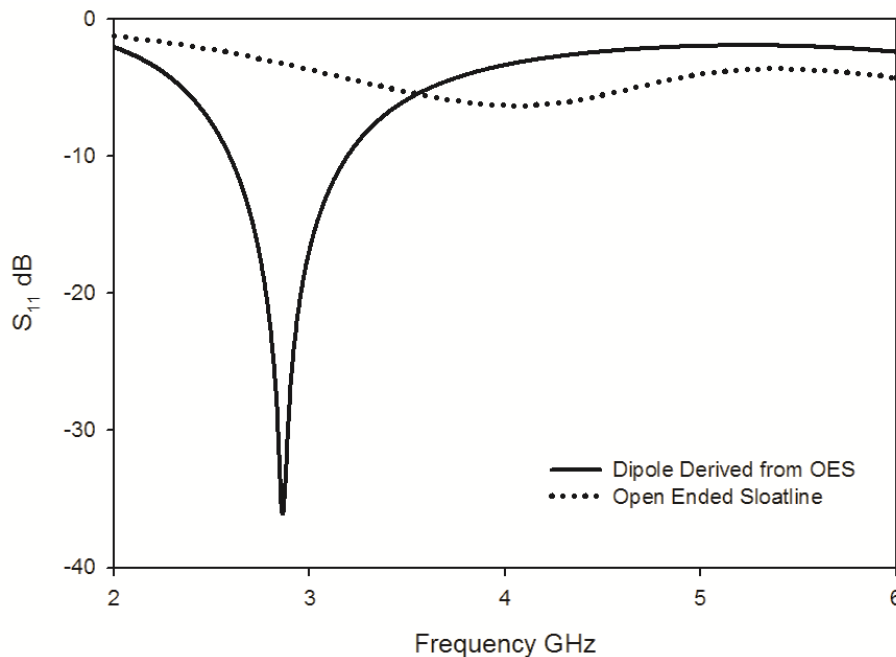


**Fig.3.17** Simulated Reflection co-efficient of a Compact Single Band Antenna derived from OES and an OES

### 3.4.2 Parametric Studies

To know the performance and characteristics of the structure with various dimensional parameters, a set of parametric analysis is carried out. To explain the variations in frequency domain response of the antenna, the variation in distributed inductance and capacitance of the antenna are also analyzed. The distributed parameters of the antenna are calculated using the method discussed in Appendix-1. These are discussed in the following sessions.

#### 3.4.2.1 Variation in reflection co-efficient with $L_1$

The variation of reflection characteristics of the antenna with the parameter  $L_1$  is shown in Fig. 3.18. A down ward shift is present in the resonant frequency with increase in  $L_1$ . This is due to the increase in resonant current path length with  $L_1$ . This can be verified from the surface current distribution of the dipole antenna given in session 3.4.4.4. The band width of the antenna is found to be constant for all values of  $L_1$ . The impedance match is found to be slightly changed with  $L_1$ . This may be due to the slight change in distributed parameters with  $L_1$ .

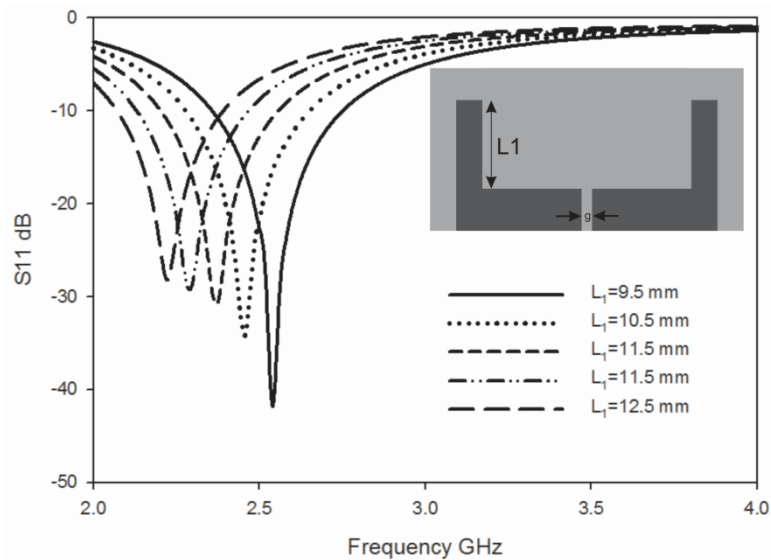


**Fig.3.18** Variation in  $S_{11}$  with  $L_1$  ( $W_1=11.75\text{mm}$ ,  $L_2=3.5\text{mm}$ ,  $W_2=3\text{mm}$ ,  $g=0.3\text{mm}$ ,  $h=1.6\text{mm}$  and  $\epsilon_r=4.4$ )

The variation in distributed capacitance and inductance of the antenna with  $L_1$  is shown in Fig.3.19. From the figure it is clear that both the reactive components will increase with increase in  $L_1$ . As  $L_1$  increases, the edge length of the metallic structure (Current path) increases which results in an increase of distributed inductance. The capacitance is increasing due to the increase in parallel conductor length with  $L_1$ . As a result the resonant frequency will come to lower side without affecting the percentage bandwidth considerably.

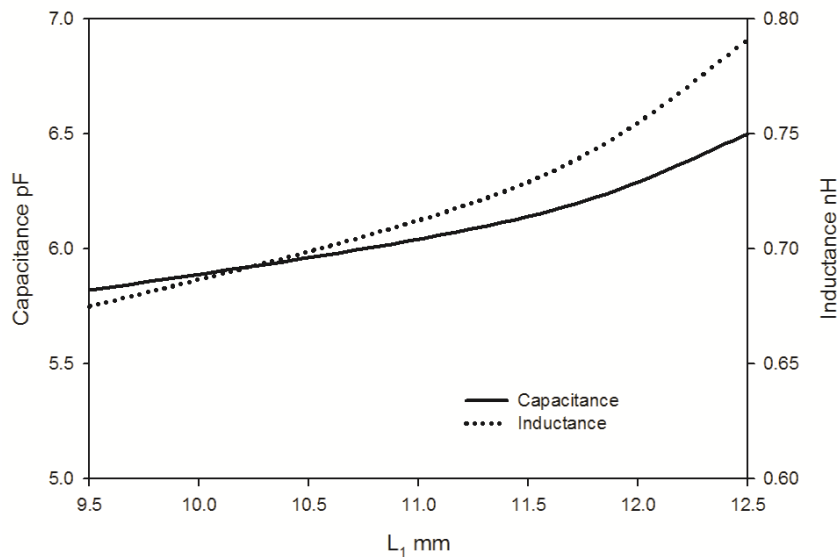


**Fig.3.19** Variation of distributed inductance and capacitance with  $L_1$  ( $W_1=11.75\text{mm}$ ,  $L_2=3.5\text{mm}$ ,  $W_2=3\text{mm}$ ,  $g=0.3\text{mm}$ ,  $h=1.6\text{mm}$  and  $\epsilon_r=4.4$ )

### 3.4.2.2 Variation in reflection co-efficient with $W_1$

The variation of reflection characteristics of the structure with the parameter  $W_1$  is shown in Fig. 3.20. Here also present a constant lower shift to the resonant frequency with increase in  $W_1$ . This is also due to the increase in surface current path length at the resonant frequency. The matching is also strongly affected with the parameter  $W_1$ . As  $W_1$  increases the matching is found to be increasing. This is due to the minute change in characteristics impedance

of the slotline with finite strip widths. The impedance of a slotline is defined for infinite strip width. The bandwidth remains unchanged with the parameter  $W_1$ .

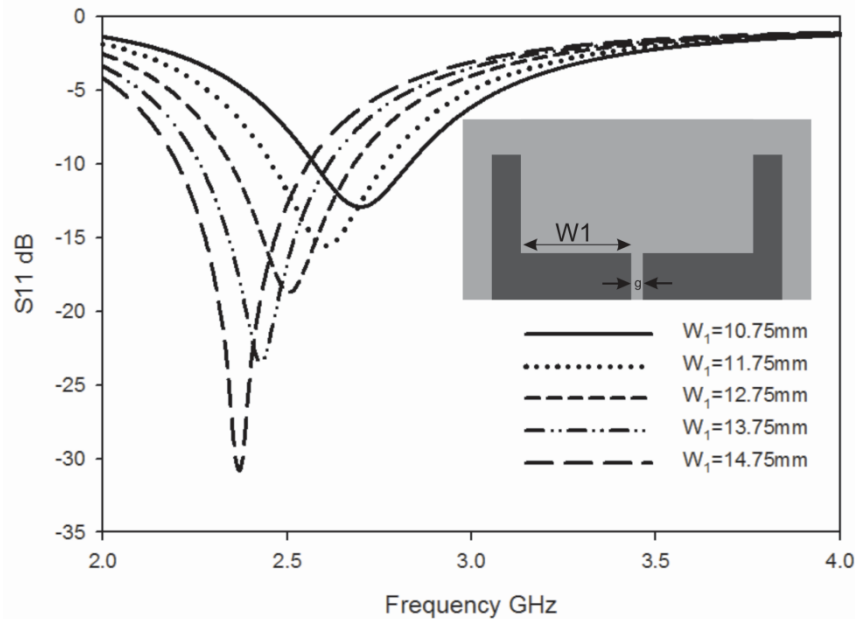


**Fig.3.20** Variation in  $S_{11}$  with  $W_1$  ( $L_1=11.5\text{mm}$ ,  $L_2=3.5\text{mm}$ ,  $W_2=3\text{mm}$ ,  $g=0.3\text{mm}$ ,  $h=1.6\text{mm}$  and  $\epsilon_r=4.4$ )

The variation in inductance and capacitance of the antenna with the parameter  $W_1$  is shown in Fig.3.21. It is clear from the plot that the capacitance decreases with  $W_1$  while the inductance increases with it. This is because, as  $W_1$  increases, the distance between the parallel edges of the antenna increases which results in a down shift in capacitance. As the edge length increases, the inductance also increases. As a result, the resonant frequency will come lower with an increase in percentage bandwidth.

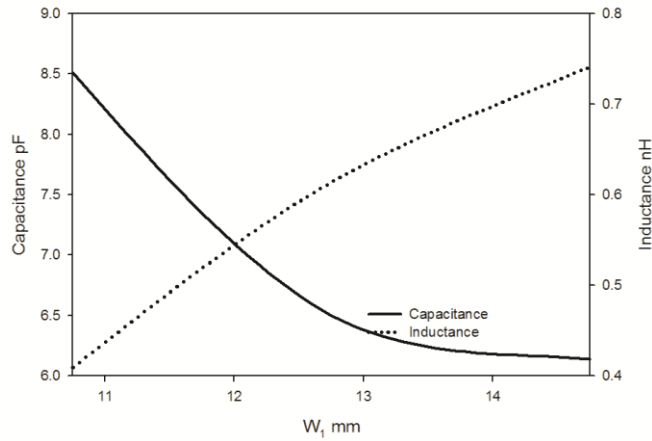


**Fig.3.21** Variation of distributed inductance and capacitance with  $W_1$  ( $L_1=11.5\text{mm}$ ,  $L_2=3.5\text{mm}$ ,  $W_2=3\text{mm}$ ,  $g=0.3\text{mm}$ ,  $h=1.6\text{mm}$  and  $\epsilon_r=4.4$ )

### 3.4.2.3 Variation in reflection co-efficient with $L_2$

Variation in reflection co-efficient with the *length* of the feed  $L_2$  is shown in Fig. 3.22. In this study the resonant frequency shows a higher shift with increase in strip width  $L_2$ . The reason for this higher shift is same as that explained in session 3.3.2.1. The shift in resonant frequency is found to be very feeble. This shows that the strip of dimension  $L_2 \times W_1$  is acting as a feed for the antenna and the length is the main frequency determining factor.

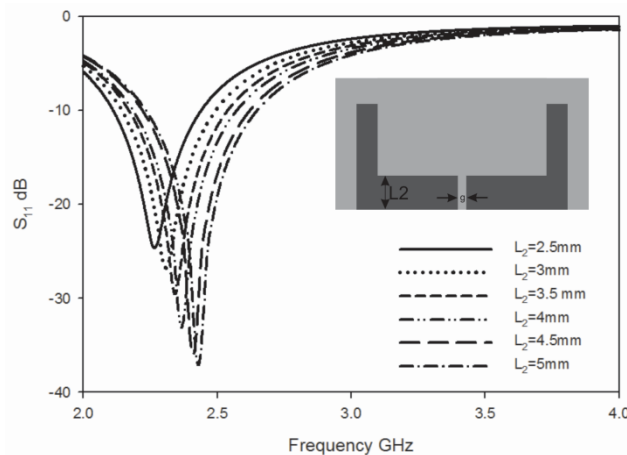


**Fig.3.22** Variation in  $S_{11}$  with  $L_2$  ( $L_1=11.5\text{mm}$ ,  $W_1=11.75\text{mm}$ ,  $W_2=3\text{mm}$ ,  $g=0.3\text{mm}$ ,  $h=1.6\text{mm}$  and  $\epsilon_r=4.4$ )

The changes in distributed components with parameter  $L_2$  is shown in Fig.3.23. The distributed capacitance is increasing while the inductance shows a down shift with  $L_2$ . Since the change inductance dominates the variations in capacitance, an increase in resonant frequency can be noticed. The change in frequency will be very low. Since the capacitance increases, an increase in Q factor is also found with  $L_2$ .

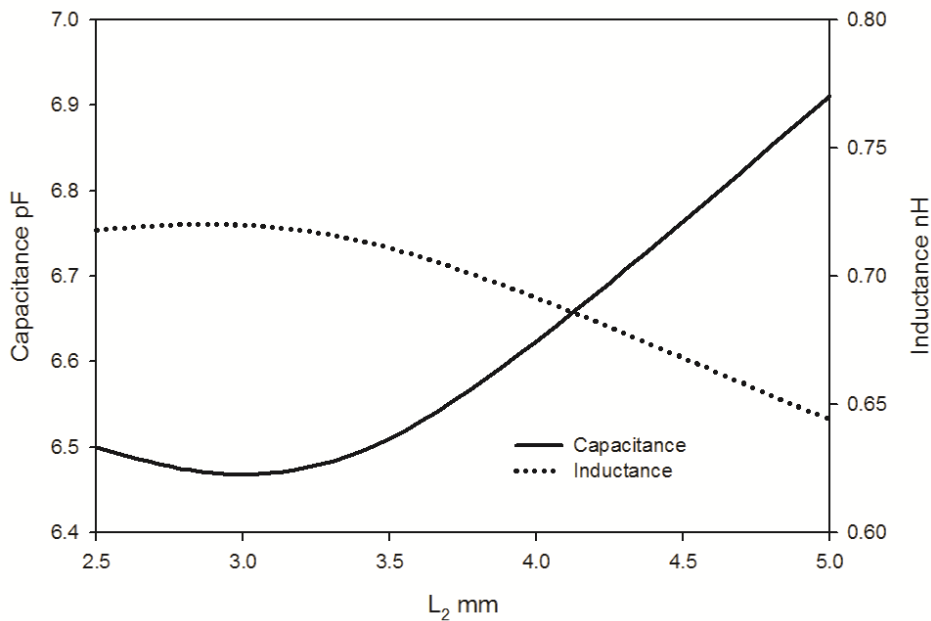


**Fig.3.23** Variation of distributed capacitance and inductance with  $L_2$  ( $L_1=11.5\text{mm}$ ,  $W_1=11.75\text{mm}$ ,  $W_2=3\text{mm}$ ,  $g=0.3\text{mm}$ ,  $h=1.6\text{mm}$  and  $\epsilon_r=4.4$ )

#### 3.4.2.4 Variation in reflection co-efficient with $W_2$

The effect of strip width  $W_2$  on reflection co-efficient is shown in Fig. 3.24. From the figure it is clear that there is a lower shift in resonant frequency with the increase in strip width. This is due to the increase in average length of the surface current path with  $W_2$ . This can be verified from the surface current plot given in Fig.3.33.



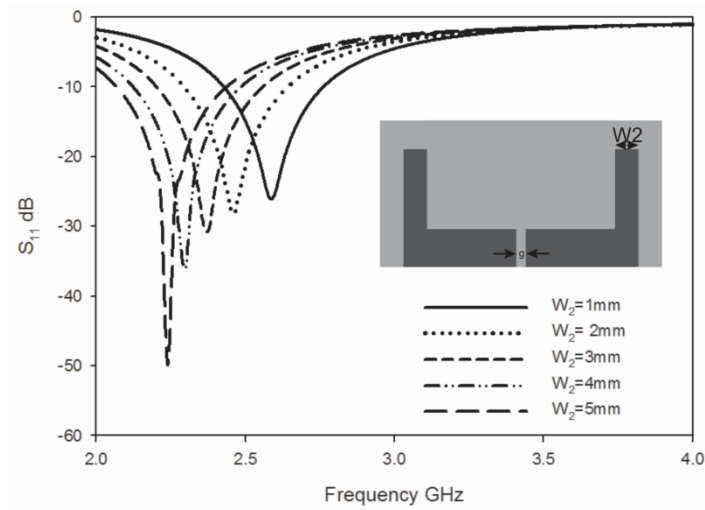


**Fig.3.24** Variation in  $S_{11}$  with  $W_2$  ( $L_1=11.5\text{mm}$ ,  $W_1=11.75\text{mm}$ ,  $L_2=3.5\text{mm}$ ,  $g=0.3\text{mm}$ ,  $h=1.6\text{mm}$  and  $\epsilon_r=4.4$ )

The variation in distributed parameters with  $W_2$  is shown in Fig.3.25. As  $W_2$  increases, the capacitance increases while the inductance decreases. This will result in a lower shift in resonant frequency with a decrease in percentage bandwidth. The selectivity will also increase with  $W_2$ .

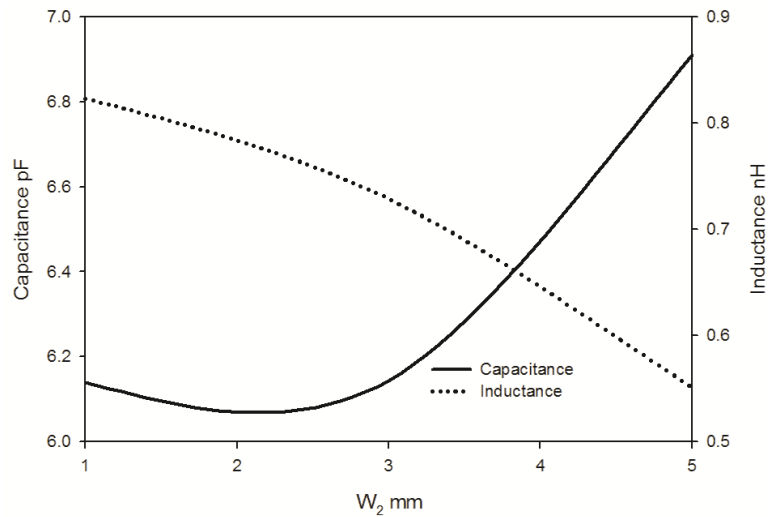


**Fig.3.25** Variation of Distributed Capacitance and inductance with  $W_2$  ( $L_1=11.5\text{mm}$ ,  $W_1=11.75\text{mm}$ ,  $L_2=3.5\text{mm}$ ,  $g=0.3\text{mm}$ ,  $h=1.6\text{mm}$  and  $\epsilon_r=4.4$ )

### 3.4.2.5 Variation in reflection co-efficient with h

The characteristic impedance of a slotline is a function of height of the substrate also. Thus it may have some impact on the reflection co-efficient and this effect is analyzed in this session. The effect of substrate height on reflection co-efficient of the antenna is given in Fig.3.26. From the figure it is found that the resonant frequency is slightly shifted towards the lower side with increase in h. As h increases, the fringing field inside the substrate increases which in turn increases the distributed capacitance. This increased capacitance results in a lower shift in resonant frequency. The impedance matching is also found to be varying with h. From equation 3.1 it is clear that the characteristic impedance varies with height of the substrate. Thus the variation in impedance matching of the structure is due to the change in input impedance of the antenna with h.

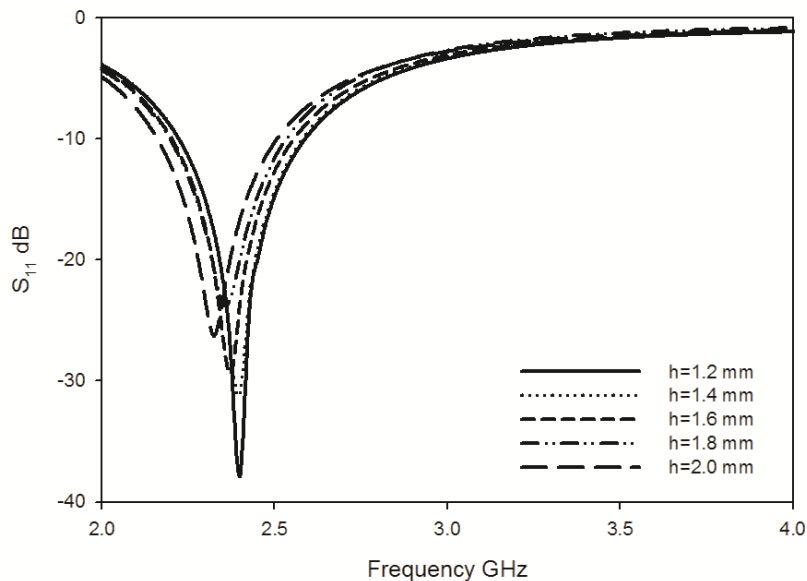


**Fig.3.26** Variation in  $S_{11}$  with height of the substrate ( $L_1=11.5\text{mm}$ ,  $W_1=11.75\text{mm}$ ,  $L_2=3.5\text{mm}$ ,  $W_2=3\text{mm}$ ,  $g=0.3\text{mm}$  and  $\epsilon_r=4.4$ )

### 3.4.3 Design Equations

From the parametric analysis of the structure and the numerical results obtained, the design equation for the antenna is obtained as

$$2 \times (L_1 + W_1) + W_2 - (0.5 \times L_2) \approx 0.625\lambda_g$$

Where  $\lambda_g$  is the guided wavelength which can be calculated from the free space wavelength  $\lambda_0$  as

$$\lambda_g = \lambda_0 / \sqrt{\epsilon_{eff}}$$

where  $\epsilon_{eff} = (\epsilon_r + 1)/2$  is the effective dielectric constant.

In order to validate the design equation, the parameters of the antennas resonating at 2.4 GHz are computed for different substrates (Table 3.1) and Table 3.2 shows the computed geometric parameters of the antenna.

**Table 3.1** Substrate Description

	<b>Antenna A</b>	<b>Antenna B</b>	<b>Antenna C</b>	<b>Antenna D</b>
<b>Laminate</b>	Rogers 5880	FR4 Epoxy	Rogers RO3006	Rogers6010LM
<b>h(mm)</b>	1.57	1.6	1.28	0.635
$\epsilon_r$	2.2	4.4	6.15	10.2
$\epsilon_{re}$	1.6	2.7	3.575	5.6
<b>g(mm)</b>	0.1	0.3	0.65	0.775

**Table 3.2** Computed Geometric Parameters of the Antenna

<b>Parameter (mm)</b>	<b>Antenna A</b>	<b>Antenna B</b>	<b>Antenna C</b>	<b>Antenna D</b>
<b>L<sub>1</sub></b>	14.9	11.5	10	7.95
<b>W<sub>1</sub></b>	15.25	11.85	10.21	8.15
<b>L<sub>2</sub></b>	4.55	3.5	3.04	2.43
<b>W<sub>2</sub></b>	3.9	3	2.6	2.1

The simulated  $S_{11}$  parameters of the antennas developed using the parameters given in the tables 3.1 and 3.2 are shown in Fig. 3.27. From the figure it is clear that all the developed antennas are operating in the 2.4 GHz WLAN band.

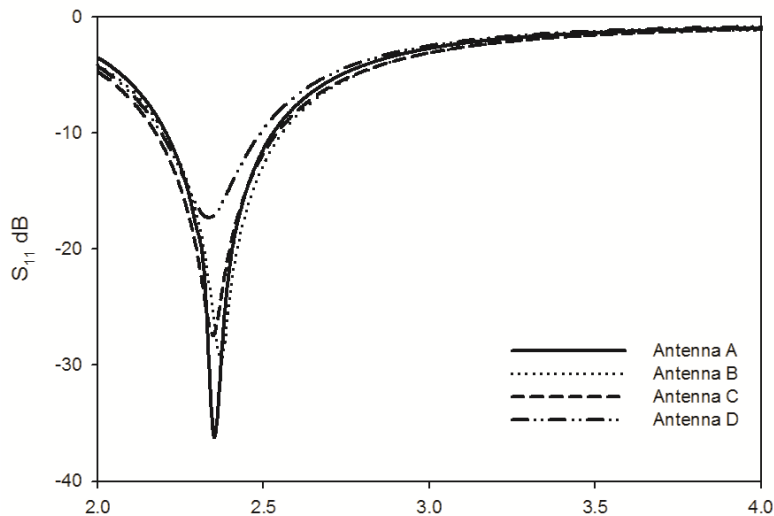


**Fig.3.27** Reflection co-efficient of the single band antenna with computed geometric parameters for different substrates.

The validation of the design equations are experimentally done for different bands also. The dimensional parameters of the antenna developed in FR4 substrate with dielectric constant 4.4 and thickness 1.6mm for different bands and their performance are depicted in the table 3.3.

**Table 3.3** Computed Geometric Parameters of the Antenna operating in different frequencies.

Designed Frequency	900 MHz	1.8 GHz	2.4 GHz	5.2 GHz
$L_1$	30.7	15.3	11.5	5.3
$W_1$	31.6	15.8	11.85	5.5
$L_2$	9.3	4.7	3.5	1.6
$W_2$	8	4	3	1.4
Resonate at	918 MHz	1.82 GHz	2.38 GHz	5.19 GHz

### 3.4.4 Coplanar strip fed Single band dipole for 2.4 GHz WLAN Band

From the design equations developed an optimized single band dipole antenna suitable for 2.4 GHz ISM band is developed and studied. The results are discussed as follows.

#### 3.4.4.1 Structure of Single band dipole

The structure of the proposed antenna is shown in Fig. 3.28. The parameters of the antenna are  $L_1=11.5\text{mm}$ ,  $W_1=11.85\text{mm}$ ,  $L_2=3.5\text{mm}$ ,  $W_2=3\text{mm}$ ,  $g=0.3\text{mm}$ . The antenna is fabricated on the commercially available FR4 substrate having height  $h=1.6\text{mm}$  relative dielectric constant  $\epsilon_r=4.4$  and loss tangent  $\tan\delta=0.02$ . The derived antenna has an overall dimension of  $30\text{mm}\times 15\text{mm}$  which is same as that of the parental OES.

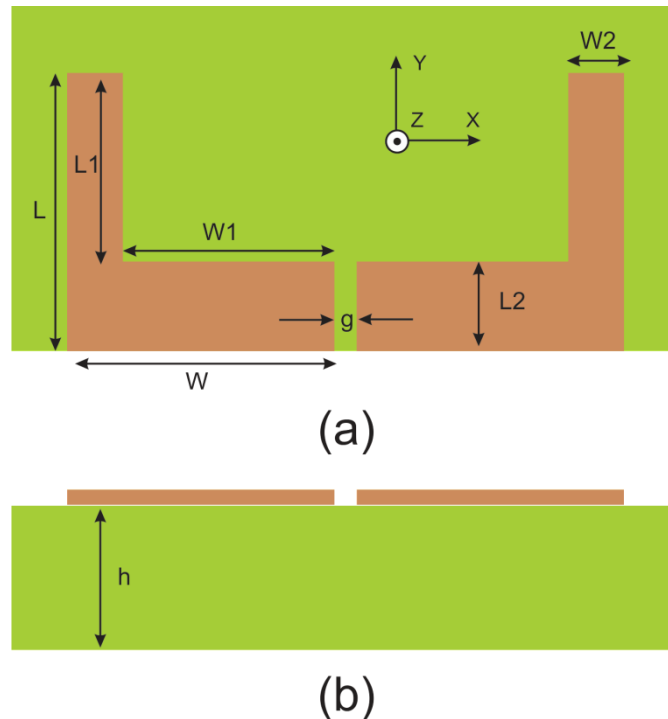


**Fig.3.28** Structure of the Single Band Dipole Antenna (a) Top view (b) Side view ( $L_1=11.5\text{mm}$ ,  $W_1=11.85\text{mm}$ ,  $L_2=3.5\text{mm}$ ,  $W_2=3\text{mm}$ ,  $g=0.3\text{mm}$ ,  $h=1.6\text{mm}$  and  $\epsilon_r=4.4$ )

### 3.4.4.2 Return Loss characteristics of Single band dipole

Simulated and measured return loss of the single band antenna derived from the OES is shown in Fig. 3.29. which are in good agreement. The antenna resonates at 2.38 GHz and offers a bandwidth of 0.46 GHz from 2.13 GHz to 2.59 GHz which is wide enough to cover the IEEE 2.4 GHz WLAN application band. The antenna offers good impedance matching also.

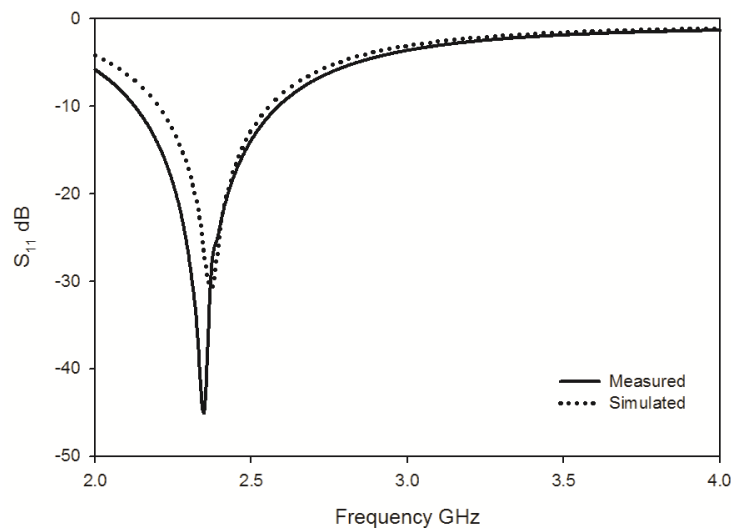


**Fig.3.29** Reflection co-efficient of the Single Band Dipole Antenna ( $L_1=11.5\text{mm}$ ,  $W_1=11.85\text{mm}$ ,  $L_2=3.5\text{mm}$ ,  $W_2=3\text{mm}$ ,  $g=0.3\text{mm}$ ,  $h=1.6\text{mm}$  and  $\epsilon_r=4.4$ )

### 3.4.4.3. Radiation characteristics of Single band dipole

The on axis received power measured by a pickup horn antenna of the single band dipole antenna derived from the OES at a distance of 30 cm is shown in Fig.3.30. From the figure it is clear that the derived structure exhibits not only good reflection characteristics but also good transmission characteristics. At the resonating frequency band, the single band structure radiate effectively than other frequencies. A transmission power level difference of about 30 dB is present between the operating band and other frequencies.

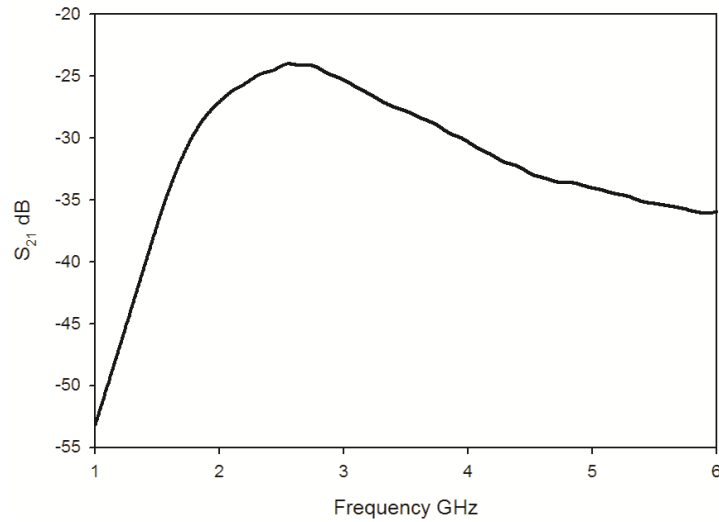


**Fig.3.30** Radiated power from the single band antennae picked by a standard horn antenna ( $L_1=11.5\text{mm}$ ,  $W_1=11.85\text{mm}$ ,  $L_2=3.5\text{mm}$ ,  $W_2=3\text{mm}$ ,  $g=0.3\text{mm}$ ,  $h=1.6\text{mm}$  and  $\epsilon_r=4.4$ )

The three dimensional radiation pattern of the single band dipole antenna at the resonant frequency is shown in Fig. 3.31. The antenna offers a figure of eight pattern along the E plane and a non directional pattern in the H plane. The beam power is found to be maximum in the direction of open end of the antenna.

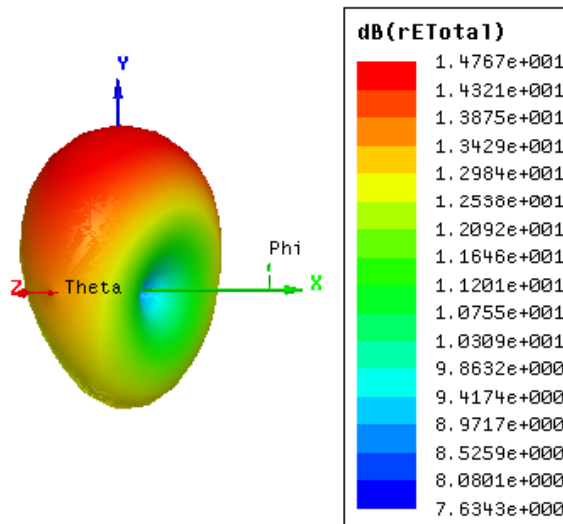


**Fig.3.31** Three dimensional Radiation Pattern of Single band Dipole ( $L_1=11.5\text{mm}$ ,  $W_1=11.85\text{mm}$ ,  $L_2=3.5\text{mm}$ ,  $W_2=3\text{mm}$ ,  $g=0.3\text{mm}$ ,  $h=1.6\text{mm}$  and  $\epsilon_r=4.4$ )

Two dimensional radiation patterns of the single band antenna in the two principal planes are shown in Fig. 3.32. Along E plane, the antenna offers a radiation pattern which offers a very small front to back ratio of nearly 1 dB. The cross polar level in the E plane is better than -25 dB along the bore sight direction. In the H principal plane the antenna offers a nearly constant power pattern with a small front to back ratio of 3 dB. A cross polar level better than 35 dB is present in the H plane pattern. From the co polar and cross polar measurement it is found that the antenna is polarized along X direction with beam maxima pointed towards positive Y direction.

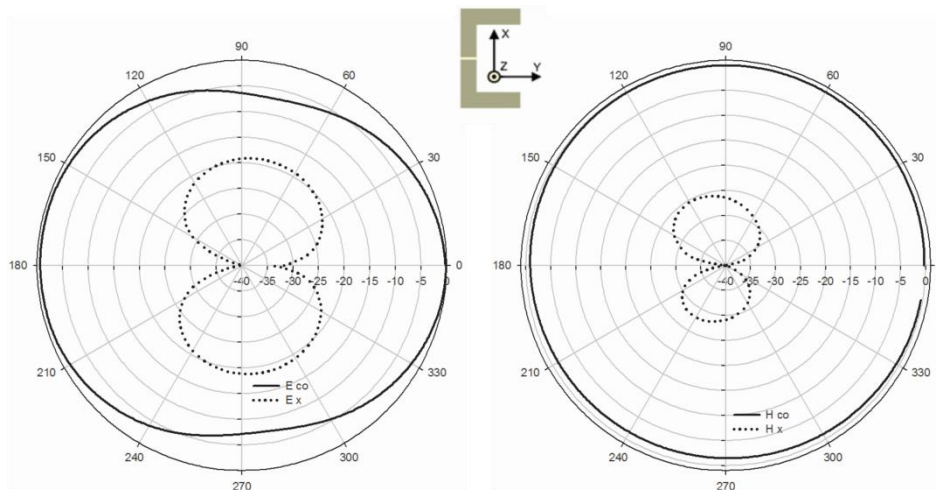


**Fig.3.32** Two dimensional Radiation Pattern of Single band Dipole ( $L_1=11.5\text{mm}$ ,  $W_1=11.85\text{mm}$ ,  $L_2=3.5\text{mm}$ ,  $W_2=3\text{mm}$ ,  $g=0.3\text{mm}$ ,  $h=1.6\text{mm}$  and  $\epsilon_r=4.4$ )

#### 3.4.4.4. Surface current analysis of Single band dipole

Simulated surface current distribution of the single band dipole at the resonant frequency is shown in Fig. 3.33. From the figure it is clear that the resonance is due to the half wavelength long variation of surface current present in the antenna strips. The two L shaped current paths are additive in nature and therefore contributes to the radiation. Since the current path is oriented along X direction, the antenna is X polarized.



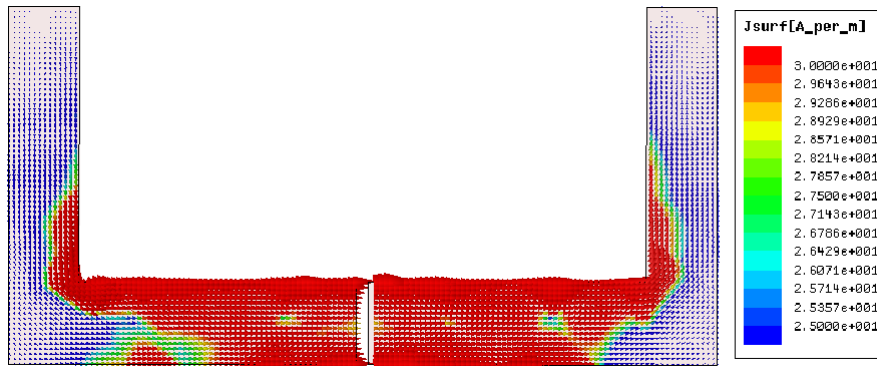


**Fig.3.33** Surface current Distribution of Single band Dipole ( $L_1=11.5\text{mm}$ ,  $W_1=11.85\text{mm}$ ,  $L_2=3.5\text{mm}$ ,  $W_2=3\text{mm}$ ,  $g=0.3\text{mm}$ ,  $h=1.6\text{mm}$  and  $\epsilon_r=4.4$ )

### 3.4.4.5 Gain and Radiation efficiency of Single band dipole

The measured gain of the antenna at the entire operating band is shown in Fig. 3.34 as solid line. The antenna offers an average gain of 2.71dB in the entire operating band and this is slightly larger than that of the dipoles. This may be due to the structural specialty of the antenna. The upward strip in the antenna not only acts as a part of the resonating structure but also contributes to direct the radiating energy in the upward (positive Y) direction.

The radiation efficiency of the antenna in the entire operating band is shown in Fig. 3.34 as dotted line. The antenna offers an average efficiency of 85% in the operating band. This high efficiency can be explained from the surface current distribution of the antenna. Almost all the metallic part of the antenna contributes to the radiation and the current present in the surfaces are additive in nature. This results in the high efficiency of the structure.

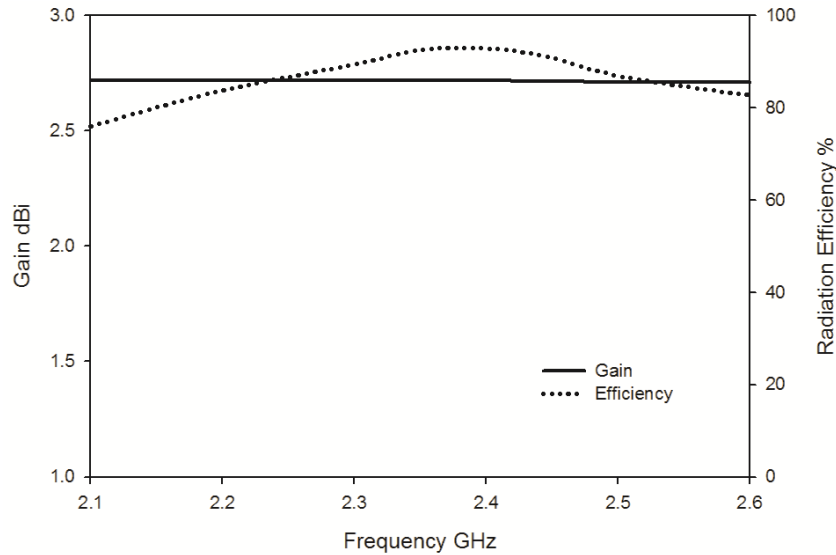


**Fig.3.34** Measured Gain and Radiation Efficiency of Single band Dipole ( $L_1=11.5\text{mm}$ ,  $W_1=11.85\text{mm}$ ,  $L_2=3.5\text{mm}$ ,  $W_2=3\text{mm}$ ,  $g=0.3\text{mm}$ ,  $h=1.6\text{mm}$  and  $\epsilon_r=4.4$ )

### 3.4.5 BALUN-Microstrip to CPS transition

Since the antenna discussed in this session is a balanced structure, there is a chance of mismatch at the SMA connector due to the transition from unbalanced to balanced transmission line. But in all the previous studies even though a balun is not used, the antenna doesn't show any degradation in performance. In order to substantiate this, the analysis of antenna characteristics are performed using a balun and the results are compared with those obtained without balun. This study is discussed in this session.

#### 3.4.5.1 Structure and S parameters of the BALUN

The structure of the developed balun is shown in Fig. 3.35. It transforms a microstrip into slotline through a shorting pin (vias). It consists of a microstrip line, from the central conductor of which a shorting pin is there to carry the energy in one perfect electric conductor of the CPS in the bottom side. The width of the ground plane in the bottom side is narrow downed suddenly at the

position of shorting. This narrow ground plane is used as the second conductor of the balanced coplanar strip.

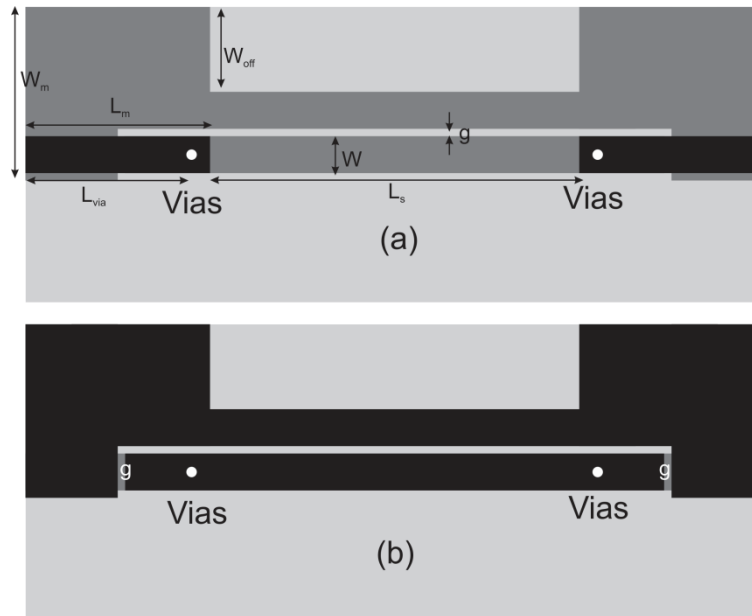


**Fig.3.35** Structure of twin balun (a) Top view (b) Bottom View ( $L_m=20$  mm,  $W_m=17.5$ mm,  $L_s=30$ mm,  $W_{off}=10$ mm,  $W=3$ mm,  $L_{via}=18$ mm,  $g=0.3$ mm,  $h=1.6$ mm)

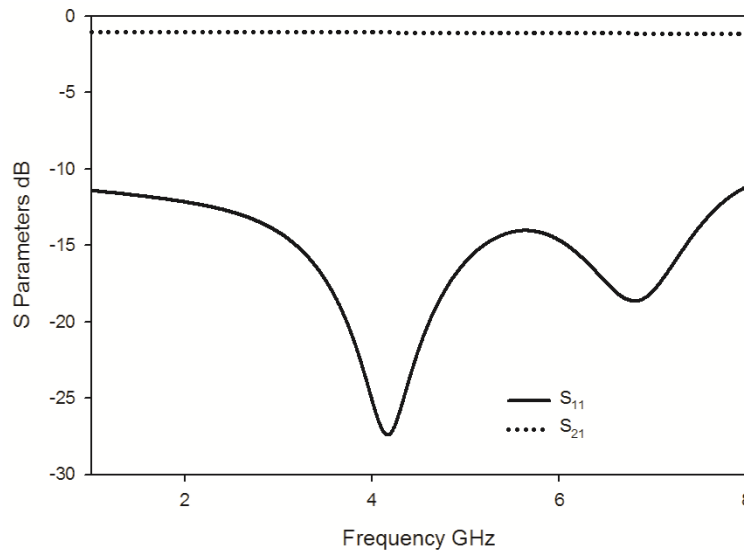


**Fig.3.36** Scattering parameters of twin balun ( $L_m=20$  mm,  $W_m=17.5$ mm,  $L_s=30$ mm,  $W_{off}=10$ mm,  $W=3$ mm,  $L_{via}=18$ mm,  $g=0.3$ mm,  $h=1.6$ mm)

The back to back Scattering parameter characteristic of the microstrip to Slotline balun is given in Fig.3.36. It has to be noted that the back to back insertion loss of a twin balun system is 1.01 dB at 2.4 GHz. This insertion loss is mainly due to two discontinuities present in the twin balun. Thus a single balun system has an insertion loss of 0.505 dB which is very small.

#### 3.4.5.2 Surface current analysis of BALUN

The intensity of surface current at 2.5 GHz in the twin balun is shown in Fig.3.37. At two far ends, the intensity of current is found to be different in two PEC parts and therefore that region of the structure is unbalanced. But at the centre part of the structure, it can be clearly inferred that both the conductors have almost similar surface current intensity. Thus the central portion ie the coplanar strip part of the structure is a balanced transmission line.

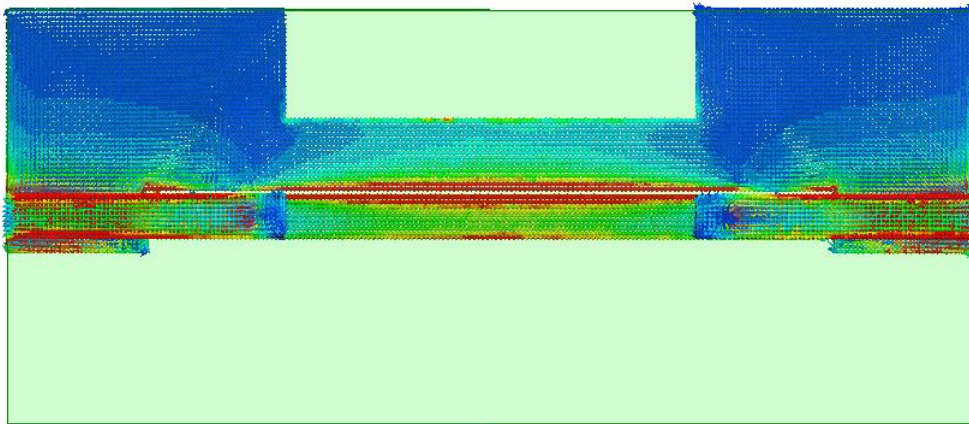


**Fig.3.37** Surface current intensity of twin balun at 2.5 GHz

#### 3.4.5.3 Antenna Characteristics with and without BALUN

For comparison of the single band antenna parameters with and without balun, an antenna is fabricated with an integrated balun. The structure of the antenna with integrated balun is shown in Fig. 3.38. Now the antenna structure

consist of an unbalanced transmission line which is a microstrip, a transition from unbalanced to balanced transmission line and a balanced transmission line which is a coplanar strip to which the antenna is directly connected. Thus the integration of balun results in a huge increase in the dimension of the antenna.

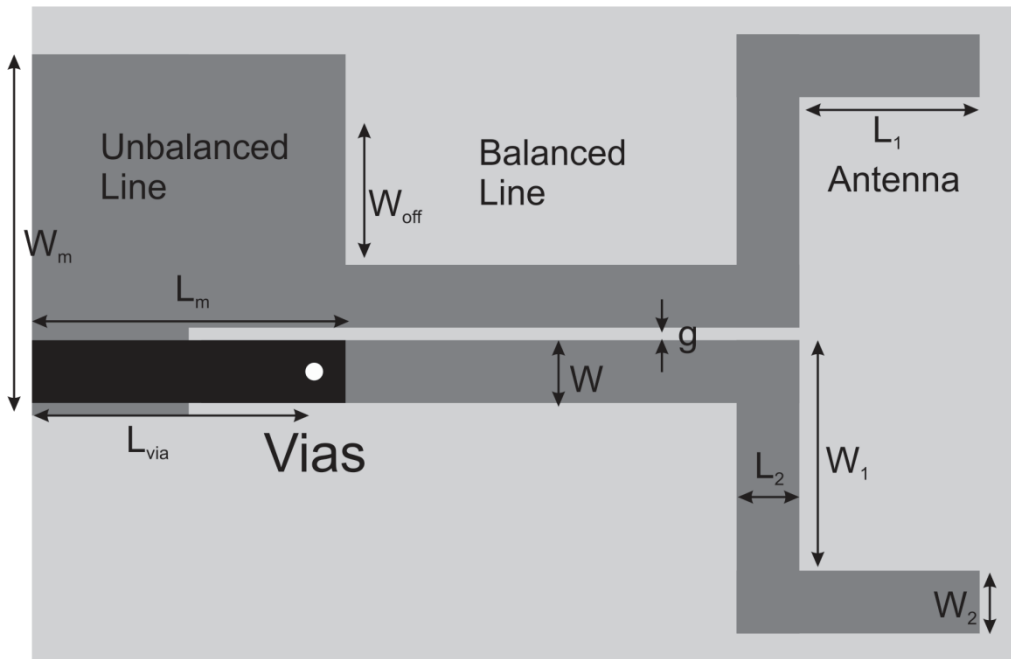


**Fig.3.38** Structure of antenna with integrated BALUN ( $L_m=20$  mm,  $W_m =17.5$ mm,  $W_{off}=10$ mm,  $W=3$ mm,  $L_{via}=18$ mm,  $g=0.3$ mm,  $h=1.6$ mm)

The reflection co-efficient of the antenna with and without the integrated balun is shown in Fig.3.39. From the Figure it is clear that there is a good agreement with both the curves. The matching of the antenna structure with integrated balun is slightly less than that without BALUN. The band width resonant frequency etc remains almost same in both the cases which implies that there is no mismatch problems when connecting a coaxial SMA connector directly to the antenna structure.

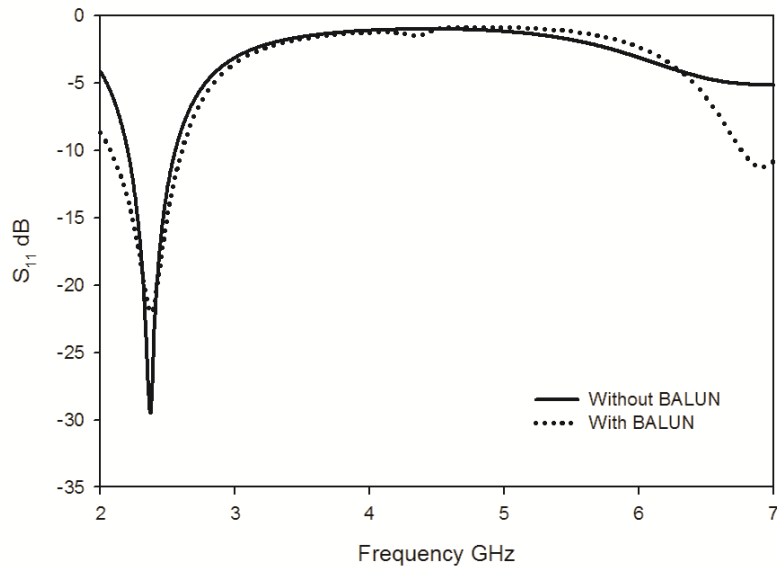


**Fig.3.39** Reflection co-efficient of the antenna with and without integrated BALUN

The radiation patterns of the antenna without and with integrated balun are shown in Fig. 3.40(a) and Fig 3.40(b) respectively. Both the pattern shows same polarization characteristics ie X polarized with power null on the same axis. Beam width of the antenna with integrated balun is slightly enhanced. This may be due to the scattering of wave by reflection from metallic parts of the balun. Power density towards the positive Y direction is slightly improved in the case of antenna with integrated balun. This is because of the reflection from metallic parts of the balun structure. Since CPS fed antenna has an inherent property of directionality towards the open end of the antenna, the enhancement due to reflection from balun is negligible.

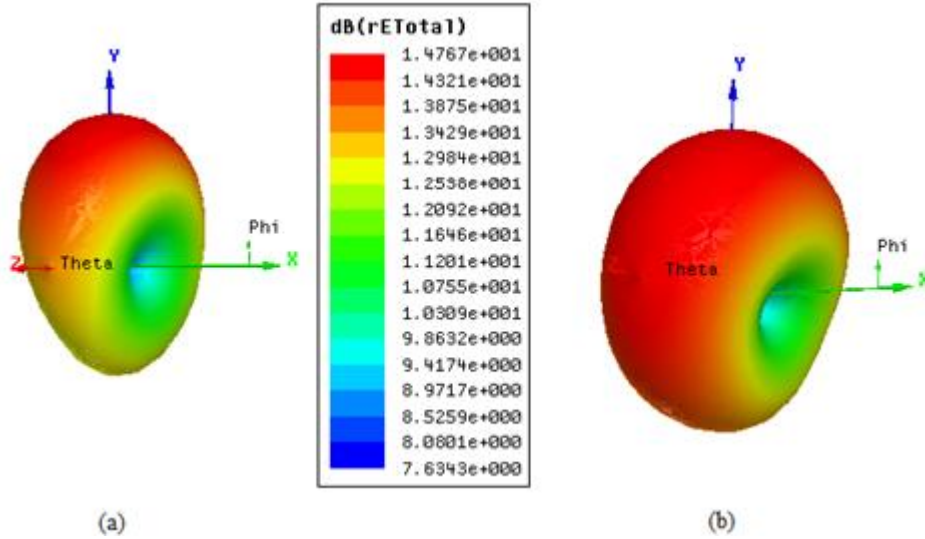


**Fig.3.40** Radiation pattern of the antenna at 2.38 GHz (a) without integrated BALUN and (b) with integrated balun

**Table.3.4** Comparison between the antennas with and without balun

Characteristics	CPS fed Single band antenna (With BALUN)	CPS fed Single band antenna (Without BALUN)
Resonance and Return loss	At 2.40 (-20 dB)	At 2.38 GHz (-30 dB)
Radiation Pattern	Slightly directional pattern with beam maxima towards Y direction.	Slightly directional pattern with beam maxima towards Y direction
Polarization	Along X direction	Along X direction
Gain	3.12 dBi	2.7 dBi
Area	50 mm x 75 mm $\epsilon_r=4.4, h= 1.6$ mm	30 mm x 15 mm $\epsilon_r=4.4, h= 1.6$ mm
Area reduction	-	Nearly 83 % compared to the antenna with balun
Efficiency	89%	85%

A comparison of parameters of the single band antenna with and without BALUN is summarized in Table. 3.4. There is no considerable difference in impedance matching. The gain and radiation efficiency of the antenna are enhanced by 0.42 dBi and 4% respectively. These enhancements in gain and

efficiency are attained by sacrificing the compactness of the antenna. Thus it is the discretion of the designer to choose the suitable configuration. The CPS fed antenna without the balun is highly useful in applications where compactness is a great concern, but at the cost of lesser gain. Since compact antenna design is our primary aim the balun less configuration is taken for the further studies.

### 3.5 Dual band Dipole Antenna

In this session the study is vectored to the development of dual band antenna from the single band dipole antenna discussed in previous session. The dual banding is attained without sacrificing the advantages of the single band antenna. After dual banding, the size of the antenna also remains the same. The technique of dual banding, the variation analysis, the antenna characteristics, gain and efficiency etc are analyzed thoroughly in this session.

#### 3.5.1 Evolution of Dual band dipole antenna from single band dipole

The derivation of dual band antenna from the single band dipole is shown in Fig. 3.41. The dual band dipole is derived from the pre discussed single band dipole by adding two metallic strips of dimension  $L_3 \times W_2$  on both arms of the single band antenna symmetrically in either side of the gap  $g$ . This addition of new strips will create additional current paths which results in another resonance.

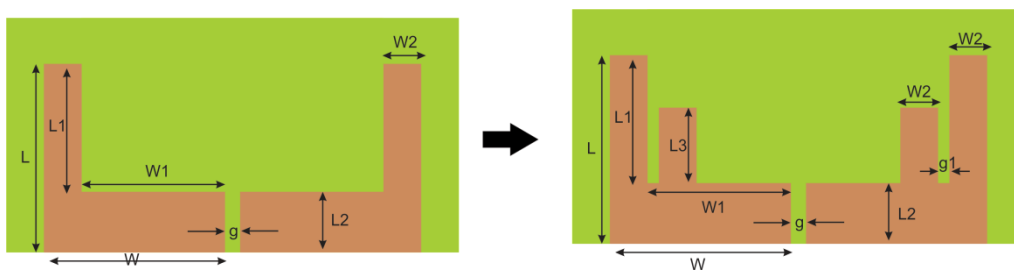


**Fig.3.41** Evolution of Dual Band Dipole antenna from Single band Antenna



The simulated reflection co-efficient of the structure after adding a strip of dimension  $L_3=5\text{mm}$  and  $W_2=3\text{ mm}$  with a gap  $g_1=0.5\text{ mm}$  from the initial strip is shown in Fig. 3.42. The newly developed antenna is resonating at two frequencies. The first resonance is found to be at 2.4 GHz with a bandwidth of 375 MHz and the second resonance is at 5.125 GHz with a bandwidth of 100 MHz. From the figure it is clear that the addition of the new strips doesnot affect the first resonance and additionally creates one new resonance. The dimension of the derived dual band antenna remains the same as that of the single band dipole discussed in the former session.

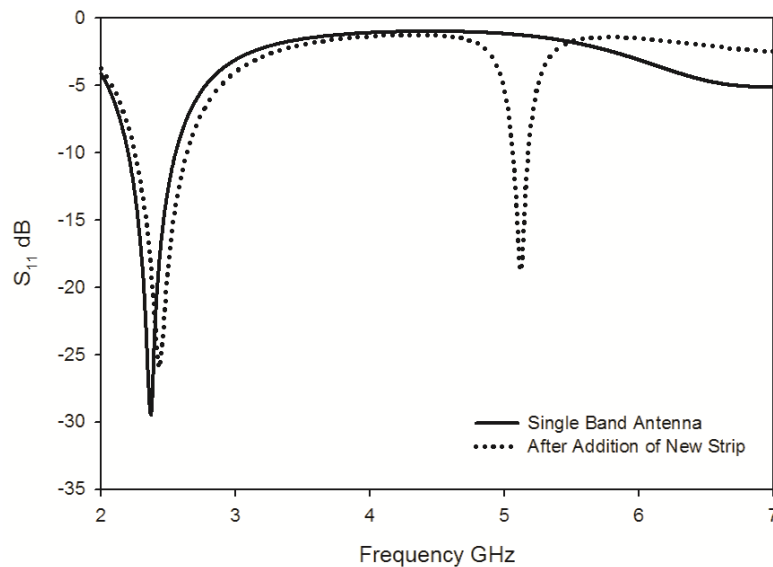


**Fig.3.42**  $S_{11}$  of Dual band Dipole antenna developed from Single band Antenna

### **3.5.2 Parametric Analysis**

For the optimization of the dual band antenna and the development of design equation for the same, the parametric analysis is very important. The variations of reflection co efficient of the antenna and the corresponding

changes in distributed inductance and capacitance with different dimensional parameters are analyzed thoroughly and are discussed in the following sessions.

### 3.5.2.1 Variation of reflection co-efficient with $L_1$

The variation of reflection co-efficient with strip length  $L_1$  is shown in Fig. 3.43. From the figure it is clear that both the resonance were affected by the change in strip length  $L_1$ . Both the resonance are lowered with the parameter  $L_1$ . This is because as the  $L_1$  increases the resonance current path length increases and correspondingly resonant frequency decreases. This can be verified from the surface current plot given in Fig. 3.63 and 3.64. The band width of the first resonance remains constant with  $L_1$ . But at second resonance the band width increases with increase in  $L_1$ . This may be due to increase in distributed inductance with strip length  $L_1$  in the second resonance frequency.

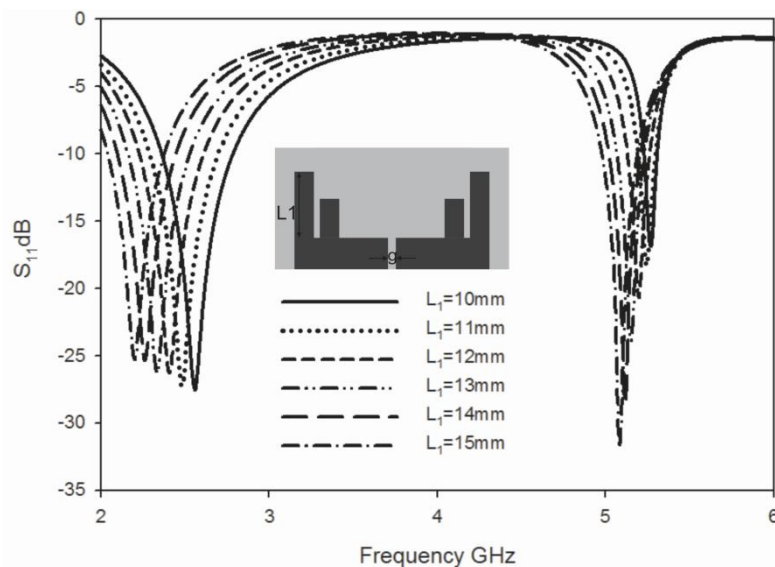


**Fig.3.43** Reflection co-efficient for different  $L_1$  ( $W_1=11.75\text{mm}$ ,  $L_2= 3.5\text{mm}$ ,  $W_2=3\text{mm}$ ,  $L_3=6.8\text{mm}$ ,  $g=0.3\text{mm}$ ,  $g_1=0.5\text{mm}$  and  $\epsilon_r=4.4$ )

From the above figure it is also to be noted that the matching of second resonance reduces with decrease in  $L_1$ . The variation of reflection co efficient of

the antenna for small values of  $L_1$  is shown in Fig. 3.44. The interesting factor inferred from the figure is that there is no second resonance when  $L_1 < L_3$ . This is due to the capacitive loading in the second resonance current path (which is clear from Fig 3.64.). As the length  $L_1$  approaches to  $L_3$  or less than  $L_3$ , the strip with length  $L_3$  will insert heavy distributed capacitance on the strip with  $L_1$ . This will change the impedance of the antenna at this frequency and deteriorates the matching. This can be verified from the imaginary part of the impedance of the antenna given in Fig. 3.45 (b). Near the second resonance region the impedance is purely capacitive.

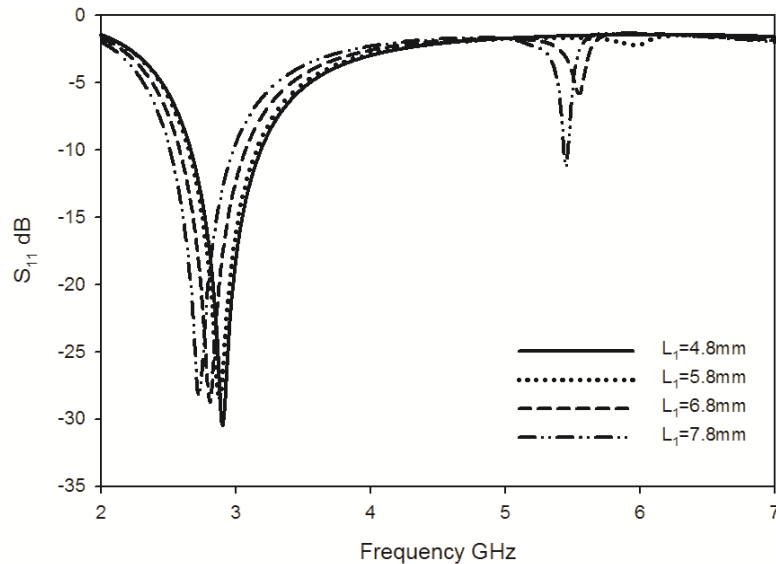


**Fig.3.44** Reflection co-efficient for small values of  $L_1$  ( $W_1=11.75\text{mm}$ ,  $L_2=3.5\text{mm}$ ,  $W_2=3\text{mm}$ ,  $L_3=6.8\text{mm}$ ,  $g=0.3\text{mm}$ ,  $g_1=0.5\text{mm}$  and  $\epsilon_r=4.4$ )

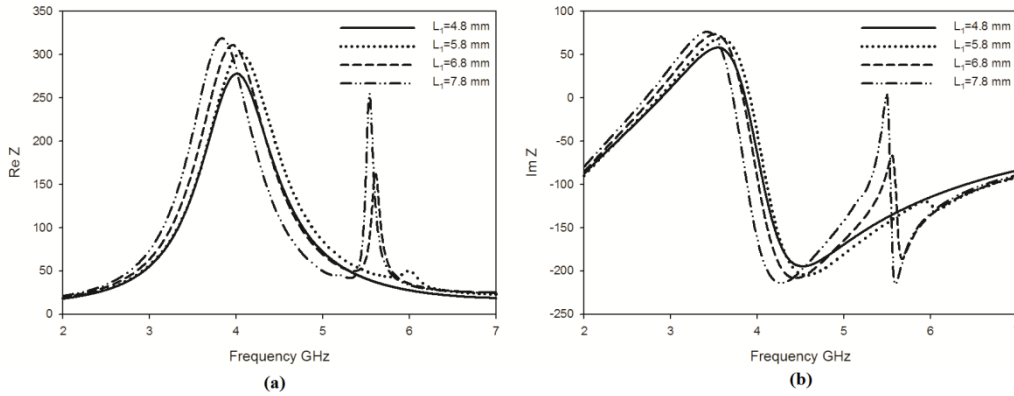


**Fig.3.45** (a) Real part and (b) Imaginary part of impedance for small values of  $L_1$ . ( $W_1=11.75\text{mm}$ ,  $L_2= 3.5\text{mm}$ ,  $W_2=3\text{mm}$ ,  $L_3=6.8\text{mm}$ ,  $g=0.3\text{mm}$ ,  $g_1=0.5\text{mm}$  and  $\epsilon_r=4.4$ )

The variation of distributed parameters corresponding to first and second resonances with parameter  $L_1$  is shown in Fig.46 (a) and (b) respectively. From the figure it is clear that both the parameters which will results in first resonance increases with  $L_1$  while the capacitance corresponding to second resonance tends to lower with  $L_1$ . Thus for very small values of  $L_1$  the reactance is fully capacitive and there will be no second resonance. As  $L_1$  increases, the capacitance will lower and the second resonance creates and it will moves to lower side with an increase in bandwidth.

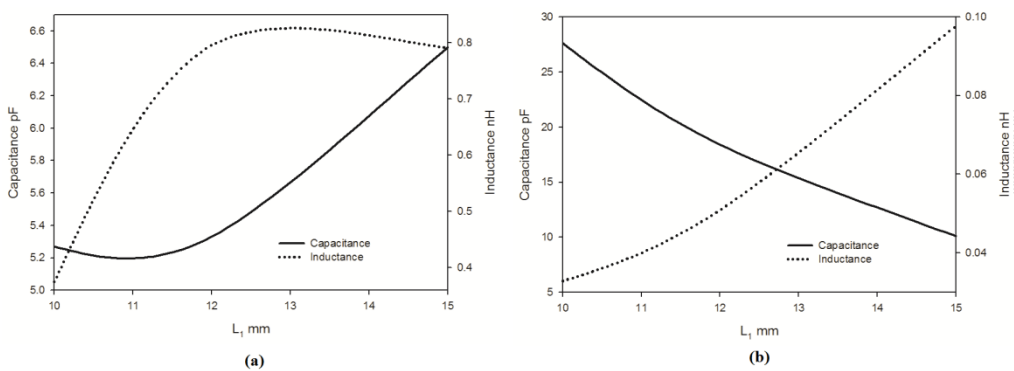


**Fig.3.46** Distributed parameters of the antenna (a) First Resonance and (b) Second Resonance for  $L_1$  ( $W_1=11.75\text{mm}$ ,  $L_2= 3.5\text{mm}$ ,  $W_2=3\text{mm}$ ,  $L_3=6.8\text{mm}$ ,  $g=0.3\text{mm}$ ,  $g_1=0.5\text{mm}$  and  $\epsilon_r=4.4$ )

### 3.5.2.2 Variation of reflection co-efficient with $W_1$

The variation of reflection co-efficient of the antenna with the parameter  $W_1$  is shown in Fig. 3.47. It is noted from the graph that as  $W_1$  increases, the frequency of first resonance decreases. The resonant current path will increase with  $W_1$  and thus the frequency reduces. The second resonance is also slightly affected with the parameter  $W_1$ . This may be due to the inductive loading in the second resonating path caused by the strip of length  $W_1$ .

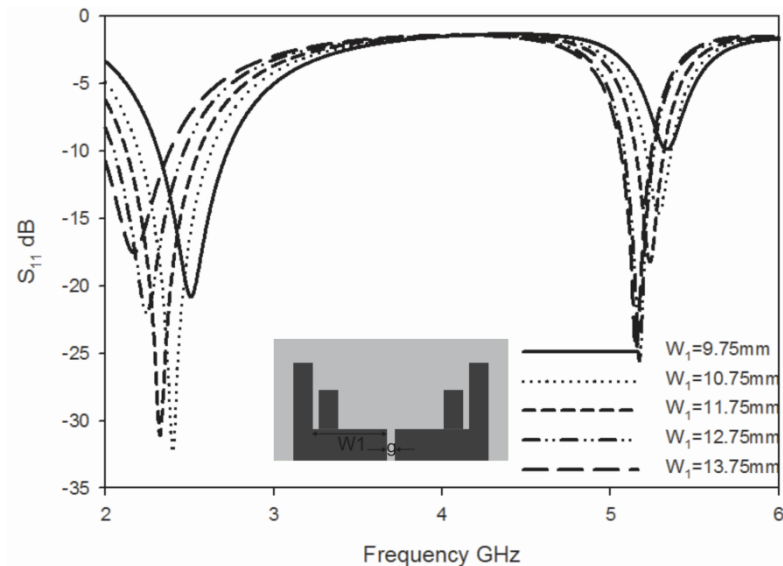


**Fig.3.47** Reflection co-efficient for different  $W_1$  ( $L_1=11.5$  mm,  $L_2= 3.5$ mm,  $W_2=3$ mm,  $L_3=6.8$ mm,  $g=0.3$ mm,  $g_1=0.5$ mm and  $\epsilon_r=4.4$ )

The variation of distributed inductance and capacitance corresponding to first and second resonances are shown in Fig. 48 (a) and (b) respectively. As  $W_1$  increases, at first resonance the inductance increases while the capacitance decreases. This will result in a lower shift in first resonance with an increase in percentage bandwidth. At second resonance also the capacitance tends to lower while the inductance increases which result in a lower shift in resonant frequency.

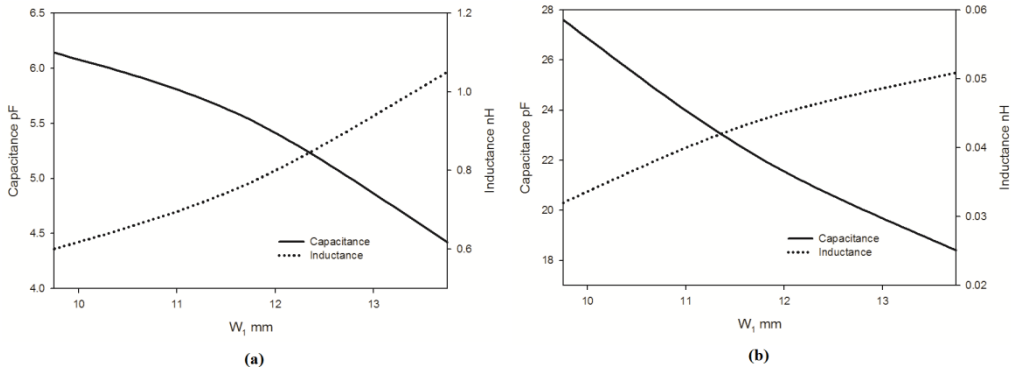


**Fig.3.48** Distributed parameters of the antenna (a) First Resonance and (b) Second Resonance with  $W_1$ . ( $L_1=11.5$  mm,  $L_2= 3.5$ mm,  $W_2=3$ mm,  $L_3=6.8$ mm,  $g=0.3$ mm,  $g_1=0.5$ mm and  $\epsilon_r=4.4$ )

### 3.5.2.3 Variation of Reflection co-efficient with $L_2$

The variation in reflection co efficient with  $L_2$  is shown in Fig. 3.49. From the plot the inference is that the first resonance is shifted towards the higher sides with  $L_2$ . The variation is similar to that in the case of length variation in OES explained in 3.3.2.1. The second resonance is not much affected with  $L_2$ .

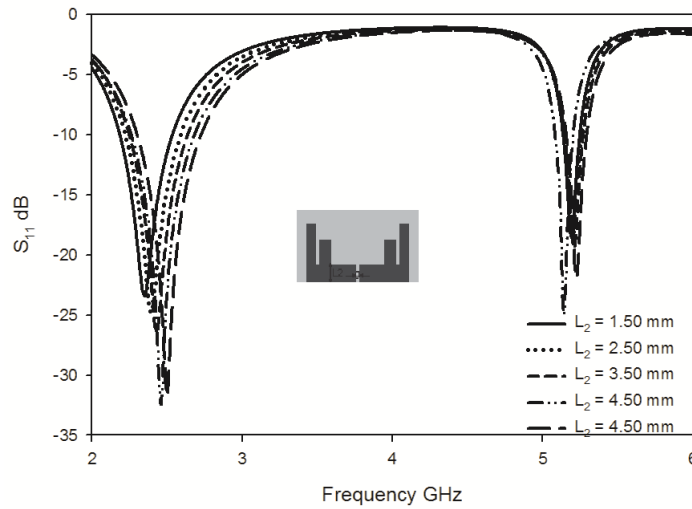


**Fig.3.49** Reflection co-efficient for different  $L_2$  ( $L_1=11.5$  mm,  $W_1=11.75$ mm,  $W_2=3$ mm,  $L_3=6.8$ mm,  $g=0.3$ mm,  $g_1=0.5$ mm and  $\epsilon_r=4.4$ )

The variation in distributed parameters of the antenna corresponding to first and second resonance with  $L_2$  are shown in Fig. 50 (a) and (b) respectively.

Capacitance corresponding first resonance increases while the inductance reduces. Both the distributed parameters which will results in second resonance remains constant for all values of  $L_2$ .

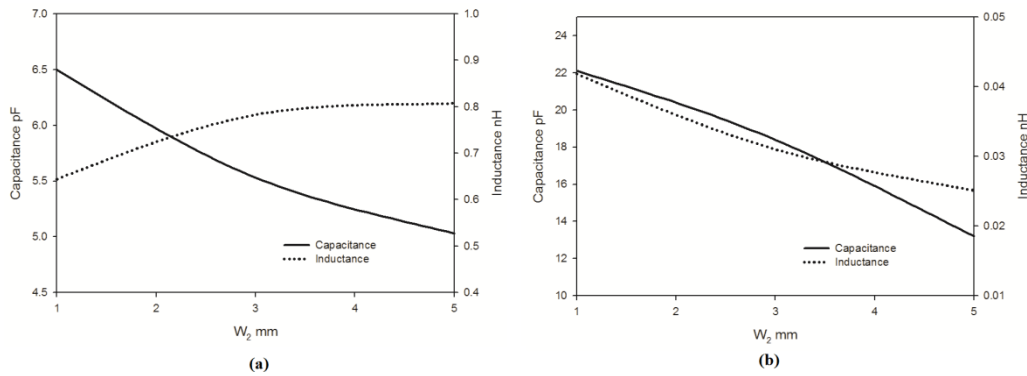


**Fig.3.50** Distributed parameters of the antenna at (a) First Resonance and (b) Second Resonance with  $L_2$ . ( $L_1=11.5$  mm,  $W_1=11.75$ mm,  $W_2= 3$  mm,  $g_1=.5$ mm,  $L_3=6.8$ mm,  $g=0.3$ mm, and  $\epsilon_r=4.4$ )

### 3.5.2.4 Variation of Reflection co-efficient with $W_2$

Variation of reflection characteristics of the antenna with the strip width  $W_2$  is shown in the Fig.3.51. There is no noticeable change in resonant frequency with the parameter  $W_2$ . The matching of either the bands are irregularly affected by the strip width  $W_2$ . The distributed reactance of a planar structure is a function of edge length and width of the planar conductive strip. Normally as the edge length increases, the inductance tends to increase and with the strip width and gap, the distributed capacitance tends to vary. In the proposed structure as the strip width varies, the reactive component ie distributed inductance and capacitance will vary which will result in the change in impedance.

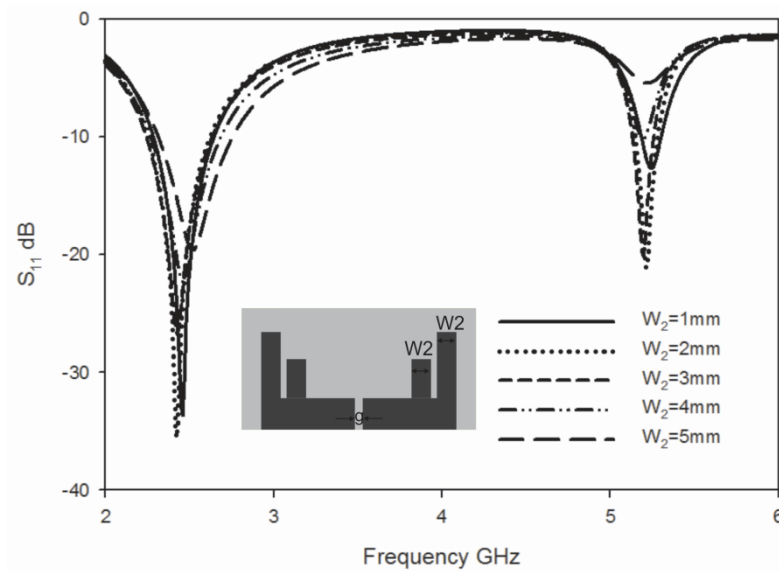


**Fig.3.51** Reflection co-efficient for different  $W_2$  ( $L_1=11.5$  mm,  $W_1=11.75$ mm,  $L_2= 3.5$ mm,  $L_3=6.8$ mm,  $g=0.3$ mm,  $g_1=0.5$ mm and  $\epsilon_r=4.4$ )

The variation in distributed capacitance and inductance of the antenna corresponding to first and second resonances as a function of  $W_2$  are shown in 3.52. From the figure it is clear that at first resonance the capacitance is found to be decreasing with  $W_2$  while the inductance is increasing. The capacitance and inductance for the second resonance shows similar variation with  $W_2$ .

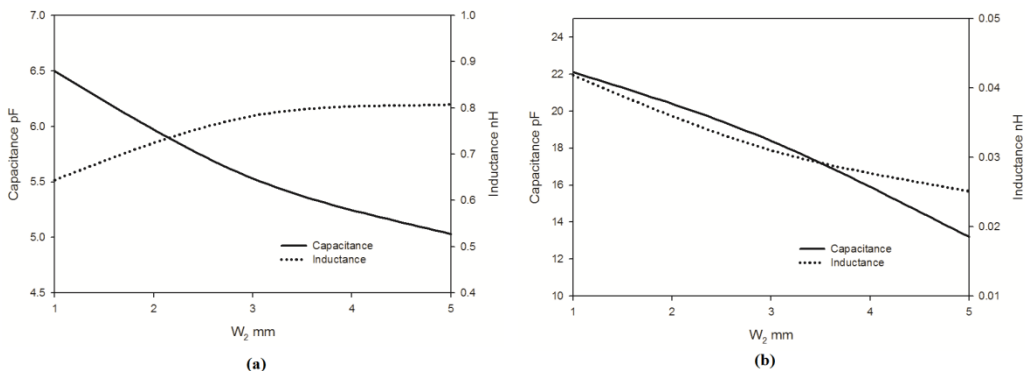


**Fig.3.52** Distributed parameters of the antenna at (a) First Resonance and (b) Second Resonance with  $W_2$ . ( $L_1=11.5$  mm,  $W_1=11.75$ mm,  $L_2= 3.5$ mm,  $g_1=.5$ mm,  $L_3=6.8$ mm,  $g=0.3$ mm, and  $\epsilon_r=4.4$ )



### 3.5.2.5 Variation of reflection co-efficient with $L_3$

The variation of reflection co-efficient of the antenna with strip length  $L_3$  is shown in Fig. 3.53. From the figure it is evident that the second resonance depends mainly on the parameter  $L_3$ . A rapid decrease in the second resonance frequency is present with a small increase in parameter  $L_3$ . This is mainly due to the quarter wavelength surface current variation present in the arm  $L_3$ (Fig 3.64.). Since the variation is quarter wavelength, a small change in  $L_3$  creates four times change in wavelength and correspondingly a large variation in the resonant frequency. Since  $L_3$  is not included in the resonant current path corresponding to first resonance, the first resonance remains unaffected with the strip length  $L_3$

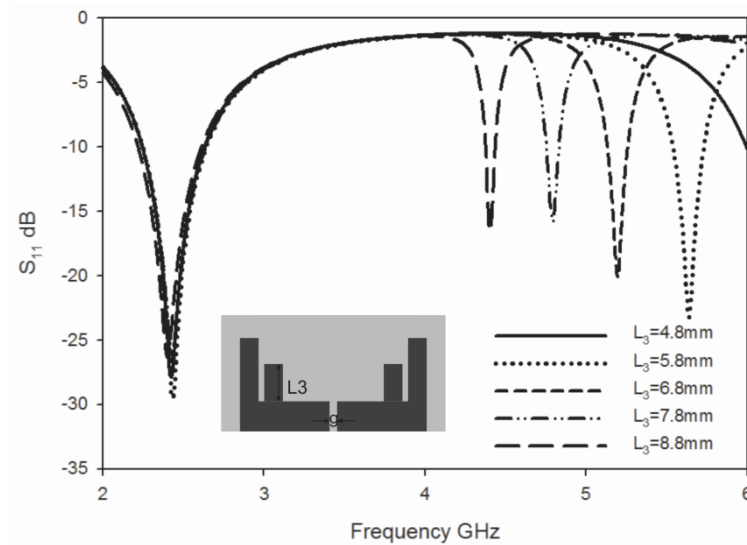


**Fig.3.53** Reflection co-efficient for different  $L_3$  ( $L_1=11.5$  mm,  $W_1=11.75$ mm,  $L_2= 3.5$ mm,  $W_2=3$ mm,  $g=0.3$ mm,  $g_1=0.5$ mm and  $\epsilon_r=4.4$ )

The variations in distributed reactive components of the antenna corresponding to first and second resonances with  $L_3$  are shown in Fig. 3.54(a) and (b). The inductance and capacitance contributing first resonance remains

constant for all values of  $L_3$ . The distributed capacitance corresponding to second resonance increases sharply while a lowering in inductance is found with  $L_3$ . Thus the second resonance will come to lower side with a reduction in bandwidth of the antenna.

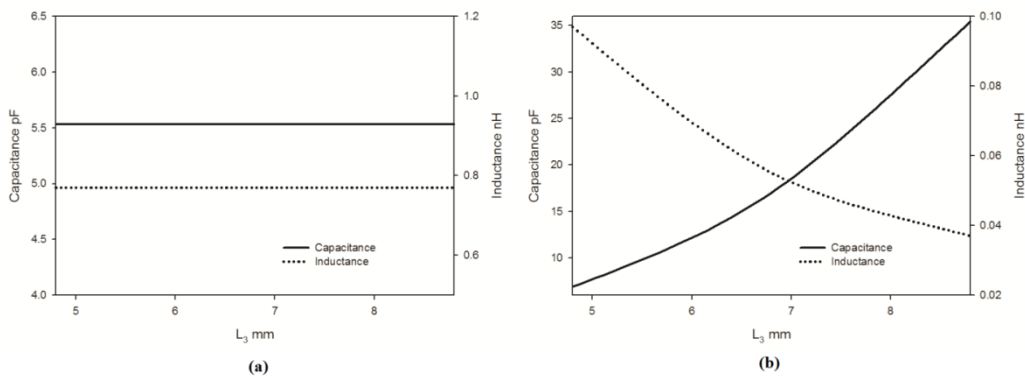


**Fig.3.54** Distributed parameters of the antenna at (a) First Resonance and (b) Second Resonance with  $L_3$ . ( $L_1=11.5$  mm,  $W_1=11.75$ mm,  $L_2= 3.5$ mm,  $W_2=3$ mm,  $g=0.3$ mm,  $g_1=0.5$ mm and  $\epsilon_r=4.4$ )

### 3.5.2.6 Variation of reflection co-efficient with $g_1$

Variation of reflection co-efficient with the gap  $g_1$  is shown in Fig.3.55, which implies that the second resonance is strongly affected with this parameter. As  $g_1$  increases, the second resonance comes to lower side and the band width remains nearly unaffected. The variation in the resonance frequency may be due to the increase in resonant path length with  $g_1$  which can be verified from the surface current distribution given in Fig.3.64. The matching of the second resonance is also affected with variation in  $g_1$ . This is because, the gap  $g_1$  adjust the capacitive reactance between the strips. As the reactance changes, the matching also changes. The first resonance remains un affected with the parameter  $g_1$ .

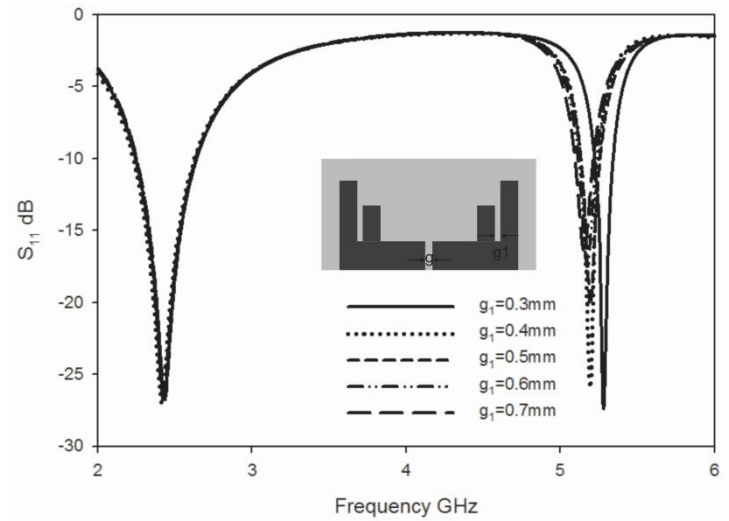


**Fig.3.55** Reflection co-efficients for different  $g_1$ . ( $L_1=11.5$  mm,  $W_1=11.75$ mm,  $L_2= 3.5$ mm,  $W_2=3$ mm,  $L_3=6.8$ mm,  $g=0.3$ mm and  $\epsilon_r=4.4$ )

The variation in capacitance and inductance corresponding to first and second resonance is shown in Fig.56 (a) and (b). The inductance and capacitance contributed by first resonant current path is remaining constant for all values of  $g_1$ . The capacitance in the second resonance is strongly affected by this parameter. The capacitance decreases with  $g_1$  and there is a small increase in inductance. This will result in a reduction in resonant frequency with a decrease in bandwidth.

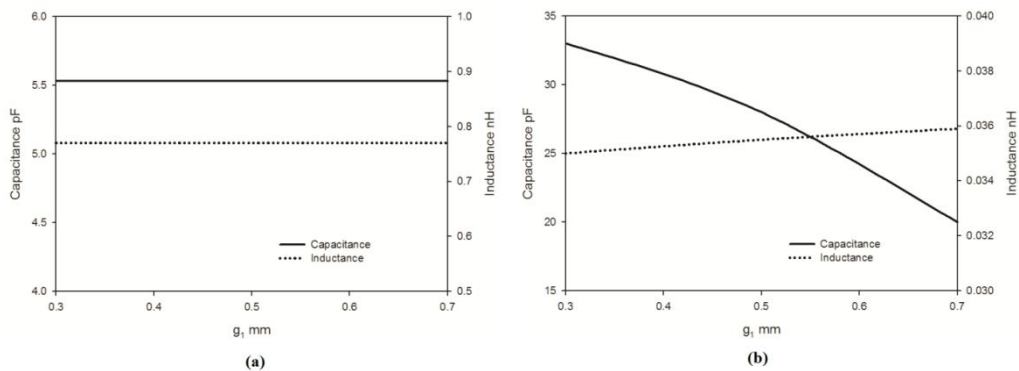


**Fig.3.56** Distributed parameters of the antenna at (a) First Resonance and (b) Second Resonance with  $g_1$ . ( $L_1=11.5$  mm,  $W_1=11.75$ mm,  $L_2= 3.5$ mm,  $W_2=3$ mm,  $L_3=6.8$ mm,  $g=0.3$ mm, and  $\epsilon_r=4.4$ )

### 3.5.3. Design Equations of dual band antenna

From the parametric analysis, the design equation for the dual band dipole in terms of the structural parameters are developed and validated. The design procedure for the dual band dipole includes the following steps. Design equation for the first resonance is given below.

$$2 \times (L_1 + W_1) + W_2 - (0.5 \times L_2) \approx 0.625 \lambda_{g1}$$

Design equation for the second resonance is given below

$$(L_1/8) + L_3 + g_1 \approx 0.113 \lambda_{g2}$$

Under the condition that  $L_1 > L_3$  otherwise no second resonance.

Where  $\lambda_{g1}$  and  $\lambda_{g2}$  are the guided wavelength corresponding to first and second resonance respectively. In order to validate the design equations, the antenna parameters were computed for different substrates (Table 3.5) and Table 3.6 shows the computed geometric parameters of the antenna.

**Table 3.5** Substrate Description

	Antenna A	Antenna B	Antenna C	Antenna D
<b>Laminate</b>	Rogers 5880	FR4 Epoxy	Rogers R03006	Rogers 6010LM
<b>h(mm)</b>	1.57	1.6	1.28	0.635
$\epsilon_r$	2.2	4.4	6.15	10.2
$\epsilon_{re}$	1.6	2.7	3.575	5.6
<b>g(mm)</b>	0.1	0.3	0.65	0.775

**Table 3.6** Computed Geometric Parameters of the Antenna

Parameter (mm)	Antenna A	Antenna B	Antenna C	Antenna D
$g_1$	0.65	0.5	0.435	0.35
$L_1$	14.9	11.5	10	7.95
$W_1$	15.25	11.75	10.21	8.15
$L_2$	4.55	3.5	3.04	2.43
$W_2$	3.9	3	2.6	2.1
$L_3$	8.8	6.8	5.9	4.72

The simulated reflection co-efficients of the antennas developed using the parameters given in the tables 3.5 and 3.6 are shown in Fig. 3.57. From the figure it is clear that all the four antennas are operated in the 2.4 and 5.2 GHz WLAN band. It is also to be noted in the figure that there is a very small shift in resonant frequencies of the antennas. This may be due to the approximation performed during the calculations of structural parameters.

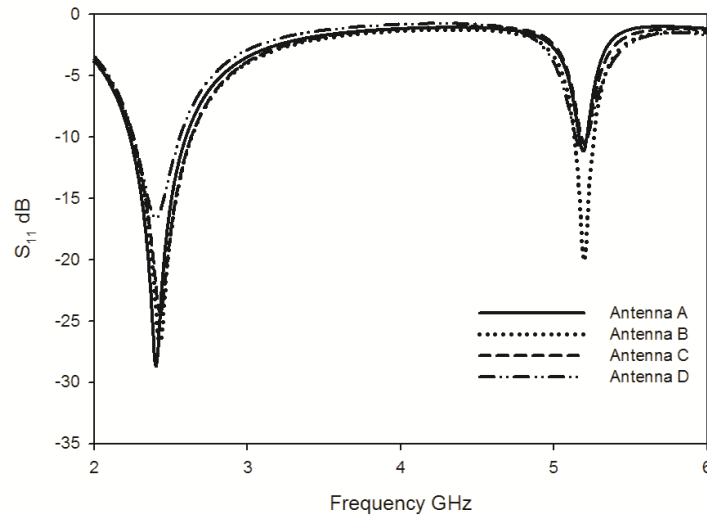


**Fig.3.57** Reflection coefficient of the Dual band antenna with computed geometric parameters for different substrates

The experimental validation is done for other frequency bands also. For this, four different antennas are fabricated in commercially available FR4 substrate with  $\epsilon_r=4.4$  and thickness 1.6mm. The dimensional parameters of the antenna and their resonant frequency are shown in Table 3.7.

**Table 3.7** Computed Geometric Parameters of the Antennas operating in different bands.

Designed Frequency	900 MHz 2.4 GHz	1.8 GHz 5.2 GHz	2.4 GHz 5.2 GHz	5.2 GHz 10. GHz
$L_1$	30.7 31.6 9.3 8	15.3	11.5	5.3
$W_1$		15.8	11.85	5.5
$L_2$		4.7	3.5	1.6
$W_2$		4	3	1.4
Resonate at	918 MHz 2.38 GHz	1.82 GHz 5.22 GHz	2.38 GHz 5.18 GHz	5.19 GHz 9.96 GHz

### 3.5.4 Coplanar Strip fed Dual band antenna for 2.4/5.2 GHz WLAN Applications

Using the developed design equations, an antenna suitable for 2.4/5.2 GHz WLAN bands is fabricated and analyzed experimentally. This is discussed in the following sessions.

#### 3.5.4.1 Structure and dimensional parameters of the Dual band antenna

The structure of the optimized dual band dipole antenna is shown in Fig.3.58. The dimensional parameters of the antennas are  $L_1=11.5$  mm,  $W_1=11.75$ mm,  $L_2= 3.5$ mm,  $W_2=3$ mm,  $L_3=6.8$ mm,  $g=0.3$ mm and  $g_1=0.5$ mm. The antenna is fabricated on an FR4 substrate whose dielectric constant is 4.4 and loss tangent is 0.02. The overall dimension of the antenna is same as that of the single band antenna discussed in previous session.

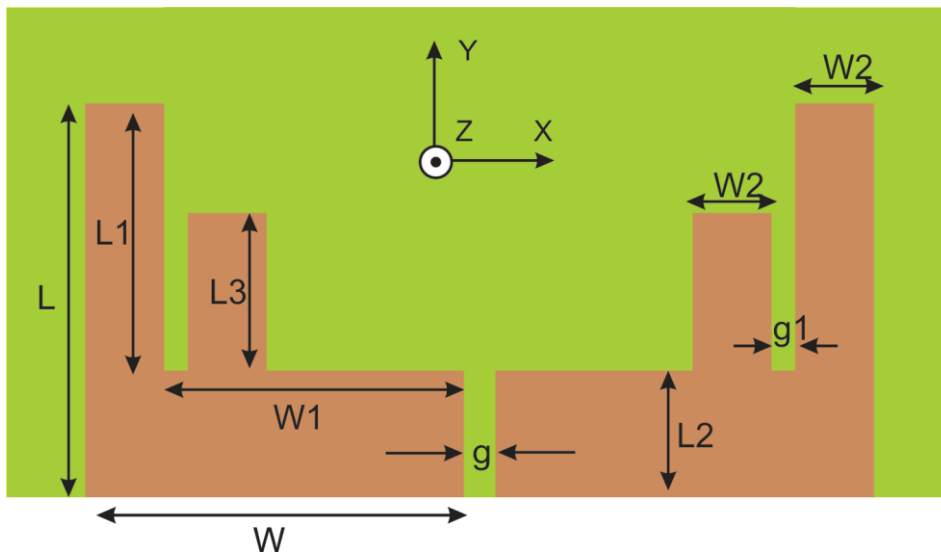


**Fig.3.58** Dimensional parameters of the dual band antenna ( $L_1=11.5$  mm,  $W_1=11.75$ mm,  $L_2= 3.5$ mm,  $W_2=3$ mm,  $L_3=6.8$ mm,  $g=0.3$ mm,  $g_1=0.5$ mm and  $\epsilon_r=4.4$ )

### 3.5.4.2 Reflection Characteristics of the Antenna

The simulated and realized reflection co-efficient of the antenna are shown in Fig. 3.59. Both the curve matches very well and proves the experimental validity of the antenna structure. The antenna offer 2:1 VSWR band width from 2.31 to 2.72 GHz and 5.13 to 5.45 GHz which is wide enough to cover both the IEEE 802.11 b/g and 802.11a WLAN bands.

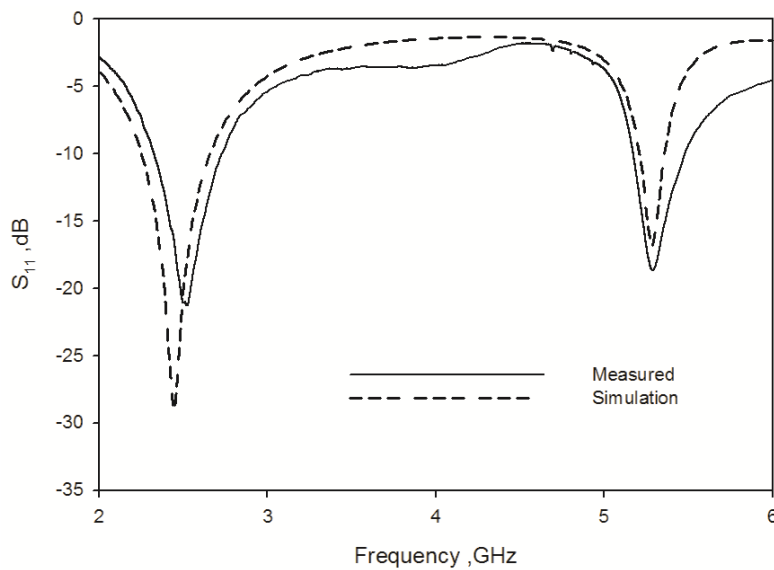


**Fig.3.59** Reflection co-efficient of dual band antenna( $L_1=11.5$  mm,  $W_1=11.75$ mm,  $L_2= 3.5$ mm,  $W_2=3$ mm,  $L_3=6.8$ mm,  $g=0.3$ mm,  $g_1=0.5$ mm and  $\epsilon_r=4.4$ )

### 3.5.4.3. Radiation Characteristics of the Antenna

The three dimensional radiation pattern of the antenna at both the resonant frequencies are shown in the Fig. 3.60. From the figure 3.60 (a) it is clear that the antenna offer an apple shaped radiation pattern at the first resonant frequency. The polarization of the antenna at first resonance is along X direction and it matches with the inference attained from surface current analysis which is explained in the later session. The beam maximum of the first resonance is pointing towards the open end of the antenna. In slotline antennas

the open edges will normally radiates and the remaining parts will push the electromagnetic energy towards the open end. This is the reason for beam maxima towards the open end. This is the reason for beam maxima towards the open end. Thus the peak gain of the antenna at the open end will be slightly enhanced. From figure 3.60 (b) it is clear that the antenna offer a polarization oriented in X direction with a slight directive radiation pattern at the second resonance. The enhancement of radiation towards the open end of the antenna is higher in the case of second resonance. This is due to the reflector like character of the outer strips of the antenna.

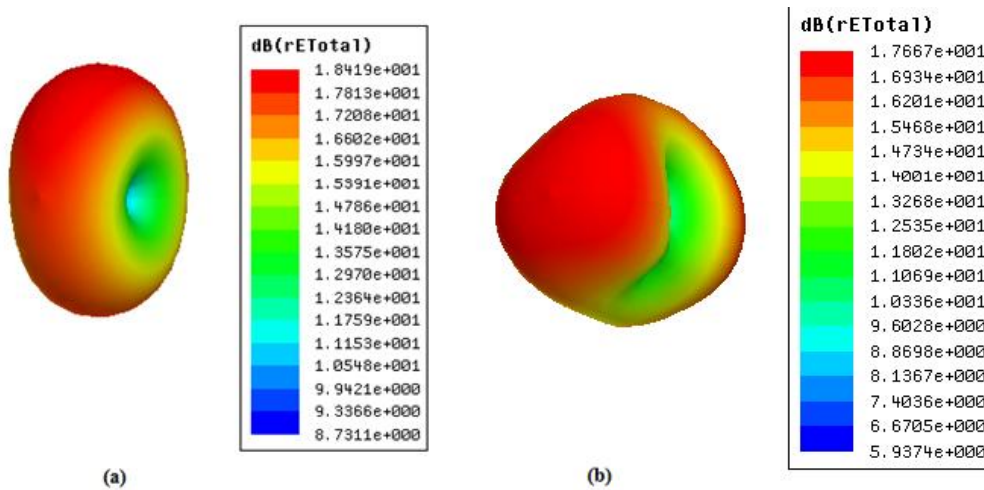


**Fig.3.60** Three dimensional Radiation pattern of the dual band antenna at (a) 2.4 GHz (b) 5.2GHz ( $L_1=11.5$  mm,  $W_1=11.75$ mm,  $L_2= 3.5$ mm,  $W_2=3$ mm,  $L_3=6.8$ mm,  $g=0.3$ mm,  $g_1=0.5$ mm and  $\epsilon_r=4.4$ )

Two dimensional radiation patterns of the antenna in the two principal planes at 2.4 GHz are shown in Fig.3.61. From the figure it is clear that the antenna offer an Omni directional pattern at 2.4 GHz. Since the two L shaped arms contribute for radiation, the null is not effective in the X direction along E plane pattern but still there is a considerable power reduction. In E plane the antenna offer a cross polar purity of greater than 30dB. In H plane the antenna posses a circular pattern with a cross polar purity of 30dB. Since the antenna



offer this much of cross polar levels, there will be a slight enhancement in the gain of the antenna.

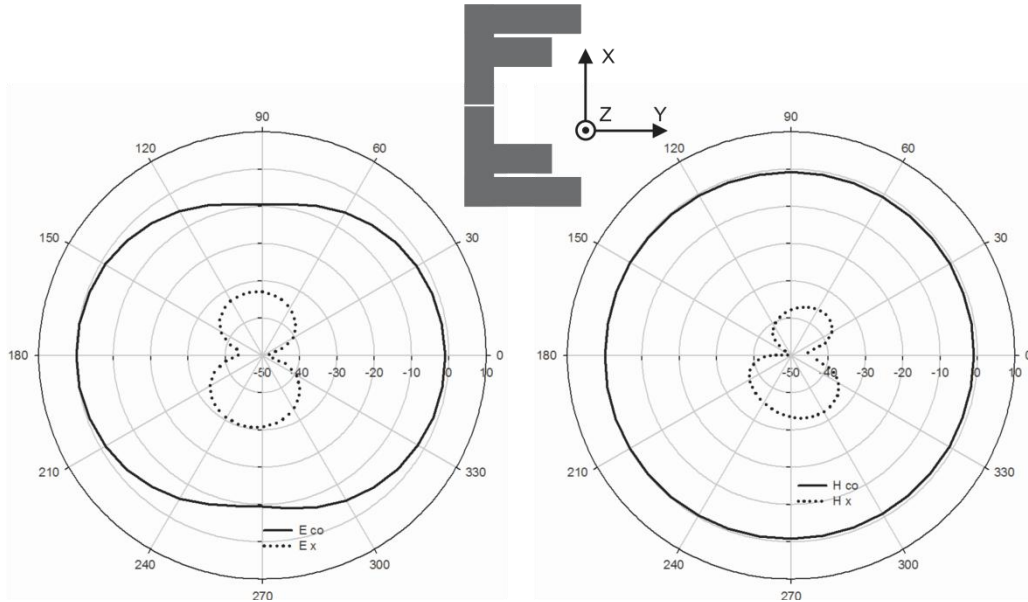


**Fig.3.61** Measured two dimensional Radiation pattern of the dual band antenna at 2.4 GHz ( $L_1=11.5$  mm,  $W_1=11.75$ mm,  $L_2= 3.5$ mm,  $W_2=3$ mm,  $L_3=6.8$ mm,  $g=0.3$ mm,  $g_1=0.5$ mm and  $\epsilon_r=4.4$ )

Two dimensional radiation patterns of the antenna in the two principal planes at 5.2 GHz are shown in Fig.3.62. At 5.2 GHz the antenna is directive towards the Y direction. From the E plane pattern it is clear that the antenna offers a pattern with a small enhancement in power towards the Y direction with a front to back ratio of nearly 5 dB. A cross polar isolation which is better than 20 dB is present in the E plane pattern. In the H plane the antenna offer a circular pattern with a front to back ratio better than 5 dB. Over an azimuth of  $180^\circ$ , the antenna offer constant power. Across polar isolation of better than 30dB is present in the H plane. Since the pattern is slightly directive and the cross polar isolation is also good, there will be a slight enhancement in the gain of the antenna and that is discussed in the later session of this chapter.

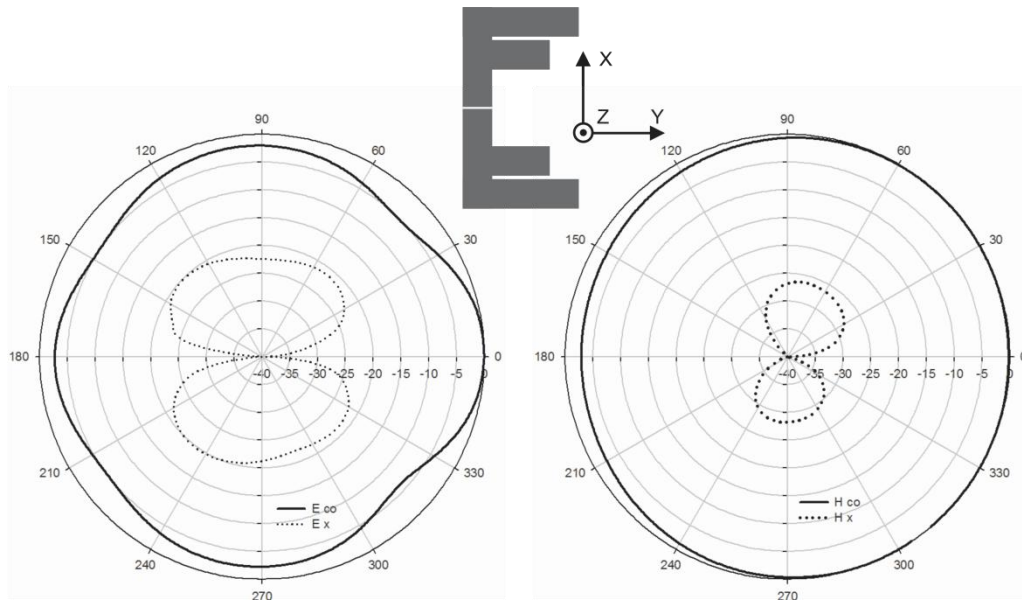


**Fig.3.62** Measured two dimensional Radiation pattern of the dual band antenna at 5.2 GHz ( $L_1=11.5$  mm,  $W_1=11.75$ mm,  $L_2= 3.5$ mm,  $W_2=3$ mm,  $L_3=6.8$ mm,  $g=0.3$ mm,  $g_1=0.5$ mm and  $\epsilon_r=4.4$ )

#### 3.5.4.4. Surface Current distribution of the Antenna

To know more about the resonant and radiating mechanism of the antenna, simulated surface current analysis of the antenna at the two resonant frequencies are performed. Polarization characteristics, Radiation pattern, Radiation efficiency, reason for Resonance etc can be explained by the detailed analysis of the surface current. This is discussed in this session.

Surface current distribution of the antenna at the first resonant frequency ie at 2.4 GHz is shown in Fig.3.63. The cause of first resonance is same as that explained in the case of the single band dipole antenna. ie the half wavelength long variation in surface current through the strips of dimensions  $L_1 \times W_1$  and  $L_2 \times W_2$ . From the figure it can also be inferred that the antenna exhibits a polarization oriented along X direction. Since more than 95% of the metallic

parts of the antenna contribute for radiation, the efficiency of the antenna is also very high.

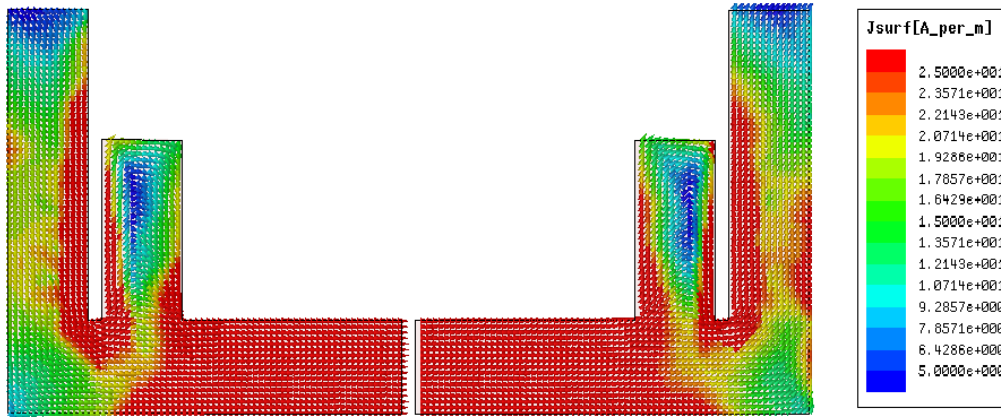


**Fig.3.63** Surface current distribution of the dual band antenna at 2.4 GHz ( $L_1=11.5$  mm,  $W_1=11.75$ mm,  $L_2= 3.5$ mm,  $W_2=3$ mm,  $L_3=6.8$ mm,  $g=0.3$ mm,  $g_1=0.5$ mm and  $\epsilon_r=4.4$ )

Simulated surface current distribution of the antenna at the second resonant frequency ie at 5.2 GHz is given in Fig. 3.64. It is clear from the current plot that the second resonance is mainly due to two antisymmetric quarter wavelength variation of surface current through the two U shaped arms formed by the two strips of dimension  $L_1 \times W_1$  and  $L_3 \times W_1$ .

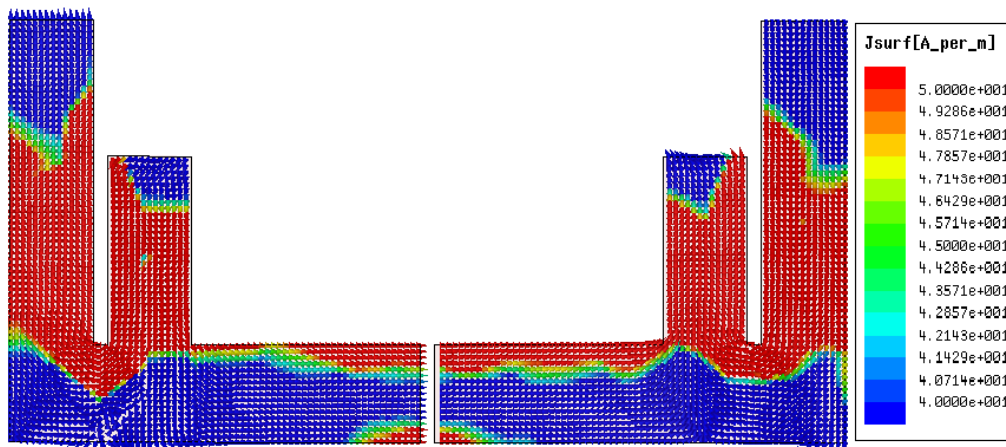


**Fig.3.64** Surface current distribution of the dual band antenna at 5.2 GHz ( $L_1=11.5$  mm,  $W_1=11.75$ mm,  $L_2= 3.5$ mm,  $W_2=3$ mm,  $L_3=6.8$ mm,  $g=0.3$ mm,  $g_1=0.5$ mm and  $\epsilon_r=4.4$ )

From the above figure it is clear that both the current patterns are anti symmetric in nature. Current through both the strips of dimension  $L_1 \times W_1$  are equal but opposite in direction. This will result in field cancellation. Similarly current through the strips of dimension  $L_3 \times W_1$  will also result in field cancellation due to the antisymmetry in their directions. Thus a small portion of these current will contribute to the additive radiation mechanism and radiation fields. Thus the efficiency of the antenna in second band may be less.

### 3.5.4.5. Gain of the Antenna

The measured gains of the coplanar strip fed dual band antenna in both the operating bands are shown in Fig. 3.65. The antenna offer an average gain of 3 dBi in the lower band with a peak directive gain of 4 dBi at 2.5 GHz. The directivity of the antenna in the second band is shown as solid curve. The gain in the second band is slightly enhanced because of the high cross polar purity of the radiation pattern and slight suppression of backward wave in the antenna. The antenna offers an average gain of nearly 4.5 dBi in the 5.2 GHz band with a peak gain of 5 dBi at 5.15 GHz.

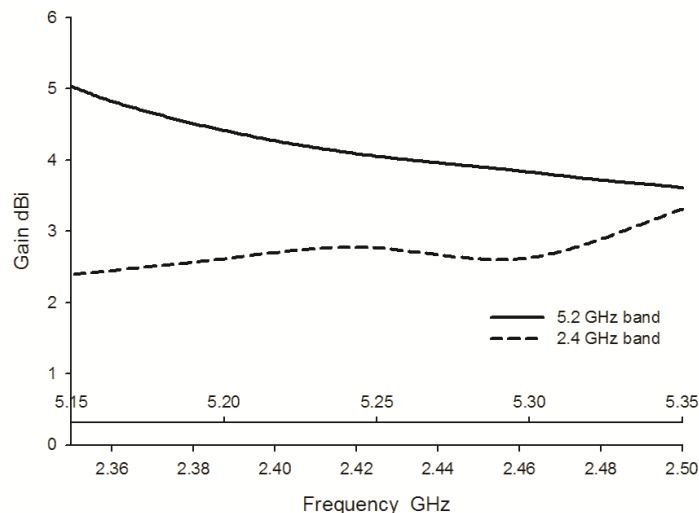


**Fig.3.65** Measured Gain of the dual band antenna in both the operating band ( $L_1=11.5$  mm,  $W_1=11.75$ mm,  $L_2= 3.5$ mm,  $W_2=3$ mm,  $L_3=6.8$ mm,  $g=0.3$ mm,  $g_1=0.5$ mm and  $\epsilon_r=4.4$ )

#### **3.5.4.6. Radiation efficiency of the Antenna**

The measured radiation efficiency of the CPS fed dual band antenna in both the operating bands is shown in Fig. 3.66. It is clear from the efficiency curves that the structure is a good radiator of electromagnetic energy in the first band of operation with greater than 95 % radiation efficiency. This high efficiency can be easily explained from the surface current path shown in Fig. 3.64. From the surface current distribution of the first resonant frequency, it is clear that almost all metallic part of the structure contributes in effective radiation and this will increase the efficiency of the structure.

In the case of second band the efficiency is less. An average efficiency of 78 % is offered by the antenna in the second operating band. This low efficiency can also be explained from the surface current distribution given in Fig. 3.64. From the surface current pattern corresponding to second resonance it is inferred that, the resonance is due to two equal but anti parallel (Oppositely directed) current path. In far field, the field is only due to a small part of current path which is additive. All fields due to other part of current paths are canceling mutually. Therefore the radiation efficiency is less in the second operating band. Since the directivity of the antenna is high, the gain will be high in second band.

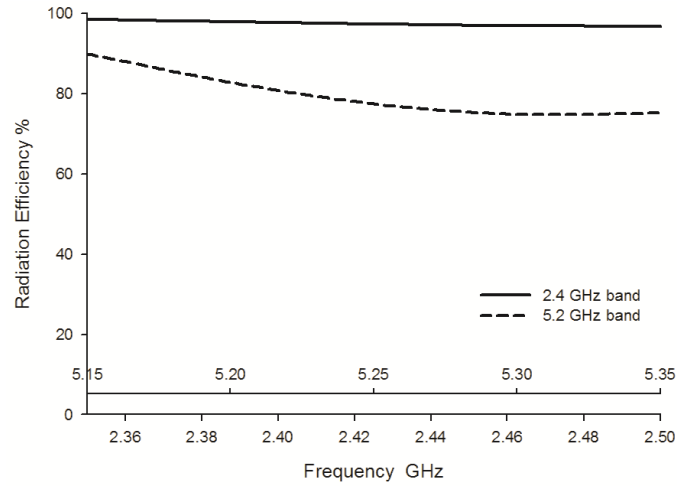


**Fig.3.66** Measured Radiation Efficiency of the dual band antenna in both the operating band ( $L_1=11.5$  mm,  $W_1=11.75$ mm,  $L_2= 3.5$ mm,  $W_2=3$ mm,  $L_3=6.8$ mm,  $g=0.3$ mm,  $g_1=0.5$ mm and  $\epsilon_r=4.4$ )

### 3.6 FDTD Analysis

For obtaining the details of radiation mechanism and further theoretical aspects of the antennas discussed in this chapter, Finite Difference Time Domain analysis is also performed. FDTD analyses of the antennas are discussed in this session.

The parameters used for FDTD calculations are depicted in table 3.8

**Table3.8** Parameters for FDTD calculations

Parameters	Value
Cell Dimension (mm)	$\Delta X=0.35$
	$\Delta Y=0.35$
	$\Delta Z=0.4$
Time Step	$\Delta t=0.88$ Ps
Number of time steps	10000
Excitation	1. Gaussian Pulse Half width $T=15$ Ps Time Delay $t_0=3T$
	2. Sinusoidal signal

### 3.6.1 Open Ended Slotline

The analyzed FDTD domain structure of the OES is shown in Fig 3.67. The  $S_{11}$  curve obtained from FDTD analysis is compared with that obtained from HFSS and are shown in Fig.3.68 which are in good agreement. This proves the validity of theoretical analysis.

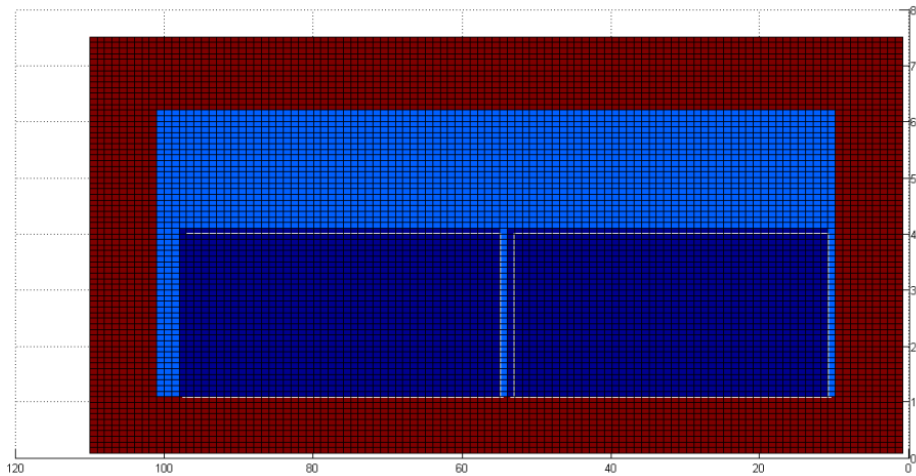


**Fig.3.67** FDTD computation domain structure of Open Ended Slotline

X component of E field vector from the antenna at resonant frequency is given in Fig 3.69 (a). it is evident that the radiation is mainly from the top edge of the antenna. Y component of E field at same frequency is also shown in Fig 3.67 (b) in which the current maxima is found to be at top edge of the OES which satisfies the inference obtained from the current pattern developed using HFSS analysis of the structure.

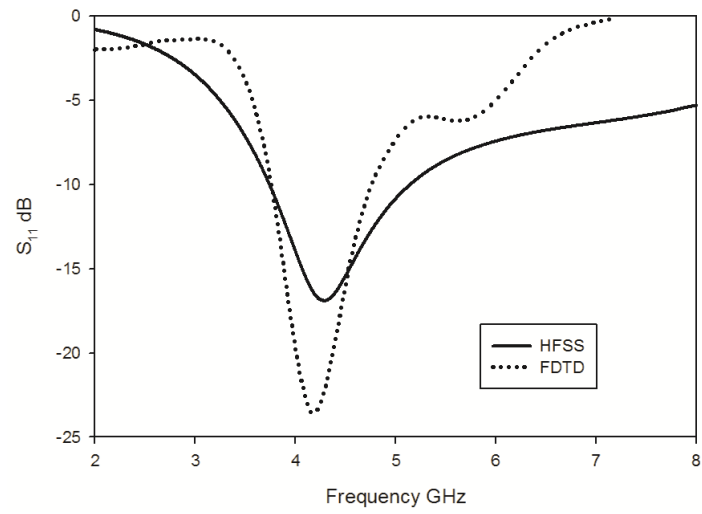


**Fig.3.68** Reflection Co-efficient of Open Ended Slotline

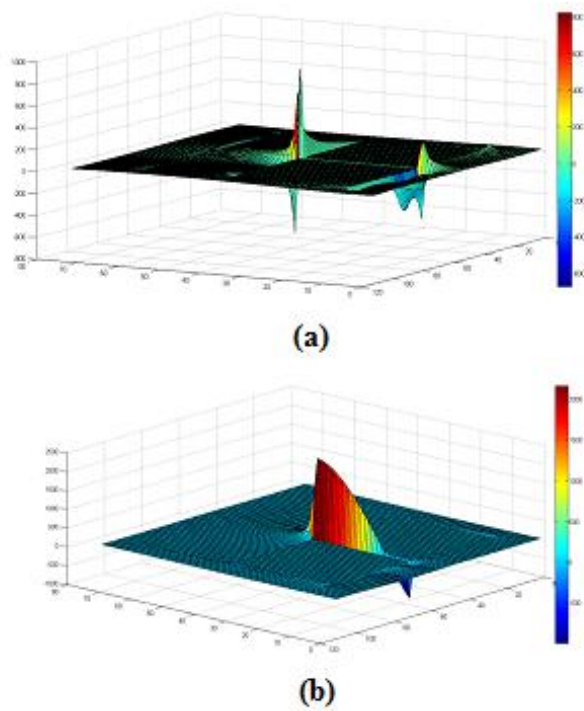


**Fig.3.69** Electric field distribution of Open Ended Slotline (a) X Component and (b) Y Component at 4.28 GHz



### 3.6.2. Coplanar Strip Fed Single Band Antenna

As the second step, FDTD analysis is done for the single band antenna. The structure analyzed and the  $S_{11}$  curve obtained is given in Fig 3.70 and 3.71 respectively. The  $S_{11}$  curve obtained from HFSS, FDTD and experimental analysis are matched very well.

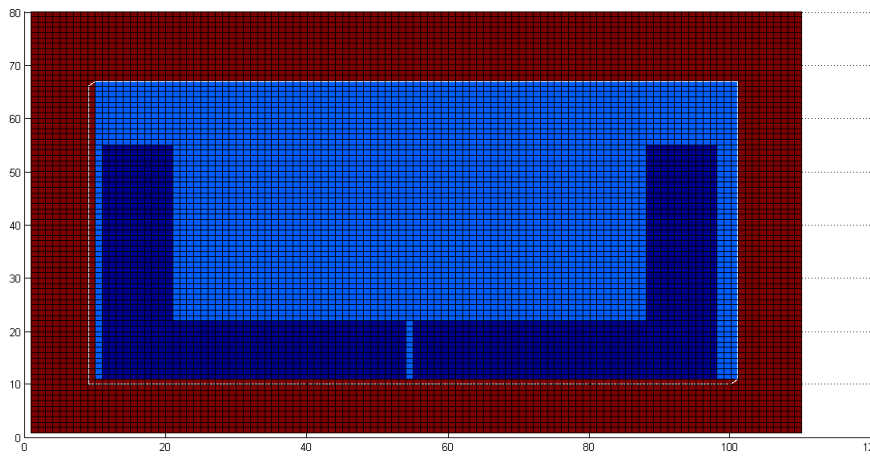


**Fig.3.70** FDTD computation Domain structure of Single Band Antenna derived from OES.

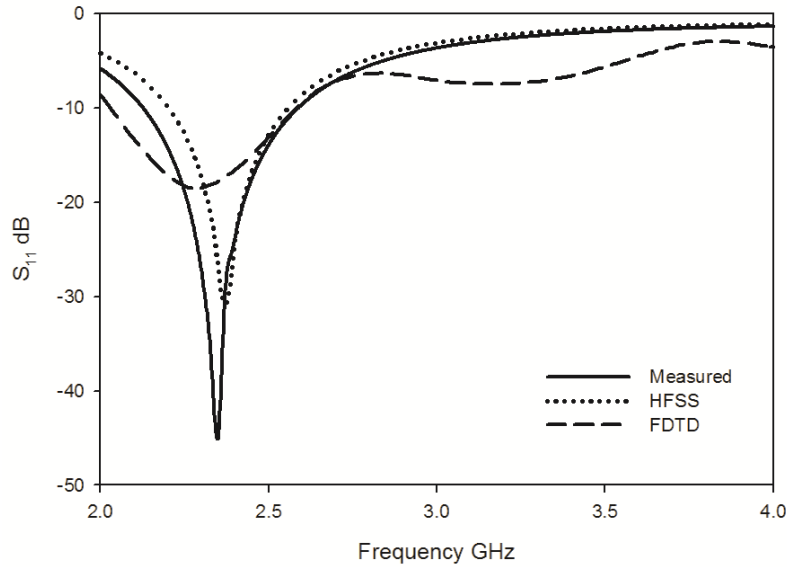
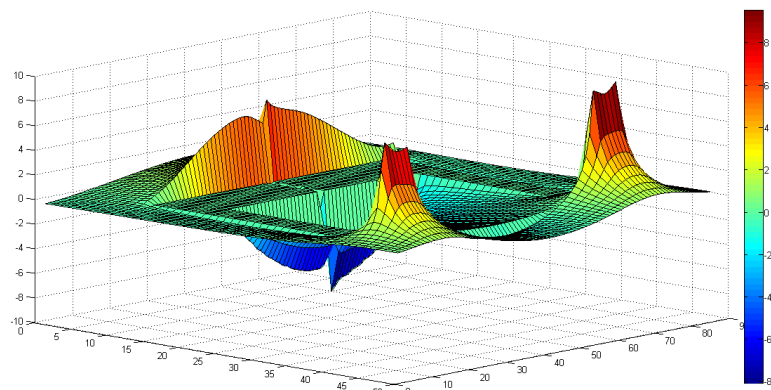
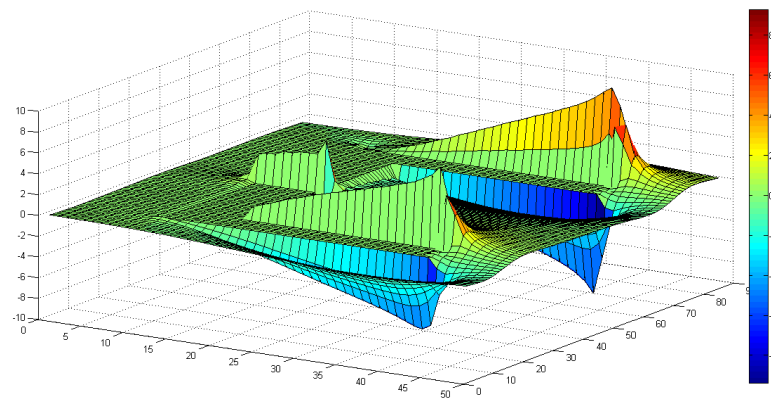


**Fig.3.71** Reflection Co-efficient of Single Band Antenna.

X component and Y component of the E field vectors at the resonant frequency ie at 2.38 GHz are shown in Fig 3.72 (a) and (b). Both the figures are in good agreement with the surface current distribution of the single band antenna which is given in the previous sessions.



(a)



(b)

**Fig.3.72** Electric field distribution of single band antenna (a) X Component and (b) Y Component at 2.38 GHz

### 3.6.3. Coplanar Strip Fed Dual Band Antenna

Analysis of the dual band dipole antenna derived from the single band antenna without affecting the compactness is discussed here. The structure in FDTD domain is shown in Fig. 3.73. The  $S_{11}$  curve obtained from the

theoretical analysis matched very well with the curve obtained experimentally. The comparison of the  $S_{11}$  curves are shown in Fig 3.74.

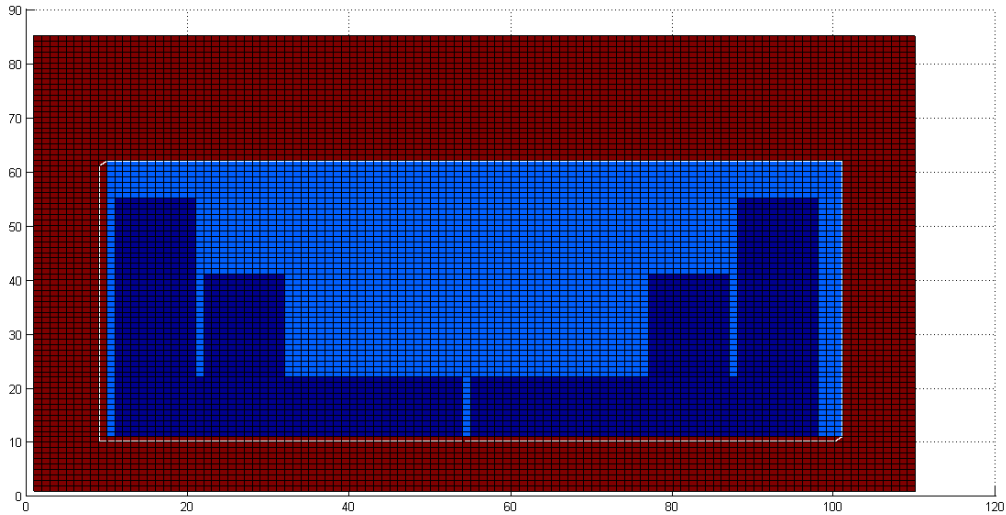


**Fig.3.73** FDTD computation Domain structure of Dual Band Antenna.

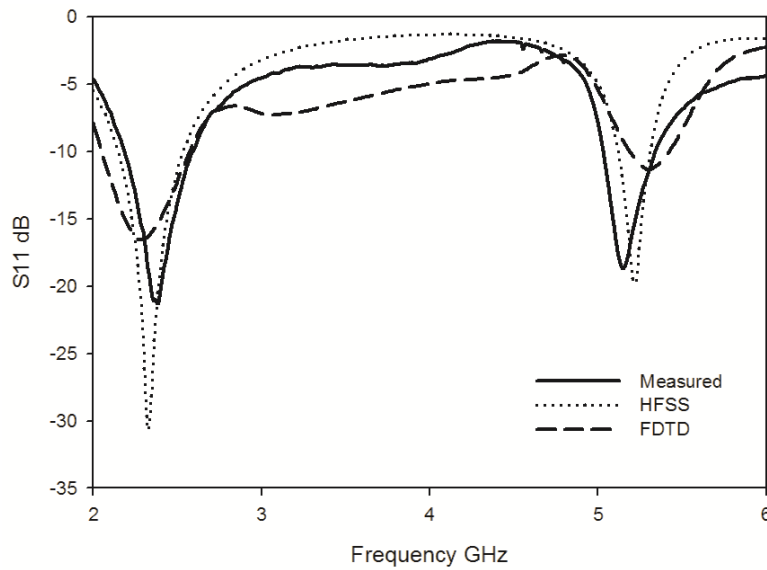
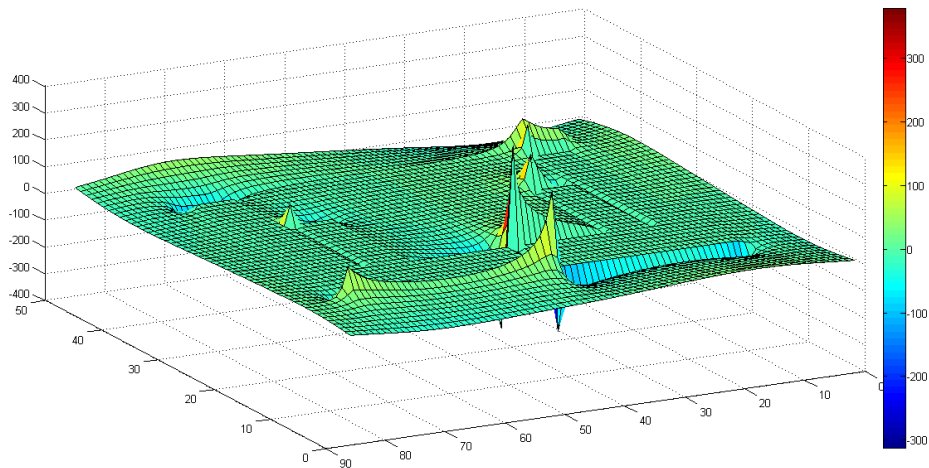


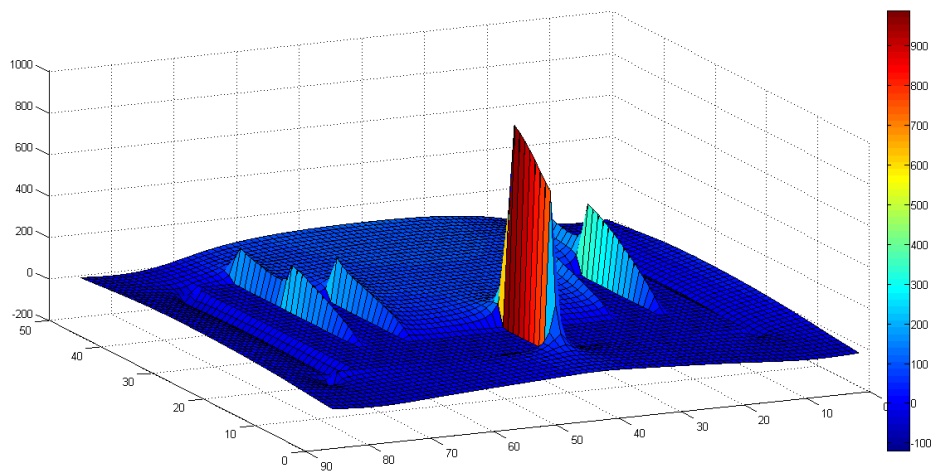
**Fig.3.74** Reflection Co-efficient of Dual Band Antenna

X and Y component of E field at 2.4 GHz and at 5.2 GHz are shown in Fig 3.75 (a&b) and 3.76 (a&b) respectively which shows similar variation of

surface current pattern obtained from HFSS analysis which are shown in Fig 3.63 and 3.64 respectively.

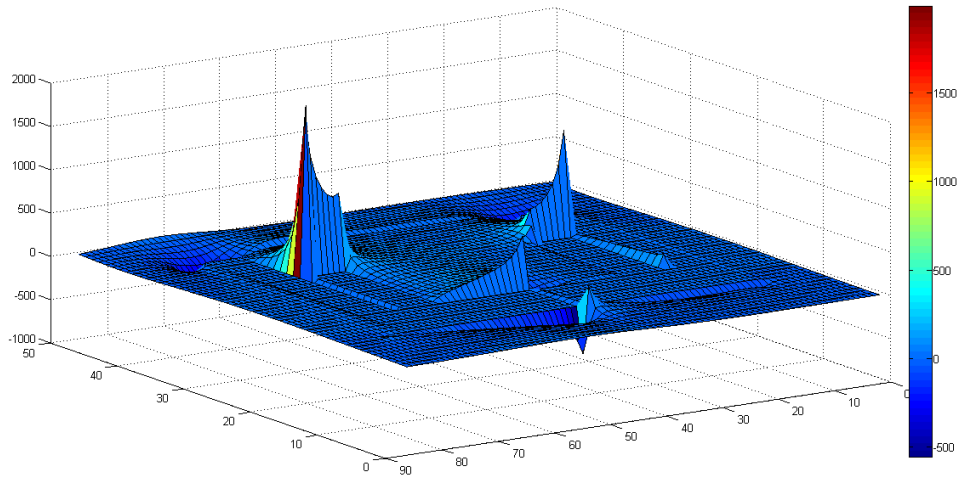


(a)

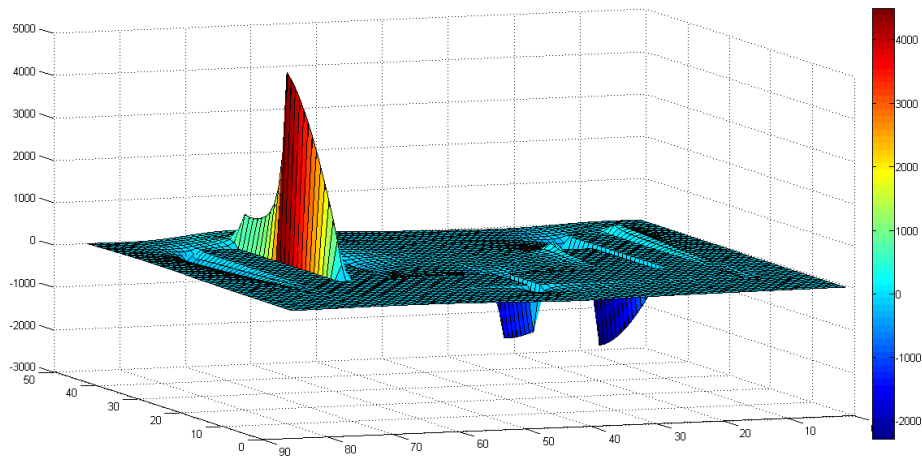


(b)

**Fig.3.75** Electric field distribution of Dual band antenna (a) X Component and (b) Y Component at 2.4 GHz



(a)



(b)

**Fig.3.76** Electric field distribution of Dual band antenna (a) X Component and (b) Y Component at 5.2 GHz

### 3.6 Chapter Summary

In the first part the chapter deals with various types of transmission lines and as a continuation it deals with the analysis of an Open Ended Slotline (OES). From the analysis of the OES it is found that it acts like an antenna with low efficiency. Then the studies are performed to derive an effective radiator

with a lower resonant frequency with the same dimension of the parental OES. This study results in the single band dipole antenna which is operating at 2.4 GHz. Analysis of all the parameters of the single band dipole antenna are performed thoroughly and the design equations for the single band dipole in terms of the dimensional parameters are obtained. All the radiation characteristics of the antenna including radiation pattern, directive gain, radiation efficiency etc are measured and analyzed carefully. Surface current distribution of the antenna is also studied well to explain various characteristics of the antenna.

As a next step, the study is vectored to develop a dual band dipole antenna without changing the dimensions of the single band dipole. This study results in a dual band dipole operating at 2.4 GHz and 5.2 GHz WLAN bands. Here also the effects of all the dimensional parameters are studied thoroughly and the design equation for the dual band antenna is developed. The design equations are validated for different substrates for the same operating frequency. The radiation characteristics such as radiation pattern, directivity and radiation efficiency of the antenna are measured practically and studied thoroughly. Surface current pattern analysis of the dual band antenna is performed to validate and explain various parameters.

Last session of the chapter deals with the FDTD analysis of different structure which are explained in the same chapter. The reflection coefficient obtained are compared with those obtained experimentally and found that they are in good agreement. The electric field distributions in different planes are also computed and compared with simulated results.

## **References**

- [1] Constantine A Balanis "Antenna theory analysis and design" John Wiley and Sons II nd edition
- [2] Mariani, E.A. Heinzman, C.P.; Agrios, J.P, Cohn, S.B, "SlotLine characteristics", **IEEE Transactions on Microwave Theory and Techniques**, Volume 17, Issue 12 Page(s):1091 – 1096, Dec 1969
- [3] Ramesh Garg,PrakashBhartia and InderBahl,Microstrip Antenna Design Hand book, 1st ed. MA Artech House, 2001.





## COPLANAR STRIP FED HIGH GAIN DIPOLE ANTENNAS



*The chapter deals with the design and development of a compact Coplanar Strip Fed High Gain Dipole Antenna suitable for IEEE 5.2 GHz and 5.8 GHz WLAN applications. Derivation of the antenna from an Open Ended Slotline (OES) is clearly discussed. After this study, conversion of this antenna in to a wideband dipole suitable for imaging and directive application is also discussed. Reflection and Radiation Characteristics of the antenna are discussed in detail. FDTD analysis of the two antenna structures are also performed and included in this chapter.*

### 4.1 High Gain Dipole Antenna

As discussed in the previous chapter, a suitable removal of metallic part from an Open Ended Slotline (OES) will result in an efficient radiating structure. In the first part of this chapter, the transformation of an OES into a high gain antenna where a portion of the transmission line acts as a reflector is discussed.

#### 4.1.1 Evolution of High Gain Dipole from OES

The evolution of the antenna structure from an Open Ended Slotline is shown in the Fig. 4.1.

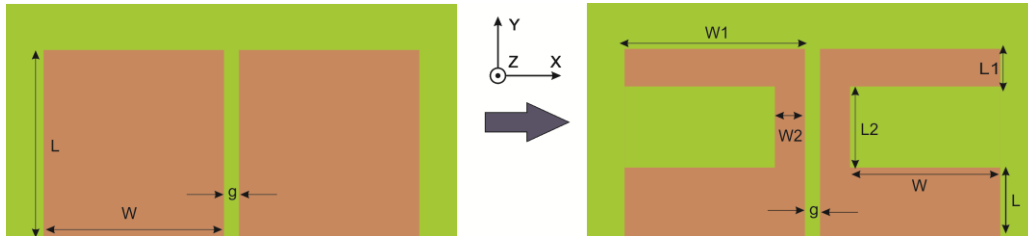


**Fig.4.1** Evolution of high gain dipole from an OES

An OES with strip length  $L$ , strip width  $W$  and gap  $g$  is shown in Fig. 4.1.(a). From the analysis of the OES performed and discussed in previous chapter, it is clear that the structure acts as a radiator. It is also inferred from the previous chapter that the selective removal of certain portions from an OES will result in high efficiency radiating devices. This removal will result in a compact antenna structure with increased bandwidth and efficiency.

Transformation of an OES into a high gain dipole antenna is explained in the above figure. The antenna is derived from an OES of dimensional parameters strip length  $L$  strip width  $W$  and gap  $g$  by removing a rectangle symmetrically from either strip of it. The simulated reflection co-efficient of the arbitrarily derived antenna by symmetrically removing rectangles of dimension  $6\text{mm} \times 8\text{mm}$  from either strips of an OES of dimension  $14.5\text{mm} \times 11\text{mm}$  along with that of the parental OES is shown in Fig.4.2. From the simulated reflection co-efficient plot it is clear that the derived structure is resonating at  $4.82\text{ GHz}$  with  $2:1$  VSWR band width of  $580\text{ MHz}$ . The resonance of the OES is found to be at  $7.627\text{ GHz}$  and it is not well matched.

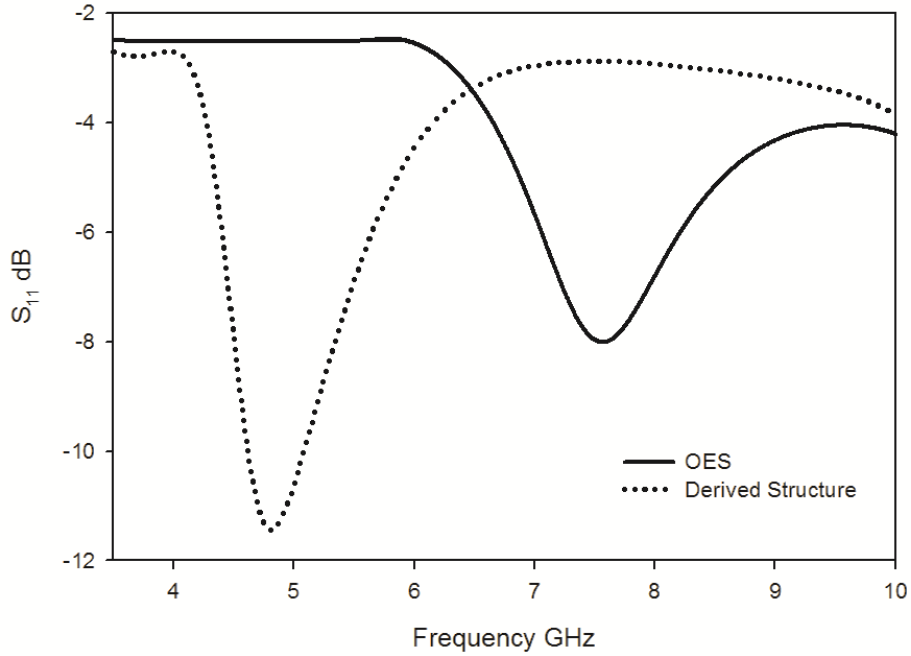


**Fig.4.2**  $S_{11}$  of newly developed high gain dipole and parental OES

The simulated three dimensional radiation pattern of the antenna derived from OES at the resonating frequency is given in Fig.4.3. From the figure it is evident that the antenna is directional in nature. The back radiation in this structure is very negligible. The directional behavior of this structure is obtained without any additional parasitic elements like reflector, director etc. A part of the radiating structure itself acts as the reflector in this case. This can be verified from the analysis performed and discussed in the later sessions of this chapter.

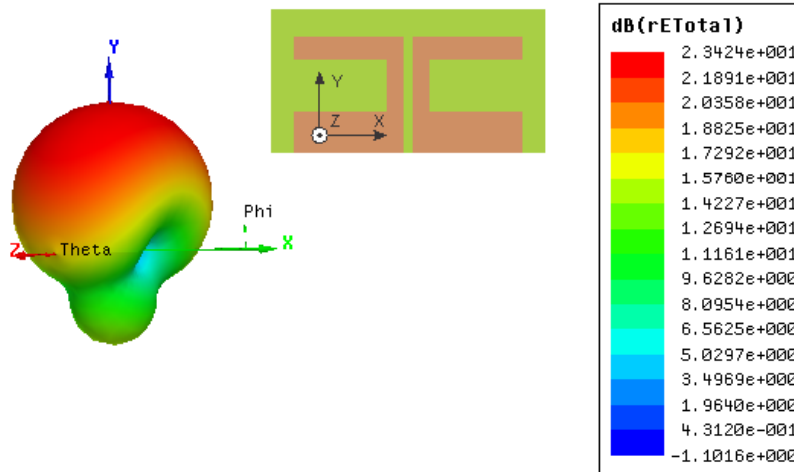


**Fig.4.3** Radiation pattern of newly developed high gain dipole

#### 4.1.2 Parametric analysis

To analyze the mechanism of the resonance and to obtain the design equation of the antenna, a set of parametric analysis are performed and explained in this session. With the parametric analysis performed, the variation of distributed parameters of the antenna as a function of dimension is also analyzed. The capacitances and inductances of the circuits/ structure are found out from the return loss characteristics using the basic network equations relating the Q factor, Resonance etc with the inductance and capacitance which is illustrated in appendix-1.

##### 4.1.2.1 Variation in reflection co-efficient with L

The variation of reflection co-efficient of the antenna with parameter L is shown in Fig. 4.4. The parameter L has no impact on antenna resonant frequency ie the *length* of the transmission line does not play an important role in determining the resonant frequency. The impedance matching is slightly affected with L but is negligible.

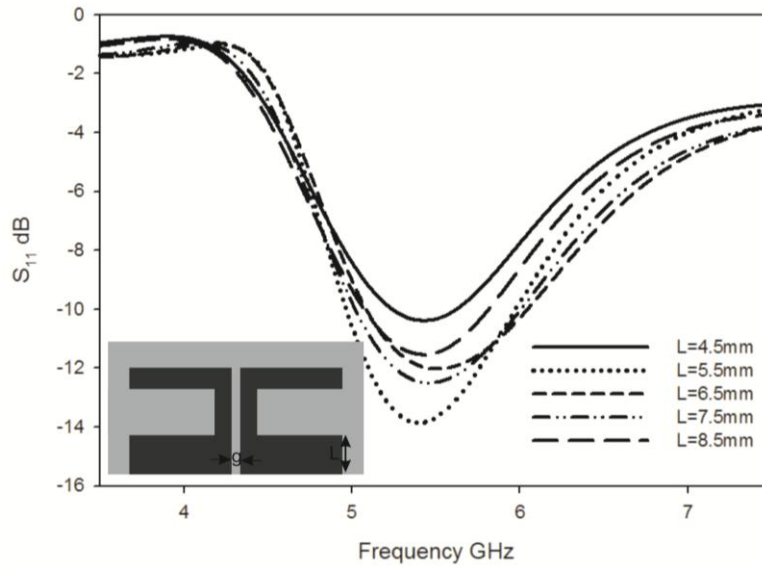


**Fig.4.4** Variation of reflection co-efficient with  $L$  ( $L_1=3$  mm,  $L_2=6$ mm,  $W=8$ mm,  $W_1=8$ mm,  $W_2=3$ mm and  $g=0.3$ mm)

The variation of distributed capacitance and inductance of the antenna with  $L$  is shown in Fig.4.5. From the plot it is inferred that the capacitance of the antenna shows a decrease while the inductance shows an increase with  $L$ . Both the changes are very feeble so that the shift in resonant frequency due to these changes are also very less. From the analysis the maximum change in inductance and capacitance for the variation of  $L$  from 4.5 mm to 8.5 mm is 8 nH and 0.04 Pf respectively. Since as the  $L$  increases, inductance increases and the capacitance decreases and the variation found to be nearly same, the resonant frequency will remain nearly same for all cases with a slight decrease in band width.

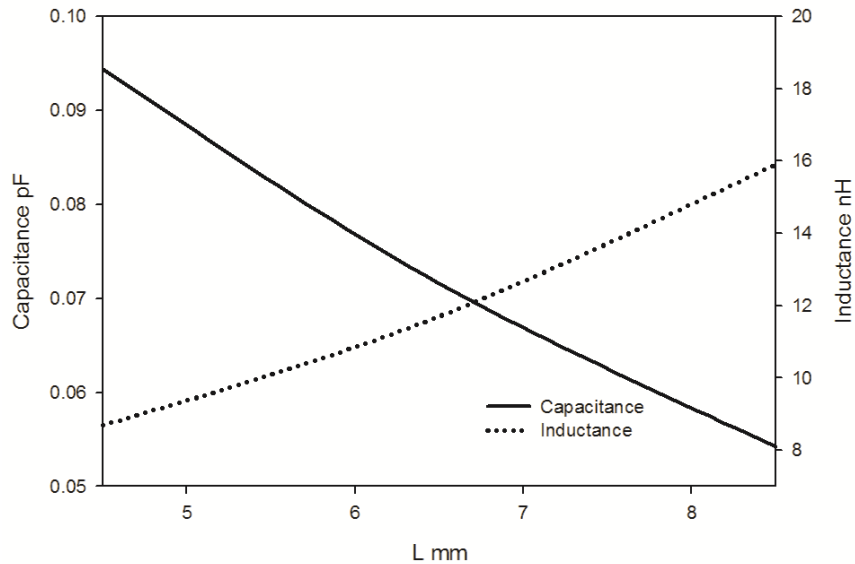


**Fig.4.5** Variation of Distributed reactive parameters with L ( $L_1=3$  mm,  $L_2=6$ mm,  $W=8$ mm,  $W_1=8$ mm,  $W_2=3$ mm and  $g=0.3$ mm)

#### 4.1.2.2 Variation in reflection co-efficient with W

Variation of reflection co-efficient of the antenna with W is shown in Fig. 4.6. The resonant frequency is found to be shifted towards lower side with increase in W. The impedance matching is strongly affected by W and it is rapidly deteriorates with increase in W. The shift in resonance is due to the change in surface current path length with the variation in strip length W. As W increases, the current path increases and correspondingly the resonance decreases. This can be verified from the surface current distribution given in Fig.4.27.

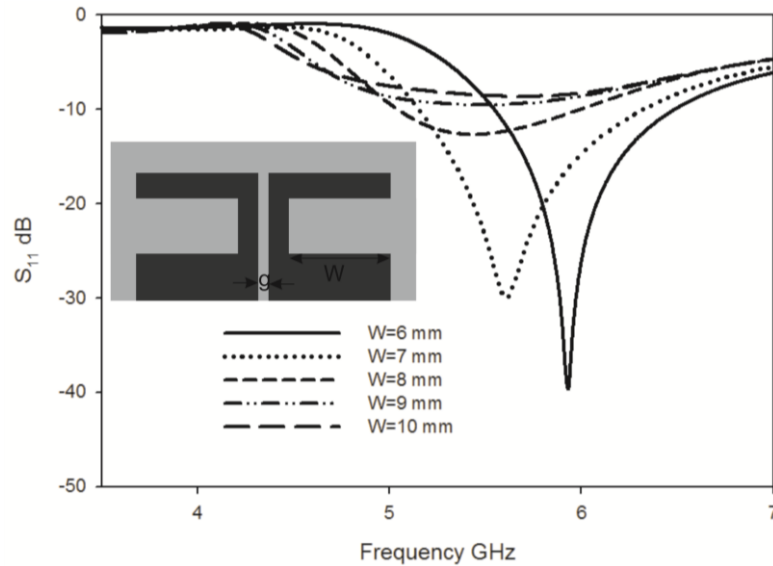


**Fig.4.6** Variation of reflection co-efficient with  $W$  ( $L=5.5\text{mm}$ ,  $L_1=3\text{ mm}$ ,  $L_2 =6\text{mm}$ ,  $W_1=8\text{mm}$ ,  $W_2=3\text{mm}$  and  $g=0.3\text{mm}$ )

The impedance matching of the antenna varies drastically with strip length  $W$ . The presence of a metallic body near the radiating structure will tend to lower the antenna impedance [1]. As the parameter  $W$  increases, a longer metallic surface is introduced near the main radiating part i.e. the strip of dimension  $L_1 \times W_1$ . This will change the impedance of the antenna and produce strong effect in the scattering parameter  $S_{11}$ . This can be verified from the real part and imaginary part of impedance of the antenna given in Fig. 4.7(a) and Fig. 4.7(b) respectively. From the impedance study it is clear that the strip with length  $W$  act not only as a radiator but also as a reflector in our antenna structure.

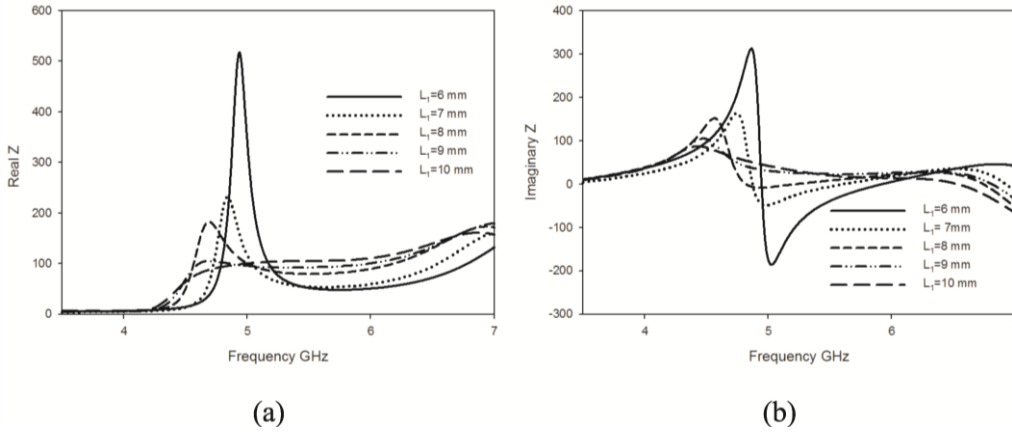


**Fig.4.7** Variation of (a) Real part of impedance and (b) Imaginary part of impedance with W (L=5.5mm, L<sub>1</sub>=3 mm, L<sub>2</sub>=6mm, W<sub>1</sub>=8mm, W<sub>2</sub>=3mm and g=0.3mm)

The variation of distributed reactive parameters with W is shown in Fig. 4.8. From the variation graph it is clear that capacitance of the structure increases with W while the inductance reduces by a small value. This will result in a lower shift in resonant frequency with a increase in bandwidth. This is because as inductance decreases, the Q of the circuit reduces which results in an increase in bandwidth.

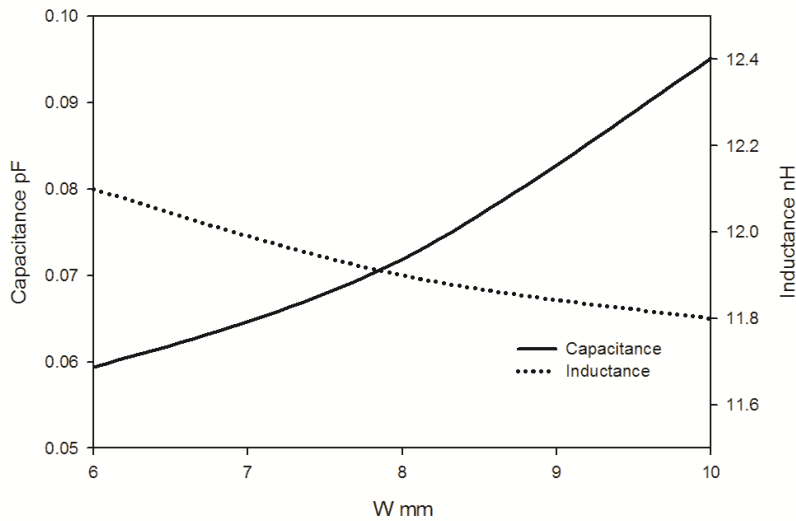


**Fig.4.8** Variation of Distributed reactive parameters with W (L=5.5mm, L<sub>1</sub>=3 mm, L<sub>2</sub>=6mm, W<sub>1</sub>=8mm, W<sub>2</sub>=3mm and g=0.3mm)



#### 4.1.2.3 Variation in reflection co-efficient with $L_1$

The effect of strip length  $L_1$  on antenna reflection co-efficient is shown in Fig. 4.9. The strip width  $L_1$  plays an important role on radiating behavior of the antenna. The matching and the bandwidth are affected by this parameter. Both the bandwidth and impedance match are decreasing with  $L_1$ . This is due to the change in distributed inductance with  $L_1$ . As  $L_1$  decreases, the distributed inductance decreases due to the reduction in edge length and therefore the Q of the circuit decreases. This will increase the band width of the antenna. The variation of antenna impedance matching may be due to the shift from inductive to capacitive behavior with increase in  $L_1$ .

The resonance is found to be not symmetrical when we reduce the parameter  $L_1$  which is owing to the presence of other resonances in the higher side of the resonating frequency. This property can be utilized to transform this antenna into a wideband structure. This is discussed as the second part of this chapter.

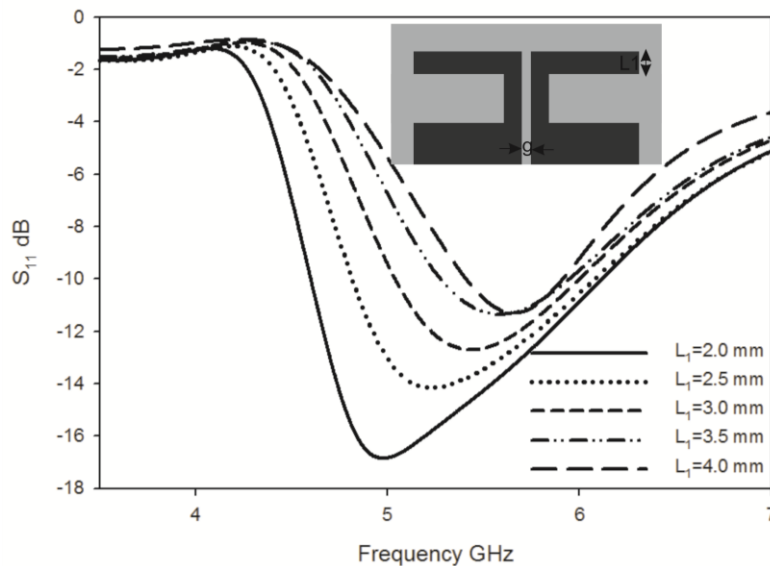


**Fig.4.9** Variation of reflection co-efficient with  $L_1$  ( $L=5.5$ mm,  $L_2=6$ mm,  $W=8$ mm,  $W_1=8$ mm,  $W_2=3$ mm and  $g=0.3$ mm)

The variation of distributed capacitance and inductance with  $L_1$  is shown in Fig.4.10. The capacitance is found to be decreasing with  $L_1$  while the inductance shows the other way. The edge length of the current path increases with  $L_1$  which in turn results in a higher shift in inductance. These changes in distributed parameter will increase the resonant frequency with an decrease in bandwidth because with  $L_1$ .

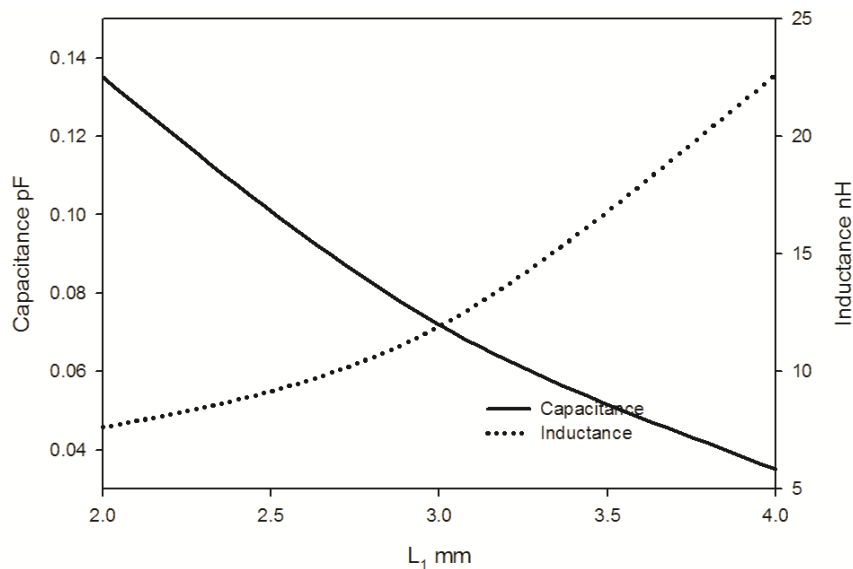


**Fig.4.10** Variation of distributed reactive components with  $L_1$  ( $L=5.5\text{mm}$ ,  $L_2=6\text{mm}$ ,  $W=8\text{mm}$ ,  $W_1=8\text{mm}$ ,  $W_2=3\text{mm}$  and  $g=0.3\text{mm}$ )

#### 4.1.2.4 Variation in reflection co-efficient with $W_1$

Variation of reflection co-efficient of the antenna with the dimensional parameter  $W_1$  is shown in Fig.4.11. As the strip length  $W_1$  increases, the resonating frequency decreases. The shift in resonant frequency is due to the increase in the resonating current path length in the antenna with increase in  $W_1$ . As the path length increases, the resonant frequency lowers. The matching of the antenna varies due to the presence of the strip of dimension  $L \times W$  just below the strip of length  $W_1$ . The presence of a metallic/conducting substance

near the radiator will change the impedance and radiation resistance of the radiator which results in a variation in impedance matching. This can be verified by the analysis of reflection co-efficient with the parameter  $W$  which is discussed in previous session 4.1.2.2.

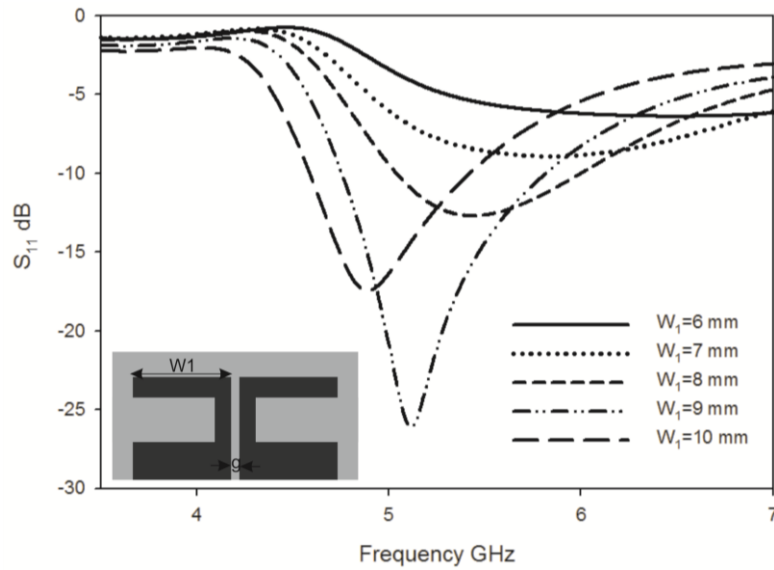


**Fig.4.11** Variation of reflection co-efficient with  $W_1$  ( $L=5.5$ mm,  $L_1=3$  mm,  $L_2 =6$ mm,  $W= 8$ mm,  $W_2=3$ mm and  $g=0.3$ mm)

The variation in distributed parameters with dimension  $W_1$  is shown in Fig.4.12. From the figure it is clear that as  $W_1$  increase both the parameters increases linearly and therefore the resonant frequency will shift towards the lower side without affecting the percentage bandwidth of the structure.

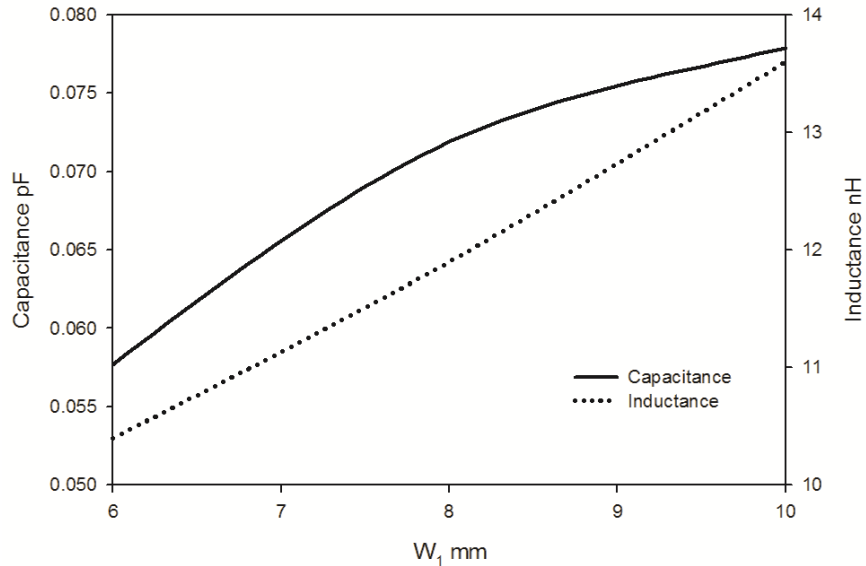


**Fig.4.12** Variation of distributed reactive components with  $W_1$  ( $L=5.5$ mm,  $L_1=3$  mm,  $L_2=6$ mm,  $W=8$ mm,  $W_2=3$ mm and  $g=0.3$ mm)

#### 4.1.2.5 Variation in reflection co-efficient with $L_2$

Variation of reflection co-efficient with strip length  $L_2$  is shown in Fig. 4.13. The resonating frequency is found to be comes towards the lower side with increase in  $L_2$ . This may be due to the increase in resonant path length with increase in  $L_2$ . This can be verified from the surface current analysis of the antenna discussed in the later session (4.1.4.4.). The variation of strip length  $L_2$  slightly affects the impedance matching of the antenna. As  $L_2$  varies, the distance between the top radiator and the reflector will vary which affect the reactive part of the impedance. But the variation in impedance mismatch is feeble in this case.

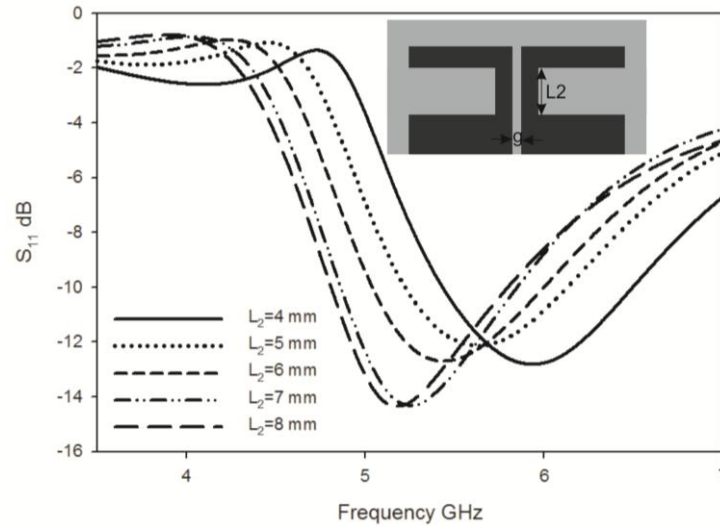


**Fig.4.13** Variation of reflection co-efficient with  $L_2$  ( $L=5.5\text{mm}$ ,  $L_1=3\text{ mm}$ ,  $W= 8\text{mm}$ ,  $W_1=8\text{mm}$ ,  $W_2=3\text{mm}$  and  $g=0.3\text{mm}$ )

The variation of distributed parameters of the antenna with  $L_2$  is shown in Fig.4.14. From the graph it is clear that both the parameters will increase with increase in  $L_2$ . Thus the resonant frequency will comes lower while the band width of the structure remains almost same for all values of  $L_2$ .

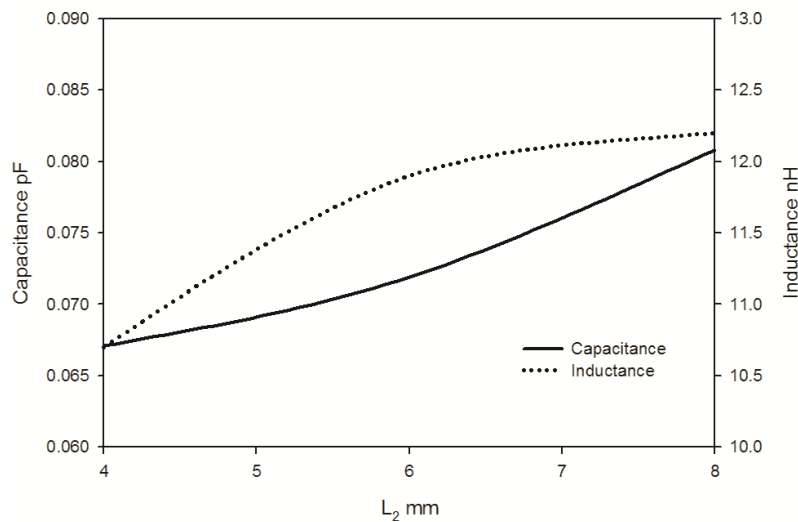


**Fig.4.14** Variation of distributed reactive components with  $L_2$  ( $L=5.5\text{mm}$ ,  $L_1=3\text{ mm}$ ,  $W= 8\text{mm}$ ,  $W_1=8\text{mm}$ ,  $W_2=3\text{mm}$  and  $g=0.3\text{mm}$ )

#### 4.1.2.6 Variation in reflection co-efficient with $W_2$

Variation of reflection co-efficient with change in strip width  $W_2$  is shown in Fig. 4.15. From the figure it is evident that as strip width increases, the resonant frequency shift to higher values and the band width and impedance matching of the antenna decreases. This is also due to the change in distributed inductance of the antenna with strip width  $W_2$ . As  $W_2$  decreases, the inductance decreases and correspondingly the bandwidth increases. Thus frequency will increase with  $W_2$ . The matching is affected because of the shift from inductive to capacitive side with increase in  $W_2$ .

The variation in distributed capacitance and inductance of the antenna structure with  $W_2$  is shown in Fig. 4.16. The capacitance shows a drastic decrease with  $W_2$  while the inductance shows an up shift with  $W_2$ . Thus the resonant frequency will decrease with an increase in bandwidth.

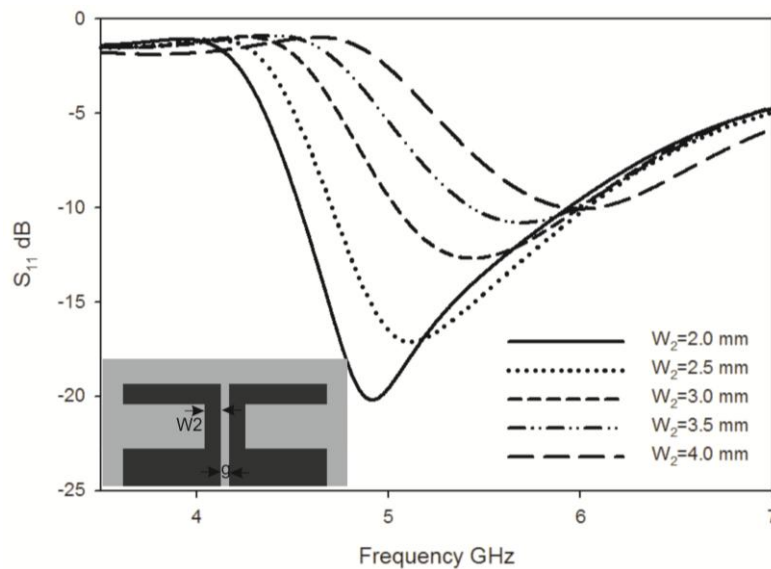


**Fig.4.15** Variation of reflection co-efficient with  $W_2$  ( $L=5.5$  mm,  $L_1=3$  mm,  $L_2=6$  mm,  $W=8$  mm,  $W_1=8$  mm and  $g=0.3$  mm)

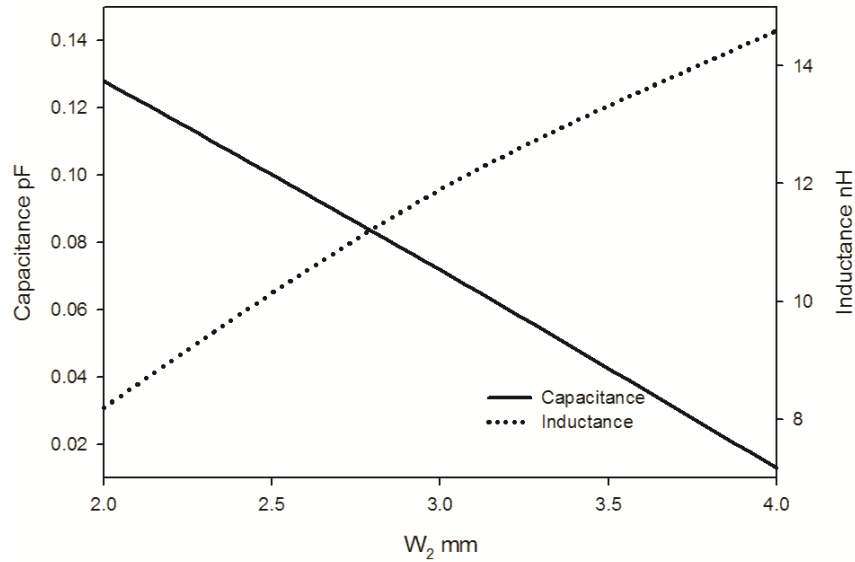


**Fig.4.16** Variation of distributed reactive components with  $W_2$  ( $L=5.5$ mm,  $L_1=3$  mm,  $L_2 =6$ mm,  $W= 8$ mm,  $W_1=8$ mm and  $g=0.3$ mm)

#### 4.1.2.7 Effect of $L_2$ on Gain of the Antenna

From the parametric analysis of the antenna, it is clear that the length of the slotline  $L$  has virtually no effect on the resonant frequency and the strip length  $W$  will effectively changes the impedance of the antenna. It may be inferred that this strip is also acting as a reflector in the radiating structure. Thus the position of this strip ie the distance between the radiating strip and the reflector strip ( $L_2$ ) will play an important role in the gain. This session deals with the variation of gain of the antenna with the distance between reflector and radiator.

The variation of the antenna gain (Simulated) with different values of  $L_2$  is shown in Fig. 4.17. From the figure it is clear that the antenna gain is strongly affected with the position of the reflector strip. A difference of 1 dBi gain is present in the antenna structure with a variation of 2 mm in the value of  $L_2$ . In the case of  $L_2 = 2$  mm, there is a dip in the gain which is due to the shift in

resonant frequency and operating band with  $L_2$  which is explained in the previous session 4.1.2.5. From the definition of reflector, the gain will be maximum at  $L_2 \approx \lambda_g/4$ .

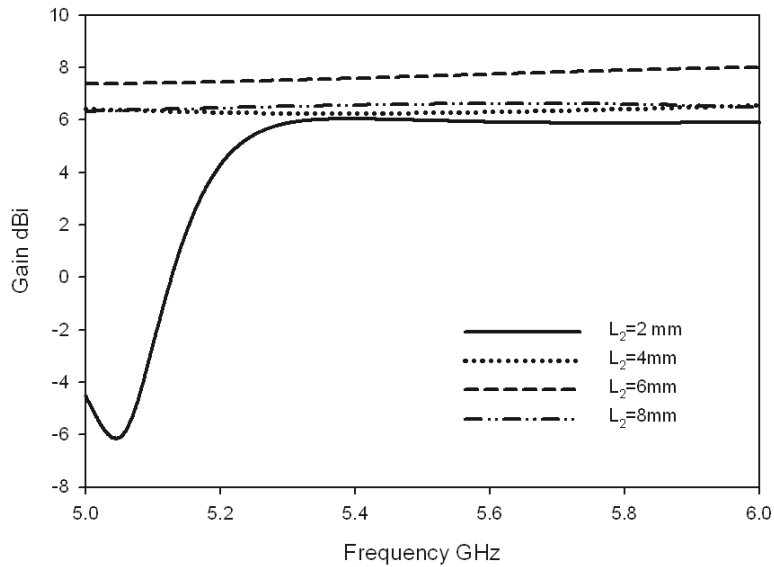


**Fig.4.17** Variation of Gain with  $L_2$  ( $L=5.5$ mm,  $L_1=3$  mm,  $W=8$ mm,  $W_1=8$ mm,  $W_2=3$ mm and  $g=0.3$ mm)

The effect of  $L_2$  on radiation patterns of the antenna are also analyzed as a part of the study of high gain dipole and are discussed in this session. The variation in co polarization radiation patterns of the antenna in the two principal planes at 5.5 GHz with  $L_2$  is shown in Fig.4.18.

The radiation patterns of the antenna for different  $L_2$  in E plane are shown in Fig 4.18 (a). Maximum power towards the bore sight direction is obtained when  $L_2 = 6$ mm. The power in the beam maximum direction is found to be decreasing when  $L_2$  is moving apart from this optimum value. The front to back ratio is also found to be maximum for the optimum value of  $L_2 = 6$ mm ie at  $L_2 \approx \lambda_g/4$ .



The two dimensional radiation patterns of the antenna in H plane for different  $L_2$  are shown in Fig. 4.18 (b). From the figure it is clear that radiated power will be maximum when  $L_2 = 6\text{mm}$ . The variation of power with  $L_2$  is found to be same as that explained in the case of E plane. From this analysis it is evident that the proposed antenna exhibits maximum directive gain at  $L_2 = 6\text{mm}$ .

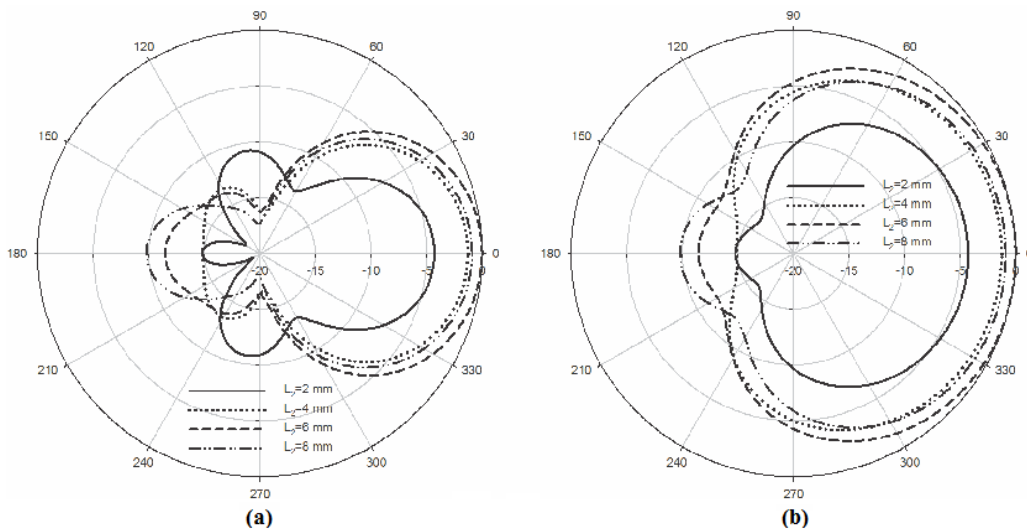


**Fig.4.18** Variation of Radiation pattern of the antenna at 5.5 GHz with  $L_2$  in (a) E Plane (b) H Plane ( $L=5.5\text{mm}$ ,  $L_1=3\text{ mm}$ ,  $W= 8\text{mm}$ ,  $W_1=8\text{mm}$ ,  $W_2=3\text{mm}$  and  $g=0.3\text{mm}$ )

#### 4.1.2.8 Effect of $W$ on Gain of the Antenna

The effect of strip length  $W$  on antenna gain is shown in Fig. 4.19. There present a small change in directive gain of the antenna with  $W$ , when the parameter  $L_1$  is equal to or greater than the length  $L$ . For  $W$  less than  $W_1$ , the gain is very less. A fall of 6 dBi gain can be noticed in the case of  $W$  less than  $W_1$ . Thus the strip length  $W$  is not an important factor in determining the gain of the antenna if its length is greater than that of the main radiator otherwise the gain is very less.

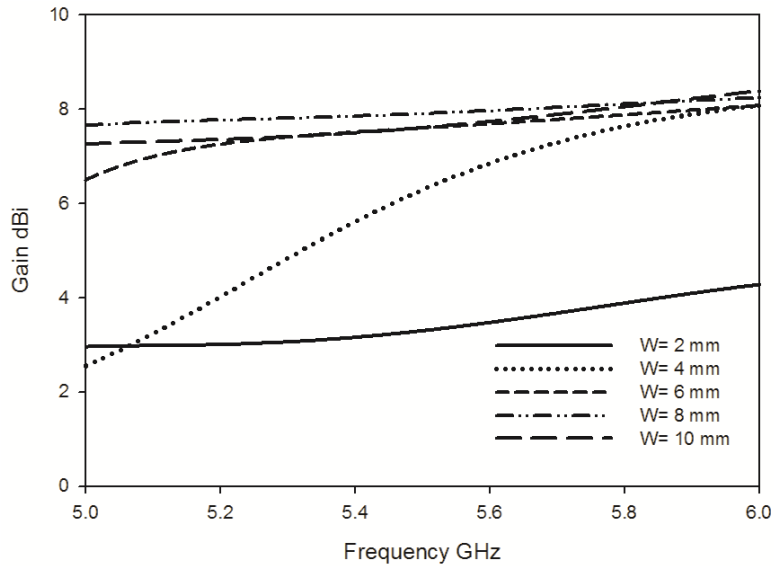


**Fig.4.19** Variation of Gain with W ( $L=5.5\text{mm}$ ,  $L_1=3\text{ mm}$ ,  $L_2 = 6\text{mm}$ ,  $W_1=8\text{mm}$ ,  $W_2=3\text{mm}$  and  $g=0.3\text{mm}$ )

From the gain analysis of the antenna with W it is clear that the gain is strongly affected by this parameter. The variation of co polarization radiation patterns of the antenna in the two principal planes at 5.5 GHz with W is shown in Fig.4.20.

The E plane radiation patterns for different W are shown in Fig 4.20 (a). From the figure it is clear that maximum power towards the bore sight direction is obtained when  $W=8\text{mm}$  ( ie  $W \approx 0.32\lambda_g$ ). The power in the beam maximum direction is found to be drastically decreasing when the parameter W goes below the length of main radiator ie  $W_1$ . Otherwise the power towards the beam maxima has only slight variation. The half power beam width of the antenna is found to be  $50^\circ$  and same for all the patterns in E plane.

The two dimensional radiation patterns of the antenna in H plane for different W are shown in Fig. 4.20 (b). Here also similar variation as that observed in E plane are found. From the observations obtained from the

radiation pattern analysis with  $W$  it is inferred that the antenna possesses maximum gain when  $W=8\text{mm}$  ( $W \approx 0.32\lambda_g$ ). The half power beam width of the antenna is found to be  $100^\circ$  and same for all the patterns in H plane.

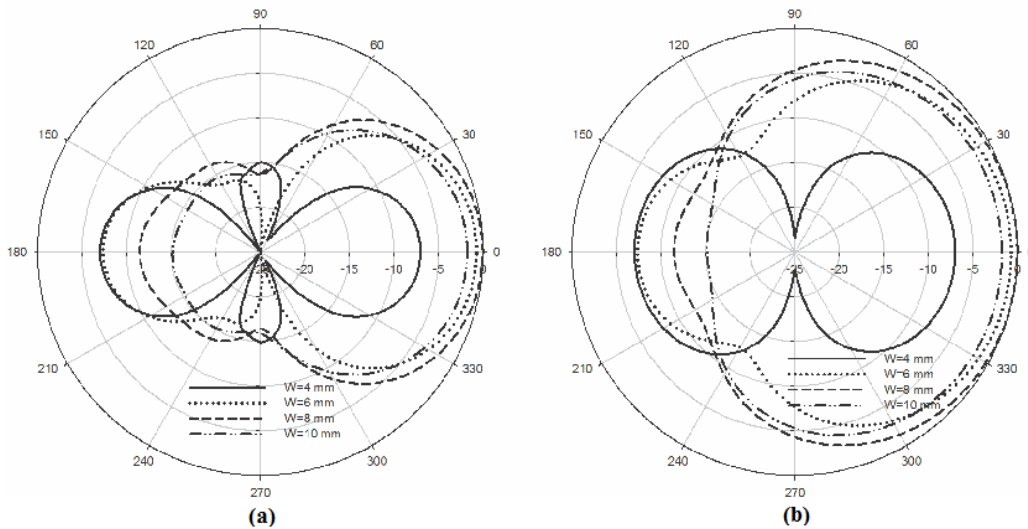


**Fig.4.20** Variation of Radiation pattern of the antenna at 5.5 GHz with  $W$  in (a) E Plane (b) H Plane ( $L=5.5\text{mm}$ ,  $L_1=3\text{mm}$ ,  $L_2=6\text{mm}$ ,  $W_1=8\text{mm}$ ,  $W_2=3\text{mm}$  and  $g=0.3\text{mm}$ )

#### 4.1.2.9 Effect of $L$ on Gain of the Antenna

The variation in the directive gain of the antenna with transmission line length  $L$  is shown in Fig. 4.21. From the figure it is clear that the gain of the antenna slightly varies with parameter  $L$  but the effect is not very dominant. The slight variation in gain may be due to the change in size/area of the reflector. Normally the gain will increase with increase in reflector area, but in this case, the area increase is not normal to the direction of propagation of wave from the antenna i.e. here the metallic area increases in  $XY$  plane and the beam maxima point towards the positive  $Y$  axis which is not normal to the  $XY$  plane and therefore the gain variation is very feeble.

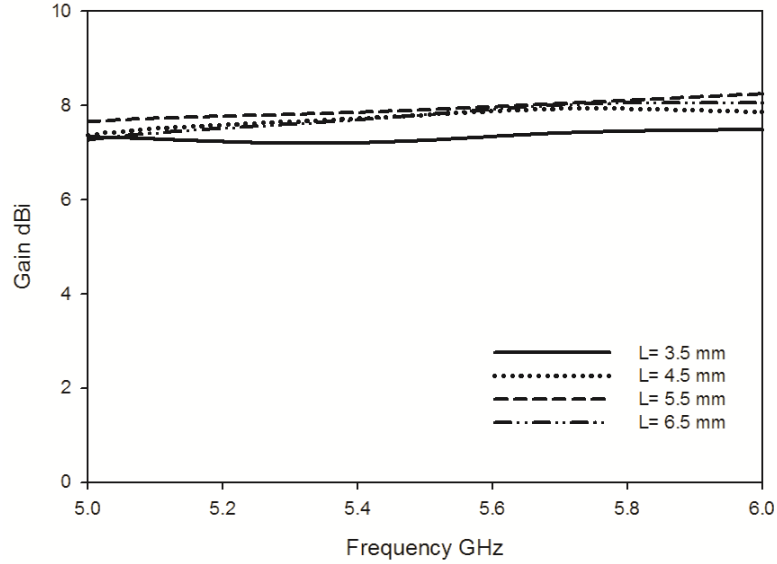


**Fig.4.21** Variation of Gain with  $L(L=8\text{mm}, L_1=8\text{mm}, L_2=6\text{mm}, W=3\text{mm}, W_2=3\text{mm}$  and  $g=0.3\text{mm}$ )

### 4.1.3 Design Equation of High Gain Dipole Antenna

From the parametric analysis performed, and the characteristic studies, the design equation of the antenna are developed and given below

$$W_1+W+L_2 -L_1-W_2 \approx 0.6 \lambda_g$$

$$L_2 + (L/2) \approx 0.25 \lambda_g$$

$$W \approx 0.32 \lambda_g$$

Here  $\lambda_g$  is the wavelength in the dielectric which is computed from the free space wavelength  $\lambda_0$  as  $\lambda_g = \lambda_0 / \sqrt{\epsilon_{re}}$

$\epsilon_{re}$  is the effective permittivity of the substrate =  $(\epsilon_r+1)/2$

In order to validate the design equations, parameters of four antennas resonating at 5.5 GHz in different substrates are computed. Table 4.1 shows the parameters of the substrates and Table 4.2 shows the computed geometric parameters of the antenna according to the developed design equations.

**Table 4.1** Substrate Description

	Antenna A	Antenna B	Antenna C	Antenna D
Laminate	Rogers 5880	FR4 Epoxy	Rogers RO3006	Rogers6010LM
h(mm)	1.57	1.6	1.28	0.635
$\epsilon_r$	2.2	4.4	6.15	10.2
$\epsilon_{re}$	1.6	2.7	3.575	5.6
g(mm)	0.1	0.3	0.65	0.775

**Table 4.2** Computed Geometric Parameters of the Antenna

Parameter (mm)	Antenna A	Antenna B	Antenna C	Antenna D
L	7.1	5.5	4.75	3.8
W	10.35	8	6.95	5.55
L <sub>1</sub>	3.9	3	2.61	2.08
W <sub>1</sub>	10.35	8	6.95	5.55
L <sub>2</sub>	7.8	6	5.21	4.16
W <sub>2</sub>	3.9	3	2.61	2.08

The simulated reflection co-efficient of the antennas developed using the specifications given by the tables 4.1 and 4.2 are shown in Fig. 4.22. From the figure it is inferred that all the four antennas are resonating at 5.5 GHz. The bandwidths of the antennas are found to be different. This may be due to the variation in Q factor of the antennas with dielectric constants of the substrates. From the very famous relation of capacitance of a plate capacitor it is clear that for high dielectric constant substrates, the distributed capacitance will be very high and therefore the Q will increase. As Q increases, the selectivity increases with a reduction in operating bandwidth.

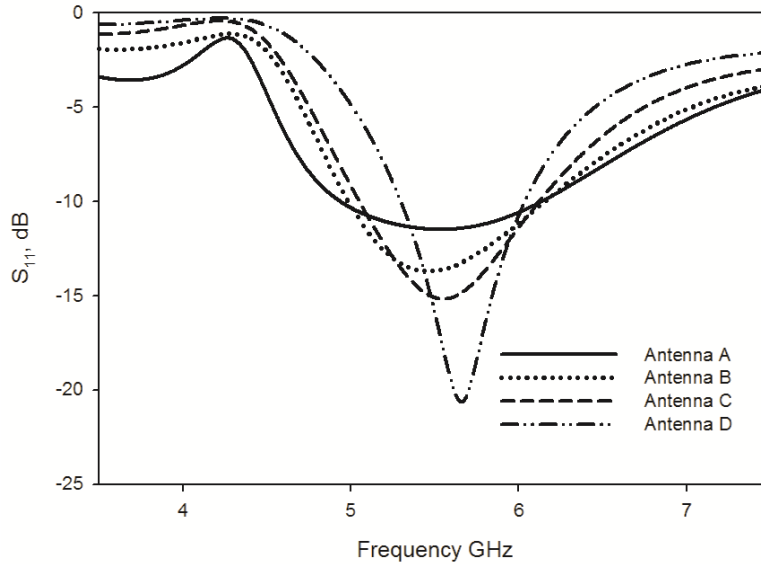


**Fig.4.22** Reflection coefficient of the antennas with computed geometric parameters for different substrates

Validation of the design equation for the high gain antenna is also done for different bands in same substrate. The parameters for different bands are calculated for FR4 substrate having dielectric constant 4.4 and thickness of 1.6 mm. The dimensional parameters and the resonance details are depicted in Table 4.3. From the tables it can be infer that the design equations are valid for any substrates and for any band of frequency.

**Table 4.3** Computed Geometric Parameters of the Antenna operating in different frequencies.

Designed Frequency	1.5 GHz	2.5 GHz	3.5 GHz	5.5 GHz
<b>L</b>	20.17	12.1	8.64	5.5
<b>W</b>	29.33	17.6	12.57	8.02
<b>L<sub>1</sub></b>	11	6.6	4.71	2.98
<b>W<sub>1</sub></b>	29.33	17.6	12.57	8.02
<b>L<sub>2</sub></b>	22	13.2	9.42	5.973
<b>W<sub>2</sub></b>	11	6.6	4.71	2.98
<b>Resonate at</b>	<b>1.52 GHz</b>	<b>2.4 GHz</b>	<b>3.52 GHz</b>	<b>5.5 GHz</b>

#### 4.1.4 Coplanar strip fed High Gain Directive Dipole Antenna for 5.2 GHz/5.8 GHz Bands

From the developed design equations, an application oriented antenna operating at 5.2 GHz and a 5.8 GHz communication band is developed for the experimental analysis. This is explained in the following session. All the radiation characteristics of the developed antenna are compared with the simulation studies.

##### 4.1.4.1 Structure of the Antenna

The structure of the proposed high gain dipole antenna is shown in Fig. 4.23. The dimensional parameters of the antenna are  $L=5.5\text{mm}$ ,  $L_1=3\text{mm}$ ,  $L_2=6\text{mm}$ ,  $W=8\text{mm}$ ,  $W_1=8\text{mm}$ ,  $W_2=3\text{mm}$  and  $g=0.3\text{mm}$ . The antenna is fabricated on commercially available FR4 substrate of dielectric constant 4.4, loss tangent 0.02 and thickness 1.6mm. The overall dimension of the antenna is about  $22.3\text{mm} \times 14.5\text{mm} \times 1.6\text{mm}$ .

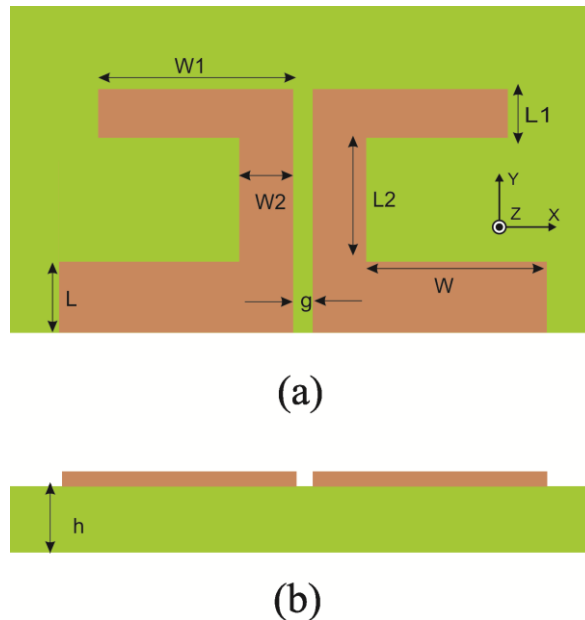


**Fig.4.23** Structure of the proposed high gain antenna. (a) Top view (b) Side view ( $L=5.5\text{mm}$ ,  $L_1=3\text{mm}$ ,  $L_2=6\text{mm}$ ,  $W=8\text{mm}$ ,  $W_1=8\text{mm}$ ,  $W_2=3\text{mm}$  and  $g=0.3\text{mm}$ .)

#### 4.1.4.2 Return loss Characteristics

The simulated and experimental reflection co-efficients of the antenna are shown in Fig. 4.24 and the two curves are matched very well. The antenna offers a 2:1 VSWR band width of 1.10 GHz from 5.08 to 6.18 GHz which is wide enough to cover both the 5.2/5.8 GHz WLAN and ISM application bands.

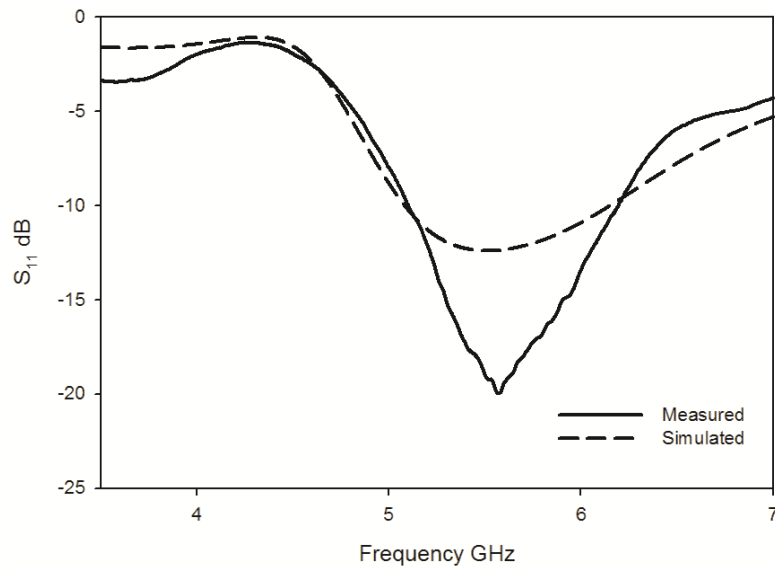


**Fig.4.24** Reflection co-efficient of high gain antenna( $L=5.5\text{mm}$ ,  $L_1=3\text{mm}$ ,  $L_2=6\text{mm}$ ,  $W=8\text{mm}$ ,  $W_1=8\text{mm}$ ,  $W_2=3\text{mm}$  and  $g=0.3\text{mm}$ .)

#### 4.1.4.3 Radiation Characteristics

The three dimensional radiation patterns of the antenna at the two application band centre frequencies are shown in Fig. 4.25. From the figure it is clear that both the radiation patterns possess a very high directional behavior. The back radiation is completely suppressed in the two patterns. Both the patterns are directed towards the bore sight direction (Y direction). The directional property of the antenna is mainly due to the reflection from the metallic strip of dimension  $L \times W$  which is an integral part of the antenna itself. This strip acts as the transmission line for the antenna and the edge of this strip



contributes in radiation also. This can be verified from the surface current distribution analysis which is explained in the next session. The main contribution of this strip in this antenna is the suppression of back radiation and reflection of electromagnetic energy into the positive Y direction, which contributes to the high gain of this structure.

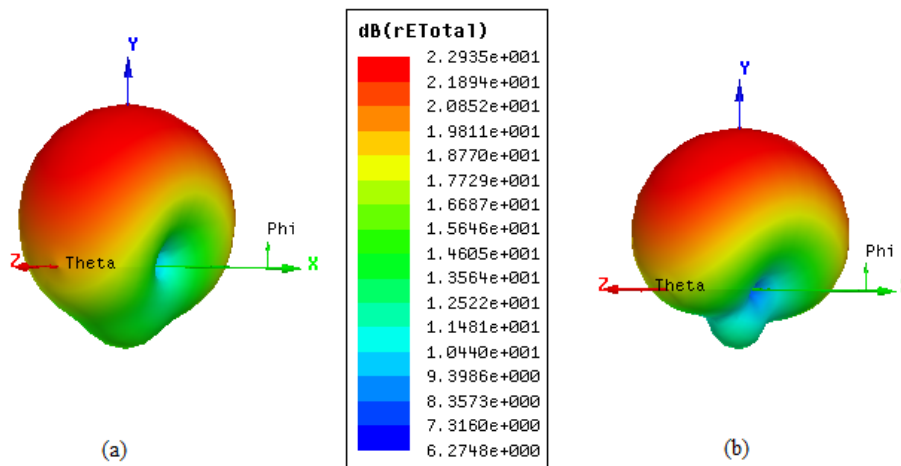


**Fig.4.25** Three dimensional Radiation Pattern of high gain antenna at (a)5.2 GHz (b) 5.8 GHz ( $L=5.5\text{mm}$ ,  $L_1=3\text{ mm}$ ,  $L_2=6\text{mm}$ ,  $W=8\text{mm}$ ,  $W_1=8\text{mm}$ ,  $W_2=3\text{mm}$  and  $g=0.3\text{mm}$ .)

To study the radiation characteristics of the antenna in the principal plane, the analysis of two dimensional radiation patterns are unavoidable. The characteristics of planar radiation patterns of the antenna in the two principal planes are discussed in this session. The two dimensional radiation patterns of the antenna in the two principal planes at different frequencies in the band of operation are shown in the Fig. 4.26.

The radiation pattern of the antenna at starting edge of the band ie at 5.08 GHz is shown in Fig.4.26.(a). The antenna is highly directional towards positive Y direction at this frequency. A front to back ratio of the order of 10 dB is present in both the E plane and H plane pattern. The cross polar level in E plane is found to be better than 30 dB while that in H plane is in the order of 40 dB. The HPBW of the antenna is found to be  $60^\circ$  in E plane and  $160^\circ$  in H plane.

The principal plane patterns of the antenna at the WLAN centre frequency 5.2 GHz is shown in Fig.4.26(b). Here also the beam maximum is pointed towards the positive Y direction. The front to back ratio in both the planes are found to be in the order of 12dB. In this frequency also the cross polar purity in E plane is 30 dB and that in H plane is 40 dB. The HPBW of the antenna is found to be  $60^{\circ}$  in E plane and  $160^{\circ}$  in H plane.

The electromagnetic energy distribution of the antenna in two principal planes at the resonant frequency 5.5 GHz are shown in Fig. 4.26.(c). The radiation pattern in this frequency is found to be almost symmetrical to that at 5.2 GHz with a small enhancement in the front to back ratio. The direction of beam maxima and the polarization etc remains the same in this pattern also. The HPBW of the antenna is found to be same as that discussed in previous frequency.

The radiation patterns of the antenna at 5.8 GHz are shown in Fig. 4.26.(d). At this frequency there is a heavy suppression of the energy towards the negative Y direction. The front to back ratio at this frequency is found to be 14 dB in both the planes with a cross polar level better than 35 dB. Here also the bore sight of the antenna is point towards positive Y direction. The HPBW of the antenna is remaining same for this frequency also.

The radiation patterns of the antenna at end frequency 6.18 GHz are shown in Fig. 4.26.(e). The front to back ratio at this frequency is found to be 15 dB in both the planes with a cross polar level better than 35 dB. At higher frequencies of the operating band it is found that the back suppression is very high. Here also the beam maximum points towards Y direction. Here also the HPBW of the antenna is  $60^{\circ}$  in E plane and  $160^{\circ}$  in H plane.

From the entire radiation pattern discussed here it is found that the antenna has excellent radiation pattern stability. All the important characteristics like beam maxima direction, polarization, position of radiation nulls etc of the radiation is found to be same in all the radiation patterns. The cross polar purity of the entire radiation patterns are also very good.

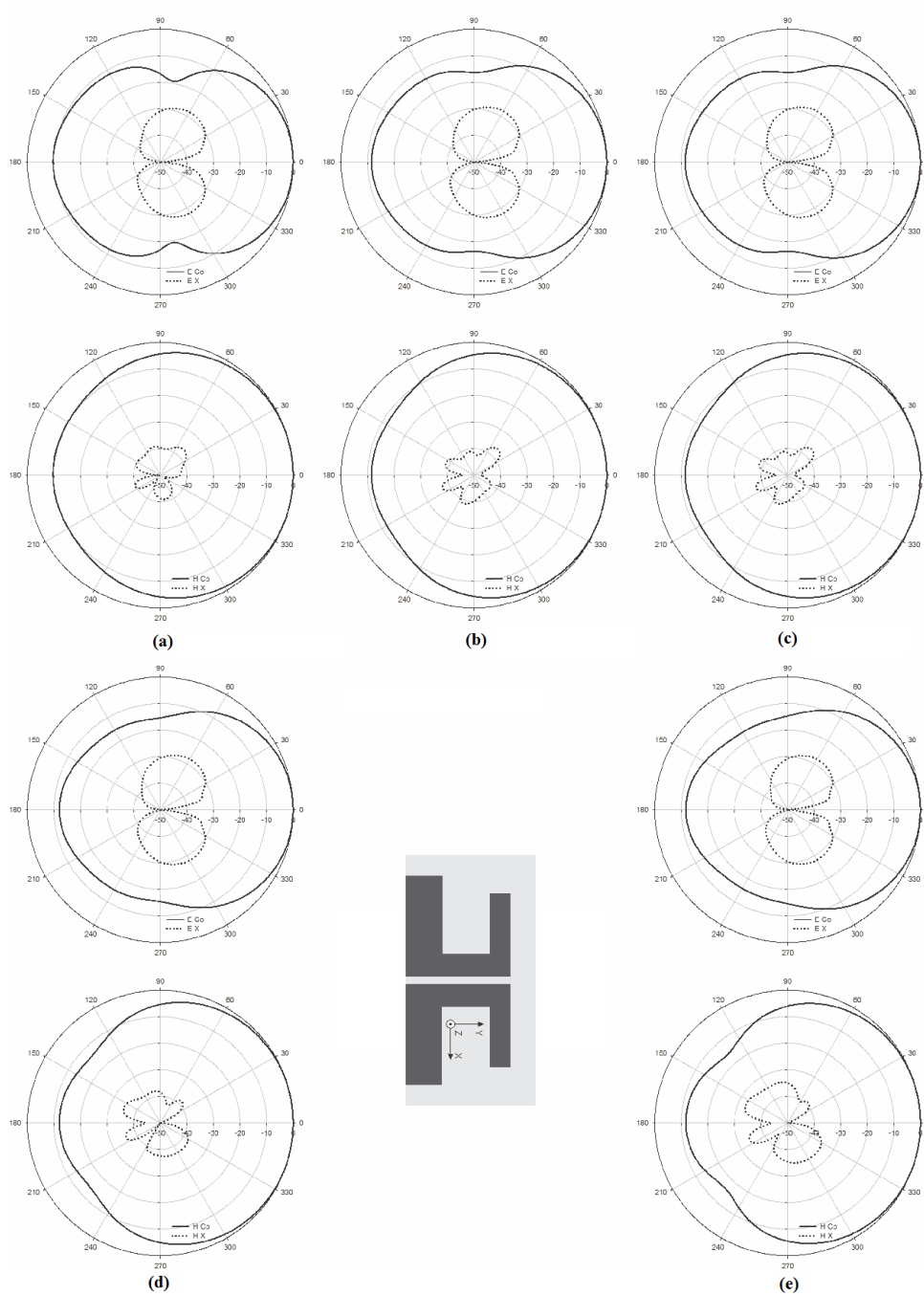


**Fig.4.26** Two dimensional Radiation Pattern of high gain antenna at (a) 5.08 GHz (b) 5.2 GHz (c) 5.5 GHz (d)5.8 GHz and (e) 6.18 GHz ( $L=5.5\text{mm}$ ,  $L_1=3\text{mm}$ ,  $L_2=6\text{mm}$ ,  $W=8\text{mm}$ ,  $W_1=8\text{mm}$ ,  $W_2=3\text{mm}$  and  $g=0.3\text{mm}$ .)

#### 4.1.4.4 Surface Current Analysis

Simulated surface current patter of the antenna at the resonant frequency is shown in Fig. 4.27. From the figure it is clear that the resonance is mainly due to the surface current through strip of length  $W_1$ . The edge of the strip of dimension  $L \times W$  is also contributes to the additive radiation. Current through strips of dimension  $L_2 \times W_2$  has large and equal amplitude but are in opposite direction which results in the field cancellation of radiation from these strips. This is the reason for the high cross polar purity which is found in the two principle plane radiation pattern of the antenna.

In the strip of dimension  $L \times W$ , except the edges, the surface current has relatively very small intensity. This shows that this part does not contributes much for the radiation but play an important role in reflecting the back radiated power into the bore sight direction. The presence of this strip is the main reason for the high front to back ratio which is found in the two principle plane radiation pattern of the antenna. This reflection will enhance the directive gain of the antenna also and is explained in the next session.

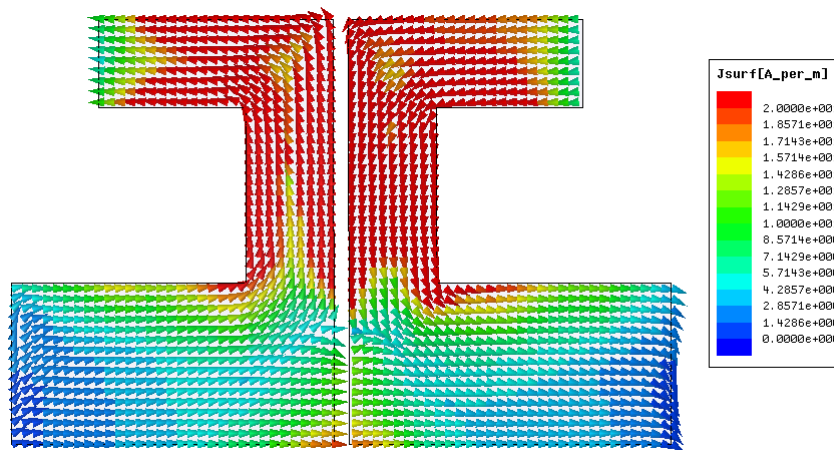


**Fig.4.27** Simulated Surface Current Distribution of the antenna at 5.5 GHz ( $L=5.5\text{mm}$ ,  $L_1=3\text{mm}$ ,  $L_2=6\text{mm}$ ,  $W=8\text{mm}$ ,  $W_1=8\text{mm}$ ,  $W_2=3\text{mm}$  and  $g=0.3\text{mm}$ .)

#### **4.1.4.5 Gain of the Antenna**

The measured gain of the antenna in the entire operating band is shown in Fig. 4.28. The antenna offers almost constant gain in the entire band with an average gain of 7.8 dBi in the entire operating band with a peak gain of 8.4 dBi at 5.8 GHz. This enhanced gain is achieved without the help of any parasitic elements. An integral part of the antenna acts as the reflector in this structure and which contributes to the enhanced gain of the antenna.

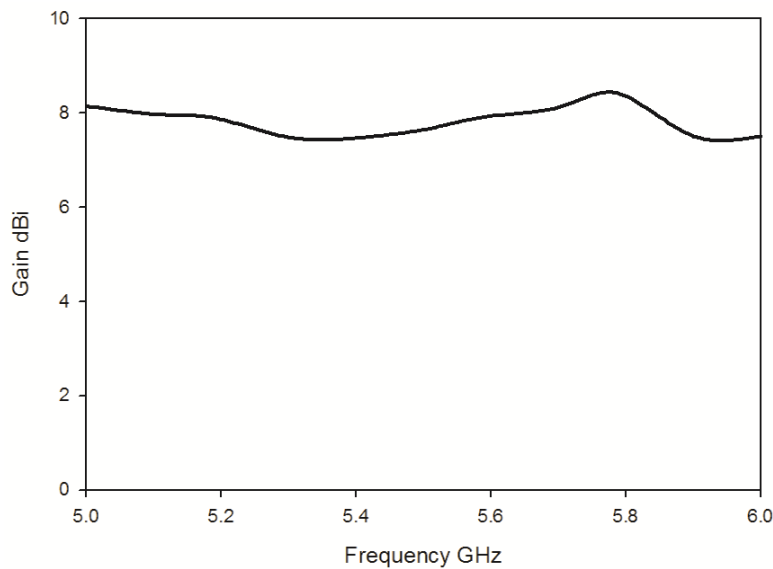


**Fig.4.28** Measured Gain of the antenna in the entire operating band ( $L=5.5\text{mm}$ ,  $L_1=3\text{ mm}$ ,  $L_2=6\text{mm}$ ,  $W=8\text{mm}$ ,  $W_1=8\text{mm}$ ,  $W_2=3\text{mm}$  and  $g=0.3\text{mm}$ .)

#### **4.1.4.6 Radiation Efficiency of the Antenna**

The radiation efficiency of the antenna in the operating band is shown in Fig. 4.29. The proposed antenna radiates the power very effectively with an average efficiency of 92%. Antenna offers efficiency greater than 90 % in the entire band of operation. Almost all metallic part of the radiating structure contributes to the radiation in far field. This may be the reason for this enhanced

efficiency. This can be verified from the surface current distribution and is explained in the previous session.

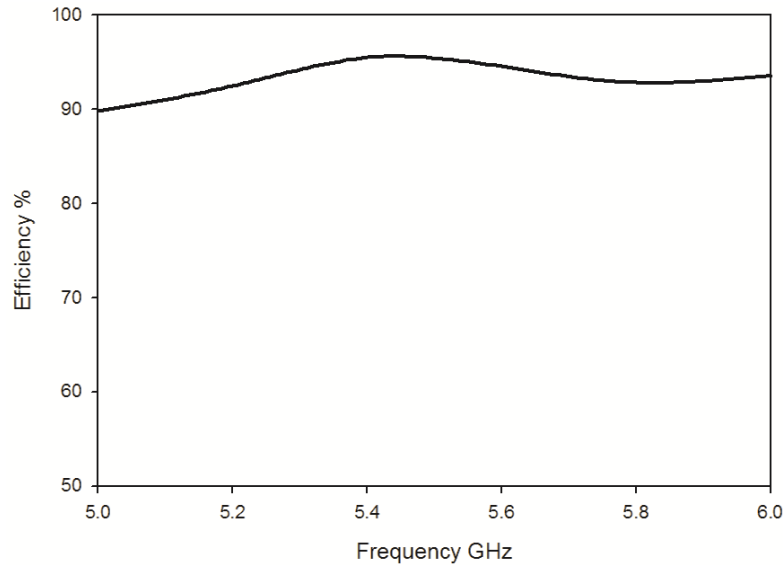


**Fig.4.29** Measured Radiation Efficiency of the antenna in the entire operating band ( $L=5.5\text{mm}$ ,  $L_1=3\text{ mm}$ ,  $L_2=6\text{mm}$ ,  $W=8\text{mm}$ ,  $W_1=8\text{mm}$ ,  $W_2=3\text{mm}$  and  $g=0.3\text{mm}$ .)

## 4.2 Bandwidth Enhancement of High Gain Dipole Antenna

From the studies discussed in previous sessions especially on the strip width variation studies (session 4.1.2.3 and 4.1.2.6), it is noticed that there is a tendency of increasing the bandwidth of the antenna structure with decrease in strip widths. With strip width  $W_1$ , there is no considerable change in resonant frequency and band width. But as we decrease the parameters  $L_1$  and  $W_2$ , ie the *width* of main radiating elements, there is a considerable change in band width of the antenna. Through the thorough study of these factors it is able to develop a wideband antenna which poses all the properties like directional behavior, high gain, high efficiency etc in the entire band with compactness. These properties make it a suitable and potential candidate for the medical imaging purpose. This is discussed in this session.

### 4.2.1 Evolution of the Wide Band Antenna

Evolution of wideband high gain antenna from the high gain antenna discussed in the previous session is shown in Fig.4.30. The wide band antenna is developed by tending the parameters  $L_1$  and  $W_2$  of the high gain antenna (Hereinafter  $L_1$  is re-notated as  $W$  for simplicity) into very small values which will reduce the edge length of the structure and results in a decrement in the distributed inductance. The decrease in inductance will results in a reduction in the Q factor. The band width is an inverse function of the Q and hence the large bandwidth.

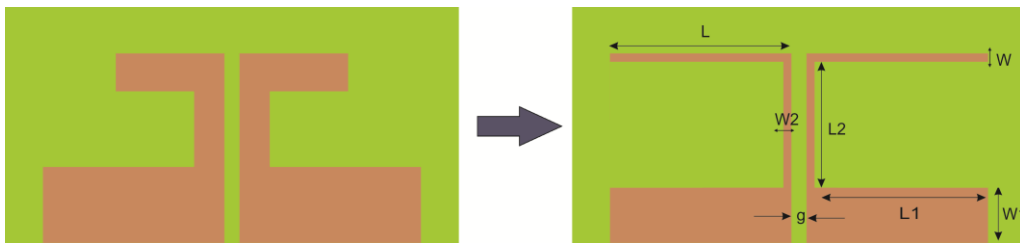


**Fig.4.30** Evolution of wide band antenna from the High Gain Antenna

To optimize the radiating structure for maximum bandwidth, uniform gain and directional radiation pattern etc a set of dimensional analysis were performed and are explained in the following sessions.

### 4.2.2 Parametric Analysis

The parametric analysis of the wideband high gain antenna developed from the antenna discussed in the previous session is carried out in this session. This study is performed to explain the reason for resonance and high band width obtained with this structure. The dimensional parameters of the antenna are varied separately and the resulting characteristics are analyzed by keeping all the other parameters constant except parameter under study. The variation in

capacitance and inductance of the structure as a function of dimension is also analyzed. The study and the results obtained are explained in this session.

#### 4.2.2.1 Variation in reflection co-efficient with L

The effect of varying the parameter L on resonance is analyzed and discussed in this session. Variation of reflection coefficient of the wideband structure with L is shown in Fig. 4.31. As L increases, the first and third resonance comes to lower side while the second resonance remains the same. Thus it is very clear that the second resonance is independent of the strip length L. The lower shift in first and third resonance is due to the increased surface current path with increase in L. These findings can be verified from the surface current distribution plot given in Fig.4.47. The band width and the impedance matching are found to be remaining same for all values of L.

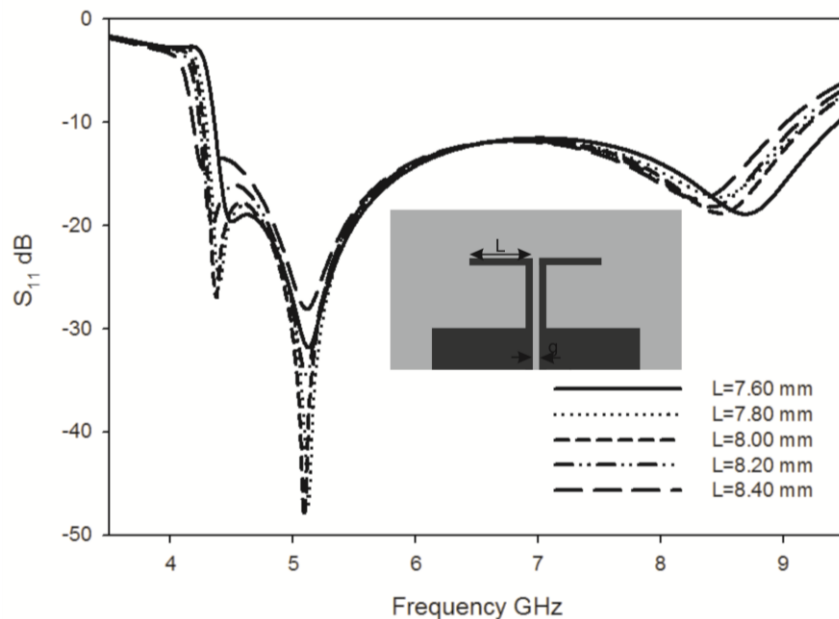


**Fig.4.31** Reflection co-efficient of the wide band antenna for different L ( $L_1=10.4\text{mm}$ ,  $L_2=5.5\text{mm}$ ,  $W=0.3\text{mm}$ ,  $W_1=3\text{mm}$ ,  $h=1.6\text{mm}$  and  $\epsilon_r=4.4$ )



The variations of distributed parameters of the antenna corresponding to the three resonances with dimension L are shown in Fig.4.32. From Fig 4.32 (a) it is evident that the distributed capacitance of the antenna at first resonance decreases with L while the inductance shows an up shift with L. The variation in inductance is predominant and this will result in a reduction in first resonant frequency with an increase in Q factor. From figure 4.32 (b), it is clear that both the distributed components corresponding to second resonance remains unaffected by the parameter L. Both the capacitance and inductance corresponding to third resonance which is given in fig.4.32.(c) tends to increase with L. This will result in a lower shift in third resonant frequency with a reduction in band width (Due to large variation in inductance) of the corresponding resonance.

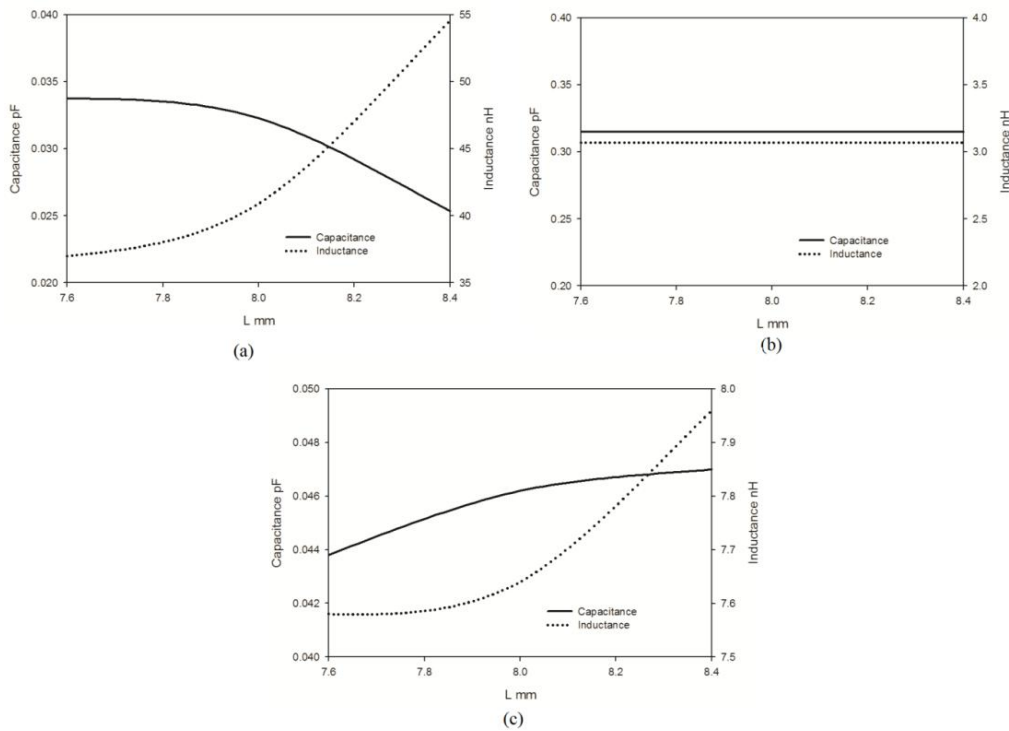


**Fig.4.32** Variation of Reactive components with L ( $L_1=10.4\text{mm}, L_2=5.5\text{mm}, W=0.3\text{mm}, W_1=3\text{mm}, h=1.6\text{mm}$  and  $\epsilon_r=4.4$ )

#### 4.2.2.2 Variation in reflection co-efficient with $L_1$

Reflection co-efficient of the wide band high gain antenna with  $L_1$  is studied and the curves showing the variation in reflection co-efficient are shown in Fig.4.33. It is the second resonance is strongly affected with the parameter  $L_1$ . The second resonance shows a drastic lower shift with increase in  $L_1$ . This may be due to the increase in surface current path length of second resonance with increase in  $L_1$ . From the figure it is also noted that both first and third resonances are unaffected by the variation in strip length  $L_1$ . Thus first and third resonances are independent of strip length  $L_1$ . This inference can be verified from the surface current distribution given in Fig.4.47.

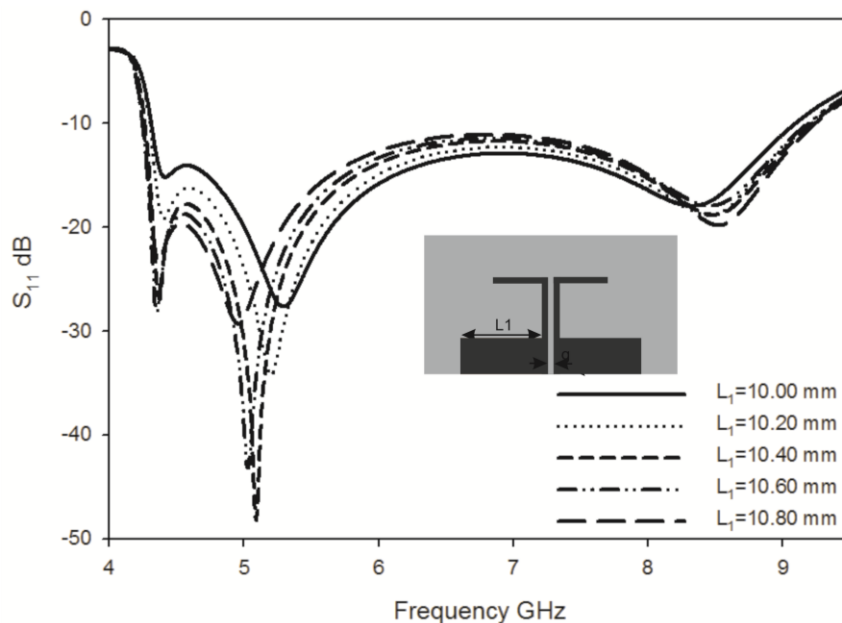


**Fig.4.33** Reflection co-efficient of the wide band antenna for different  $L_1$  ( $L=8\text{mm}$ ,  $L_2=5.5\text{mm}$ ,  $W=0.3\text{mm}$ ,  $W_1=3\text{mm}$ ,  $h=1.6\text{mm}$  and  $\epsilon_r=4.4$ )

The variations of the distributed parameters of the antenna with parameter  $L_1$  corresponding to first, second and third resonances are shown in Fig.4.34 (a), (b) and (c) respectively. From the graphs it is clear that the

capacitance and inductance corresponding to first and third resonances are unaffected by the changes in  $L_1$ . Thus both the resonant frequencies were remaining same for all values of  $L_1$ . Both the distributed parameters corresponding to third resonance is found to be steadily increasing with  $L_1$ . This will result in a decreasing of second resonant frequency.

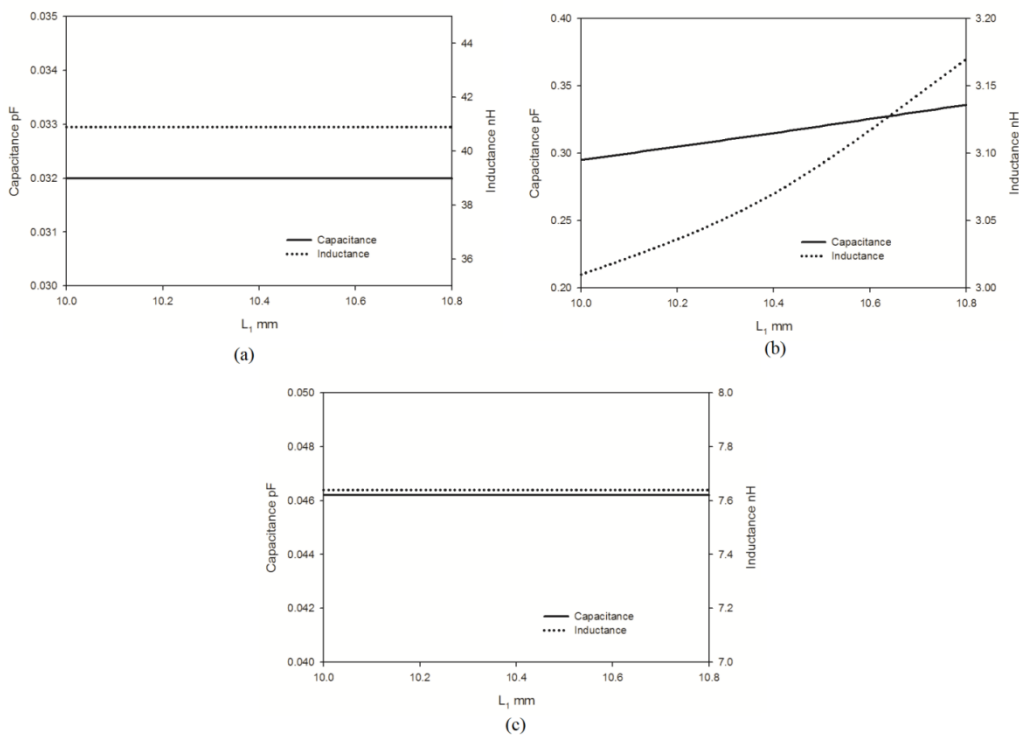


**Fig.4.34** Variation of Reactive components with  $L_1$  ( $L=8\text{mm}$ ,  $L_2=5.5\text{mm}$ ,  $W=0.3\text{mm}$ ,  $W_1=3\text{mm}$ ,  $h=1.6\text{mm}$  and  $\epsilon_r=4.4$ )

#### 4.2.2.3 Variation in reflection co-efficient with $L_2$

In this session the dimensional parameter  $L_2$  is varied symmetrically and the results are analyzed. The variation of reflection co-efficient with the parameter  $L_2$  is shown in Fig. 4.35. Both the first and second resonances are remaining same for all values of  $L_2$ . The third resonance is strongly affected by  $L_2$  and it is shifted towards the lower side with increase in  $L_2$ . The down

shifting of third resonance with increase in  $L_2$  is mainly due to the increased current path. The band width and the impedance matching remains the same for all values of  $L_2$ .

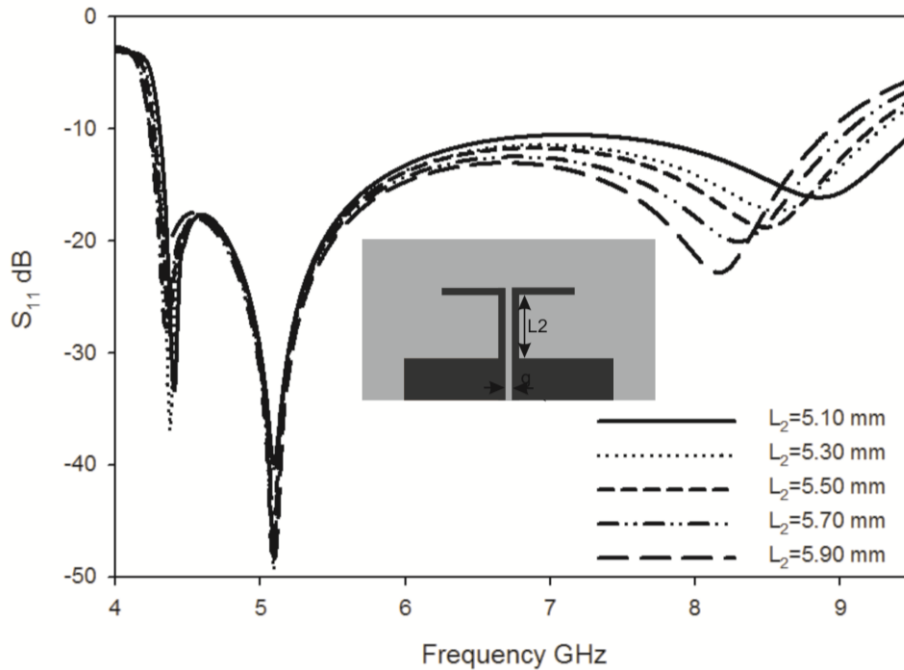


**Fig.4.35** Reflection co-efficient of the wide band antenna for different  $L_2$  ( $L=8$ mm,  $L_1=10.4$ mm,  $W=0.3$ mm,  $W_1=3$ mm,  $h=1.6$ mm and  $\epsilon_r=4.4$ )

The variations in distributed inductance and capacitance of the antenna corresponding to the three resonances with  $L_2$  are shown in Fig.4.36. From figures 4.36 (a) and (b) it is evident that the capacitance and inductance of the antenna at first and second resonance are independent of  $L_2$ . The distributed elements at third resonance are strongly affected by  $L_2$ . The capacitance at this frequency increases while the inductance decreases. This will result in a lower shift in resonant frequency with an increase in bandwidth at third resonance.

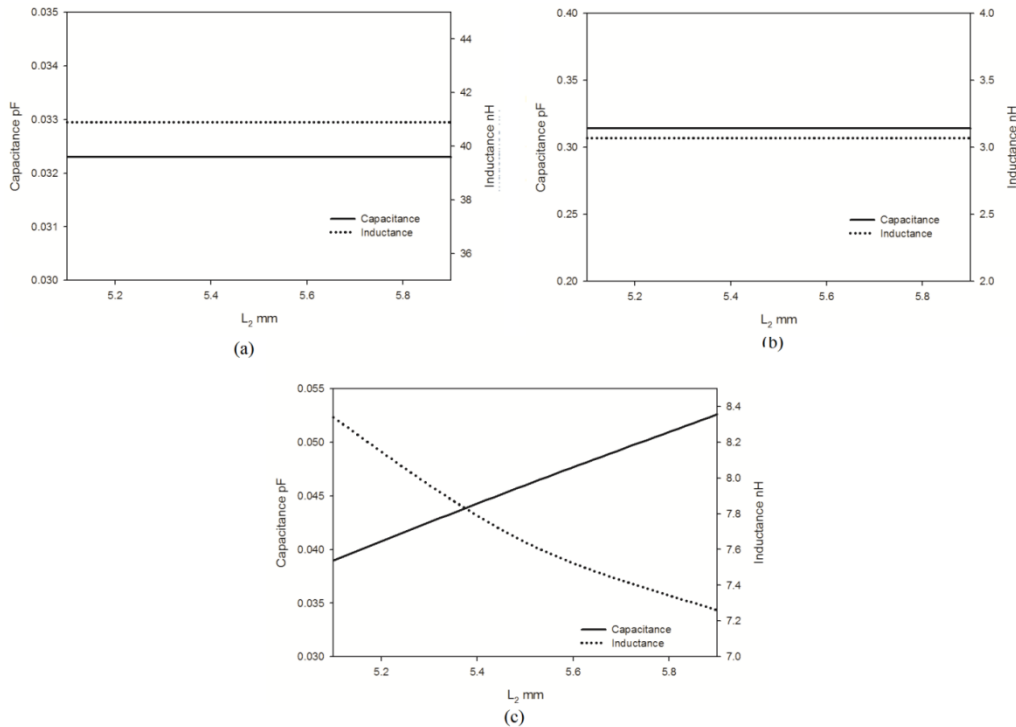


**Fig.4.36** Variation of Reactive components with  $L_2$  ( $L=8$ mm,  $L_1=10.4$ mm,  $W=0.3$ mm,  $W_1=3$ mm,  $h=1.6$ mm and  $\epsilon_r=4.4$ )

#### 4.2.2.4 Variation in reflection co-efficient with $W_1$

The effect of variation of transmission line length  $W_1$  on reflection co-efficient is discussed in this session. Variation of reflection co-efficient with  $W_1$  is shown in Fig. 4.37 and from that it is evident that as  $W_1$  increases, the first and third resonances remains unaffected but there is a very feeble up shift on resonant frequency of the second resonance with  $W_1$ . The reason for this higher shift in frequency is same as that explained in the case of OES in session 3.3.2.1 of the previous chapter ie as the length of the slotline increases, the fringing field tends to concentrate near the slot and at the far ends of the conducting planes the surface current density is nearly zero. Thus in an OES with higher length, the resonance current will tends to maximize near the slot which results in reduction of length of resonant current path and thus increases the resonant

frequency. The impedance matching and band width are found to be same for all the values of  $W_1$ . Since the frequency shift of second resonant is very feeble with  $W_1$ , it is not an important design parameter for this antenna.

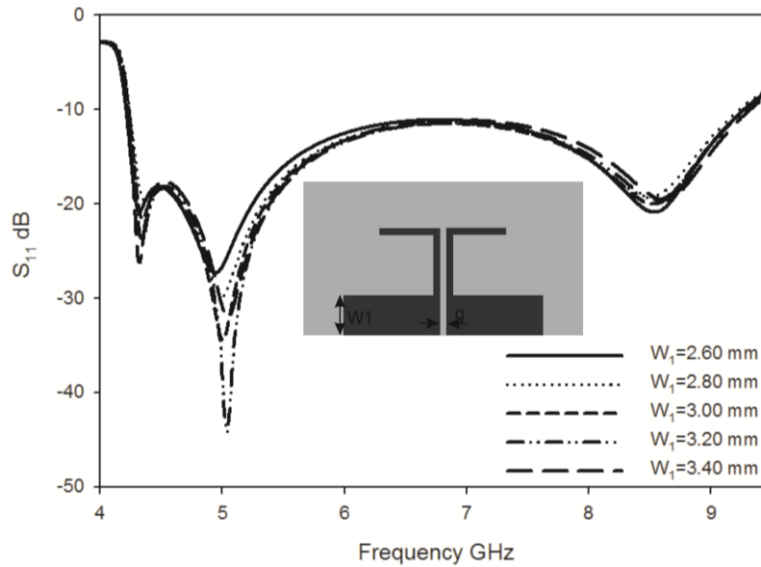


**Fig.4.37.** Reflection co-efficient of the wide band antenna for different  $W_1$  ( $L=8\text{mm}$ ,  $L_1=10.4\text{mm}$ ,  $L_2=5.5\text{mm}$ ,  $W=0.3\text{mm}$ ,  $h=1.6\text{mm}$  and  $\epsilon_r=4.4$ )

#### 4.2.2.5 Variation in reflection co-efficient with $L$ and $L_2$ by keeping $L+L_2$ constant

From the parametric analysis mentioned in session 4.5.2.1 and 4.5.2.3, it is evident that the third resonances is strongly affected by the strip lengths  $L$  and  $L_2$  while the first resonance is affected by  $L$ . To determine the effect of these strip lengths on resonances a study is carried out by varying  $L$  and  $L_2$  simultaneously by keeping their sum a constant. The variation of reflection co-efficient of the antenna by varying  $L$  and  $L_2$  simultaneously and by keeping their sum as 13.5mm is shown in Fig.4.38. Only first resonance is affected by the variation. The other two resonances are remaining nearly same for all the values of  $L$  and  $L_2$  with  $L + L_2$  a constant. From this it is inferred that the first

resonance is mainly due to the strip length  $L$  and the third resonance is due to strip length  $L + L_2$ .

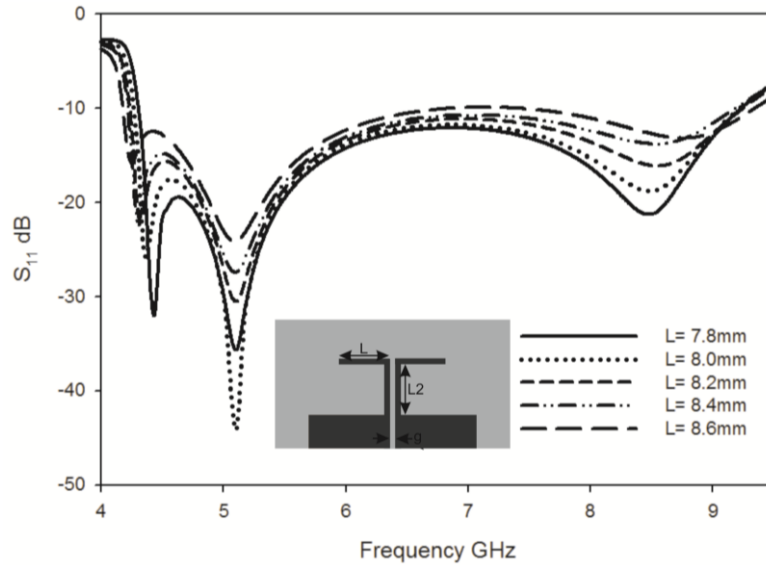


**Fig.4.38.** Reflection co-efficient of the wide band antenna for different  $L$  Keeping  $L+L_2$  a constant ( $L=8\text{mm}$ ,  $L_1=10.4\text{mm}$ ,  $L+L_2=13.5\text{mm}$ ,  $W=0.3\text{mm}$ ,  $h=1.6\text{mm}$  and  $\epsilon_r=4.4$ )

From the variation analysis of the antenna structure, it is found that the strip with dimensions  $L_1$  and  $W_1$  acts as a reflector for a wide range of frequencies at first and third resonances. Since the gain of the antenna depends on the parameters like reflector spacing and length of the reflector, it is important to analyze the effect of these parameter on the directive gain. Simulation analyses are performed to analyze the effect of these parameters and are discussed in the next two sessions

#### 4.2.2.6 Variation in reflection co-efficient with substrate height $h$

The variation of reflection co-efficient for different substrate height is shown in Fig. 4.39. From the figure it is evident that the parameter  $h$  hasn't any considerable impact on antenna resonance. All the resonant frequencies are remaining the same for all values of  $h$ . The matching is slightly affected by

variation in substrate height but the effect is very feeble so that the impedance bandwidth is remaining the same.

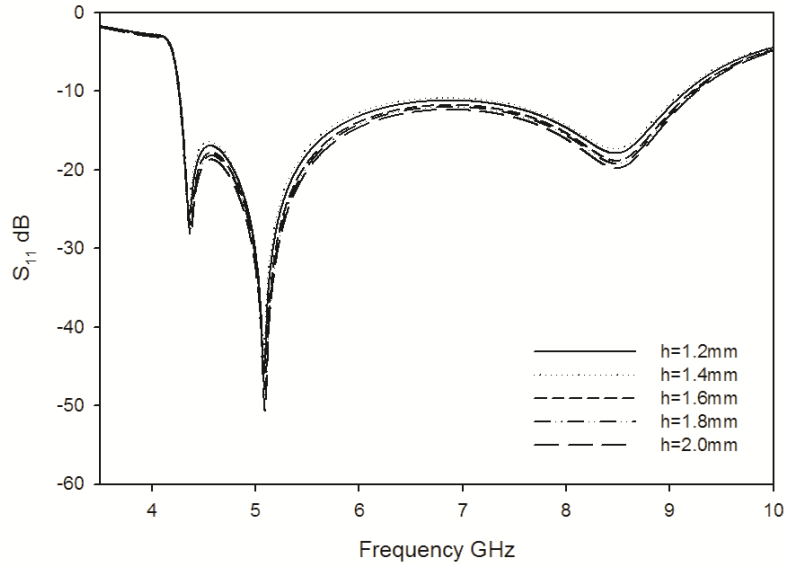


**Fig.4.39** Reflection co-efficient of the wide band antenna for different  $h$  ( $L=8\text{mm}$ ,  $L_1=10.4\text{mm}$ ,  $L_2=5.5\text{mm}$ ,  $W=0.3\text{mm}$ ,  $W_1=3\text{mm}$  and  $\epsilon_r=4.4$ )

#### 4.2.2.7 Effect of $L_1$ on Gain of the antenna

Variation of directive gain of the antenna for different reflector length  $L_1$  is shown in Fig.4.40. From the gain variation plot it is clear that the directive gain is maximum at an optimum value of  $L_1=10.4$  mm. The gain is found to be reducing when  $L_1$  changing from the optimum value. The variation in gain is found to be very feeble which infer that the reflector length hasn't a strong impact on gain of the antenna when it is greater than the length of radiating element.



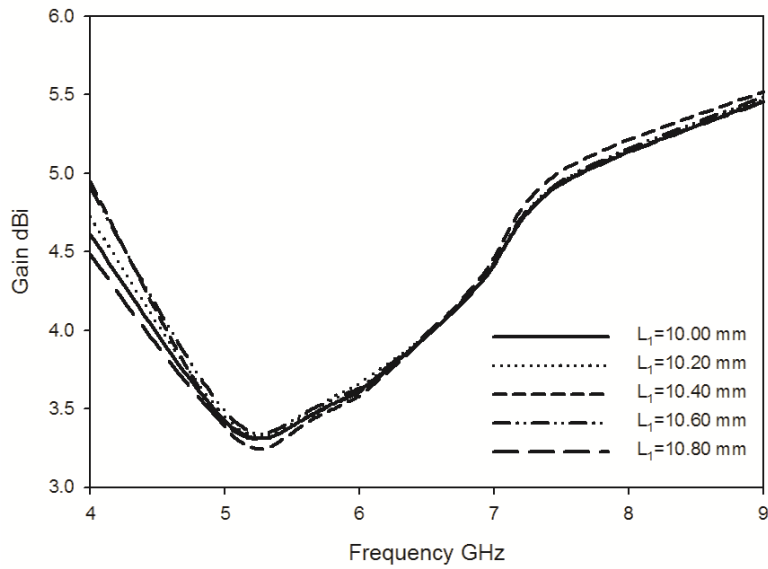


**Fig.4.40** Gain of the wide band antenna for different  $L_1$  ( $L=8\text{mm}$ ,  $L_2=5.5\text{mm}$ ,  $W=0.3\text{mm}$ ,  $W_1=3\text{mm}$  and  $\epsilon_r=4.4$ )

#### 4.2.2.8 Effect of $L_2$ on Gain of the antenna

The variation of gain of the antenna for different radiator and reflector spacing is shown in Fig. 4.41. From the figure it is evident that the strip length  $L_2$  has a strong effect on determining the gain of the antenna. The gain is found to be maximum at  $L_2=5.5\text{mm}$  and found to be decreasing if  $L_2$  is changing away from the optimum value.

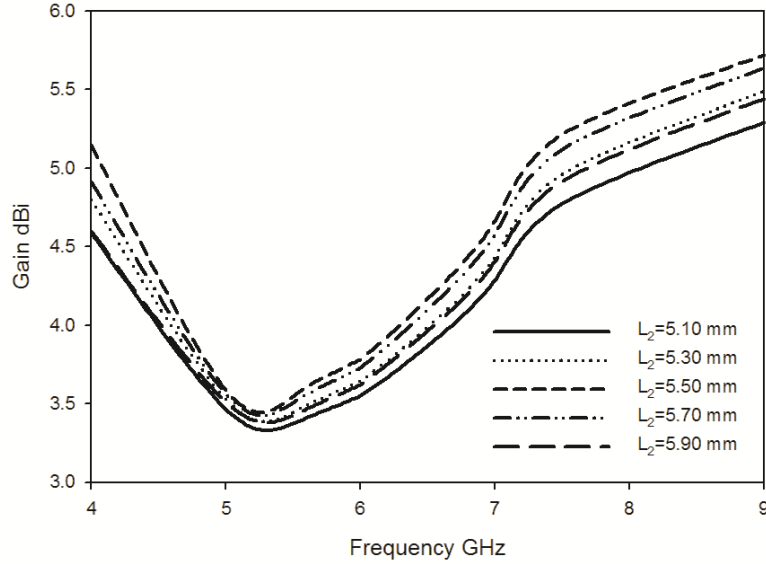


**Fig.4.41** Gain of the wide band antenna for different  $L_2$  ( $L=8\text{mm}$ ,  $L_1=10.4\text{mm}$ ,  $W=0.3\text{mm}$ ,  $W_1=3\text{mm}$  and  $\epsilon_r=4.4$ )

### 4.2.3 Design equations of the wide band antenna

From the variation analysis of different parameters of the structure, the design equations for the wideband antenna are developed as follows.

$$\mathbf{L} + (\mathbf{g}/2) \approx 0.2 \lambda_{g1}$$

$$\mathbf{L}_1 + (\mathbf{g}/2) + \mathbf{W} \approx 0.3 \lambda_{g2}$$

$$\mathbf{L} + \mathbf{L}_2 + (\mathbf{g}/2) \approx 0.64 \lambda_{g3}$$

Where  $\lambda_{g1}$ ,  $\lambda_{g2}$  and  $\lambda_{g3}$  are the guided wavelengths corresponding to the first, second and third resonances.

In order to validate the design equations, parameters of four antennas with resonating frequencies at 4.3 GHz, 5GHz and 8.5 GHz in different substrates are computed. Table 4.4 shows the parameters of the substrates and Table 4.5 shows the computed geometric parameters of the antenna according to the developed design equations.

**Table 4.4** Substrate Description

	<b>Antenna A</b>	<b>Antenna B</b>	<b>Antenna C</b>	<b>Antenna D</b>
<b>Laminate</b>	Rogers 5880	FR4 Epoxy	Rogers R03006	Rogers6010LM
<b>h(mm)</b>	1.57	1.6	1.28	0.635
$\epsilon_r$	2.2	4.4	6.15	10.2
$\epsilon_{re}$	1.6	2.7	3.575	5.6
<b>g(mm)</b>	0.1	0.3	0.65	0.775

**Table 4.5** Computed Geometric Parameters of the Antenna

<b>Parameter (mm)</b>	<b>Antenna A</b>	<b>Antenna B</b>	<b>Antenna C</b>	<b>Antenna D</b>
<b>L</b>	10.39	8	6.95	5.55
<b>L<sub>1</sub></b>	13.51	10.4	9.04	7.22
<b>L<sub>2</sub></b>	7.14	5.5	4.78	3.82
<b>W</b>	0.3	0.3	0.3	0.3
<b>W<sub>1</sub></b>	3.9	3	2.61	2.09

The simulated  $S_{11}$  parameters of the antennas developed using the specifications given by the tables 4.4 and 4.5 are shown in Fig. 4.42. It is found that all the four antennas having three resonating frequencies in the desired band and all of them have the required bandwidth. Thus the developed design equation can be used to develop wide band directive antennas in any substrates.

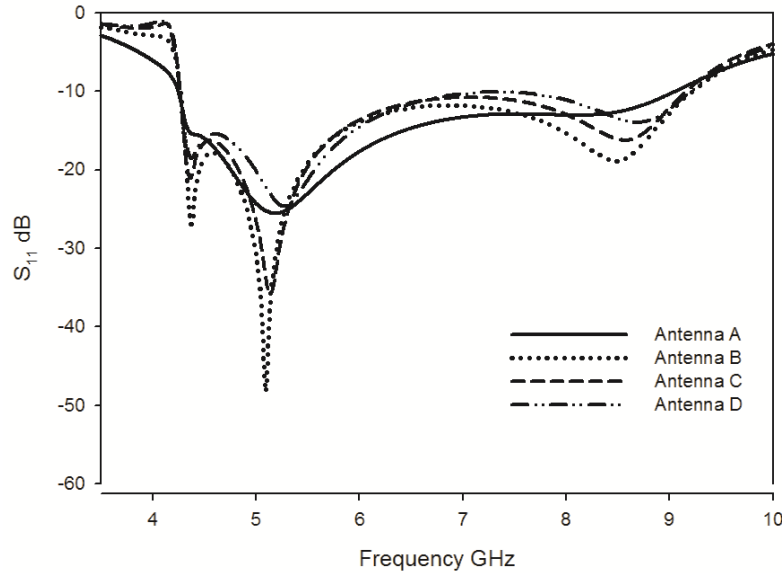


**Fig.4.42.** Reflection coefficient of the antennas with computed geometric parameters for different substrates

#### 4.2.4 Coplanar strip fed Directive dipole antenna for wide band applications

From the design equations developed, an optimized version of the wide band antenna is fabricated and tested. The studies performed and the results obtained are discussed in the following sessions.

##### 4.2.4.1 Structure of Wide Band Directive dipole Antenna

The structure of the optimized antenna which is experimentally developed for the analysis is shown in Fig.4.43. The dimensional parameters of the antenna are  $L=8\text{mm}$ ,  $L_1=10.4\text{ mm}$ ,  $L_2 =5.5\text{mm}$ ,  $W=0.3\text{mm}$  and  $W_1=3\text{mm}$ . The antenna is fabricated on commercially available FR4 substrate with dielectric constant  $\epsilon_r=4.4$ , loss tangent  $\tan \delta=0.02$  and height  $h=1.6\text{mm}$ . the overall dimation of the antenna is  $21.1\text{mm} \times 8.8\text{ mm} \times 1.6\text{ mm}$ .

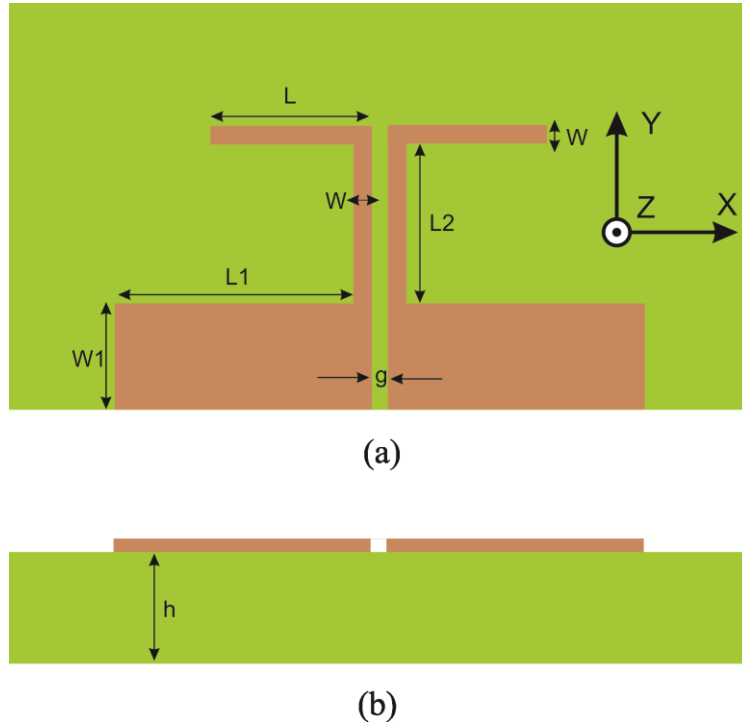


**Fig.4.43** Structure of wide band antenna ( $L=8\text{mm}$ ,  $L_1=10.4\text{mm}$ ,  $L_2 =5.5\text{mm}$ ,  $W=0.3\text{mm}$ ,  $W_1=3\text{mm}$ ,  $g=0.3\text{mm}$ ,  $h=1.6\text{mm}$  and  $\epsilon_r=4.4$ )

#### 4.2.4.2 Return loss Characteristics

The simulated and measured reflection co-efficient of the wide band high gain antenna is shown in Fig. 4.44. The antenna offers a 2:1 band width of 6.4 GHz starting from 3.8 GHz to 10.2 GHz or a percentage band width of 97.27 %. This wide band width is obtained by merging three resonances centered at 4.3775 GHz, 5.0925 GHz and 8.505 GHz which is wide enough to cover many application bands listed in Table1 of Chapter1 and can be used for many wide band applications.

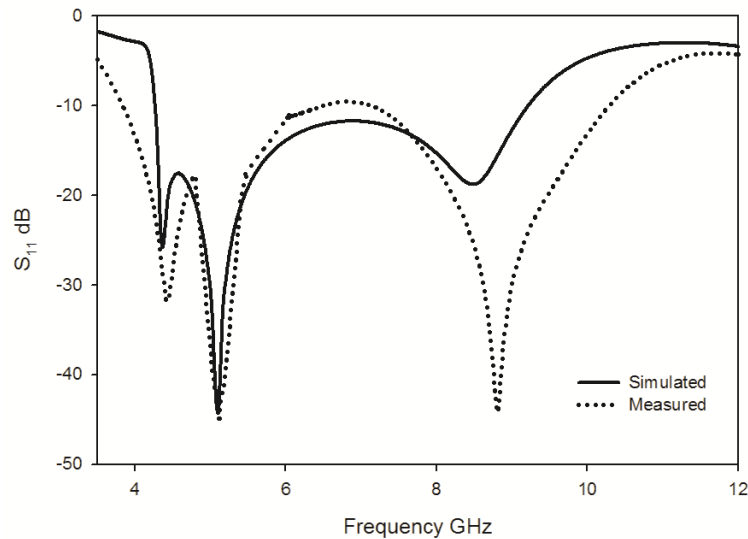


**Fig.4.44.** Simulated and measured reflection co-efficient of the wideband antenna ( $L=8\text{mm}$ ,  $L_1=10.4\text{mm}$ ,  $L_2=5.5\text{mm}$ ,  $W=0.3\text{mm}$ ,  $W_1=3\text{mm}$   $h=1.6\text{mm}$  and  $\epsilon_r=4.4$ )

#### 4.2.4.3 Radiation Characteristics

Three dimensional radiation patterns of the wide band high gain antenna at the three resonances are shown in Fig. 4.45. From the figure 4.45 (a) it is clear that the antenna offers a directional radiation pattern with radiation maxima towards the positive Y direction at 4.3775 GHz. The large directive property at first resonance is due to the reflection from strip of dimension  $L_1 \times W_1$ . The same strip will suppress the back ward power towards the negative Y direction and push these energy to positive Y direction. The polarization of the antenna at the first resonance lies in the X direction.

Three dimensional radiation pattern of the antenna at 5.0925 GHz is shown in Fig. 4.45 (b). At the second resonance also ie at 5.0925 GHz the antenna is slightly directive with beam maxima towards Y direction. The directivity of the antenna at the second resonance is found to be less when

compared to the other two radiation pattern. This is because; the second resonance is produced by the stub of dimension  $L_1 \times W_1$  which acts as the reflector for the other two resonances. Thus in second resonance, there is no reflector to increase the directivity. A slight enhancement in the directive property at second resonance is due to the inherent directive nature of the slotline and the director like behavior of the two strips of dimension  $L \times W$ . The polarization of the antenna at second resonance is in X direction with radiation nulls occurs along the X axis.

The radiation pattern of the structure at third resonance ie at 8.505 GHz is shown in Fig 4.45 (c). The radiating structure acts as a highly directional antenna at the third resonance with beam maxima pointing towards positive Y direction. At high frequencies the reflector spacing is generally minimum due to lower wavelength and therefore the directive property of the structure increases with increase in frequency. Here also the polarization of the antenna lies in the X axis.

All the three radiation patterns says that the antenna is a directive radiating structure. The directional property of the antenna is mainly due to the reflection from the strips of width  $W_1$ . Beam width of the antenna is found to be same for all the radiation patterns. Since the characteristics like beam maxima direction, polarization, beam width etc of the antenna are similar for the radiating structure, we can conclude that the antenna offers a stable radiation characteristics in the entire band of operation.

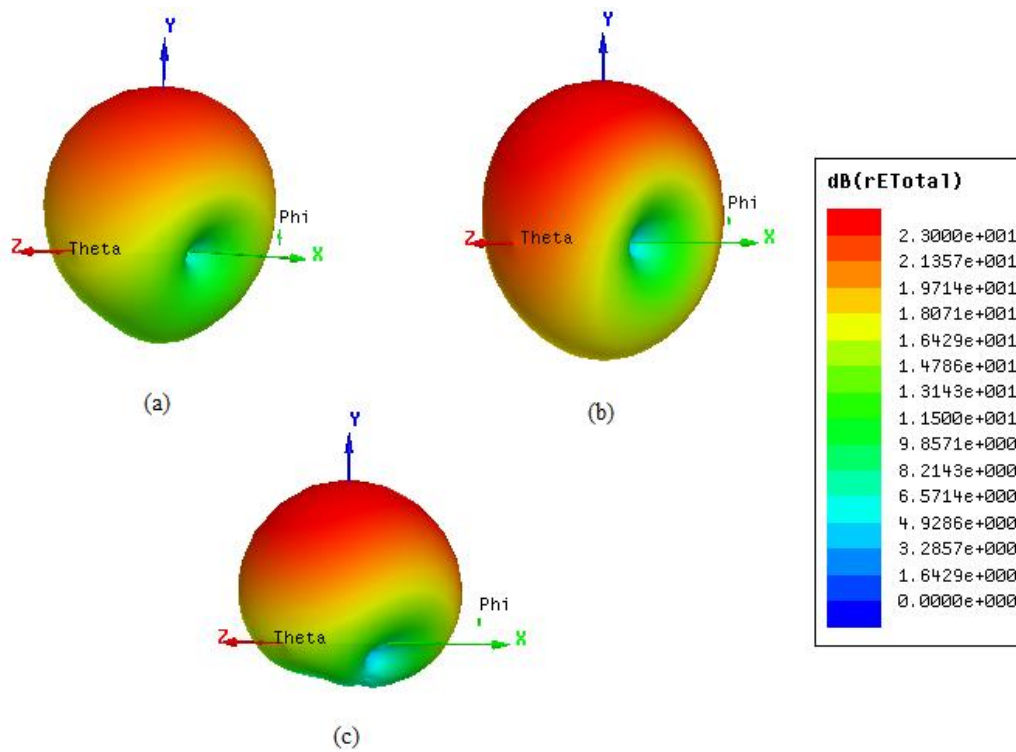


**Fig.4.45.** Three dimensional Radiation pattern of the wideband antenna at (a) 4.3775 GHz (b) 5.0925 GHz and (c) 8.505 GHz ( $L=8\text{mm}$ ,  $L_1=10.4\text{mm}$ ,  $L_2=5.5\text{mm}$ ,  $W=0.3\text{mm}$ ,  $W_1=3\text{mm}$   $h=1.6\text{mm}$  and  $\epsilon_r=4.4$ )

To substantiate the simulated radiation patterns and to study the radiation performance of the antenna at the two principal planes, the two dimensional radiation patterns are measured and analyzed. Fig 4.46 shows the measured radiation patterns of the antenna in the two principal planes at different frequencies of the operating band including the three resonances.

The E and H plane patterns of the antenna at 3.8 GHz are shown in Fig.4.46 (a). From the figure it is clear that the antenna offers a front to back ratio of 17 dB in the two principal planes. The cross polar level in the E plane



and H plane is about 25 dB. The beam maxima in the two planes are towards the positive Y direction.

The E and H plane patterns of the antenna at 4.375 GHz are shown in Fig.4.46 (b). At this frequency the antenna offers a front to back ratio of 15 dB in the two principal planes. The cross polar level in the E plane is about 25 dB while that in the H plane is about 30 dB. The beam maxima in the two planes are towards the positive Y direction as discussed in the earlier session.

The radiation patterns of the antenna at 5.0925 GHz in the two principal planes are shown in Fig. 4.46 (c). Antenna offers an eight shaped pattern in E plane with a front to back ratio better than 5 dB. In H plane the antenna offers a nearly omnidirectional radiation pattern with a small enhancement in power of 5 dB towards the positive Y direction. The cross polar isolations of both the planes are of in the order of 30dB. The nulls of E plane pattern are in X direction and the polarization is also in the same direction.

The principle plane radiation patterns of the antenna at 6.5 GHz are shown in Fig. 4.46 (d). From the figure it is clear that the antenna offers an eight shaped pattern in E plane with a front to back ratio better than 8 dB. In H plane also the antenna offers a front to back ratio of 8 dB. The cross polar isolation in both the planes is of the order of 35dB. The polarization of the antenna at 6.5 GHz is along X direction.

The two dimensional radiation patterns of the antenna at the third resonance ie at 8.505 GHz are shown in Fig. 4.46 (e). At the third resonance, the antenna is highly directional one with a high suppression of backward power towards the negative Y direction. At this frequency, the antenna offers a

front to back ratio of the order of 20 dB. The cross polar isolation of the structure in the E plane is of 20 dB and that in H plane is in the range of 30 dB.

The E and H plane patterns of the antenna at 10.2 GHz are shown in Fig.4.46 (f). From the figure it is evident that the antenna offers a front to back ratio better than 20 dB in the two principal planes. The cross polar isolation in the E plane is about 35 dB in the bore sight direction while that in the H plane is about 30 dB. The beam maxima in the two planes are towards the positive Y direction.

From the radiation pattern analysis it is clear that the proposed wideband antenna is a directional radiator without the help of any parasitic reflector or director elements. The important feature of this antenna is its radiation pattern stability in the entire band of operation. The beam maxima direction and the polarization of the antenna are remaining the same for all the frequencies in the operating region. The directivity of the antenna at the second resonance is found to be slightly less. For all other frequencies the antenna acts as a good directive radiator. Since the directivity of the antenna is higher than normal dipoles, the peak gain also will be enhanced in this case.

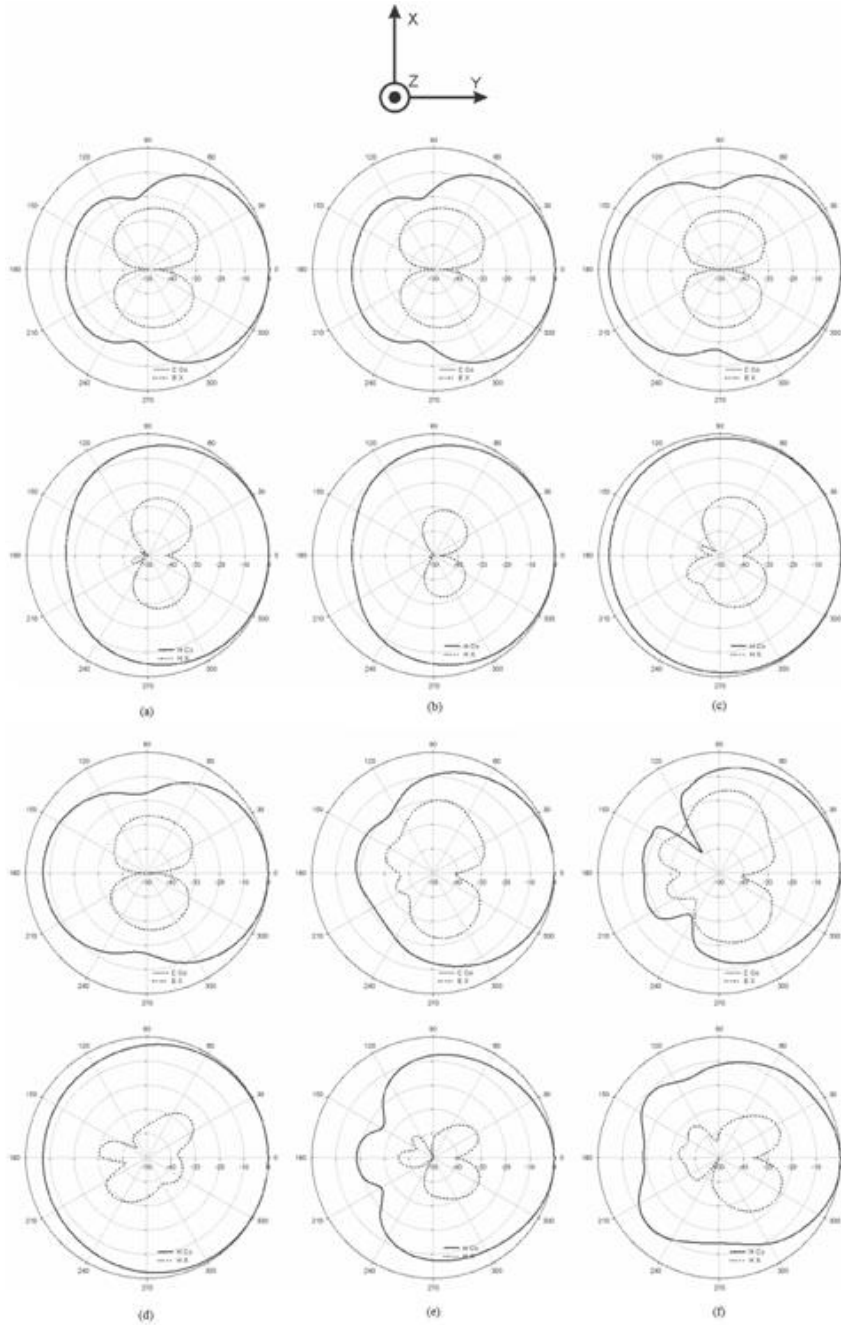


**Fig.4.46.** Two dimensional Radiation pattern of the wideband antenna at (a) 3.8 GHz (b) 4.377 GHz (c) 5.0925 GHz (d) 6.5 GHz (e) 8.505 GHz and (f) 10.2 GHz ( $L=8\text{mm}$ ,  $L_1=10.4\text{mm}$ ,  $L_2=5.5\text{mm}$ ,  $W=0.3\text{mm}$ ,  $W_1=3\text{mm}$   $h=1.6\text{mm}$  and  $\epsilon_r=4.4$ )

To obtain an in-depth knowledge about the radiation mechanism of the antenna, the surface current analysis is performed and discussed as the next session.

#### 4.2.4.4 Surface Current Analysis

To get further insight of the radiation mechanism of the proposed wide band structure, the surface current analysis is necessary. The surface current studies of the antenna at the three resonant frequencies are performed in detail and are discussed in this session. The simulated surface current distributions of the antenna at the three resonant frequencies are shown in Fig 4.47. The surface current distribution of the antenna at the first resonance ie at 3.4775 GHz is shown ion Fig. 4.47(a). From the figure it is clear that the first resonance is due to the half wavelength ( $\lambda_g/2$ ) long variation of surface current present in the strips of length L. This inference is already obtained from the parametric analysis discussed in sessions 4.5.3.1. The strip of width  $W_1$  has only very small amount of surface current density in the first resonance and thus it acts as the reflector.

The surface current distribution of the antenna at the second resonance is shown in Fig 4.47(b). According to the plot the second resonance is mainly due to the half wavelength ( $\lambda_g/2$ ) long variation of surface current present in the strips of dimension  $L_1 \times W_1$ . These strips acts as a half wave dipole at this frequency. The other two strips have only a feeble current density at this frequency. Since at this frequency there is no reflector, the directive property is slightly less.

The surface current distribution of the antenna at the third resonating frequency 8.505 GHz is shown ion Fig. 4.47(c). The third resonance is due to a  $3\lambda_g/2$  long variation of surface current present in the strips of length L and  $L_2$ . ie

the third resonance is the third harmonics of the first resonance. Here also the strips of dimension  $L_1 \times W_1$  have a very feeble surface current density and thus it acts as a reflector of power at this frequency.

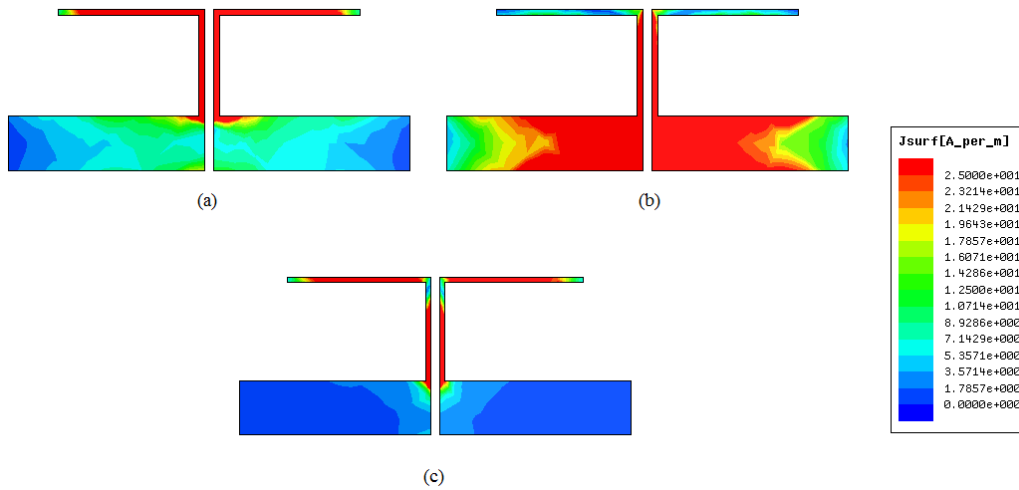


**Fig.4.47** Simulated Surface current distribution of the wideband antenna at (a) 4.3775 GHz (b) 5.0925 GHz and (c) 8.505 GHz ( $L=8\text{mm}$ ,  $L_1=10.4\text{mm}$ ,  $L_2=5.5\text{mm}$ ,  $W=0.3\text{mm}$ ,  $W_1=3\text{mm}$   $h=1.6\text{mm}$  and  $\epsilon_r=4.4$ )

#### 4.2.4.5 Gain of the Wide band Antenna

For directional antennas, gain is an important factor because the directive gain determines the ability of the structure to concentrate the radiated energy into a particular direction. The measured gain of the wide band antenna in the entire band of operation is shown in Fig. 4.48. From the figure it is clear that the antenna offers an average gain of 5.2 dBi in the entire operating band which is very much higher than the gain of normal dipoles.

The directive gain of the antenna near to the second resonance is found to be slightly less than that in the other region of the band. The reason for this small reduction can be explained from the current distribution of the antenna. As explained in parametric analysis in session 4.5.3.2 and the surface current

distribution given in Fig.4.47 (b), the second resonance is due to the variation of current through strip of dimension  $L_1 \times W_1$ . This strip acts as the reflector for all other frequencies in the operating band. Thus there is no reflector for the second resonance and the gain at this frequency is slightly less. The enhancement of directive gain at these frequencies without reflector is due to the effect of slotline's inherent high gain and the director like action of strips of dimension  $L \times W$ .

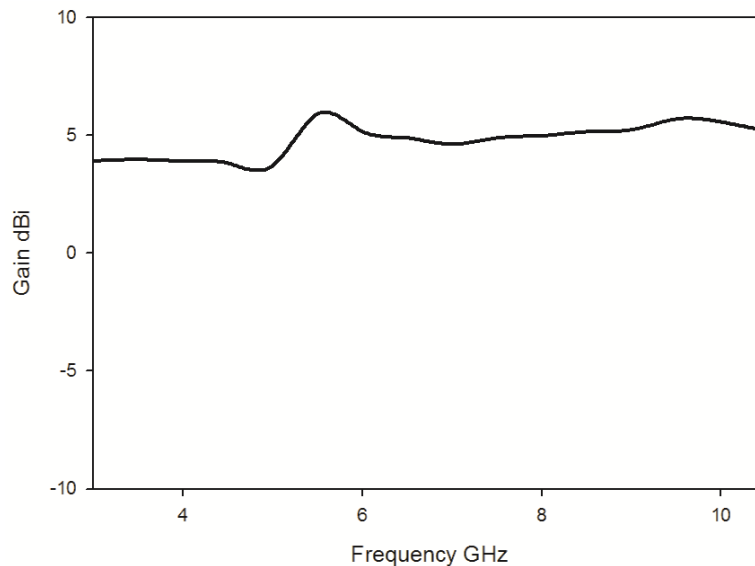


**Fig.4.48** Directive Gain of the antenna in the entire operating band ( $L=8\text{mm}$ ,  $L_1=10.4\text{mm}$ ,  $L_2=5.5\text{mm}$ ,  $W=0.3\text{mm}$ ,  $W_1=3\text{mm}$   $h=1.6\text{mm}$  and  $\epsilon_r=4.4$ )

#### 4.2.4.6 Radiation efficiency of the Wide band Antenna

This session deals with the radiation efficiency of the wideband dipole antenna. Measured radiation efficiency of the antenna in the entire operating band is given in Fig 4.49. From the figure it is evident that the structure is an effective radiator with almost uniform radiation efficiency of more than 91 %.

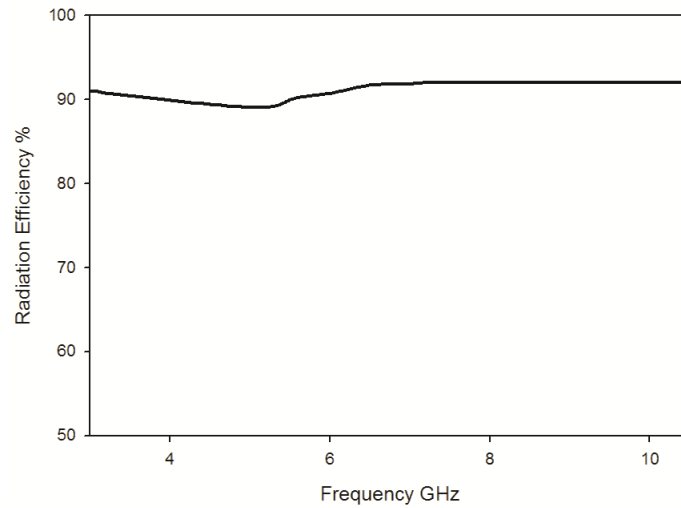


**Fig.4.49** Radiation Efficiency of the antenna in the entire operating band ( $L=8\text{mm}$ ,  $L_1=10.4\text{mm}$ ,  $L_2=5.5\text{mm}$ ,  $W=0.3\text{mm}$ ,  $W_1=3\text{mm}$   $h=1.6\text{mm}$  and  $\epsilon_r=4.4$ )

### 4.3 FDTD Analysis

Results obtained from numerical analysis of the antenna structures discussed in previous sessions of this chapter are presented here. The specifications of the FDTD domain like cell dimensions, time steps, excitations etc are same as that used in chapter 3.

#### 4.3.1 Coplanar Strip fed High Gain Dipole Antenna

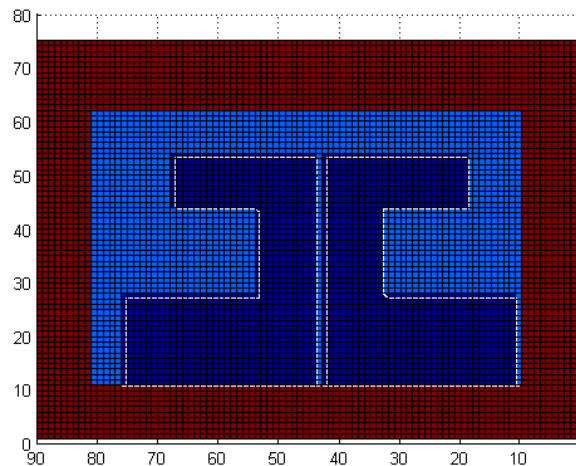


**Fig.4.50.** FDTD computation domain of high gain dipole antenna.

FDTD computational domain of the high gain dipole antenna formed by structural transformation of OES is shown in Fig 4.50. Reflection co-efficient of the antenna obtained from experiment and HFSS are compared with the result obtained from FDTD calculations and are shown in Fig 4.51. All the curves show a very good agreement.

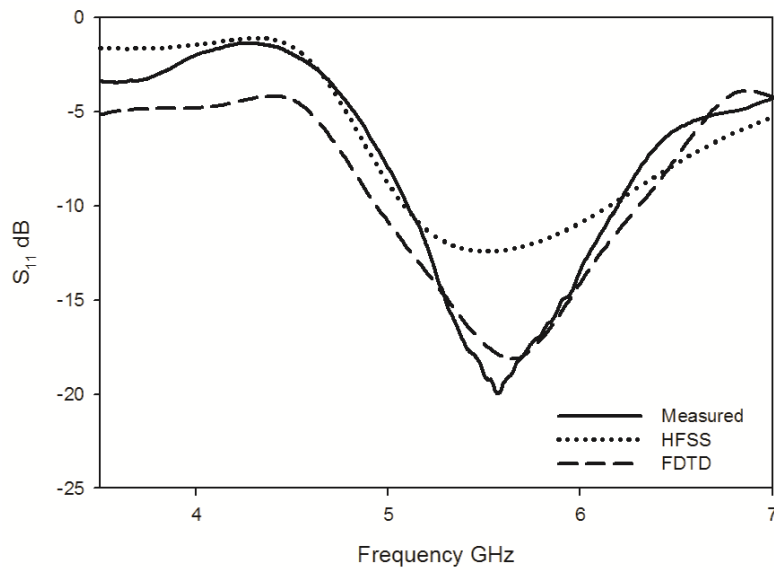


**Fig.4.51** Comparison of reflection co efficiencies of High gain dipole antenna.

X and Y component of electric field vector at 5.5 GHz are shown in Fig 4.52 (a) and (b) respectively. They matches very well with the inference that obtained from the HFSS simulated surface current distribution plot of the antenna given in Fig.4.27.



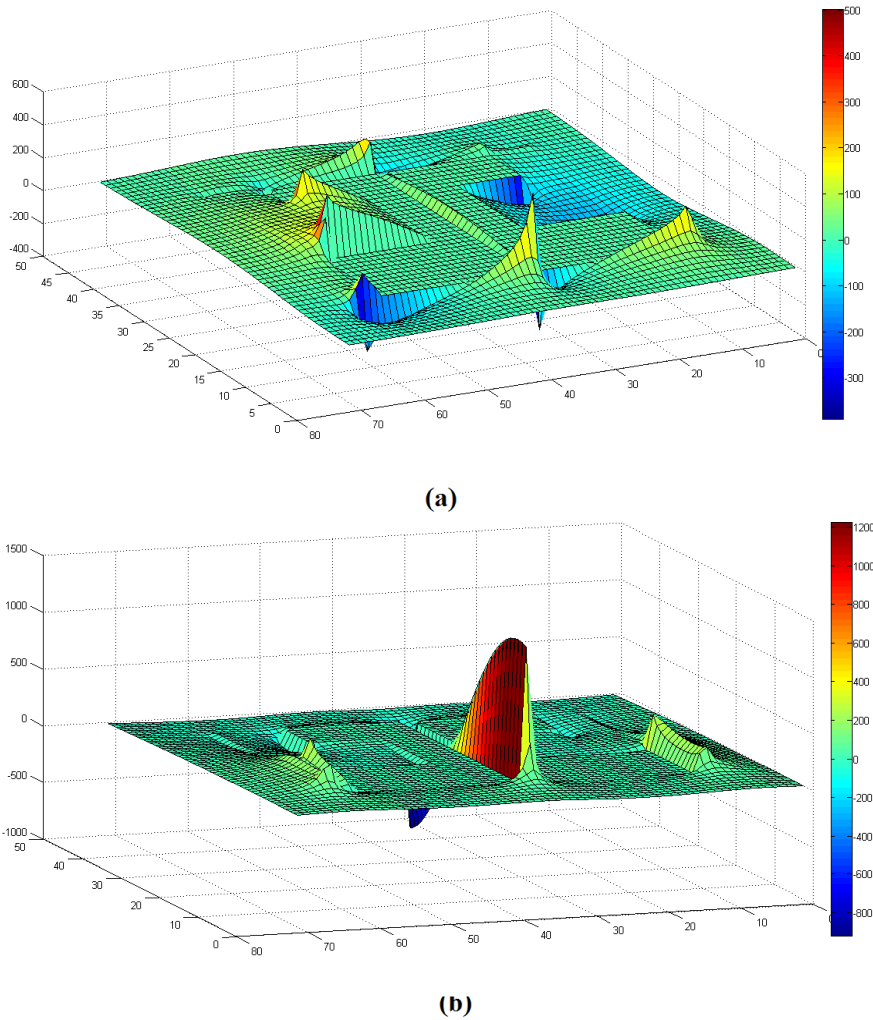


**Fig.4.52** Electric field distribution of High gain dipole antenna at 5.5 GHz (a) X Component and (b) Y component.

### 4.3.2 Coplanar Strip fed Wide band Directive Dipole Antenna

The second part of this chapter is going through the analysis of a high gain wide band antenna derived from a high gain single band antenna. Thus FDTD analysis is also performed in this structure. The results obtained are discussed here.

The computational domain of the high gain wide band dipole is shown in Fig.4.53. Reflection co efficient obtained from FDTD is compared with those obtained from HFSS and experiment. They matches very well as shown in Fig. 4.54.

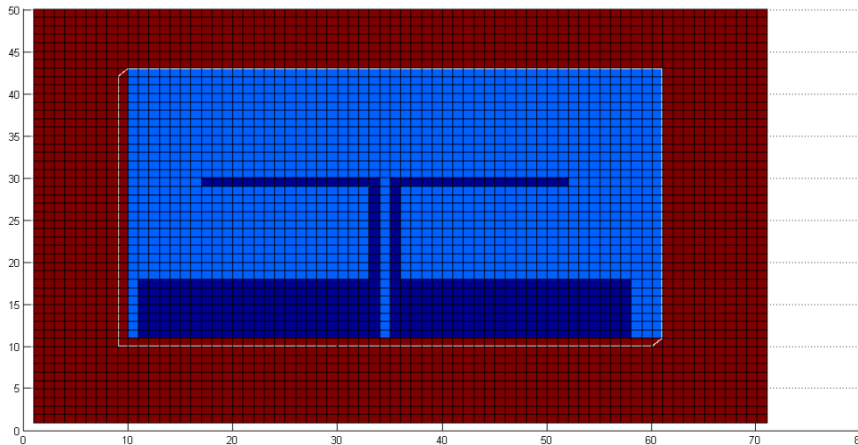


**Fig.4.53.** FDTD computation domain of high gain wide band dipole antenna

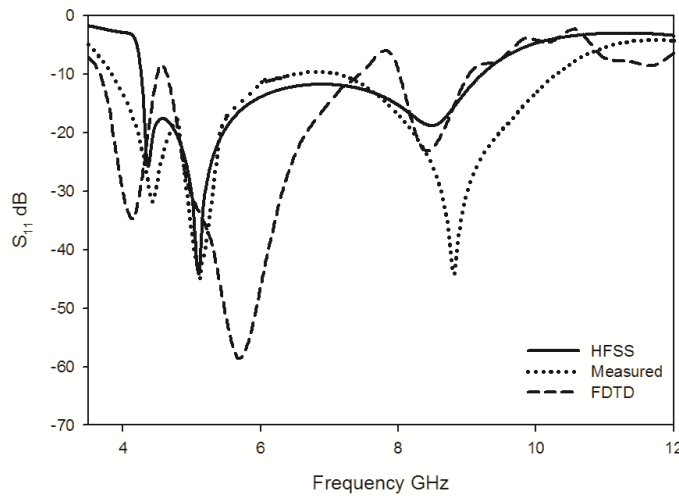


**Fig.4.54** Reflection co efficient of High gain dipole antenna from FDTD, HFSS and Experiment.

The wide band effect of the antenna is derived by combining three different resonances. Thus the electric field analysis is performed in three different resonant frequencies for obtaining the technical knowhow of the resonance. These results are discussed in the following sessions.

The X and Y component of the E field vector at first resonant frequency ie at 4.37 GHz is shown in Fig.4.55 (a) and (b) respectively. The field distributions of the high gain wide band dipole antenna at 5.1 GHz and 8.5 GHz are shown in Fig 4.56 and 4.57.

The field distributions are perfectly in agreement with the surface current analysis of the wide band directive dipole antenna present in session 4.2.4.4.

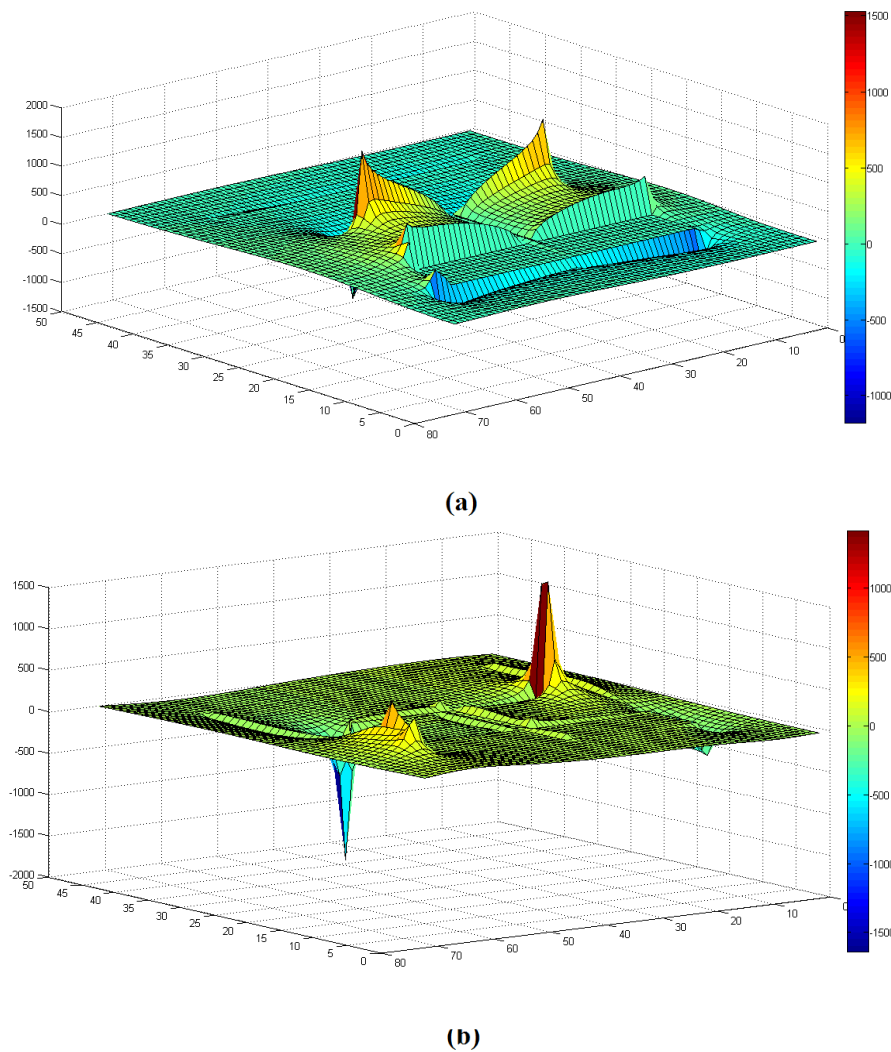
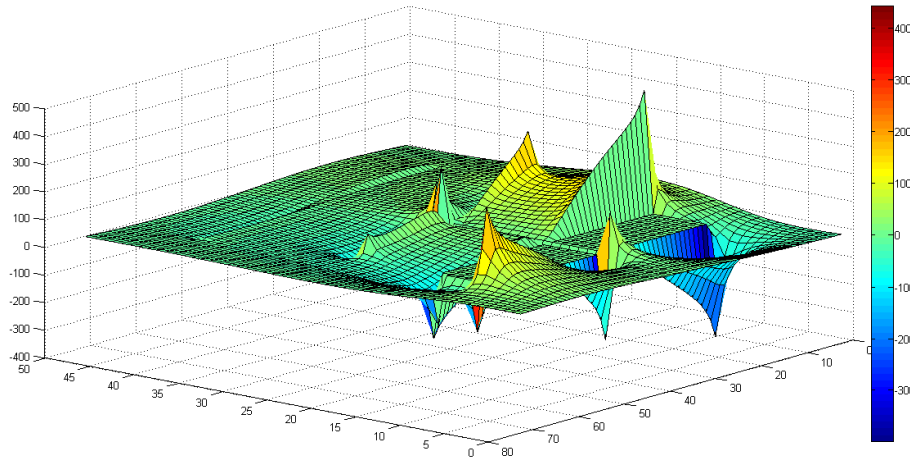
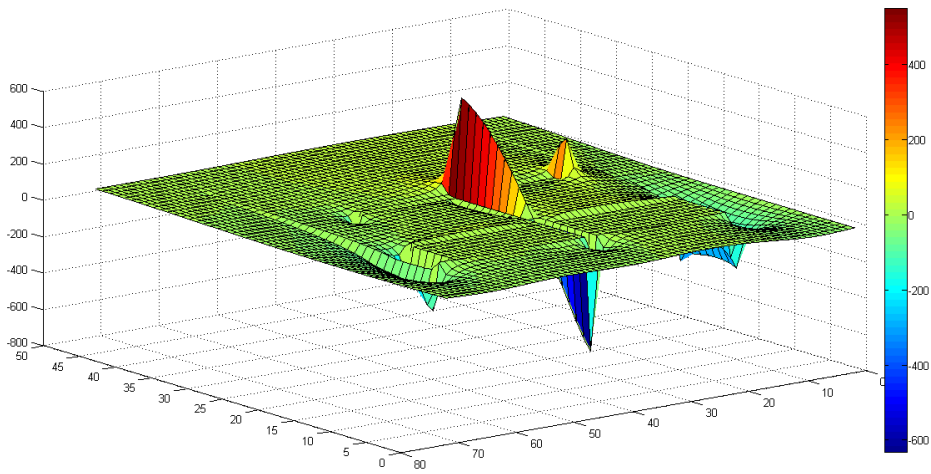


**Fig.4.55.** Electric field distribution of High gain Wide band dipole antenna at 4.37 GHz (a) X Component and (b) Y component. .

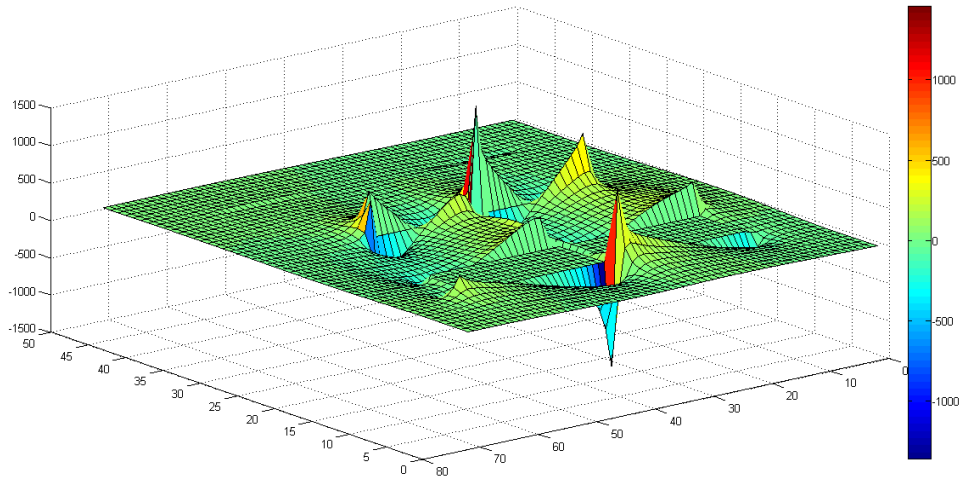


(a)

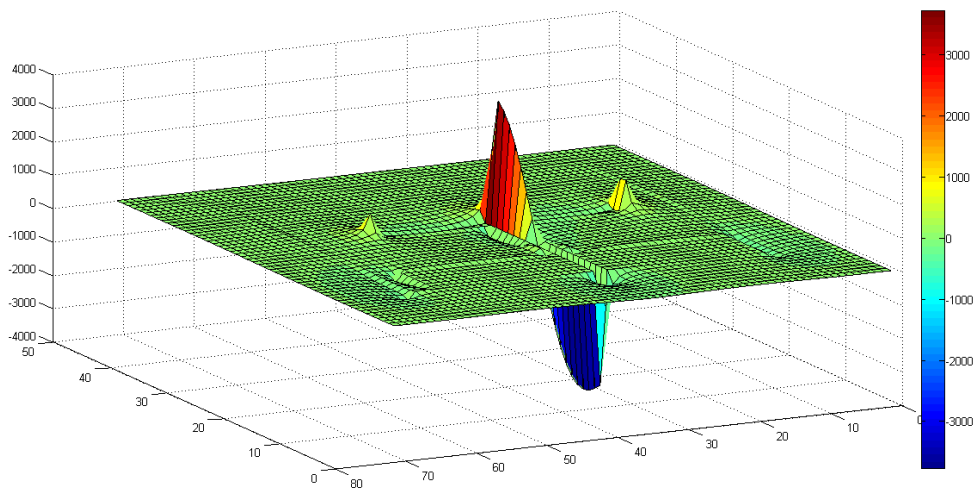


(b)

**Fig.4.56.** Electric field distribution of High gain Wide band dipole antenna at 5.1 GHz (a) X Component and (b) Y component.



(a)



(b)

**Fig.4.57.** Electric field distribution of High gain Wide band dipole antenna at 8.50 GHz (a) X Component and (b) Y component.

## **4.7 Chapter Summary**

The first part of this chapter deals with the evolution of a high gain dipole antenna from an open ended transmission line. Effects of all the dimensional parameters are studied thoroughly and design equations for the high gain antenna are developed. Using the developed design equations a prototype of the antenna operating at 5.2/5.8 GHz WLAN band is experimentally developed and analyzed. All the radiation and reflection characteristics of the antenna like reflection co-efficient, radiation pattern, surface current analysis, gain, radiation efficiency etc are analyzed experimentally and verified by comparing with simulation results.

As the next step of the chapter, the study is pointed towards the development of a wideband antenna from the high gain dipole. Here also an in-depth parametric study is carried out to get the technical know-how of radiation mechanism from the antenna. The design equation of the wideband antenna is also developed from the parametric analysis and validated by developing four antennas on different substrates. From the developed design equation, a prototype of wideband antenna is experimentally developed. All the characteristics of the developed antenna are analyzed thoroughly. The explanation for the radiation mechanism is also substantiated from the surface current study.

As the last part of the chapter, FDTD analysis is also performed to obtain more insight about the radiation mechanism. Results obtained from the numerical analysis are compared with those obtained from simulation and experimental studies and found that all of them match very well.

A comparison of the proposed high gain antenna suitable for 5.2/5.8 GHz with some of the high gain antennas already presented in literature were compared and the observations are depicted in table 4.6. From the table it is very clear that the proposed antenna exhibits high gain without any parasitic elements and offer moderate bandwidth.

**Table 4.5 Comparison of Proposed Antenna parameter with existing antennas**

Antenna	Size	No of Parasitic elements	Percentage Band width	Gain dBi	Front to back ratio dB	Cross polar isolation dB
Ref 2	$0.75 \lambda_g \times 0.5 \lambda_g$	1	38	4	12	-15
Ref 3	$0.75 \lambda_g \times 1.25 \lambda_g$	3	2.5	9.3	11	-25
Ref 4	$3.2 \lambda_g \times 0.8 \lambda_g$	13	20	12	15	-
Ref 5	$2.5 \lambda_g \times 2.5 \lambda_g \times 0.9 \lambda_g$	5	14	10	-	-
Ref 6	$0.9 \lambda_g \times 1.4 \lambda_g$	3	15	7.1	15	-20
Ref 7	$1.38 \lambda_g \times 2.26 \lambda_g$	3	3	-	10	-
Ref 8	$2.5 \lambda_g \times 3 \lambda_g$	7	1.6	9	20	-16
Ref 9	$2.27 \lambda_g \times 2.72 \lambda_g$	1	55	4.9	20	-
Ref 10	$0.36 \lambda_g \times 0.7 \lambda_g$	1	49	6.5	10	-15
<b>Proposed antenna</b>	<b><math>0.5 \lambda_g \times 0.3 \lambda_g</math></b>	<b>0</b>	<b>19.63</b>	<b>7.9</b>	<b>20</b>	<b>-20</b>

## References.

- [1] Constantine A Balanis "Antenna theory analysis and design" John Wiley and Sons II<sup>nd</sup> edition.
- [2] N. Kaneda, W. R. Deal, Y. Qian, R. Waterhouse, and T. Itoh, "A broadband planar Quasi-Yagi antenna," IEEE Trans. Antennas Propag., vol. 50, no. 8, pp. 1158–1160, Aug. 2002
- [3] P. R. Grajek, B. Schoenlinner, and G. M. Rebeiz, "A 24-GHz high-gain Yagi-Uda antenna array," IEEE Trans. Antennas Propag., vol. 52, pp. 1257–1261, May 2004.

- [4] Jean-Marie Floch, Jean-Michel Denoual and Khaled Sallem “Design of Printed Dipole with Reflector and Multi Directors” Loughborough Antennas & Propagation Conference 2009.
- [5] Olivier Kramer, Tarek Djerafi, and Ke Wu “Vertically Multilayer-Stacked Yagi Antenna With Single and Dual Polarizations” IEEE Trans. Antennas Propag, VOL. 58, NO. 4, APRIL 2010.
- [6] Le Huu Truong, Yong Hyun Baek, Seok Gyu Choi, Mun Kyo Lee, Du Hyun Ko, Sang Jin Lee, Dao Ngoc Chien\*, Yeon Sik Chae and Jin Koo Rhee “A high performance 94 GHz planar quasi Yagi antenna on GaAs” Microwave and optical technology Lett. VOL 51, Issue 10, JUL 2009.
- [7] Anatoly P. Gorbachev, Member, IEEE, and Vladimir M. Egorov “A Modified Planar Quasi-Yagi Antenna for Wireless Communication Applications IEEE Antennas and wireless propagation Lett, VOL. 8, 2009.
- [8] Ramadan A. Alhalabi and Gabriel M. Rebeiz “High-Gain Yagi-Uda Antennas for Millimeter-Wave Switched-Beam Systems” IEEE Trans. Antennas Propag, VOL. 57, NO. 11, NOVEMBER 2009.
- [9] Son Xuat Ta; Byoungchul Kim; Hosung Choo; Ikmo Park; “Slot-line-fed quasi-Yagi antenna “ Antennas Propagation and EM Theory (ISAPE), 2010 9th International Symposium on Digital Object Identifier: 10.1109/ISAPE.2010.5696461 Publication Year: 2010 , Page(s): 307 – 310.
- [10] V. Deepu, S. Mridula, R. Sujith and P. Mohanan. “Slot line FED dipole antenna for wide band applications” Microwave and Optical Technology Letters Volume 51, Issue 3, March 2009, Pages: 826–830.



**COPLANAR STRIP FED ULTRA WIDE BAND ANTENNAS**

*This chapter highlights the design and development of compact Coplanar Strip Fed V Groove, Semicircular Slot and Semicircular Ultra Wide Band Antennas with enhanced gain and directivity. Reflection and Radiation Characteristics of the antenna are discussed in detail. Since the chapter dealt with UWB designs, the time domain analysis of the antenna are also performed. The transmission analysis like EIRP, Pulse Response, Fidelity etc are also carried out and found that the discussed antennas are very much suited for high data rate UWB applications.*

**5.1 Coplanar Strip fed V Groove UWB antenna**

This session deals with a coplanar strip fed antenna which has a V groove on the top edge of the conducting strip. The evolution of the V groove antenna from the Open Ended Slotline (OES) is shown in Fig. 5.1. The antenna is derived from an OES by symmetrically removing a right angled triangle of base  $W_{\text{off}}$  and altitude  $L_{\text{off}}$  from either conducting strips. The overall dimension of the antenna after the transformation will remain the same as that of the parental OES.

The basic idea of derivation of this antenna structure came from the Vivaldi antennas in which there is an exponential tapering of both the conducting strips. Here in this structure, the tapering is not an exponential one but linear. The size of the proposed structure is also found to be very compact when compared to that of Vivaldi structures. Since the tapering is linear, it can be compared with horn antennas in which a linear tapering is included to increase the radiation behavior.

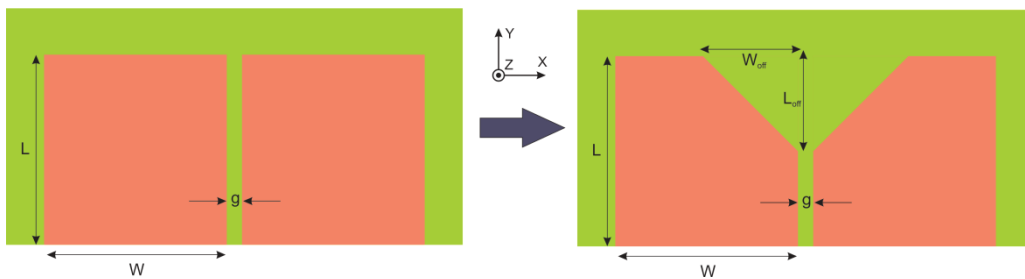


**Fig.5.1.** Evolution of V Groove UWB from an OES

The effect of introducing a V groove on the upper edge of an open ended slotline is discussed here. The reflection coefficients of an OES and the OES with a V groove of different dimensions are shown in Fig. 5.2. The figure says that the OES without V groove will act as a single band dipole with total length approximately equal to half of the wavelength of resonant frequency. The introduction of a flaring portion at the top edge of the OES will introduce an additional resonance near the initial resonant frequency. This resonance is due to the creation of a new surface current path through the either sides of the slot and through flared and upper edges of the structure. It is also inferred from the figure that the newly created resonance is found to be increasing with increase in dimensions  $L_{off}$  and  $W_{off}$ . This is due to the removal of a part from the current path with these parameters. The effects of all the dimensional

parameters are thoroughly analyzed in the parametric analysis and are explained in the following sessions.

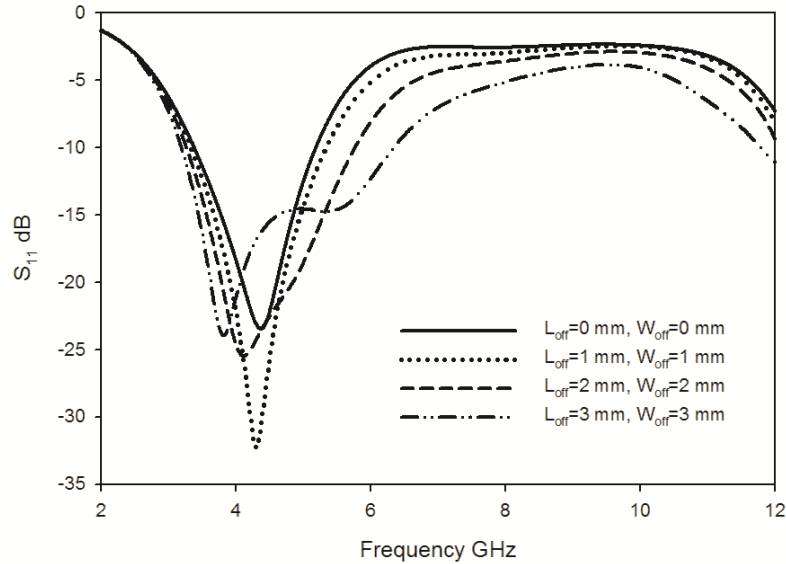


**Fig.5.2.** Reflection co efficient of an OES and OES with V groove of different dimensions ( $L=10\text{mm}$  &  $W=15.75\text{mm}$ )

### 5.1.1 Parametric analysis of the V groove antenna

To get further insight to the radiation mechanism and to analyze the effect of various dimensional parameters of the antenna on reflection coefficient, it is important to perform a detailed parametric analysis of the antenna. This is discussed in the following sessions.

#### 5.1.1.1 Variation in reflection co-efficient with L

The variation of reflection co-efficient of the antenna with L is shown in Fig. 5.3. All the resonances are affected by L. The second and third resonance shows a down shift with L while the first resonance shows a very feeble higher shift in frequency with increase in L. This higher shifting of frequency is due to the tendency of fringing field concentration near the slot of the structure and is

explained in session 3.3.2.1 of chapter.3. The decrease in resonant frequencies of second and third resonance is due to the increase in surface current path length and can be verified from the surface current distribution given in Fig.5.13. From the variation analysis performed, for the better impedance matching of the structure in the UWB frequency range  $L$  of the antenna is optimized as 10 mm.

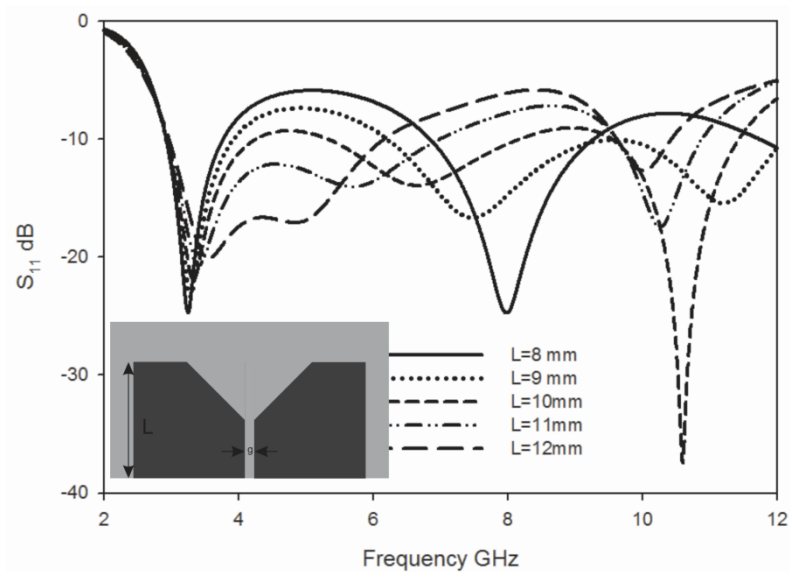


**Fig.5.3.** Variation of Reflection co-efficient with  $L$  ( $W=15.75\text{mm}$ ,  $L_{\text{off}}=5\text{mm}$ ,  $W_{\text{off}}=4\text{mm}$ ,  $g=0.3\text{mm}$  and  $h=1.6\text{mm}$ )

### 5.1.1.2 Variation in reflection co-efficient with $W$

This session deals with the dependency of resonances on  $W$ . The variation of reflection co-efficient of the antenna with  $W$  is shown in Fig.5.4. All the three resonances were strongly affected by  $W$ . All the three resonances shows a decrease with increase in  $W$ . This is due to the increase in length of surface current path with the parameter  $W$ . This can be easily verified from the surface current distribution of the antenna given in Fig.5.13.

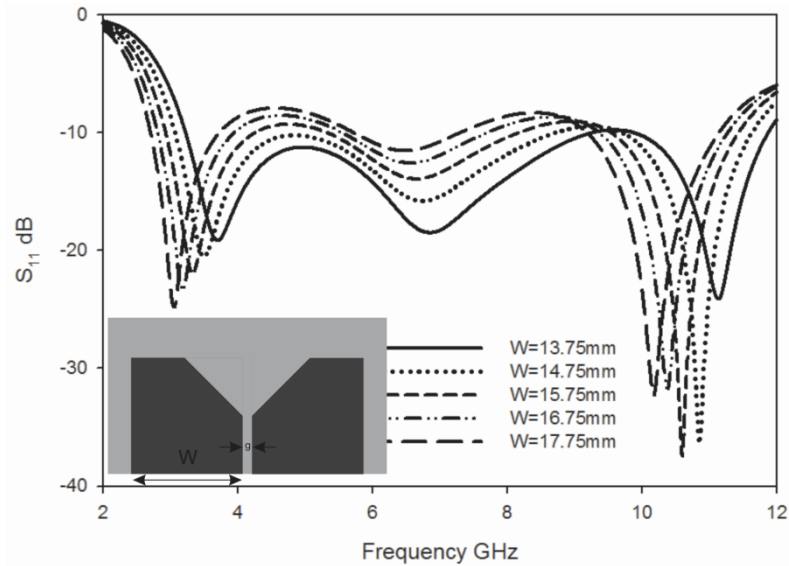


**Fig.5.4.** Variation of Reflection co-efficient with  $W$  ( $L=10\text{mm}$ ,  $L_{\text{off}}=5\text{mm}$ ,  $W_{\text{off}}=4\text{mm}$ ,  $g=0.3\text{mm}$  and  $h=1.6\text{mm}$ )

### 5.1.1.3 Variation in reflection co-efficient with $L_{\text{off}}$

The effect of  $L_{\text{off}}$  on resonance is discussed here. The variation of reflection co-efficient of the antenna with  $L_{\text{off}}$  is shown in Fig.5.5. According to the figure it is evident that the impedance band width is strongly affected by the parameter  $L_{\text{off}}$ . All the resonances are strongly affected by this parameter with first and third resonance show a reduction in frequency while the second resonance shows a higher shift in resonant frequency with increase in  $L_{\text{off}}$ . This higher shift in second resonant frequency with  $L_{\text{off}}$  is due to the reduction in initial vertical current path length  $L$ . The same variation of second resonant frequency may be noted in the case of  $W_{\text{off}}$  also which is discussed in the next session.

Since the separation between second and third resonance increases and the total band width reduces with the reduction in  $L_{\text{off}}$  and the antenna will acts as a dual band radiator for small  $L_{\text{off}}$ .

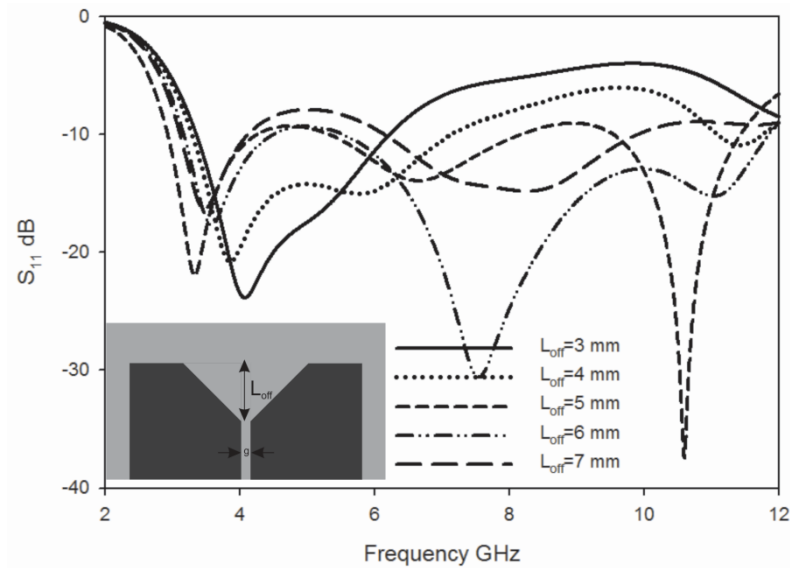


**Fig.5.5.** Variation of Reflection co-efficient with  $L_{off}$  ( $L=10\text{mm}$ ,  $W=15.75\text{mm}$ ,  $W_{off}=4\text{mm}$ ,  $g=0.3\text{mm}$  and  $h=1.6\text{mm}$ )

#### 5.1.1.4 Variation in reflection co-efficient with $W_{off}$

This session deals with the analysis of the parameter  $W_{off}$ . The variation of reflection co-efficient of the antenna with  $W_{off}$  is shown in Fig.5.6. Figure shows that all the resonances are affected by the parameter  $W_{off}$ . The first and third resonances show a lower shift with  $W_{off}$  while the second resonance shows an up shift in resonant frequency with increase in  $W_{off}$ . The variation in resonant frequency is found to be similar to that in the case of  $L_{off}$ . The shift in frequency of first resonance is found to be very feeble. As  $W_{off}$  increases, that portion of metallic part is removed from the initial horizontal surface current path corresponding to the second resonance of the antenna which results in an increase in frequency at second resonance.

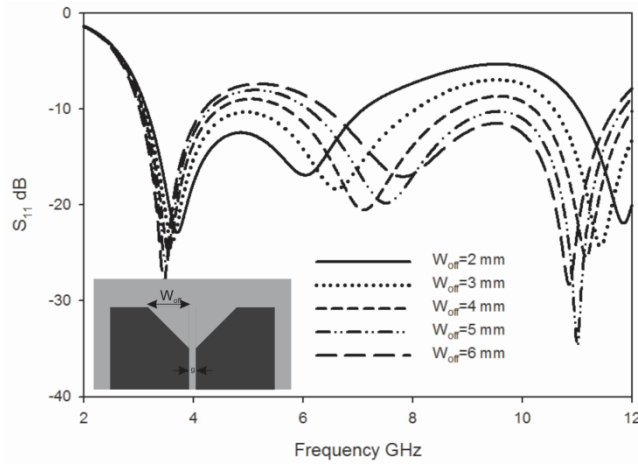


**Fig.5.6.** Variation of Reflection co-efficient with  $W_{off}$  ( $L=10\text{mm}$ ,  $W=15.75\text{mm}$ ,  $L_{off}=5\text{mm}$ ,  $g=0.3\text{mm}$  and  $h=1.6\text{mm}$ )

### 5.1.1.5 Variation in reflection co-efficient with h

The effect of substrate height on reflection co efficient of the antenna is discussed here. The variation of reflection coefficient of the V groove antenna with substrate height  $h$  is shown in Fig. 5.7. All the resonances are unaffected by the height of the substrate. The matching is slightly affected by the parameter  $h$ . This may be due to the variation of input impedance of the antenna with  $h$ .

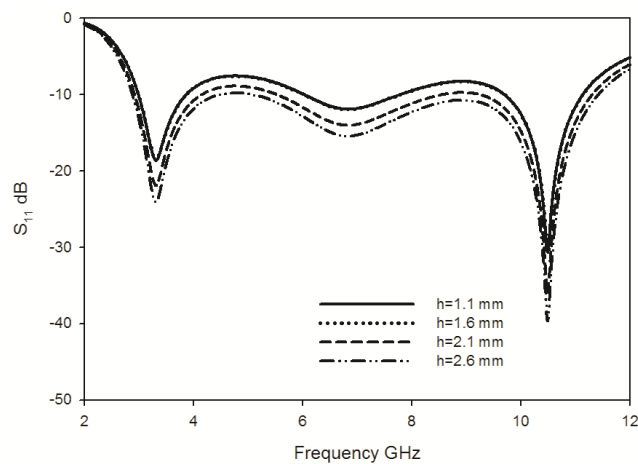


**Fig.5.7.** Variation of Reflection co-efficient with  $h$  ( $L=10\text{mm}$ ,  $W=15.75\text{mm}$ ,  $L_{off}=5\text{mm}$ ,  $W_{off}=4\text{mm}$  and  $g=1\text{mm}$ )

### 5.1.2 Design Equation of the V Groove Antenna

From the parametric analysis of the V groove antenna, it is able to develop the design equation of the V groove ultra wideband antenna and is discussed in this session. The developed design equations are validated for different substrates with different dielectric constant and are also discussed.

The design equations of the antenna are given below.

$$2\left(W - W_{off} + \sqrt{W_{off}^2 + L_{off}^2}\right) \cong 0.63\lambda_{g1}$$

$$2\left(L + W - L_{off} - W_{off} + \sqrt{W_{off}^2 + L_{off}^2}\right) \cong 1.82\lambda_{g2}$$

$$2\left(L + W - W_{off} + \sqrt{W_{off}^2 + L_{off}^2}\right) \cong 3.17\lambda_{g3}$$

Where  $\lambda_{gn}$  is the guided wavelength corresponding to the  $n^{\text{th}}$  resonant frequency and can be calculated from free space wavelength  $\lambda_{0n}$  as,

$$\lambda_{gn} = \lambda_{0n} / \sqrt{\epsilon_{eff}}$$

Where  $\epsilon_{eff} = (\epsilon_r + 1)/2$  is the effective dielectric constant.

In order to validate the developed design equation, the parameters of the antennas operating in UWB region are computed for different substrates (Table 5.1) and Table 5.2 shows the computed geometric parameters of the different V groove UWB antennas.



**Table 5.1** Substrate Description

	Antenna A	Antenna B	Antenna C	Antenna D
<b>Laminate</b>	Rogers 5880	FR4 Epoxy	Rogers R03006	Rogers6010LM
<b>h(mm)</b>	1.57	1.6	1.28	0.635
$\epsilon_r$	2.2	4.4	6.15	10.2
$\epsilon_{re}$	1.6	2.7	3.575	5.6
<b>g(mm)</b>	0.1	0.3	0.65	0.775

**Table 5.2** Computed Geometric Parameters of the Antenna

Parameter (mm)	Antenna A	Antenna B	Antenna C	Antenna D
<b>L</b>	13.8	10	8.6	6.75
<b>W</b>	20	15.75	13.75	11
<b>L<sub>off</sub></b>	6	4	3.2	2.45
<b>W<sub>off</sub></b>	6.75	5	4	2.9

The simulated reflection co-efficient of the antennas developed using the parameters given in the tables 5.1 and 5.2 are shown in Fig. 5.8 and all the four antennas are with ultra wide band characteristics and offer sufficient band width with three resonances. From the figure it is also clear that the developed design equations can be utilized to develop antennas operating in UWB region in any substrates.

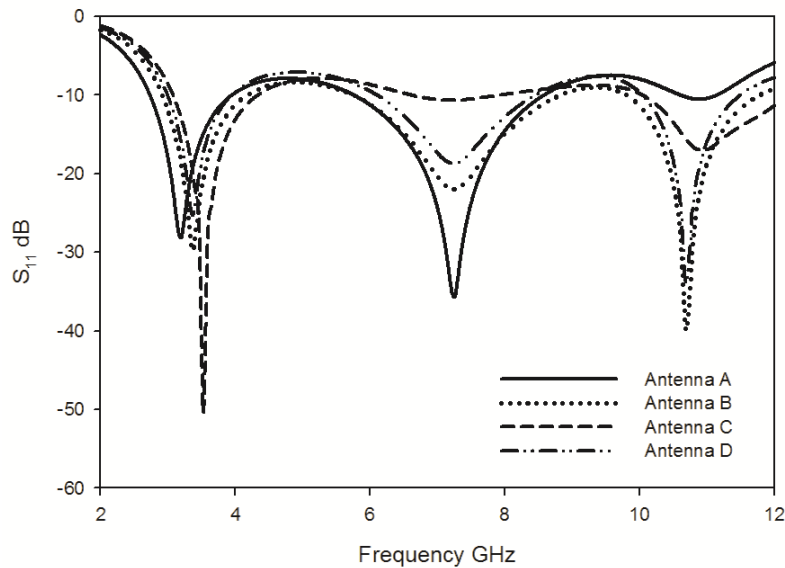


**Fig.5.8.** Reflection co-efficient of the V groove antenna with computed geometric parameters for different substrates.

### 5.1.3 Optimized Structure of the V Groove UWB antenna

To substantiate the simulation studies, a prototype of the proposed V groove UWB antenna is fabricated and analyzed experimentally. The results obtained are discussed in the following sessions.

The structure of the V groove UWB antenna is shown in Fig.5.9. It consist of a coplanar strip of metallic strip dimension  $L \times W$  from which a right angled triangle of dimensions  $L_{\text{off}}$  and  $W_{\text{off}}$  is removed symmetrically from either strips. The antenna is fabricated on commercially available FR4 substrate having relative dielectric constant  $\epsilon_r=4.4$ , height  $h=1.6\text{mm}$  and loss tangent  $\tan\delta=0.02$ . The dimensional parameters of the antenna are  $L=10\text{mm}$ ,  $W=15.75\text{mm}$ ,  $L_{\text{off}}=5\text{mm}$ ,  $W_{\text{off}}=4\text{mm}$  and  $g=0.3\text{mm}$ . The overall dimension of the antenna is  $10\text{mm} \times 31.8\text{mm} \times 1.6\text{mm}$  which is very compact when compared to the existing UWB antennas.

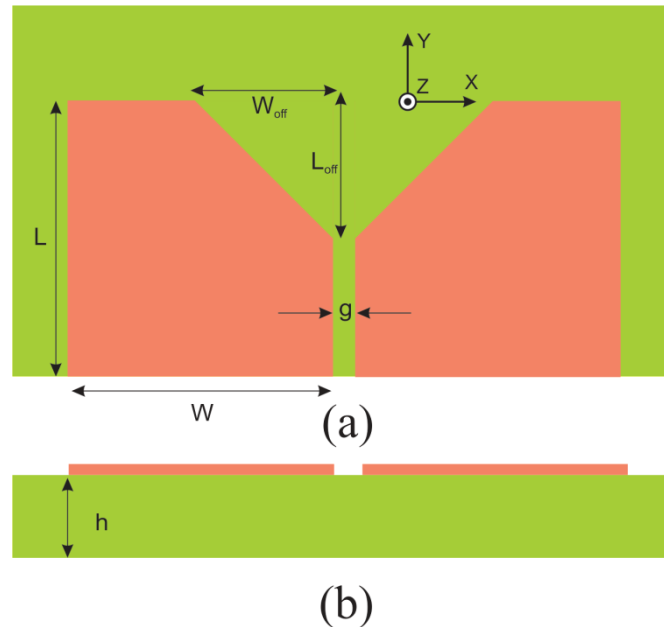


**Fig.5.9.** Structure of the V Groove UWB Antenna ( $L=10\text{mm}$ ,  $W=15.75\text{mm}$ ,  $L_{\text{off}}=5\text{mm}$ ,  $W_{\text{off}}=4\text{mm}$ ,  $g=0.3\text{mm}$  and  $h=1.6\text{mm}$ )

### 5.1.4 Reflection characteristics of the antenna

The simulated and measured reflection co-efficient of the V groove ultra wideband antenna is shown in Fig.5.10. The antenna offers a 2:1 VSWR bandwidth of more than 10 GHz starting from 3.08 GHz. This large bandwidth enables the antenna as a potential candidate for operating in FCC specified ultra wideband range. This large bandwidth is obtained by merging three resonances centered at 3.365GHz, 7.215GHz and 11.68GHz.

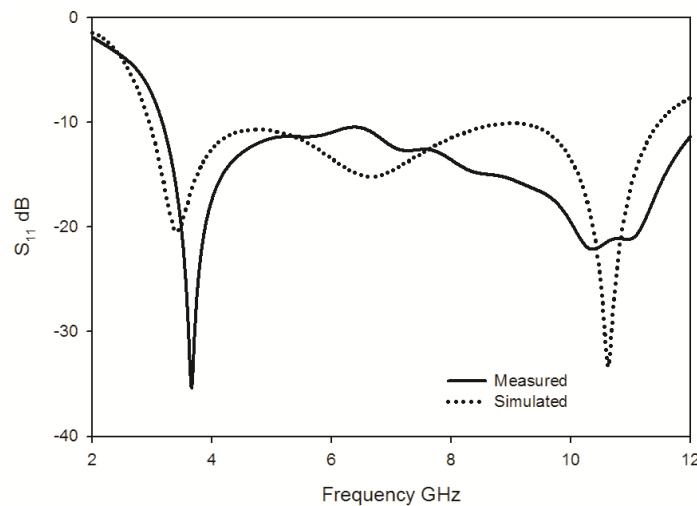


**Fig.5.10.**Reflection co-efficient of the V Groove UWB Antenna ( $L=10\text{mm}$ ,  $W=15.75\text{mm}$ ,  $L_{\text{off}}=5\text{mm}$ ,  $W_{\text{off}}=4\text{mm}$ ,  $g=0.3\text{mm}$  and  $h=1.6\text{mm}$ )

### 5.1.5 Radiation Characteristics of the Antenna

The three dimensional radiation pattern of the antenna at first resonance ie at 3.365 GHz is shown in Fig. 5.11(a). It is inferred from the figure that the antenna offers an apple shaped radiation pattern at this frequency with radiation nulls along the X axis.

The radiation pattern of the antenna at second resonance ie at 7.215GHz is shown in Fig.5.11.(b). At second resonance the antenna is highly directive towards the positive Y direction. The power towards the negative Y direction is highly suppressed. The reason for this directive phenomenon can be explained

from the surface current distribution given in Fig.5.13.(b). From the surface current distribution it is evident that the second resonance is generated due to the current which is maximized at the inclined edge of the antenna ie at the V grooves. This portion is considered as analogous to the flaring in the horn antennas. Thus there will be a forward push to the electromagnetic energy and therefore the directivity increases.

The simulated three dimensional radiation pattern of the antenna at the third resonating frequency is shown in Fig. 5.11(c). At this frequency the antenna offer a distorted radiation pattern with a beam maxima pointing towards positive Y direction. The resonance at this frequency is due to the higher harmonics of the first resonance and that is the reason for pattern distortion. Since the energy is not pointing towards a single direction here, the directivity may be slightly less at the higher frequencies.

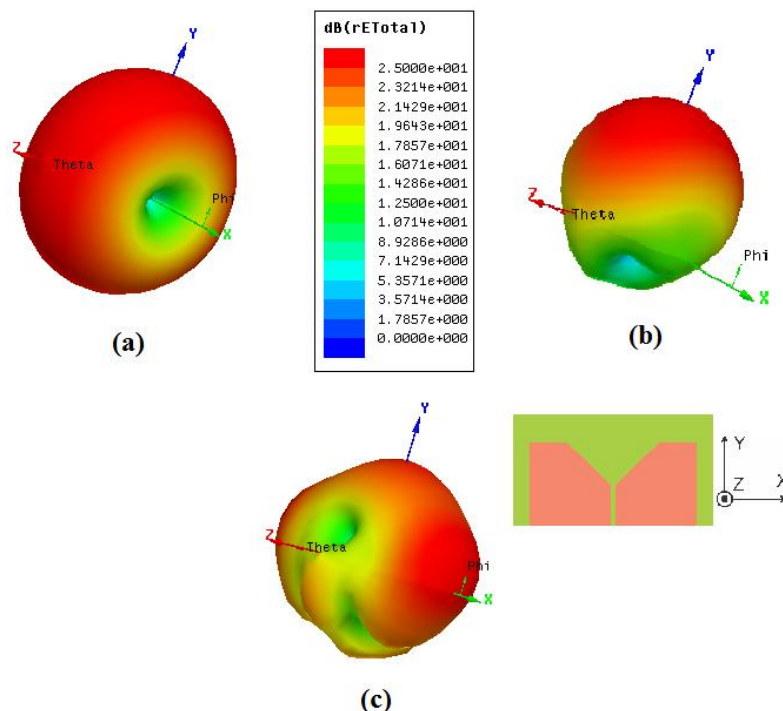


**Fig.5.11.**Three dimensional Radiation pattern of the V Groove UWB Antenna at (a) 3.365 GHz (b) 7.215 GHz and (c) 10.68 GHz ( $L=10\text{mm}$ ,  $W=15.75\text{mm}$ ,  $L_{\text{off}}=5\text{mm}$ ,  $W_{\text{off}}=4\text{mm}$ ,  $g=0.3\text{mm}$  and  $h=1.6\text{mm}$ )

The two dimensional radiation pattern of the antenna in the two principal planes at different frequencies including the three resonances are given in Fig.5.12.

The principal plane radiation patterns of the antenna at starting edge frequency is shown in Fig. 5.12.(a). At 3.1 GHz the antenna offers nearly constant radiation pattern in H plane and an eight shaped radiation pattern in the E plane like a dipole antenna. The cross polar isolation of the antenna at this frequency is found to be better than 15 dB in both the planes.

E and H plane radiation patterns of the antenna at first resonance ie at 3.365 GHz is shown in Fig.5.12(b). At first resonance the radiation pattern is omnidirectional like a dipole. The pattern is non directional along H plane and directional along E plane. The radiation Nulls occur along the X axis. The cross polar level at this frequency is found to be better than 20 dB in both the planes.

The two dimensional radiation pattern of the antenna at second resonance ie at 7.215 GHz is shown in Fig. 5.12(c). The figure clarifies that the antenna exhibits a highly directional behavior at this frequency. In H plane the antenna offers a slightly directive pattern with maxima pointed towards the positive Y direction. The front to back ratio of the radiation patterns at this plane is found to be better than 5 dB. In E plane the antenna offers a directive radiation pattern with a front to back ratio of 7 dB. The cross polar isolation at this frequency is founded as 30 dB in E plane and 40 dB in H plane. Here also the radiation nulls lay along the X axis.

Principal plane patterns of the antenna at 10 GHz is shown in Fig. 5.12(d). At this frequency also the antenna is slightly directive towards the positive Y direction. A front to back ratio of 3 dB is present in both the planes with a cross polar isolation of 15 dB in E plane and 20 dB in H plane.

Two dimensional radiation patterns of the antenna at the third resonance ie at 10.68 GHz is shown in Fig. 5.12(e). According to the figure the antenna at this frequency offers a directional radiation pattern with a slight enhancement in power towards the positive Y direction in both the planes. The cross polar isolation of the antenna is observed as 15 dB in E plane and 20 dB in H plane.

The radiation pattern of the antenna in two principal planes at the end frequency (at 12 GHz) is shown in Fig. 5.12(f). From the figure it is clear that the radiation pattern of the antenna at this frequency is almost similar to that in the third resonance. Here also the antenna offers a slight enhancement in power radiated towards the positive Y direction. A front to back ratio of 3 dB is present in the E plane radiation pattern. The cross polar isolation in E plane is found to be 13dB while that in H plane is observed as 18 dB.

From the three dimensional and planar radiation pattern analyses, it is evident that the antenna offers a radiation pattern whose beam maxima pointed towards the positive Y direction in the entire operating frequency band. Since the directional property of the antenna is maximum at the second resonance, the directive gain of the antenna will be peak at this part of the operating band. The reason for this directional property at the second resonance can be explained from the surface current distribution of the antenna given in Fig. 5.13.(b). From the current distribution it is clear that the second resonance is generated by the surface current peaks at the flaring edges of the V groove antenna. This V groove will give a forward push to the electromagnetic energy which is fed into the antenna.

Since the beam maxima of the antenna pointed towards the same direction and the polarization of it remains the same orientation it can be concluded that the antenna has very good radiation pattern stability in the entire band of operation.

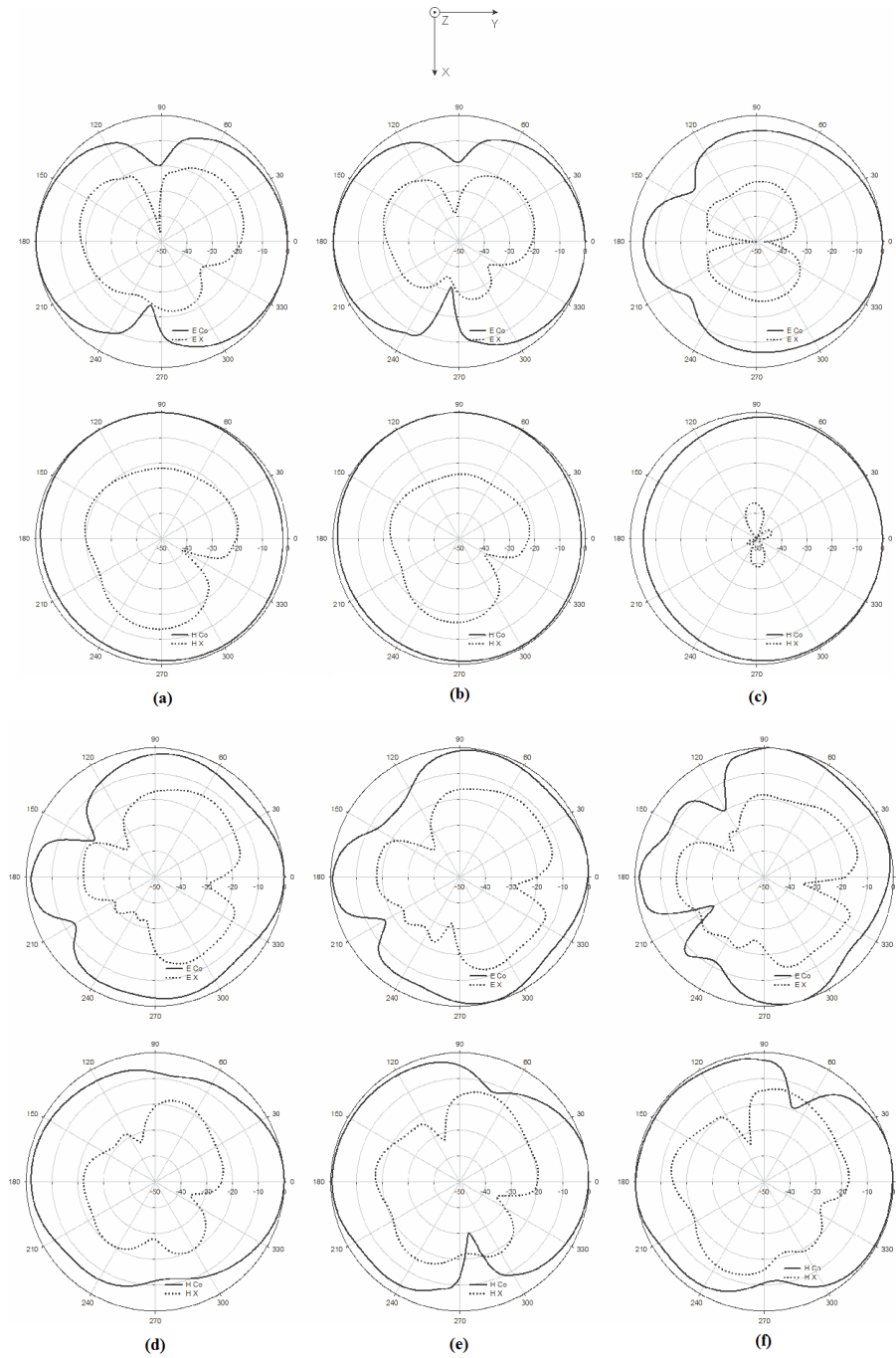


**Fig.5.12.**Principal Plane radiation pattern of the V Groove UWB Antenna at (a) 3.08 GHz (b) 3.365 GHz (c)7.215 GHz (d) 10GHz (e)10.68GHz and (f)12 GHz ( $L=10\text{mm}$ ,  $W=15.75\text{mm}$ ,  $L_{\text{off}}=5\text{mm}$ ,  $W_{\text{off}}=4\text{mm}$ ,  $g=0.3\text{mm}$  and  $h=1.6\text{mm}$ )

### 5.1.6 Surface Current Distribution of the Antenna

The explanation for radiation mechanism of the antenna cannot be completed without the analysis of the surface current distribution of the antenna. Surface current distribution analysis will give more insight about the resonance. Simulated surface current distributions of the antenna at the three resonating frequencies are shown in Fig.5.13.

The surface current distribution of the antenna at first resonance ie at 3.365 GHz is shown in Fig 5.13(a). From the plot it is evident that the resonance is due to the half wavelength long variation of surface current through the entire upper edge of the antenna. This can be verified from the parametric analysis explained in the previous session (5.1.1.). The first resonance is shifting towards lower side with  $W$ ,  $L_{\text{off}}$  and  $W_{\text{off}}$  (Fig.5.4, 5.5 and 5.6) while remaining nearly same for all values of  $L$  (Fig.5.3.). The length of upper edge will increase with  $W$ ,  $L_{\text{off}}$  and  $W_{\text{off}}$  and thus the resonance lowered. The current is maximum at the centre and is minimum at the edges. Since the current is directed along the  $X$  axis, the polarization of the antenna lies in  $X$  direction.

The surface current distribution of the antenna at 7.215 GHz is shown in Fig. 5.13(b). According to the figure the second resonance is created by a three half wave surface current variations through upper edges ( $X$  direction oriented edges and the flaring) and upward edges (four  $Y$  direction oriented edges) of the structure. These can also be verified from the parametric analysis. With  $L$  and  $W$  the resonating frequency gets lowered but with  $L_{\text{off}}$  and  $W_{\text{off}}$  the resonance shows an upward shift. Since the  $Y$  direction oriented current variation in two plates have equal amplitude and exactly opposite phase characteristics, they will cancel each other resulting in a high cross polar purity and a polarization along



X direction. Since the surface current peak occurs at the flaring, the gain may enhance at this frequency [1].

The surface current distribution of the antenna at third resonance ie at 10.68 GHz is shown in Fig 5.13(c). The third resonance is due to the excitation of an approximately five wavelength long surface current variation through the upper edges and the two extreme upward edges. The phase cancellation in both Y directional variation of surface currents present in two conducting planes of the antenna will result in a polarization oriented along X direction and a high degree of cross polar purity.

All the resonances are found to be the odd multiple of half wavelength. The even multiples of the fundamental mode are found to be suppressed in this structure. The second harmonics of the first resonance is close to the second resonance in the optimized structure since the length corresponding to second resonance current path  $(2(W + 2L - W_{off} - L_{off} + \sqrt{L_{off}^2 + W_{off}^2}))$  is approximately twice that of first resonance  $(2(W - W_{off} + \sqrt{L_{off}^2 + W_{off}^2}))$ .

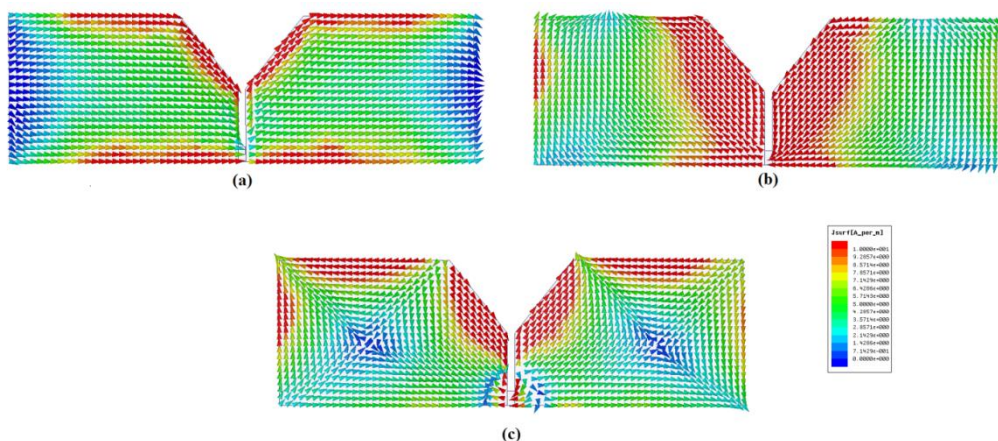


**Fig.5.13.**Surface current distribution of the V Groove UWB Antenna at (a) 3.365 GHz (b) 7.215 GHz and (c) 10.68 GHz ( $L=10\text{mm}$ ,  $W=15.75\text{mm}$ ,  $L_{off}=5\text{mm}$ ,  $W_{off}=4\text{mm}$ ,  $g=0.3\text{mm}$  and  $h=1.6\text{mm}$ )

### 5.1.7 Gain and efficiency of the Antenna

Measured directive gain of the antenna in the entire operating band is given in Fig 5.14 as solid line. The antenna offers an average gain of 4.84 dBi in the entire operating band with a peak gain of 6.24 dBi near the second resonance. The enhancement in directive gain near the second resonance is explained in the previous sessions.

The radiation efficiency of the antenna in the entire operating frequencies is shown in Fig.5.14 as dotted line. The proposed V Groove ultra wide band antenna offers an average radiation efficiency of 92% in the entire operating band which is a very good value.

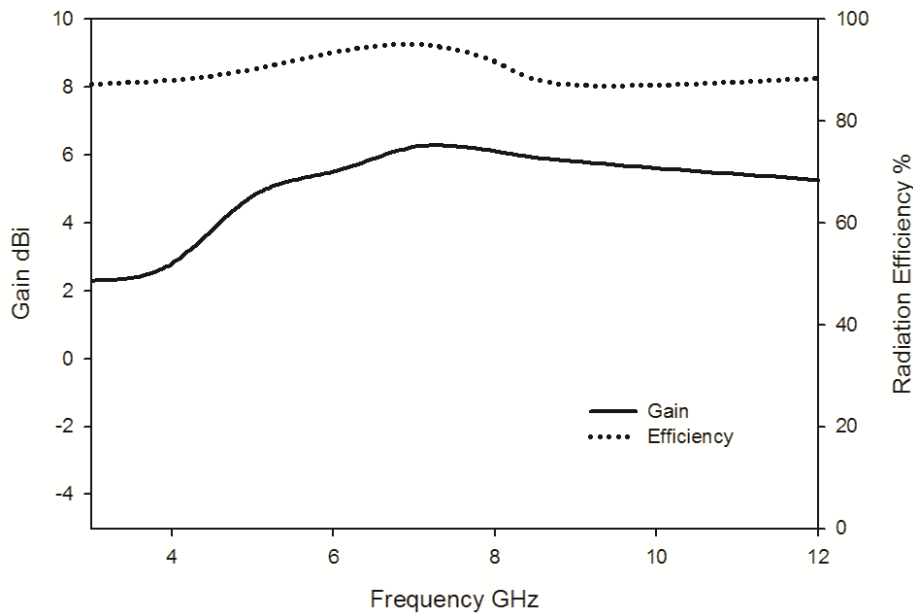


**Fig.5.14.** Gain and Efficiency of the V Groove UWB Antenna ( $L=10\text{mm}$ ,  $W=15.75\text{mm}$ ,  $L_{\text{off}}=5\text{mm}$ ,  $W_{\text{off}}=4\text{mm}$ ,  $g=0.3\text{mm}$  and  $h=1.6\text{mm}$ )

## **5.2 Coplanar Strip fed Ultra compact Semicircular slot UWB antenna**

The second part of this chapter is describing the development of an ultra compact UWB antenna. The evolution of the ultra compact UWB antenna is shown in Fig. 5.15. The antenna is obtained from an OES by removing a semicircle of radius  $R$  from the top edge of the OES with centre of the semicircle lies in the intersection of middle point of the slot along X axis and upper edge of the OES. The overall dimension of the antenna after the transformation will remain the same as that of the parental OES.

The idea behind this antenna is derived from the previously discussed V groove antenna in which a linear tapering is used to attain the UWB performance. Here in this structure the tapering is not linear one but circular. The size of the proposed structure is also found to be very compact when compared to that of existing structures. Since the tapering proposed here is of circular one, the size of the antenna become very compact than the V groove UWB discussed in the earlier session.

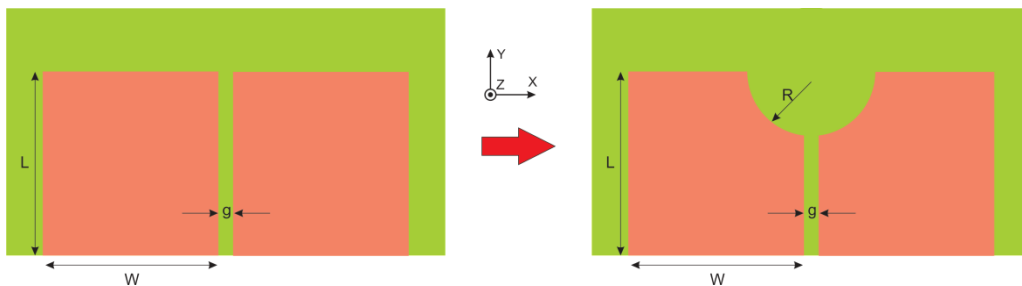


**Fig.5.15.** Evolution of Ultra compact semicircular slot UWB from an OES

The creation of a new circular slot on the top edge of an OES will change the reflection characteristics of OES. The reflection coefficients of an OES and the OES with a semicircular slot of different dimensions are shown in Fig. 5.16.

The figure clarify that the OES without semicircular slot will acts as a single band dipole with total width approximately equal to half of the wavelength of resonant frequency. The introduction of a semicircular slot at the top edge of the OES will increase the band width. Since the resonance created due to the introduction of semicircular slot with higher radius is asymmetric, there is a possibility of creating an additional resonance near the initial resonant frequency. By properly selecting the parameters this structure can perform like a UWB antenna. The optimization of the antenna is discussed in the parametric analysis session.

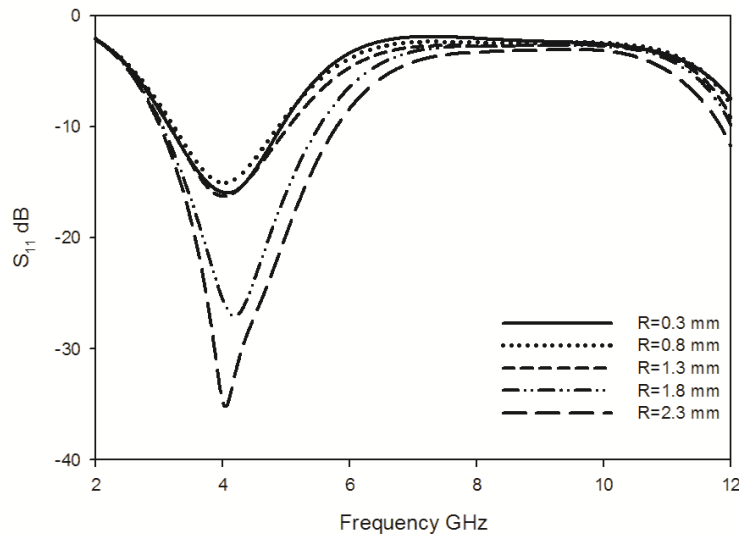


**Fig.5.16.** Reflection co efficient of an OES with small R of different dimensions (L=110mm &W=14mm)

### 5.2.1 Parametric Analysis of the antenna

The parametric analysis of the antenna is performed to get the reason for resonance and to get further technical knowhow of the radiation mechanism. It is also helpful in developing the design equation of the antenna. The results obtained are discussed here.

### 5.2.1.1 Variation in reflection co-efficient with L

The variation of reflection co-efficient of the antenna with L is shown in Fig. 5.17. According to the figure all the resonances are found to be strongly affected by L. The second and third resonance shows a down shift with L while the first resonance show a very feeble higher shift in frequency with increase in L. This higher shifting of frequency is due to the tendency of fringing field concentration near the slot of the structure and is explained in session 3.3.2.1 of chapter.3. The decrease in resonant frequencies of second and third resonance is due to the increase in surface current path length and can be verified from the surface current distribution given in Fig.5.26. From the variation analysis performed, for the better impedance matching of the structure in the UWB frequency range L of the antenna is optimized as 10 mm.

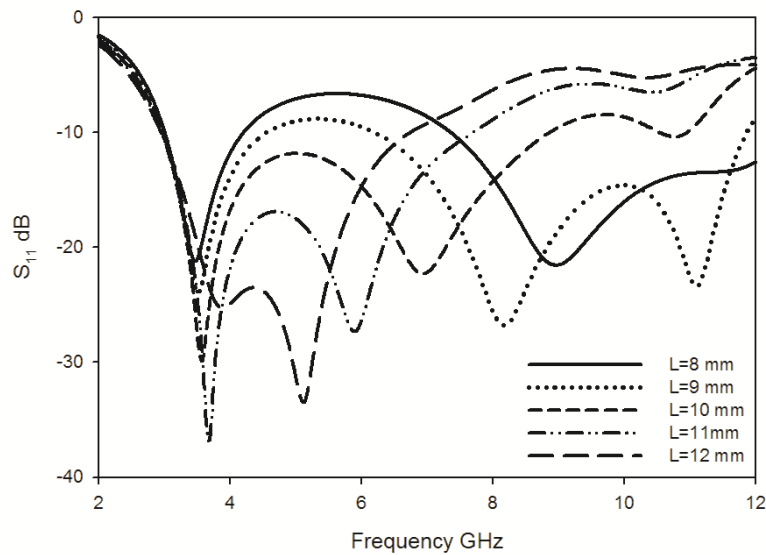


**Fig.5.17.** Variation of Reflection co-efficient with L (W=14mm, R=4.38mm, g=0.3mm and h=1.6mm)

### 5.2.1.2 Variation in reflection co-efficient with W

The variation of reflection co efficient of the antenna with W is shown in Fig.5.18. From the figure it is observed that all the three resonances are affected by this parameter. There is a considerable down shift for all the resonant frequencies with W. This is due to the increase in surface current path length of the antenna. This can be easily verified from the surface current distribution of the antenna given in Fig.5.26. The impedance matching of all the curves is found to be good. The W of the antenna is optimized as 14 mm to get the FCC specified impedance bandwidth.

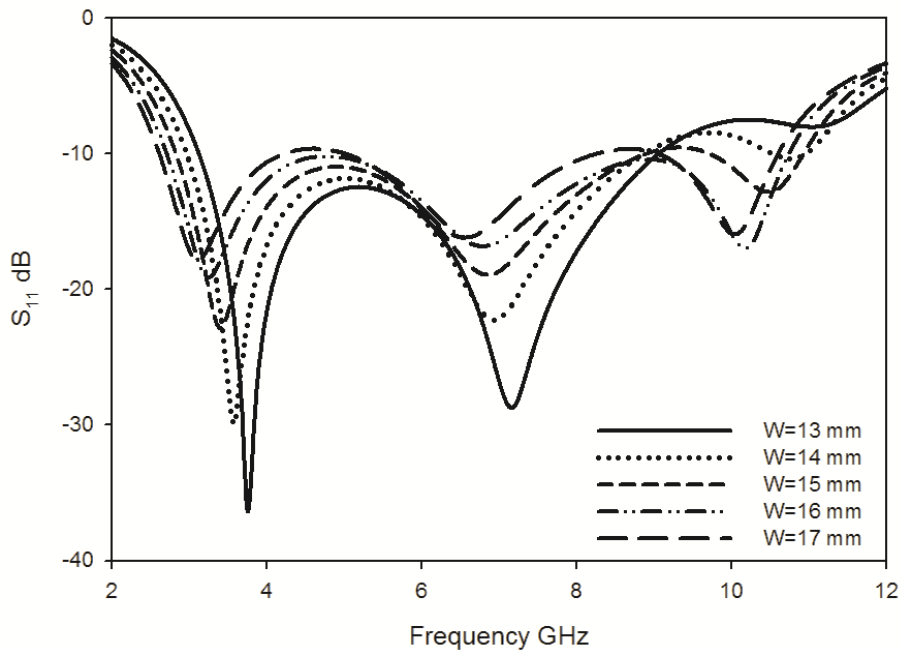


**Fig.5.18.** Variation of Reflection co-efficient with W ( $L=10\text{mm}$ ,  $R=4.38\text{mm}$ ,  $g=0.3\text{mm}$  and  $h=1.6\text{mm}$ )

### 5.2.1.3 Variation in reflection co-efficient with R

The variation of reflection co efficient of the antenna with radius R of the semicircle is shown in Fig.5.19. For small values of R, the antenna acts as a single band antenna with moderate band width. But for larger values of R, the

first and third resonant frequencies show a down shift with increase in R. This is due to the increase in resonant current path length corresponding to these resonances. The second resonant frequency increases with R and is due to the removal of metallic part from the initial current path corresponds to second resonance, which will decrease the current path length.

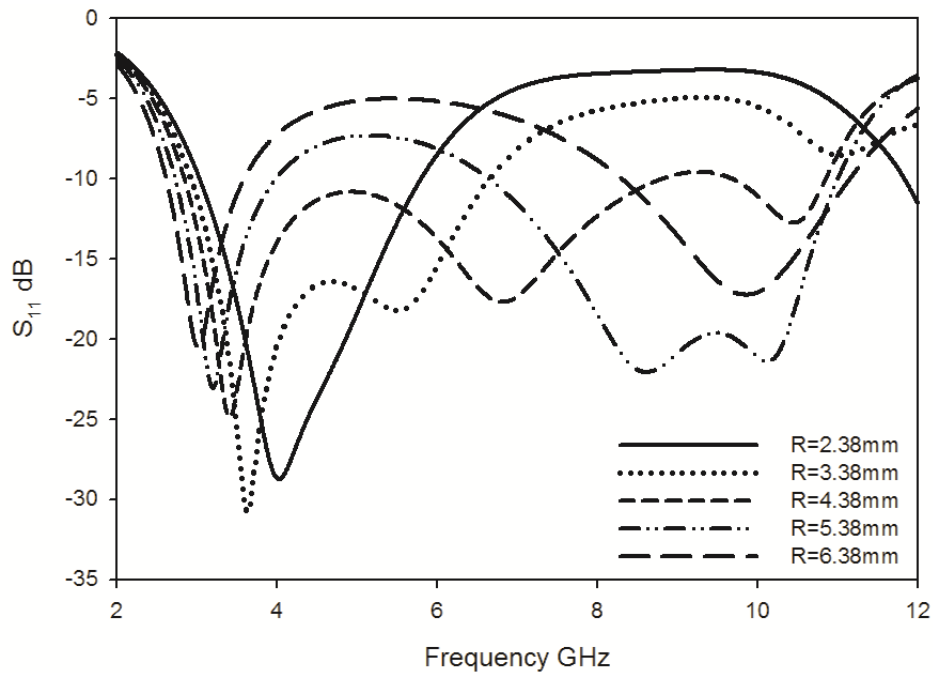


**Fig.5.19.** Variation of Reflection co-efficient with R (L=10mm, W=14mm, g=0.3mm and h=1.6mm)

#### 5.2.1.4 Variation in reflection co-efficient with h

This session deals with the effect of substrate height on reflection co efficient of the antenna. The variation of reflection coefficient of the antenna with substrate height h is shown in Fig. 5.20. From the figure it is clear that all the resonances are unaffected by the height of the substrate. The matching is slightly affected by the parameter h. This may be due to the variation of input impedance of the antenna with h.

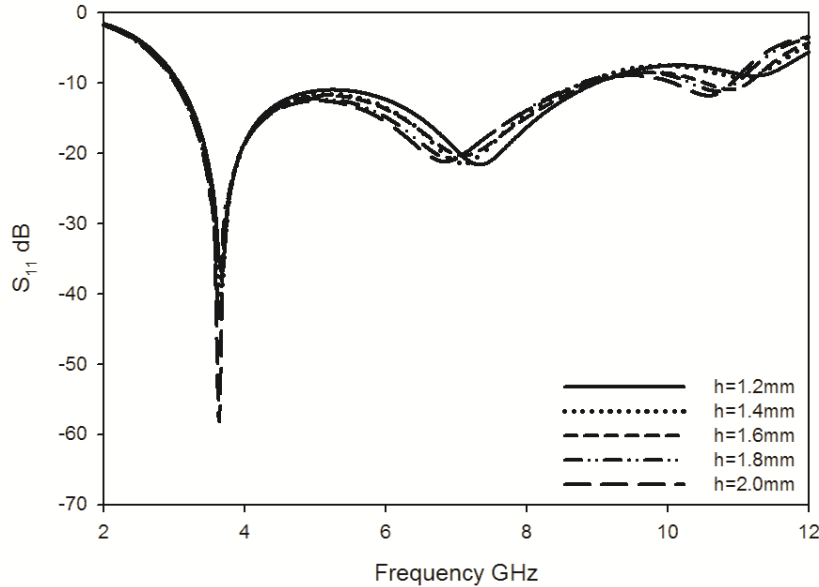


**Fig.5.20.** Variation of Reflection co-efficient with  $h(L=10\text{mm}, W=14\text{mm}, R=4.38\text{mm}$  and  $g=0.3\text{mm}$ )

### 5.2.2 Design Equation of the semicircular slot Antenna

From the parametric analysis of the antenna performed in the previous session, the design equation of the semicircular slot ultra wideband antenna is developed and is discussed in this session. The developed design equations are validated for different substrates with different dielectric constant.

The design equations of the antenna are given below.

$$2(W - R) + \pi R \cong 0.65\lambda_{g1}$$

$$2(L + W - 2R) + \pi R \cong 1.72\lambda_{g2}$$

$$2(L + W - R) + \pi R \cong 3.2\lambda_{g3}$$

Where  $\lambda_{g1}$ ,  $\lambda_{g2}$ ,  $\lambda_{g3}$ , are the guided wavelengths corresponding to the first, second and third resonant frequencies and can be calculated from free space wavelength  $\lambda_{0n}$  as,



$$\lambda_g = \lambda_0 / \sqrt{\epsilon_{eff}}$$

Where  $\epsilon_{eff} = (\epsilon_r + 1)/2$  is the effective dielectric constant.

In order to prove the developed design equation, the parameters of the antennas operating in UWB region are computed for different substrates. The substrate parameters of the developed antenna are shown in Table 5.3 and the calculated dimensional parameters of the antenna are shown in table 5.4.

**Table 5.3** Substrate Description

	<b>Antenna A</b>	<b>Antenna B</b>	<b>Antenna C</b>	<b>Antenna D</b>
<b>Laminate</b>	Rogers 5880	FR4 Epoxy	Rogers R03006	Rogers6010LM
<b>h(mm)</b>	1.57	1.6	1.28	0.635
$\epsilon_r$	2.2	4.4	6.15	10.2
$\epsilon_{re}$	1.6	2.7	3.575	5.6
<b>g(mm)</b>	0.1	0.3	0.65	0.775

**Table 5.4** Computed Geometric Parameters of the Antenna

<b>Parameter (mm)</b>	<b>Antenna A</b>	<b>Antenna B</b>	<b>Antenna C</b>	<b>Antenna D</b>
<b>L</b>	13.8	10	7.4	6.75
<b>W</b>	17.8	14	13.1	10
<b>R</b>	5.9	4.38	2.8	2.1

The simulated reflection co-efficient of the antennas developed using the parameters given in the tables 5.3 and 5.4 are shown in Fig. 5.21. All the four antennas are ultra wide band in nature and offer sufficient band width with three resonances. The developed design equations are very suitable for developing antennas operating in UWB region in any substrates.

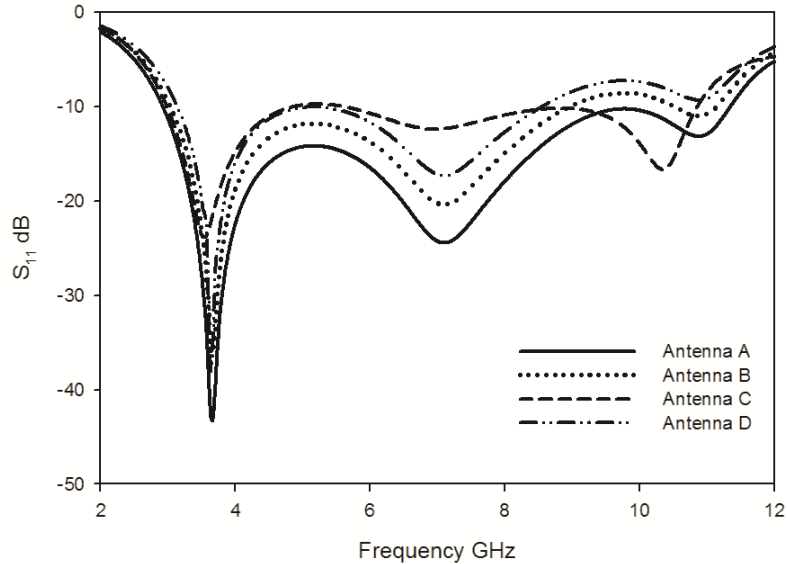


**Fig.5.21.** Reflection co-efficient of the Semicircular slot antenna with computed geometric parameters for different substrates

### 5.2.3 Optimized Structure of the semicircular slot UWB antenna

In order to validate the simulation results an optimized prototype of the proposed antenna is fabricated and experimentally analyzed. The results are discussed in this session of the chapter. The structure of the semicircular slot UWB antenna is shown in Fig.5.22. It consist of a slotline of metallic strip dimension  $L \times W$  from the top of which a semicircle of radius  $R$  is removed. The antenna is fabricated on commercially available FR4 substrate having relative dielectric constant  $\epsilon_r=4.4$ , height  $h=1.6\text{mm}$  and loss tangent  $\tan\delta=0.02$ . The dimensional parameters of the antenna are  $L=10\text{mm}$ ,  $W=14\text{mm}$ ,  $R=4.8\text{mm}$  and  $g=0.3\text{mm}$ . The overall dimension of the antenna is  $10\text{mm} \times 28.3\text{mm} \times 1.6\text{mm}$  which is very compact when compared to the V groove UWB antenna.

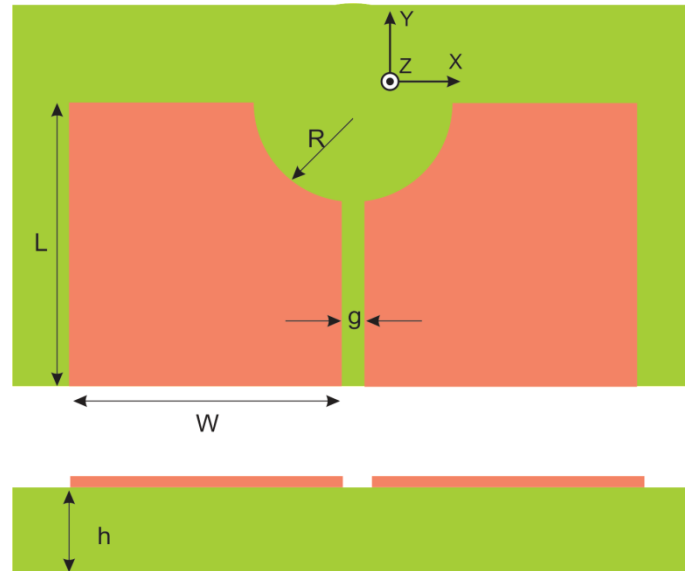


**Fig.5.22.** Structure of the Ultra compact Semicircular slot UWB Antenna ( $L=10\text{mm}$ ,  $W=14\text{mm}$ ,  $R=3.48\text{mm}$ ,  $g=0.3\text{mm}$  and  $h=1.6\text{mm}$ )

#### **5.2.4. Reflection co-efficient of the semicircular slot UWB antenna**

The simulated and measured reflection co-efficient of the proposed semicircular slot ultra wideband antenna is shown in Fig.5.23. The proposed semicircular cut UWB antenna offers a large 2:1 VSWR bandwidth starting from 2.92 GHz to 11.34 GHz. This large bandwidth ensure that the antenna can be used in FCC specified UWB applications. This bandwidth is obtained by merging three resonances centered at 3.67 GHz, 7.2 GHz and 10.85 GHz. From the figure it is clear that both the curves are in good agreement.

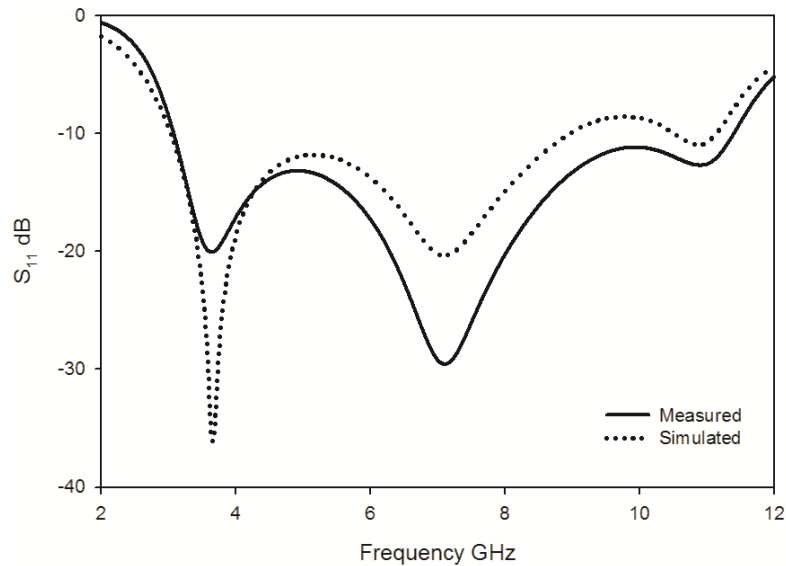


**Fig.5.23.** Reflection co-efficient Ultra compact Semicircular slot UWB Antenna (L=10mm, W=14mm, R=3.48mm, g=0.3mm and h=1.6mm)

### 5.2.5. Radiation Characteristics of the semicircular slot UWB Antenna

The simulated three dimensional radiation patterns of the semicircular slot UWB antenna at three resonances are shown in Fig.24.

The radiation pattern of the proposed antenna at 3.67 GHz is shown in Fig.24 (a). The figure shows that the antenna pattern is apple shaped similar to a dipole antenna. There is a small enhancement of power towards the positive Y direction and is due to the inherent directive property of the OES discussed in Chapter 3. The null of the pattern is occurred along the X direction.

Three dimensional radiation patter of the antenna at second resonance ie at 7.2 GHz is shown in Fig.24 (b). The antenna offers a directive radiation pattern at this frequency with beam maxima pointed towards the positive Y direction. A high amount of back lobe suppression is noticed in this pattern. This effect can be substantiated from the explanation of the surface current

pattern of the antenna given in Fig.5.26 (b). From the current pattern it is found that the current is maximum at the curved edges of the antenna and at all other parts the current is minimum. Thus the other parts of the radiating structure will acts as a suppressor of backward power. In this pattern also the radiation null lies along the X direction.

The simulated 3 dimensional radiation pattern of the antenna at third resonance is shown in Fig.5.24 (c). At 10.85 GHz the antenna offers a highly directive radiation pattern with a noticeable back radiation suppression. The pattern is slightly distorted with radiation null of the antenna along X axis.

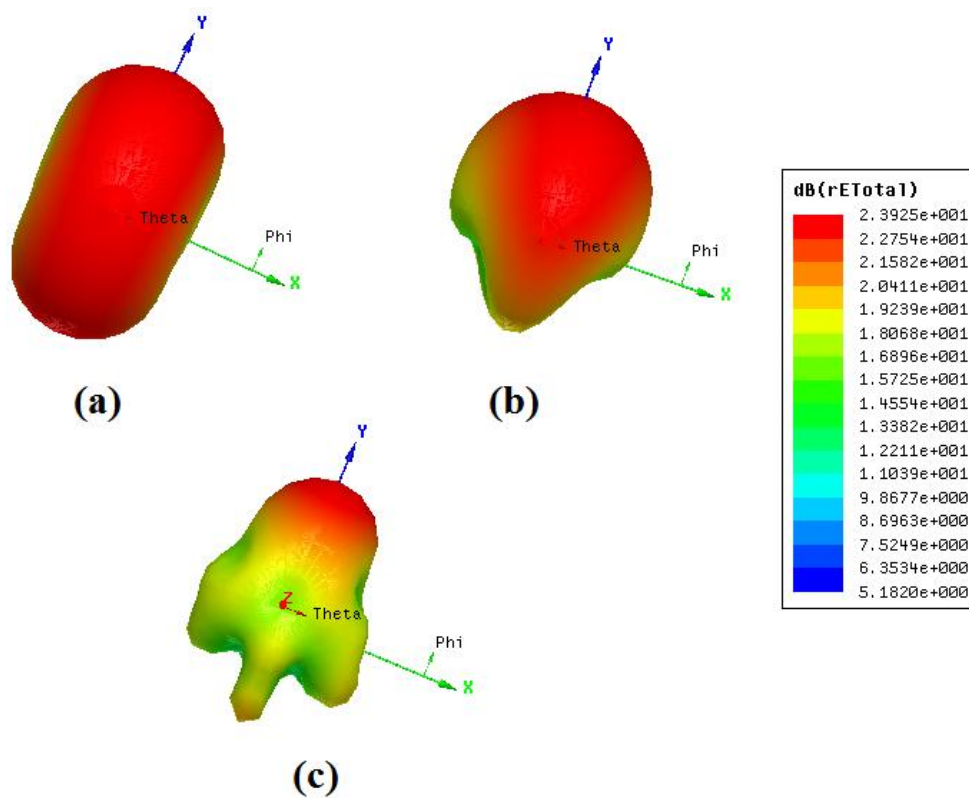


**Fig.5.24.**Three dimensional Radiation pattern of the Ultra compact Semicircular slot UWB Antenna at (a) 3.67 GHz (b) 7.20 GHz and (c) 10.85 GHz (L=10mm, W=14mm, R=3.48mm, g=0.3mm and h=1.6mm)

The two dimensional radiation pattern of the antenna in the two principal planes at different frequencies including the three resonances are given in Fig.5.25.

The principal plane radiation patterns of the antenna at starting frequency ie at 2.92 GHz is shown in Fig. 5.25.(a). At this frequency the antenna offer nearly constant radiation pattern in H plane and an eight shaped radiation pattern in the E plane like a dipole antenna. The cross polar isolation of the antenna at this frequency is found to be better than 20 dB in both the planes. Polarization of the antenna at this frequency lies along X axis.

E and H plane radiation patterns of the antenna at first resonance ie at 3.67 GHz is shown in Fig.5.25.(b). At first resonance the radiation pattern is omnidirectional similar to a dipole antennaie in H plane the pattern is non-directional and along E plane it offers a directional radiation pattern with radiation nulls along X axis. The cross polar level at this frequency is found to be in the order of 20 dB in both the planes. The polarization of the antenna remains same as the previous frequency.

The principle plane patterns of the antenna at a mid-frequency 5.2GHz is shown in Fig.5.25.(c). At this frequency the antennas offer a slightly directional pattern in both planes with a front to back ratio of 3 dB. The cross polar level of E plane pattern is better than 30 dB while that of H plane is better than 40 dB. Thus the gain at this frequency may be enhanced. The radiation null of E plane pattern occurs at X direction. The polarization at 5.2 GHz is found to be X oriented and the radiation maximum is towards the positive Y direction.

The two dimensional radiation pattern of the antenna at second resonance ie at 7.20 GHz is shown in Fig. 5.25.(d). The antenna exhibits a highly directional behavior at second resonance. The front to back ratio of either plane is found to be better than 5 dB. The cross polar levelsalong E and H plane are found to be better than 30 dB and 40 dB respectively. The radiation

null and polarization of the antenna are along the X direction with a radiation maxima occur in the positive Y direction.

Principal plane patterns of the antenna at third resonance 10.85 GHz is shown in Fig. 5.25.(e). From the figure it is clear that at this frequency also the antenna is directive towards the positive Y direction and the directive property of the antenna increases with frequency. F/B ratio of 7 dB is present in both the planes with a cross polar isolation of 30 dB in E plane and that of 40 dB in H plane. The polarization of the antenna at this frequency also found to be oriented along X direction.

Two dimensional radiation patterns of the antenna at the end frequency at 11.34 GHz is shown in Fig. 5.25.(f). Here the radiation pattern is directional with maximum power points towards the positive Y direction in both the planes. The cross polar isolation of the antenna is observed as 20 dB in both E plane and H plane. The beam width of the antenna is found to be slightly less in this frequency.

From the three dimensional and planar radiation pattern analyses, it is evident that the antenna offers a radiation pattern whose beam maxima pointed towards the positive Y direction in the entire operating frequency band. Since the directional property of the antenna is maximum at the second and third resonances, the directive gain of the antenna will be peak at the vicinity of these resonances in the operating band. The reason for this directional property at the second and third resonances can be explained from the surface current distribution of the antenna given in Fig. 5.26.(b).

Since the beam maxima of the antenna pointed towards the same direction and the polarization of it remains the same orientation it can be concluded that the antenna has very good radiation pattern stability in the entire band of operation.

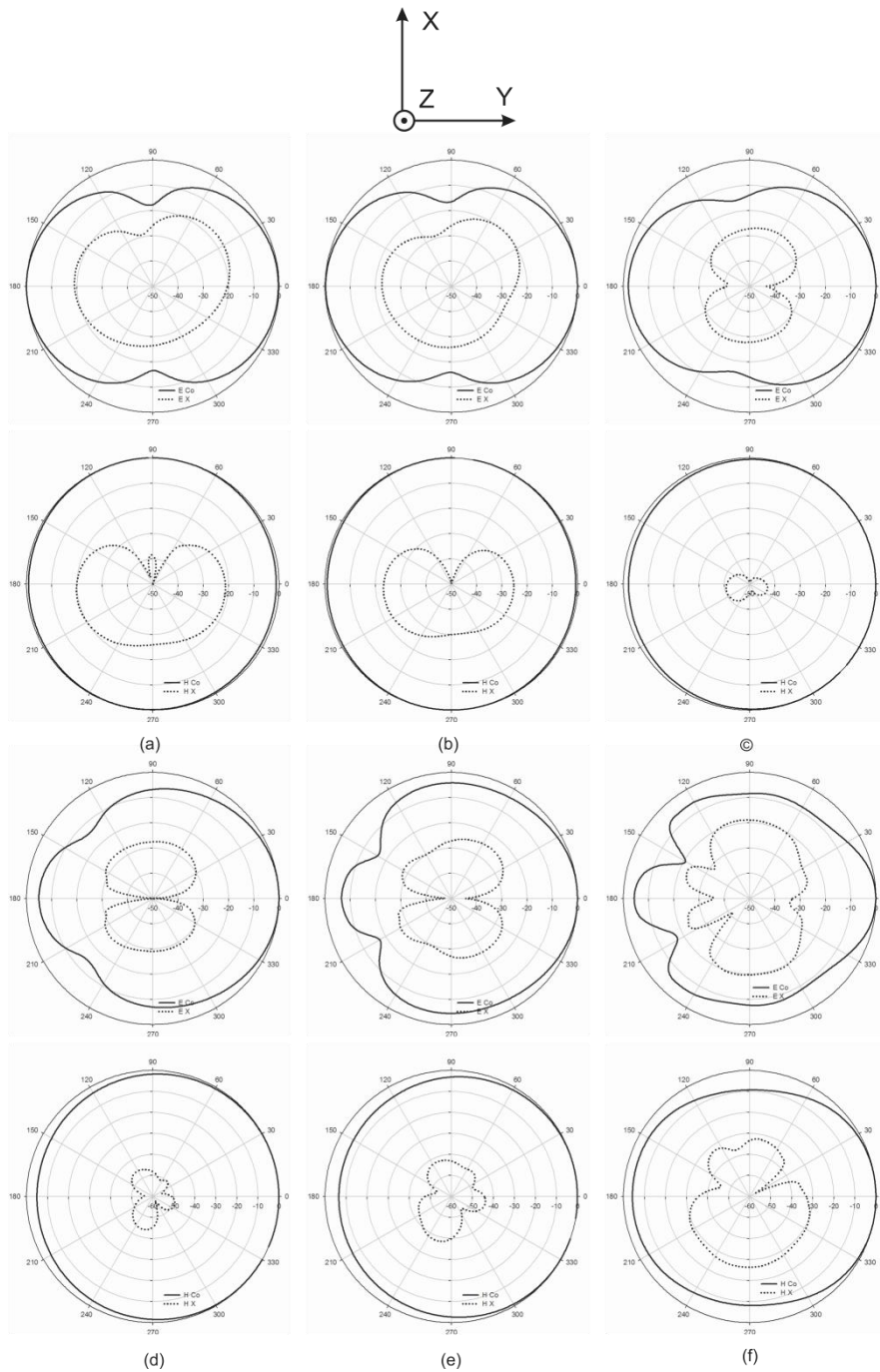


**Fig.5.25.**Principal Plane radiation pattern of the Ultra compact Semicircular slot UWB Antenna at (a) 2.92 GHz (b) 3.67 GHz (c)5.2 GHz (d) 7.20GHz (e)10.85GHz and (f)11.34 GHz ( $L=10\text{mm}$ ,  $W=14\text{mm}$ ,  $R=3.48\text{mm}$ ,  $g=0.3\text{mm}$  and  $h=1.6\text{mm}$ )



### **5.2.6. Surface Current Distribution of the Antenna**

To explain the radiation mechanism and the reason for resonances, the surface current analysis is very important and unavoidable. Simulated surface current distributions of the antenna at the three resonating frequencies are shown in Fig.5.26.

The surface current distribution of the antenna at first resonance ie at 3.64 GHz is shown in Fig 5.26 (a). The first resonance is created due to the half wavelength long variation of surface current through the entire upper edge length of the antenna. The current is found to be maximum at the centreie near the slot and is minimum at the edges. This can be also verified from the parametric studies of the parameter W and R. As W increases, the upper edge length increases and result in an increase in current path which will reduce the resonant frequency (Fig.5.18). Similar variation of first resonant frequency is found in the case of parameter R also. As R increases, the perimeter of the semicircle increases which result in increase in the current path length (Fig.5.19). As a result resonance gets lowered. Since the current is flowing along the X axis, the polarization of the antenna lies along X direction.

The surface current distribution of the antenna at second resonating frequency 7.105 GHz is shown in Fig. 5.26 (b). The second resonance is due to the surface current variation through the upper edge and upward edges which are similar in the case of pre explained V groove antenna. This can be inferred from the parametric analysis. As L and W increases, the lengths of upper and upward edges increases which result in a lower shift in second resonance (Fig. 5.17 and 5.18). As R increases, a portion from the upper upward edge is removed from the strip, which resulting in a higher shift in resonant frequency (Fig.5.19). Since the variation of surface current in Y direction has exactly

opposite phase characteristics, they will cancel each other and the polarization of the antenna remains in X direction. This phase cancellation is the reason for High cross polar purity.

The surface current distribution of the antenna at third resonance ie at 10.9 GHz is shown in Fig 5.26 (c). Here also the surface current shows similar variation as explained in the case of second resonance, but the upward current is through the far edges from the slot. The phase cancellation in both Y directional variation of field will result in a polarization oriented along X direction and a high degree of cross polar purity.

From the parametric analysis and the detailed surface current studies, it can be concluded that the structure and resonance mechanism of the semi circular slot antenna is almost similar to that of the V groove UWB antenna. Thus removal of elliptical portions from upper edges, exponential tapering of the upper edges etc also results in compact enhanced gain UWBs.

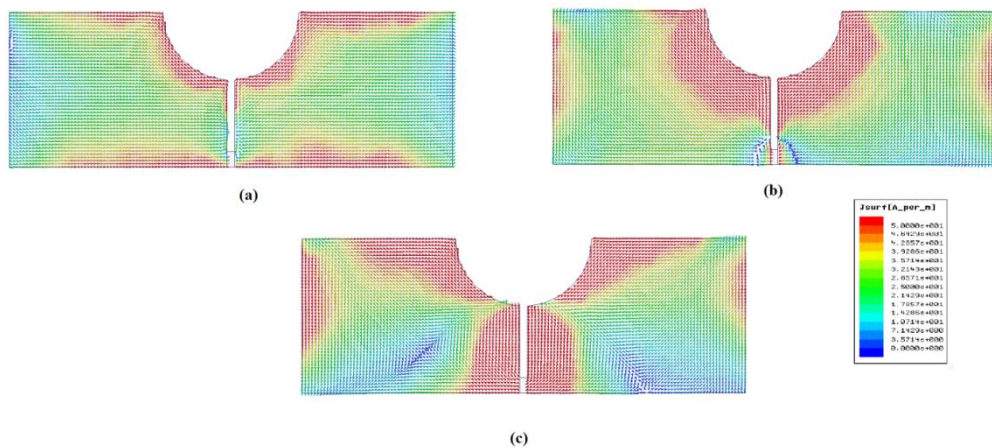


**Fig.5.26.** Surface current distribution of the Ultra compact Semicircular slot UWB Antenna at (a) 3.67 GHz (b) 7.20 GHz and (c) 10.85 GHz (L=10mm, W=14mm, R=3.48mm, g=0.3mm and h=1.6mm)

### 5.2.7 Gain and efficiency of the Antenna

Measured directive gain of the antenna as a function of operating frequency and the radiation efficiency of the antenna are given in Fig 5.27 as solid and dotted lines respectively. The antenna offers an average gain of 4.92dBi in the entire operating band with a peak gain of 6.9dBi at higher frequencies. The enhancement in directive gain near the second and third resonance is explained in the previous surface current analysis sessions. The radiation efficiency of the antenna is found to be better than 90% in the entire operating band with an average value of 93 %.

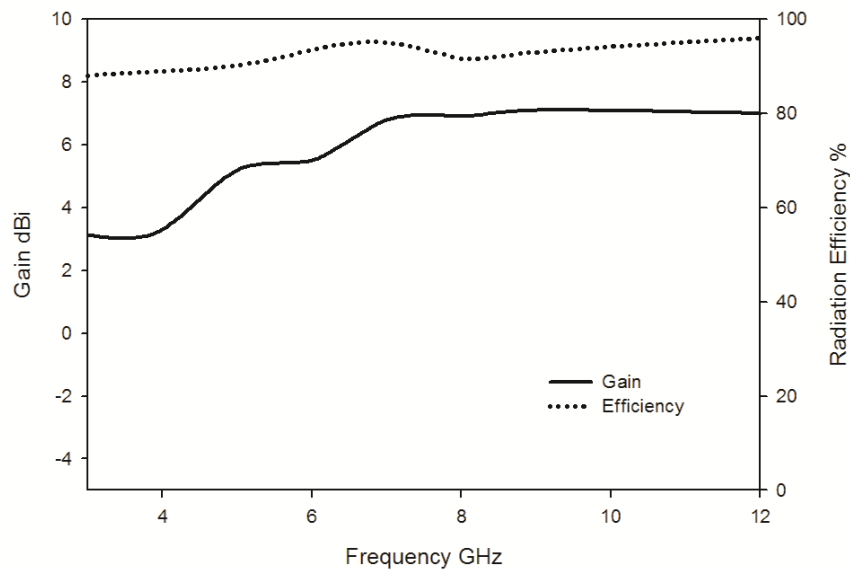


**Fig.5.27.** Gain and Efficiency of the Ultra compact Semicircular slot UWB Antenna ( $L=10\text{mm}$ ,  $W=14\text{mm}$ ,  $R=3.48\text{mm}$ ,  $g=0.3\text{mm}$  and  $h=1.6\text{mm}$ )

### 5.3 Coplanar strip fed Enhanced Gain UWB antenna

In this session, the study is vectored to the development of a compact highly directive UWB antenna with high efficiency and enhanced gain. Evolution of the coplanar strip fed compact semicircular Ultra Wide Band

antenna from the Open Ended Slotline (OES) is shown in Fig. 5.28. It is derived from the OES of dimension  $L \times W$  by adding two semicircular perfect electric conductors on the top edge of both the strips of OES.



**Fig.5.28.** Evolution of semicircular UWB antenna from an OES

### 5.3.1. Parametric Analysis of the Semicircular UWB Antenna

Further insight on the antenna performance is obtained by carrying out a detailed parametric analysis. The variation of reflection coefficients with different antenna parameters are discussed in the following session.

#### 5.3.1.1. Variation in reflection co-efficient with R

Variation of reflection co-efficient of the antenna with radius  $R$  of the semicircle is shown in Fig.5.29. As the radius of the circle  $R$  increases all the three resonant frequencies are shifted towards the lower side. The reason for this down shift is due to the increase in length of the current paths which produce the resonances. This phenomenon can be easily verified from the surface current distribution of the antenna which is discussed in the coming session. The matching remains nearly same for all the values of  $R$  which shows that there is no noticeable variation in the impedance of the antenna with  $R$ .

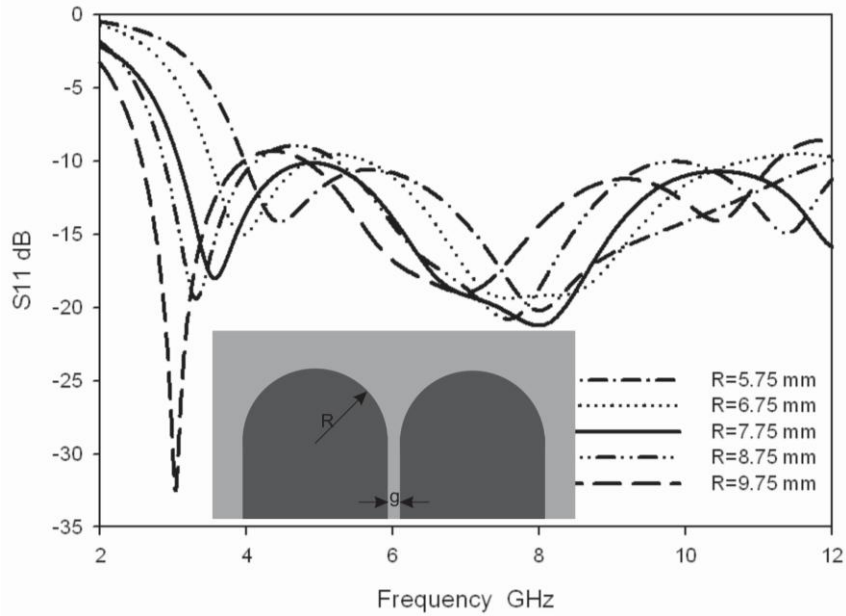


**Fig. 5.29** Variation of Reflection co-efficient of coplanar strip fed semicircular UWB antenna with R ( $L=3$  mm,  $g=0.3$  mm,  $h=1.6$  mm).

### 5.3.1.2 Variation in reflection co-efficient with L

The variation of reflection co-efficient of the antenna for different slotline length  $L$  is shown in Fig. 5.30. The first resonance shows a very feeble up shift in frequency with  $L$ . This higher shifting of frequency is also due to the tendency of fringing field concentration near the slot of the structure and is explained in session 3.3.2.1 of chapter.3. Both the higher resonances are shifted towards lower side with increase in  $L$ . This is also due to the increase in surface current path length corresponding to those resonances with  $L$ . The impedance matching at the higher bands is also strongly affected by the variation of  $L$ . This implies that the variation in slotline length affect the input impedance of the higher band strongly because at the higher band, due to small wavelength, a small change in transmission line length creates a huge variation in the impedance.

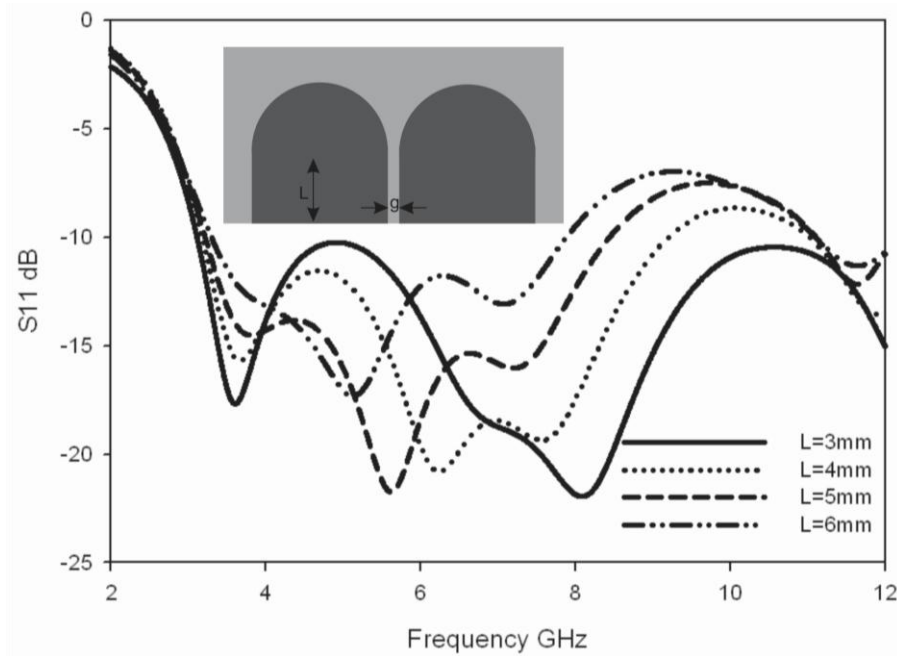


**Fig. 5.30** Variation of Reflection co-efficient of coplanar strip fed semicircular UWB antenna with  $L$  ( $R=7.75$  mm,  $g=0.3$  mm,  $h=1.6$  mm).

### 5.3.1.3 Variation in reflection co-efficient with $h$

The effect of substrate height of the semicircular UWB antenna on the reflection characteristics are discussed in this session. The variation of reflection co efficient of the antenna with  $h$  is shown in Fig. 5.31. According to the figure it is evident that the band width is not affected by the parameter  $h$ . Only a slight variation is found in the impedance matching of the antenna. This is due to the variation of the characteristic impedance of the antenna with substrate height.

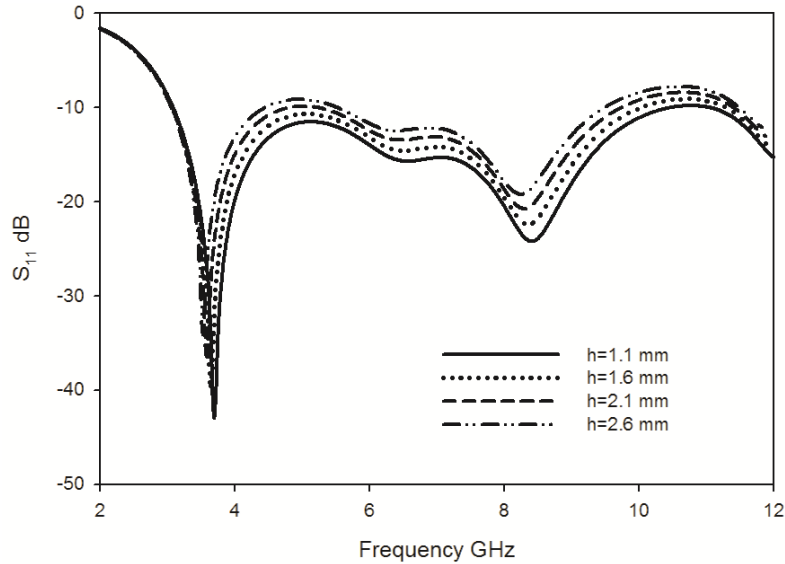


**Fig. 5.31** Variation of Reflection co-efficient of coplanar strip fed semicircular UWB antenna with h (R=7.75mm, L=3 mm, g=0.3mm)

### 5.3.2 Design equation of semicircular UWB Antenna

From the parametric analysis of the semicircular UWB antenna, it is able to develop the design equation of the antenna and is discussed in this session. The developed design equations are validated for different substrates with different dielectric constant and are also discussed.

The design equations of the antenna are given below.

$$R=0.16\lambda_g$$

$$L=0.06\lambda_g$$

Where  $\lambda_g$  is the guided wavelength corresponding to the lower resonant frequency and can be calculated from free space wavelength  $\lambda_0$  as,

$$\lambda_g = \lambda_0 / \sqrt{\epsilon_{eff}}$$

where  $\epsilon_{eff} = (\epsilon_r + 1)/2$  is the effective dielectric constant.

The developed design equations of the compact semicircular ultra wide band antenna are validated for four different antennas in different substrates with substrate parameters given in Table 5.5. The computed dimensional parameters of the antennas according to the design equations are given in Table 5.6.

**Table 5.5** Substrate Description

	Antenna A	Antenna B	Antenna C	Antenna D
<b>Laminate</b>	Rogers 5880	FR4 Epoxy	Rogers R03006	Rogers6010LM
<b>h(mm)</b>	1.57	1.6	1.28	0.635
$\epsilon_r$	2.2	4.4	6.15	10.2
$\epsilon_{re}$	1.6	2.7	3.575	5.6
<b>g(mm)</b>	0.1	0.3	0.65	0.775

**Table 5.6** Computed Geometric Parameters of the Antenna

Parameter (mm)	Antenna A	Antenna B	Antenna C	Antenna D
<b>L</b>	3.9	3	2.61	2.08
<b>R</b>	10.06	7.75	6.735	5.38

The simulated reflection co-efficient of the antennas developed according to the specifications given in the tables 5.5 and 5.6 are shown in Fig. 5.32. Figure proves that all the four antennas are with ultra wide band characteristics and offer sufficient band width with three resonances. From the figure it is also clear that the developed design equations can be utilized to develop antennas operating in UWB region in any substrates.



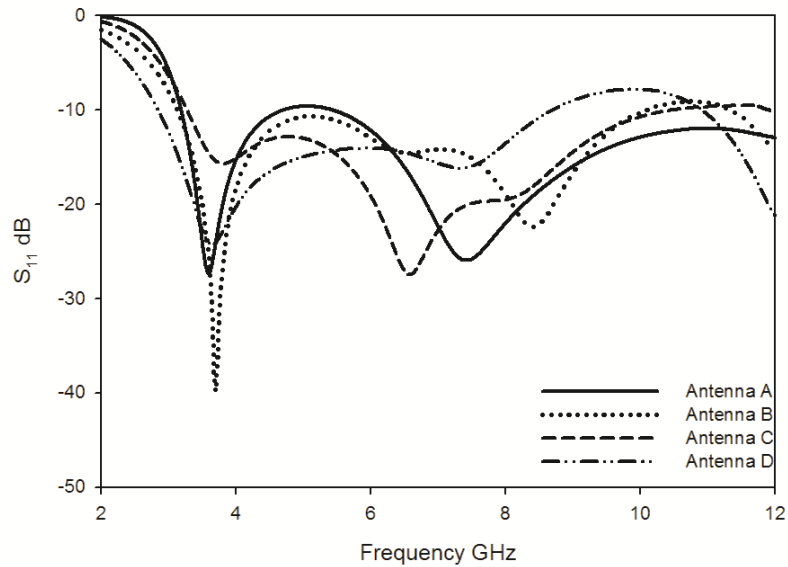


**Fig.5.32.** Reflection co-efficient of the Semicircular UWB antenna with computed geometric parameters for different substrates.

### 5.3.3 Optimized Structure of Semicircular UWB Antenna

The structure of the CPS fed semicircular UWB antenna is shown in Fig.5.33. It consist of a slotline of dimension  $L \times W$  on which a semicircular patch of radius  $R$  is integrated. The width of the coplanar strip is selected such that  $W=2R$ . The antenna structure is created on commercially available substrate having relative dielectric constant  $\epsilon_r= 4.4$ , loss tangent  $\tan\delta= 0.02$  and thickness  $h= 1.6$  mm. The main attractions of this uniplanar antenna structure is its compactness (size is only  $31.3\text{mm} \times 10.75\text{mm} \times 1.6$  mm) and the lesser number of design parameters.

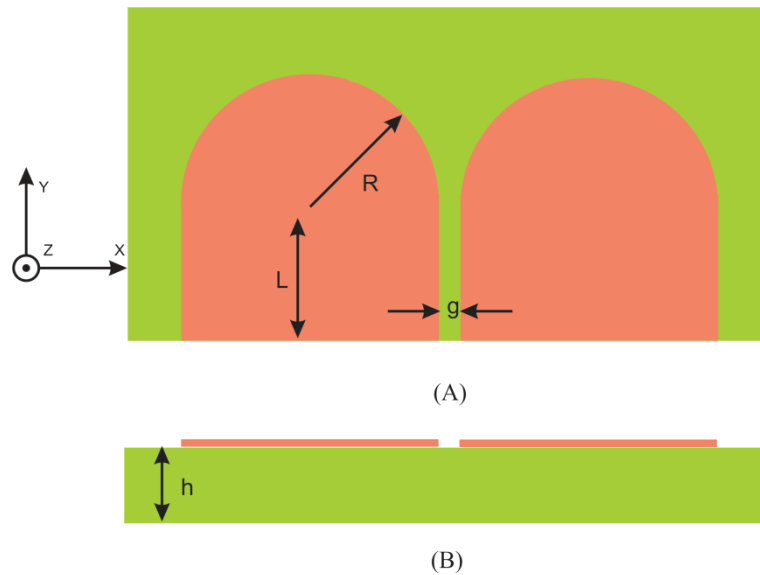


**Fig.5.33.** Structure of Semicircular UWB antenna (A) Top view (B) Side View ( $L=3$  mm,  $R=7.75$  mm,  $g=0.3$ mm,  $h=1.6$  mm).

### 5.3.4 Reflection Characteristics of Semicircular UWB Antenna

The simulated and measured reflection coefficient of the optimal design of the antenna is shown in Fig.5.34. The parameters of the antenna are same as that given in Figure 5.33. The -10dB bandwidth appears to span an extremely wide frequency range from 3.1GHz to more than 12 GHz. This wide bandwidth is obtained by merging three resonances centered at 3.69 GHz, 6.5 GHz and 8.26 GHz. Here a slight variation is noticeable inbetween the simulated and measured reflection co-efficient. This may be due to the fabrication tolerance.

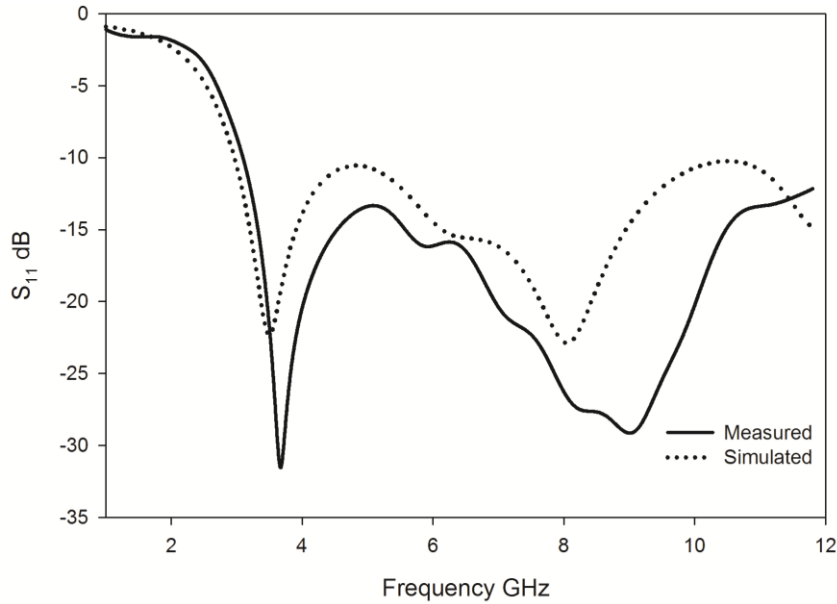


**Fig.5.34** Reflection co-efficient of Semicircular UWB ( $L=3$  mm,  $R=7.75$  mm,  $g=0.3$ mm,  $h=1.6$  mm).

### 5.3.5 Radiation Characteristics of the Semicircular UWB Antenna

The radiation characteristics of the coplanar strip fed Semicircular UWB antenna is analyzed thoroughly and is discussed in this session. The simulated three dimensional radiation patterns at the three resonant modes are given in Fig.5.35.

The three dimensional radiation pattern of the antenna at 3.69 GHz is given in Fig 5.35.(a). At this frequency the maximum radiation is directed towards the Y direction. A reduction in power to the negative Y direction is noticeable in the radiation pattern. The nulls of the beam are along X direction.

Radiation pattern of the antenna at 6.5 GHz is given in Fig.5.35. (b). The antenna offers a radiation pattern similar to that of a microstrip patch antenna. Power towards the negative Y direction is entirely suppressed in this structure

and is highly directional towards the positive Y direction. Here also both the nulls and the polarization are along same direction ie along X axis.

The radiation characteristics of the antenna at the third resonant frequency 8.26 GHz is given in Fig.5.35.(c). At the third resonant frequency also the pattern is found to be highly directional and pointed towards the plus Y direction and suppress the power towards negative Y direction.

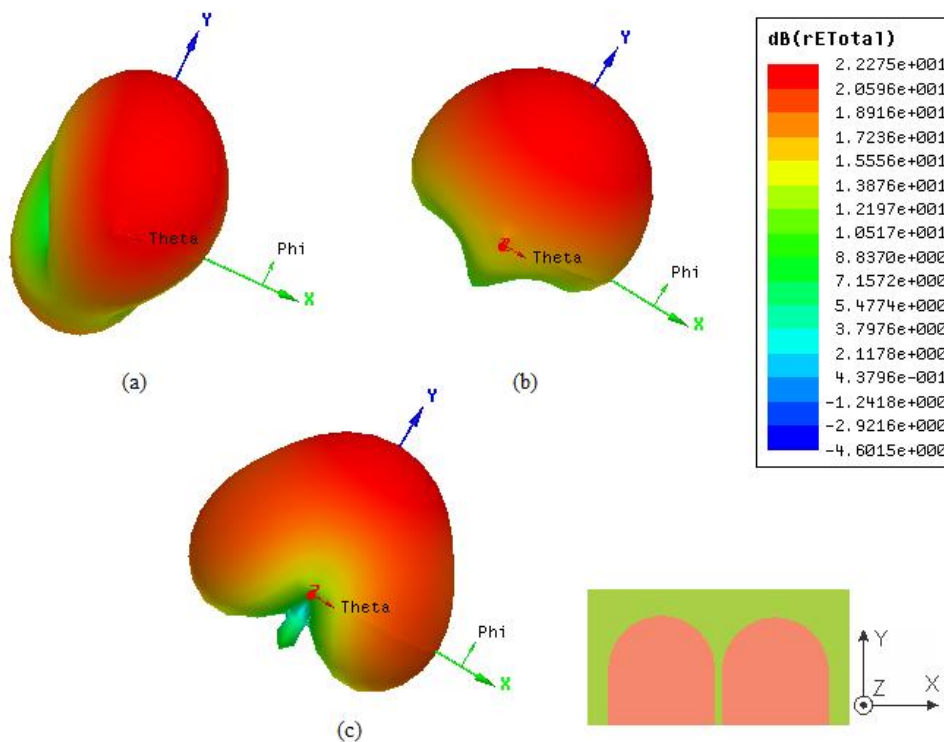


**Fig.5.35.** Three dimensional radiation pattern of Semicircular UWB at (a)3.69 GHz, (b) 6.5 GHz and (c)8.26 GHz (L=3 mm, R=7.75 mm, g=0.3mm, h=1.6 mm).

In all the discussed cases, the pattern seems to be directional along positive Y direction and the radiations of energy along the negative Y direction are suppressed. Thus it is evident that the antenna has a very good radiation pattern stability which is a main attraction of this coplanar strip fed semicircular UWB radiating structure. To analyze the radiating behavior of the antenna in

the principal planes, two dimensional radiation pattern of the antenna are also measured and is discussed in this session. The two dimensional radiation patterns of the antenna at different frequencies including the three resonances are shown in Fig.5.36.

The two dimensional radiation pattern of the antenna at the band starting frequency 3.1 GHz is shown in Fig. 5.36.(a). From the figure it is inferred that at this frequency the antenna offer an eight shaped pattern in E plane and circular radiation pattern with 1 dB front to back ratio in the H plane. The cross polar isolation is found to be better than 20 dB in both the patterns.

The principal plane radiation pattern of the antenna at first resonance ie at 3.69 GHz is shown in Fig. 5.36.(b). At first resonance the antenna offers almost similar radiation patterns to that of the dipole antenna. There is a small front to back ratio of 2.5 dB can be noticeable in both the radiation patterns. The cross polar level in E and H plane is found to be better than 25 dB.

The radiation patterns of the antenna at 5 GHz in the E and H plane are shown in Fig. 5.36.(c). From the figure it is clear that the directivity of the antenna is increased in this frequency when compared to lower frequencies. The antenna offers a front to back ratio of 3 dB in both the planes. The cross polar isolation is found to be better than 30 dB in E plane and 40 dB in H plane. The beam maximum of the antenna is pointed towards positive Y direction.

E plane and H plane radiation pattern of the antenna at second resonance ie at 6.5 GHz is shown in Fig. 5.36.(d). The antenna is found to be highly directive at this frequency. A front to back power ratio better than 8 dB is present in both the radiation pattern with a cross polar isolation of 30 dB in E plane and 40 dB in H plane. Since the cross polar isolation at this frequency is

very good and a better F/B ratio is present, the directive gain of the antenna at this frequency may be highly enhanced.

The principal plane patterns of the antenna at third resonance ie at 8.26 GHz is shown in Fig. 5.36.(e). At third resonance the antenna offers a directional pattern pointed towards Y direction. Front to back ratio at this frequency is found to be greater than 12 dB in both the planes. The cross polar isolation of the antenna is found to be better than 30 dB in E plane and 40 dB in H plane.

The radiation patterns of the antenna at the band ending frequency 10.6 GHz is shown in Fig. 5.36.(f). It can be founded from the figure that the antenna offer a directive radiation pattern at this end frequency also with bore sight towards positive Y direction. The front to back ratio of the antenna at this frequency is found to be better than 10 dB in E plane and 8 dB in H plane. The cross polar level is found to be better than 35 dB in both the planes.

From the radiation pattern analysis of the antenna it is found that the directivity is a common nature of all the patterns. This property is found to be maximum in the middle of the application band. The polarization of the antenna and the beam maxima direction are also remains the same for all the frequencies within the band. Thus the antenna has high radiation pattern stability in the entire frequency of operation.

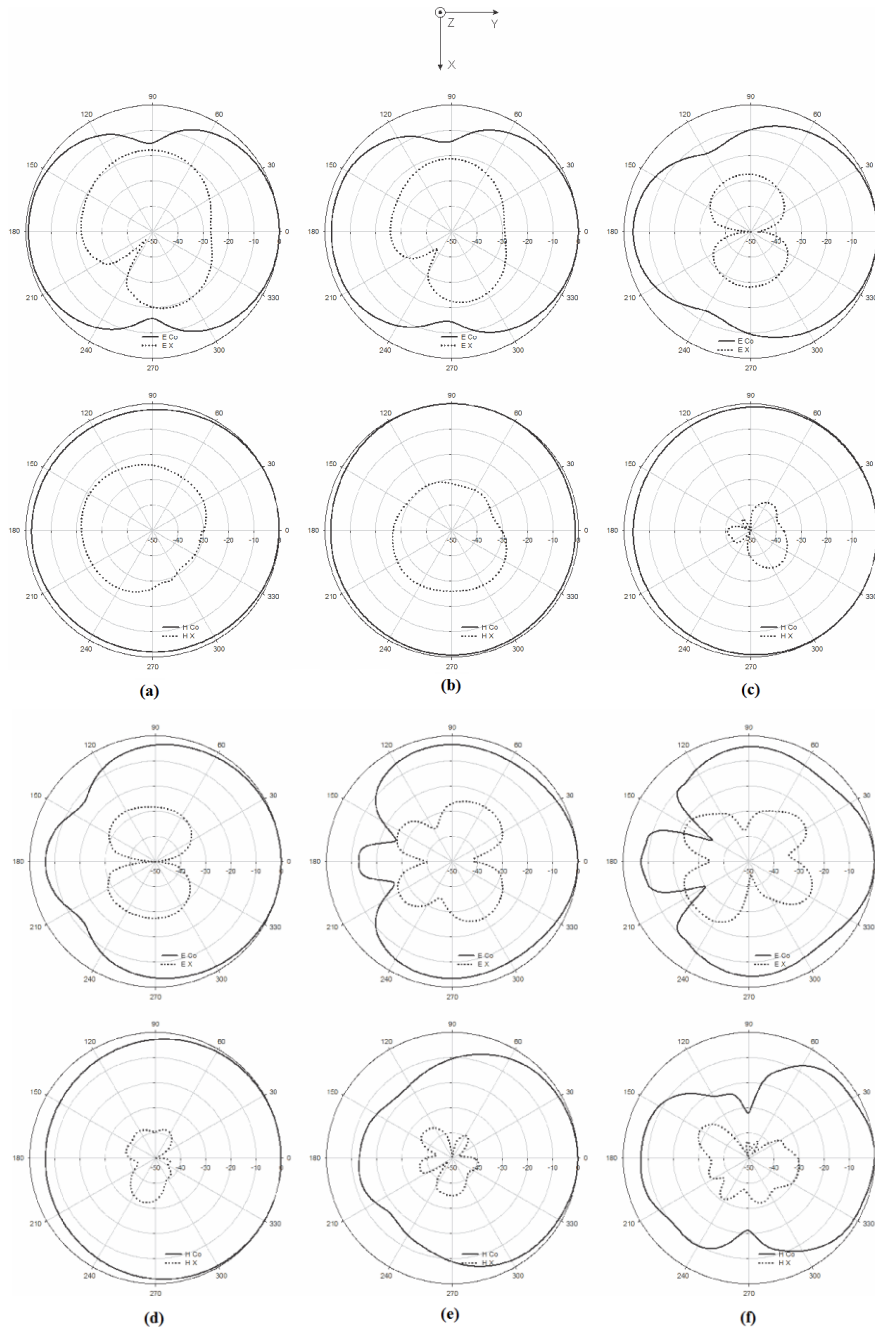


**Fig.5.36.** Principal plane radiation pattern of Semicircular UWB at (a)3.1 GHz (b)3.69 GHz, (c) 5 GHz (d) 6.5 GHz (e) 8.26 GHz and (e)10.6 GHz ( $L=3$  mm,  $R=7.75$  mm,  $g=0.3$ mm).

From the performed two dimensional radiation pattern analysis it is evident that the antenna is a highly directive in the entire band of operation with good radiation pattern stability. All the measured results show good agreement with the simulated three dimensional radiation patterns. Further explanation of the resonant modes and radiation patterns are obtained from the surface current distribution analysis which is explained in the next session.

### **5.3.6 Surface Current Analysis of the Semicircular UWB Antenna**

To explain the radiation mechanisms and the reasons for resonant modes, it is necessary to analyze the surface current distribution of the antenna. Detailed analyses of the surface current distributions of the antenna at the three resonant modes are carried out by simulation and are explained in this session. The simulated current distribution of the antenna is given in Fig.5.37.

Simulated surface current distribution of the antenna at 3.69 GHz is given in Fig.5.37 (a). From the figure it is clear that the first resonant mode is due to a half wavelength long current path through the entire upper edge of the antenna with current maxima at the centre and minima at the two extremes of the structure. The antenna is therefore polarized in the X direction in first resonating frequency. Since the antenna is flared towards the positive Y direction, the antenna offer a beam maxima towards the same direction [1].

Surface current distribution of the antenna at the second resonant frequency 6.5 GHz is given in Fig.5.37 (b). The second resonant mode is excited due to a combined effect of surface current variation in X and Y direction. The variations in surface current in Y direction have equal magnitude and opposite direction which results in an X oriented linear polarization. Since the radiated fields due two ends are equal in magnitude and opposite in direction, they will cancel each other and effectively the  $\lambda/2$  variation in



centre part contributes in far field radiation. This will increase the directive behavior of the antenna since the far field radiating current is present at the flared edge [1] of the antenna pointing towards the Y direction without creating distortions in pattern.

From the surface current distribution given in Fig.5.37 (c) corresponding to third resonant mode, it is evident that the resonance at 8.26GHz is excited due to surface current variation in X and Y directions as explained in the previous case. Here also the polarization is along X direction due to cancellation of field along Y direction. Since the current which results in far-field radiation flow through the curved edges, the directivity will be enhanced.

From the analysis of the surface current distribution of the antenna it is evident that the antenna's radiation is mainly from the centre part of the structure and it will increase its directionality just as like Vivaldi antennas [1]. Since all the current path is through the edge of the antenna, the remaining part of the structure will contribute in suppressing the back radiation. The polarization of the antenna is in X direction with two nulls of the radiation patterns in the X axis which can be verified from the three dimensional radiation pattern given in Fig.5.35.

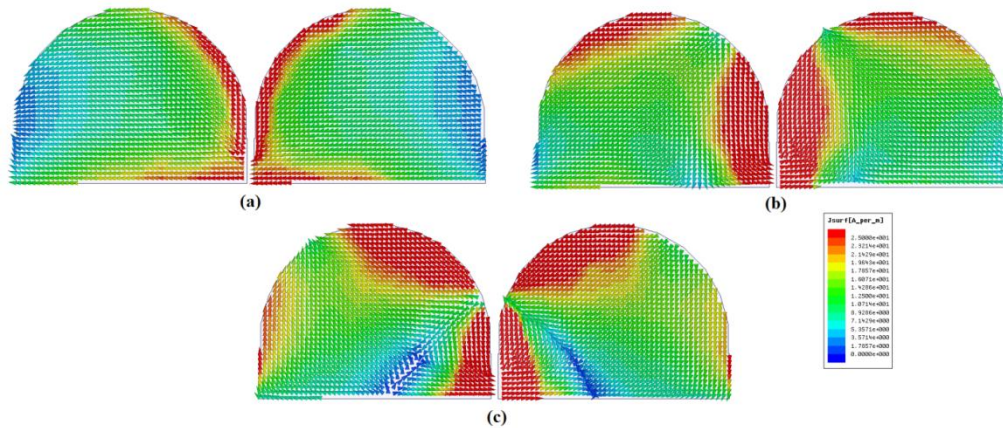


**Fig.5.37.** Surface current distribution of Semicircular UWB at (a)3.69 GHz, (b) 6.5 GHz and (c)8.26 GHz ( $L=3$  mm,  $R=7.75$  mm,  $g=0.3$ mm,  $h=1.6$  mm).

### 5.3.7 Gain and Efficiency of the Semicircular UWB Antenna

The measured gain of the antenna in the entire band of operation is shown in Fig.5.38. The semicircular UWB radiating structure offer an average gain of 8 dBi in the operating band with a peak gain of 8.74dBi around 7 GHz. It is to be noted from the gain plot that the antenna offer nearly uniform flat gain in the entire bandwidth.

The measured radiation efficiency of the antenna using wheeler cap method in the entire bandwidth is shown in Fig.5.38 as dotted line. From the figure it is clear that the antenna offer a uniform flat efficiency in the entire operating band width with an average value of 90 %.

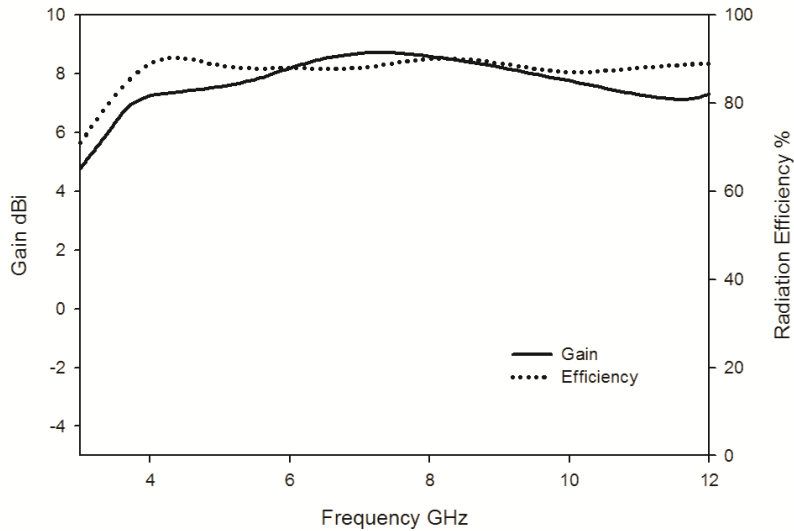


**Fig. 5.38** Measured Gain and Radiation efficiency of the UWB ( $L=3$  mm,  $R=7.75$  mm,  $g=0.3$ mm,  $h=1.6$  mm).

## 5.4 Time Domain analysis of the Antennas

In the previous sessions we have analyzed the frequency domain parameters of all the developed ultra wide band antennas. Since the UWB systems are dealing with extremely narrow pulses, time domain analysis is also equally important for UWB antennas as frequency domain analysis and is unavoidable. The following sessions describes the time domain analysis and performance of the proposed UWB antenna.

### 5.4.1 Group delay

Group delay is defined as the negative derivative of the signal phase with respect to angular frequency. When a signal passes through a device or medium, it experiences both amplitude and phase distortion. A particular wave incident at the input of a device, it may have several frequency components. The group delay gives a measure of average time delay of input signal at each frequency OR it gives a measure of the dispersive nature of the device. In order to be a good UWB system the group delay must be as small as possible.

The group delay of the developed three UWB antennas as a function of frequency is shown in Fig.5.39. In the proposed antenna measurements the side by side orientation means the orientations are along bore. From the group delays shown, it is evident that all the three antennas offer a group delays less than 0.5 nS which indicate that the dispersion is very less in all the three antennas. The group delay is found to be very smooth for the semicircular UWB antenna and is shown in Fig 5.39 (c). Thus it will show excellent prevention against pulse dispersion.

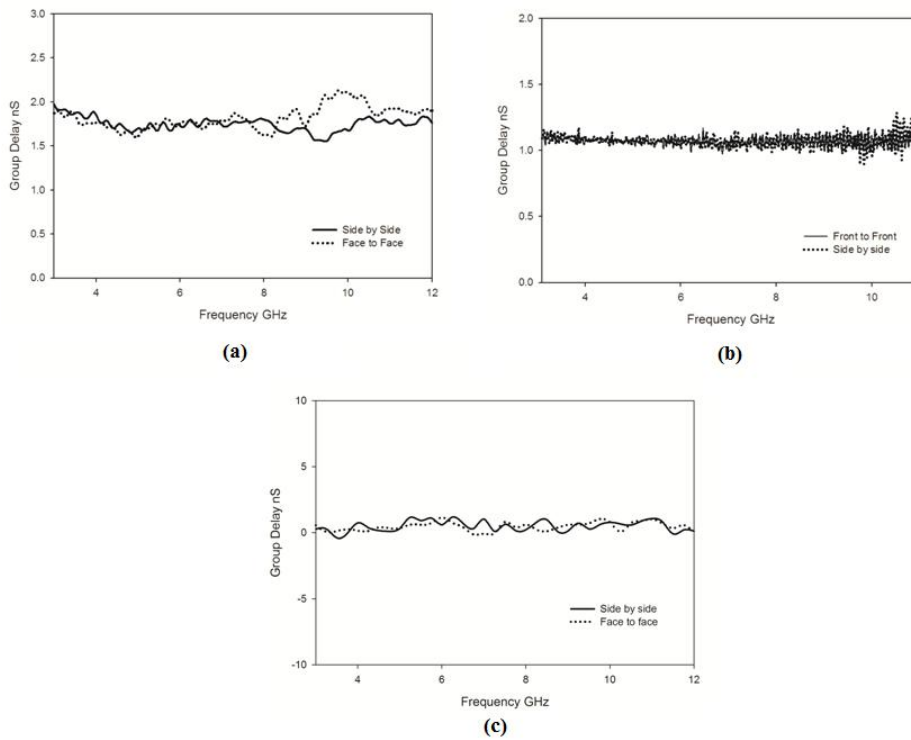


**Fig.5.39.** Group Delay of the of the UWB Antennas (a) V Groove UWB (b) Semicircular cut UWB and (c) Semicircular UWB

### 5.4.2 Transfer functions

Transfer function of an antenna system is the frequency domain transformation of impulse response of the system. In UWB application, to

minimize the potential interferences between the UWB system and the narrowband systems, the variations of the transfer function magnitude and the group delay should be minimum as possible.

The transfer function of the V groove antenna as a function of  $\phi$  and  $\theta$  at the three resonant frequencies are shown in Fig.5.40(1) From the figure it is evident that the maximum of the transfer function occurs at bore sight direction where  $\phi$  and  $\theta$  values equal to  $90^0$ ie at the positive Y direction. It is also clear from the figure that the maximum value of transfer function has almost same value in the first two resonances and at the third resonance it is slightly less. This indicates that there is minimum variation for the transfer function in the range of frequencies formed by the merging of first and second resonances but a slight variation in the third resonant frequency range.

The transfer function of the semicircular slot UWB antenna as a function of  $\phi$  and  $\theta$  at the three resonant frequencies are shown in Fig.5.40.(2). Here also the maximum of the transfer function occurs at bore sight direction where  $\phi$  and  $\theta$  equal to  $90^0$ . It is also clear from the figure that the maximum value of transfer function has almost same value in the second and third resonances and at the first resonance it is slightly enhanced. This indicates that there is minimum variation for the transfer function in the range of frequencies formed by the merging of second and third resonances but a slight enhancement in the first resonant frequency range.

The simulated planar transfer functions of the antenna at the three resonant frequencies are shown in Fig. 5.40. (3). It is evident from the plot that the antenna is highly directive towards the direction with  $\theta=90^0$  and  $\phi=90^0$  with almost same power in that particular direction in all the three resonant

frequencies. This indicates that the semicircular ultra wide band antenna offers a transfer function with minimum variation in the operating band.

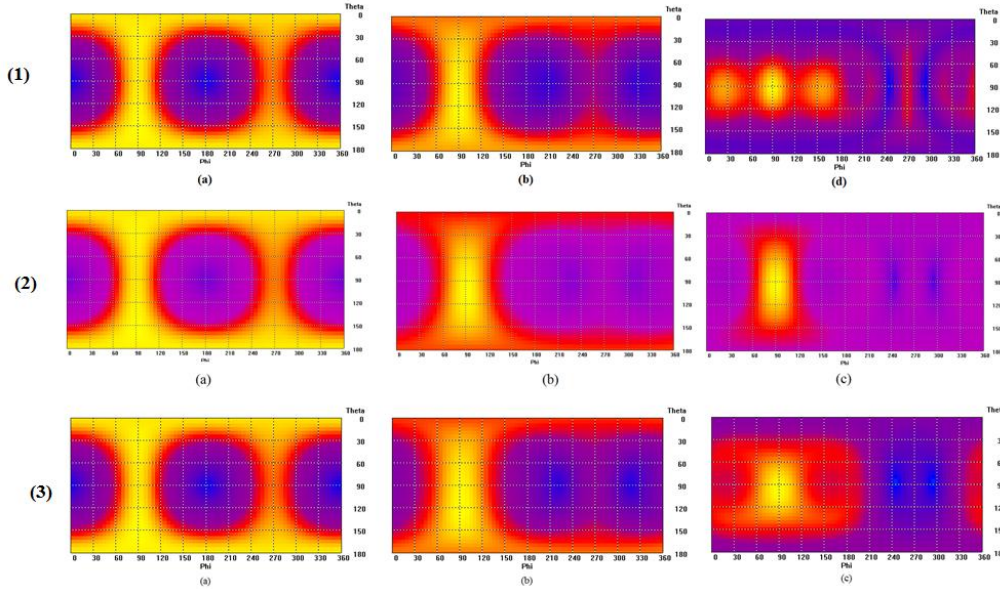


**Fig.5.40.** Simulated Transfer function of the UWB Antennas at three resonances (1) V Groove UWB (2) Semicircular cut UWB and (3) Semicircular UWB in bore sight orientation

From the Fig.5.40, it is already proved that for all the developed antennas, the maximum magnitude of transfer function is occurring at the bore sight direction. Thus it is very necessary to analyze the transfer function in bore sight orientation in the entire frequency band. The measured transfer function all the UWB antennas in beam maxima direction are shown in Fig.5.41. All the transfer functions are characterized with minimum variation in the frequency ranges. The variation is found to be extremely minimum for the semicircular high gain UWB antenna.

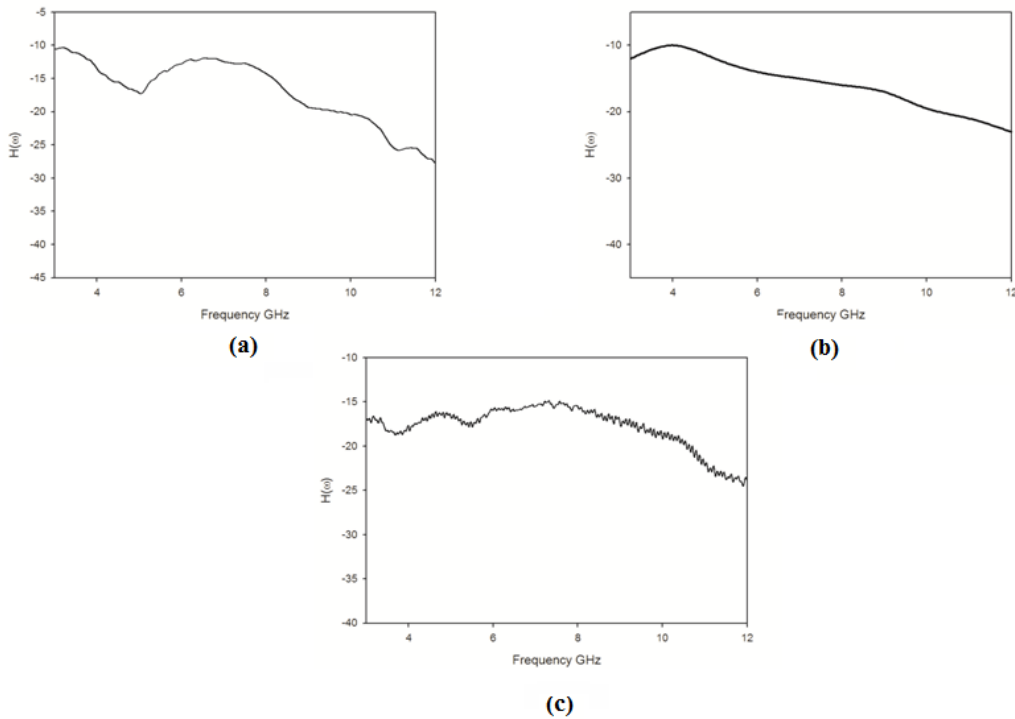


**Fig.5.41.** Transfer Function of the UWB Antennas (a) V Groove UWB (b) Semicircular cut UWB and (c) Semicircular UWB

### 5.4.3 Impulse Responses

Impulse response of an antenna system is defined as the response of the system for the impulse signal as input. It is obtained from the transfer function by performing the inverse Fourier transform of it. Calculated impulse response of the proposed UWB antennas along the bore sight direction orientation is shown in Fig. 5.42. All the figures are showing good impulse response waveforms with minimum ringing. There is a small ringing is present in the first two waveforms around 100 nS from the peak value. This may be due to the edge diffraction of signals from those antennas. The impulse response also shows that the semicircular high gain UWB is the best suited candidate for UWB high data rate applications.

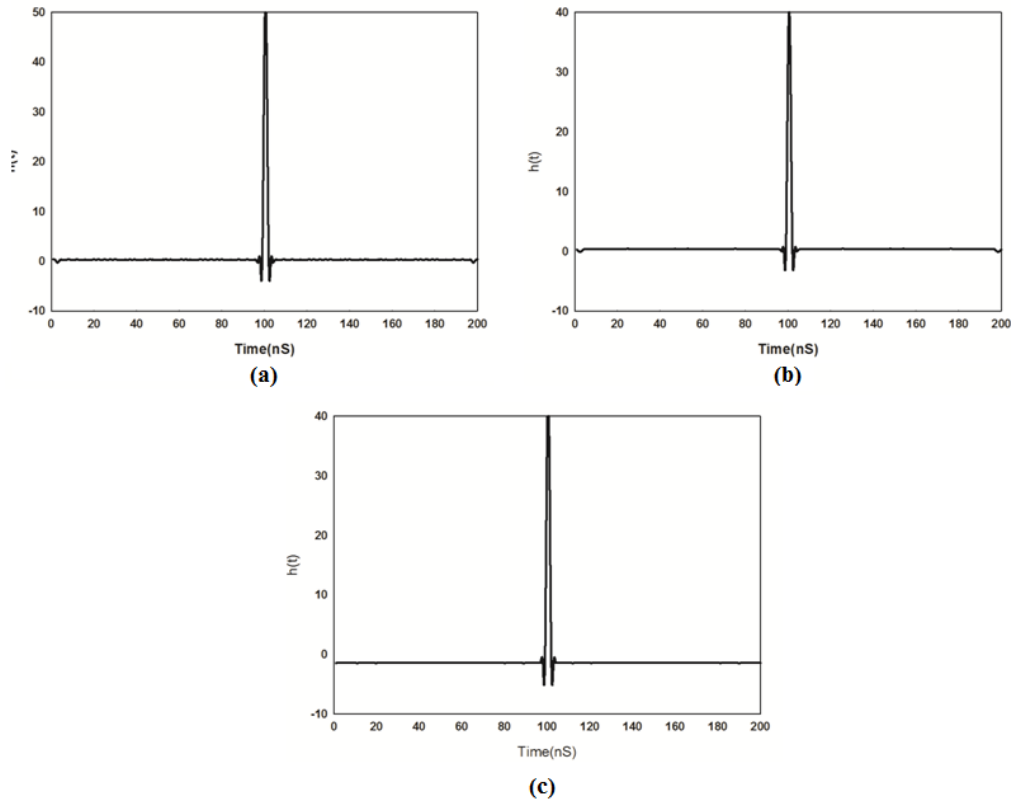


**Fig.5.42.** Impulse Response of the of the UWB Antennas (a) V Groove UWB (b) Semicircular cut UWB and (c) Semicircular UWB

#### 5.4.4 Received signal waveforms

For a UWB system, it is important that the received signal should match the source pulse with minimum distortions because the signal envelope is the carrier of useful information. The received waveform is determined by convoluting both the source pulse and inverse Fourier transform of the system transfer function (impulse response of the system)

Transmitted and received pulses of the pre discussed UWB antennas along the bore sight orientation ie side by side orientation is shown in Fig.5.43. From the figure it is clear that almost all the received waveforms preserve the shape of the transmitted pulse. The amplitude of the received pulse is less than



that of transmitted pulse because of the loss created by the antenna systems and free space loss.

A small amount of ringing is found in both the received pulses given in Fig.5.43. (a) and (b) before the excitation begins. This may be due to the effect of channel noise. However, the pulse shape is preserved in both the received pulses which indicate lossless reception of transmitted data. The ringing is found to be minimum in the case of semicircular UWB antenna and thus from the pulse response analysis also it is evident that the high gain semicircular UWB antenna performance of preserving the signal envelope is very much better than that of other two UWBs.

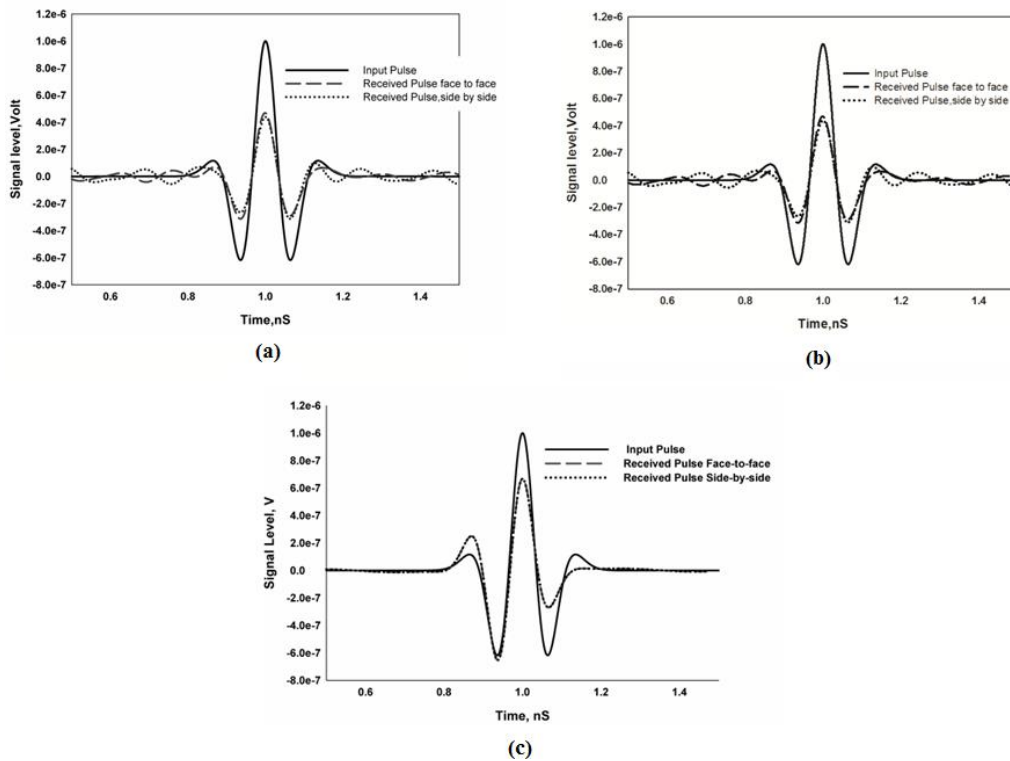


**Fig.5.43.** Pulse Response of the of the UWB Antennas (a) V Groove UWB (b) Semicircular cut UWB and (c) Semicircular UWB

### 5.4.5 Fidelity Factor

Co-relation between the transmitted and received pulses OR fidelity is an important measure of quality of an ultra wideband antenna system. Fidelity factor of the proposed UWB antennas as a function of azimuth angle are shown in Fig.4.44.

Maximum fidelity of the V groove antenna is found to be 94% with almost constant value in all orientation which is given in Fig 5.44. (a). According to Fig 5.44 (b), the semicircular cut antenna offer 95 % maximum fidelity. The fidelity factor of the semi circular high gain UWB antenna has a maximum value of 98%. From the fidelity analysis, it is clear that even though the developed antennas are directional radiators, all of them preserve the shape of the waveform in all the directions.

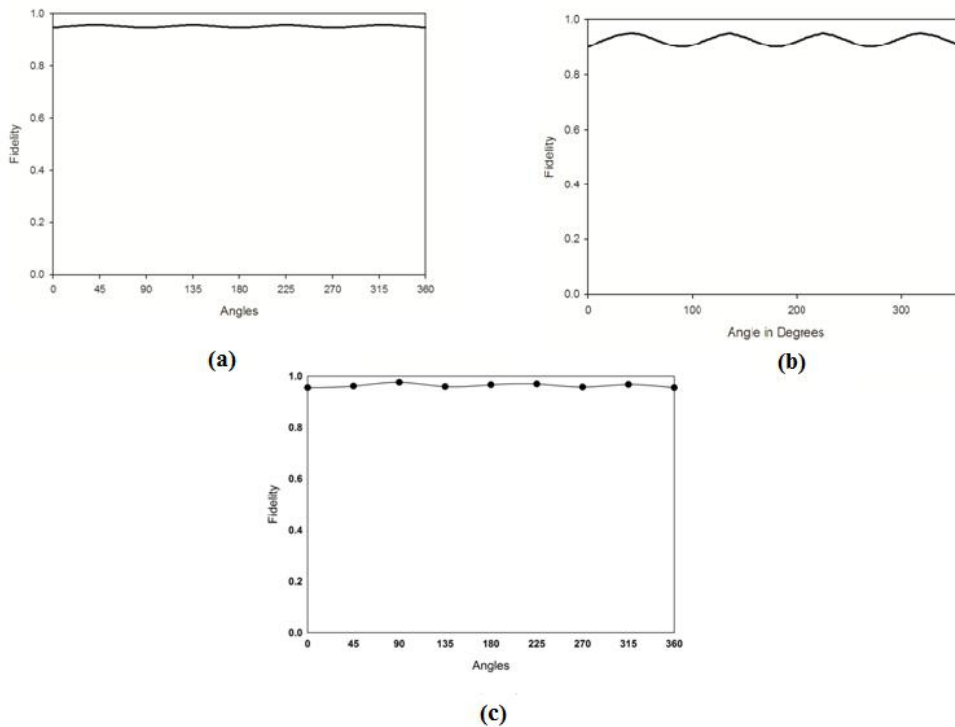


**Fig.5.44.** Fidelity factor of the of the UWB Antennas (a) V Groove UWB (b) Semicircular cut UWB and (c) Semicircular UWB

### 5.4.6 Effective Isotropic Radiated Power

EIRP is the amount of power that would have to be emitted by an isotropic antenna to produce the peak power density of the antenna under test. Measured EIRPs of all the three UWB antennas are shown in Fig.4.45. From the figure it is found that EIRPs of the proposed antennas are within both the indoor and outdoor masks specified by FCC.

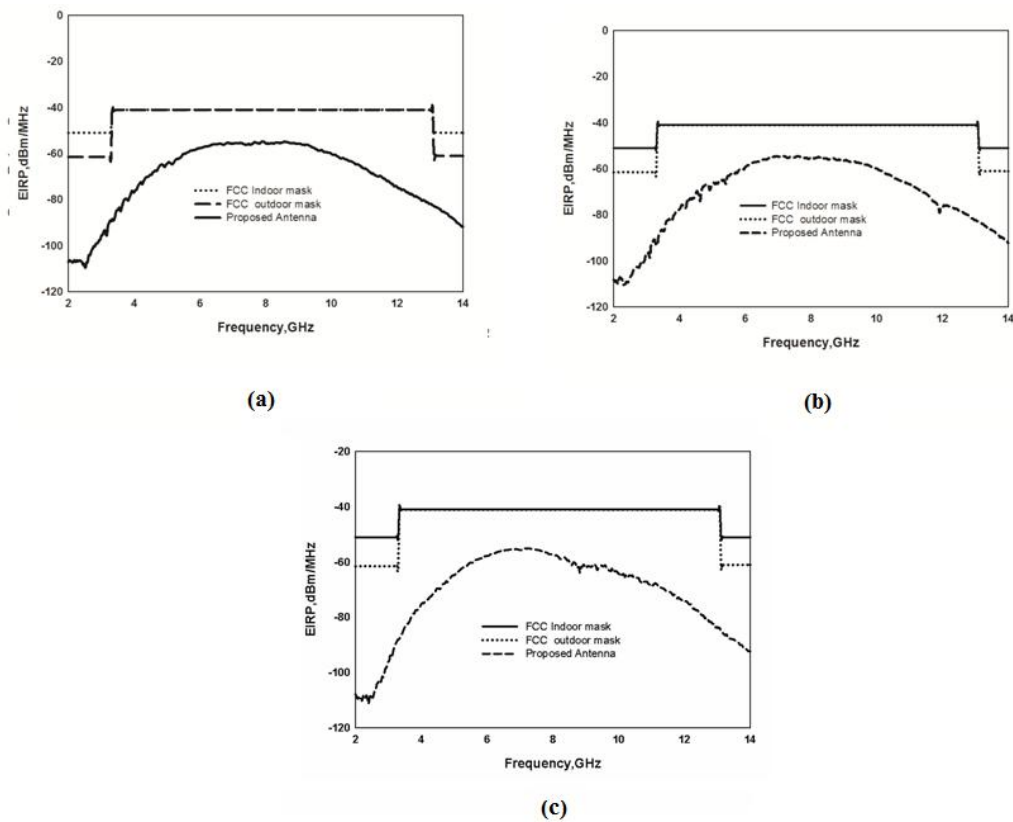


**Fig.5.45.** EIRP of the of the UWB Antennas (a) V Groove UWB (b) Semicircular cut UWB and (c) Semicircular UWB

## 5.5 Chapter Summary

This chapter deals with coplanar strip fed dipole antennas suitable for ultra wideband applications. Mainly two types of UWB antennas are developed

and analyzed thoroughly. All the time domain and frequency domain analysis of the antennas developed are carried out and found that these antennas are very much suitable for compact UWB applications.

The first part of the chapter deals with the design of a coplanar strip fed compact ultra wideband V groove antenna operating from 3.08 GHz to 12GHz. Less number of dimensional parameters, radiation pattern stability, polarization uniformity, flat gain and efficiency etc are the main attractions of this design. The overall dimension of the antenna is only  $10 \times 32 \times 1.6 \text{ mm}^3$  when fabricated on a substrate of dielectric constant 4.4 and thickness 1.6 mm.

The time domain analysis of the antenna is also performed and found that the antenna is very much suitable for pulse transmission applications.

As an extension, the second part of the chapter is devoted for the design and development of an ultra compact coplanar strip fed ultra wideband semi circular cut antenna operating from 3.1 to more than 12GHz with almost similar characteristics of the V Groove antenna. The antenna has simple structure with minimum design parameters. It is very interesting to note that this antenna has only  $10 \times 28.3 \text{ mm}^2$  in size which is the most compact UWB antenna till presented in the literatures.

The third part of the chapter is vectored to the design of a compact coplanar strip fed ultra wideband semi circular antenna with enhanced gain and directive properties which is operating from 3.1 to more than 12GHz. The antenna has simple structure with minimum design parameters. The discussed antenna possesses a directional radiation pattern which makes it suitable for imaging applications. The antenna offers a peak gain of 8.74 dBi in the operating band. The antenna has an overall dimension of  $10.75 \times 30.3 \text{ mm}^2$ .

From the frequency domain analysis of the antennas, it is clear that the antenna appears to be an ideal candidate for the 3.1 to 10.6GHz UWB operation. Since the antenna operates over a multi-octave bandwidth, it would be excellent to transmit pulses of the order of nanosecond duration with minimal distortion. The directional gain of the semi circular antenna is found to be very high and found tremendous attraction in communication and imaging applications.

The time domain performance of these antennas for validating their suitability for pulsed applications is also carried out at the end of the chapter. From these studies also it is clear that the proposed design is very much suitable for UWB communication and imaging purposes.

## **References**

- [1] Y. Yang, Y. Wang, and A. E. Fathy "Design of Compact Vivaldi Antenna Arrays for UWB see Through Wall Applications" Progress In Electromagnetics Research, PIER 82, 401-418,2008.



## CONCLUSION AND FUTURE PERSPECTIVE



*This chapter brings up the total outcome of the research carried out by the author and highlights the achievements of the research work. This is followed by few suggestions for future work. The results presented in the thesis have been published by the author in different international journals.*

### 6.1 Thesis Summary and Conclusions

The aim of this study is to develop compact coplanar strip fed planar antennas in different category. Six different types of coplanar strip fed antennas are mainly developed during the research. They are Coplanar Strip Fed Dual-Band Antenna operating at 2.4/5.2 GHz WLAN bands, Enhanced Gain Dipole Antenna operating at 5.2/5.8 GHz bands, Wideband Directive Dipole Antenna, V groove Dipole for UWB applications, Ultra compact semicircular slot Dipole for UWB applications and compact coplanar strip fed semi circular UWB antenna. The different parameters and characteristics of the antenna are analyzed thoroughly during the study.

The first part of the study of the antenna is parametric analysis ie all the dimensional parameters of the antenna are varied and the corresponding

variation in reflection coefficient is analyzed. From these analysis the critical dimensional parameters affecting the resonance, impedance match, band width, gain etc are identified. The design equations for various antenna structures are also developed with the help of the results of the parametric study. The parametric analysis is carried out using simulation software.

Next step in antenna study includes the experimental development of the antenna structure and practical studies. The antenna structure is fabricated through photolithography and chemical etching. Then various characteristics such as reflection coefficient, radiation pattern, directive gain, radiation efficiency, transfer function, group delay etc are measured using network analyzer. In case of ultra wide band antenna time domain transformations are performed on these measured results to analyze the time domain characteristics of the antenna such as impulse response, pulse response, fidelity, EIRP etc.

To explain the reason for resonance, the surface current distribution is also analyzed. This is performed with the help of surface current patterns given by simulation software. From the pattern we can identify the resonant current path which creates the resonance in antenna. This can also provide the reason for High/Low/Medium value of efficiency etc.

The newly developed antennas during the research are

### **1. Coplanar Strip fed Dual band antenna for 2.4/5.2 GHz WLAN applications**

A printed compact CPS fed dual band coplanar dipole antenna having a dimension of  $0.39\lambda_g \times 0.20\lambda_g$  suitable for both 2.4 and 5.2 GHz (IEEE 802.11 b/g and 802.11a) WLAN application is developed. The structure comprises of a slot line fed symmetrical L strips to achieve dual band operation. Design equations of the antenna are developed and validated on different substrates.



The simulation and experimental results show that the proposed antenna exhibits good impedance match, gain and stable radiation patterns in both the frequency bands.

## **2. Coplanar Strip fed High gain Directive dipole for 5.2/5.8 GHz applications**

A high-efficiency and high gain CPS fed directive dipole antenna is developed for 5.2GHz and 5.8 GHz microwave applications. The antenna offers an average gain of 7.9 dBi with a front to back ratio better than 20 dB and a cross polar level better than -20 dB. Design equations of the antenna are developed and validated on different substrates. The simulation and experimental results show that the proposed antenna exhibits high gain and stable radiation patterns in the entire frequency band. A wide band version of the antenna is also developed and analyzed during the study.

## **3. Coplanar Strip fed Directive dipole for Wideband Applications**

A wideband directive dipole antenna with an operating band of 3.8 GHz to 10.2 GHz is developed and analyzed. The ultra compact antenna developed has a very good directive radiation pattern in the entire operating band with a uniform directive gain of 6 dBi. Design equations for the antenna are also developed and are validated for different substrates. From the measured and simulated results it is evident that the proposed ultra compact antenna is a potential candidate for directive wide band applications with good efficiency.

## **4. Coplanar Strip fed V Groove Dipole for UWB applications**

CPS fed dipole antenna with a V Groove suitable for UWB application is developed. The antenna offers a 2:1 VSWR bandwidth starting from 3.1 GHz to 12 GHz which is wide enough to cover the FCC specified UWB applications. This antenna offers an average gain of 5 dBi in the entire

frequency band. From the simulation and experimental studies it is clear that the proposed antenna exhibits moderate gain and stable radiation patterns in the entire frequency band. The time domain analysis of the antenna is also performed and from these results it is found that the proposed antenna is very much suited for the UWB high data rate communication applications.

### **5. Coplanar Strip fed Ultra compact Semicircular slot Dipole for UWB applications**

CPS fed dipole antenna with a semicircular slot suitable for UWB application is developed. The developed antenna is very compact and offers a 2:1 VSWR bandwidth starting from 2.92 GHz to 11.34 GHz which is wide enough to cover the FCC specified UWB frequency spectrum. This antenna offers an average gain of 5.1 dBi in the entire frequency band with greater than 90% radiation efficiency. From the simulation and experimental studies it is clear that the proposed antenna exhibits moderate gain and stable radiation patterns in the entire frequency band which ensure that the antenna a potential candidate for UWB applications. The time domain analysis of the antenna is also performed and from these results it is found that the proposed antenna is very much suited for the UWB high data rate communication applications.

### **6. Coplanar Strip fed Enhanced Gain Semicircular Dipole for UWB applications**

A high gain CPS fed semicircular directive dipole antenna suitable for UWB application is developed. The antenna offers a 2:1 VSWR bandwidth greater than 10 GHz starting from 3.1 GHz. This antenna offers an average gain of 8 dBi in the entire frequency band. The simulation and experimental results show that the proposed antenna exhibits high gain and stable directive radiation patterns in the entire frequency band. The time domain analysis of the antenna is also performed

and from these results it is found that the proposed antenna is suitable for the UWB high data rate communication and imaging applications.

## **6.2 Suggestions for future work**

The following are some of the prospects for future work:

The antennas can be designed and developed on low temperature co-fired ceramic (LTCC) substrates which have the advantage of direct integration with monolithic microwave circuits.

The antennas can be designed and developed on flexible and transparent substrates for using it on various networks such as BANs etc.

The SAR measurements of these antennas are not performed and as a future work, SAR measurements and impact of the energy radiated from these structures on human body can also be investigated.

Further investigations to develop Ultra compact antennas and wearable antennas can be performed as a future work.

Performance of an antenna array using these antennas as unit cells is not performed. I hope this will be a good study and can improve the range and quality of communication.

Antenna integration with a low noise amplifier (LNA) is also a good future work since it improves the quality of communication.

All the studies of this thesis are on open ended slotline based antennas. It will be very interesting that a series of study about the shorted ended slotline (SES) based antennas and coplanar strip fed slot antennas.

Band notched version of the UWBs are not incorporated in this thesis. As a future work one can perform the analysis on band notched UWB antennas also.

All the results presented in the thesis are measured in noise free atmosphere. Issues on practical implementation of the antenna are not considered. It will be a good study of the antenna when all these analyses are performed in practical implementation situations.

## EXTRACTION OF DISTRIBUTED RLC PARAMETERS.

*The thesis deals with the values of distributed components which are responsible for the resonance and their analysis for obtaining a clear technical knowhow of the mechanism for resonance in Chapter 3 and 4. The extraction of these distributed capacitance, inductance and resistance are discussed in this section.*

### 1.1 Introduction

The antenna is considered as a resonant circuit with its own resonant frequency and band width. From the literatures it can be seen that, antennas can be approximated to series RLC networks [1] with a specific resonant frequency and Q factor. The circuit of an antenna is shown in Fig.App1.1

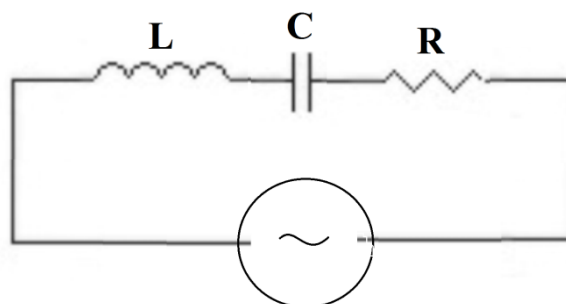


**Fig.App1.1.** Equivalent Circuit of an Antenna.

The circuit consists of a resistance, capacitance and inductance connected in series with an alternating, frequency variable voltage source. At zero frequency ie DC condition, the steady state current through the circuit is zero. As the frequency increases, the current flows through the circuit. As the frequency increases and approaches a particular value, the reactance of the capacitance and inductance become complex conjugates. At that point of frequency, the reactance will cancel each other and the remaining impedance is only due to the resistance R of the circuit. At this time, maximum current will flow through the circuit and that condition is known as Resonance. For all the frequencies below resonance, the capacitive reactance ( $\frac{1}{C\omega}$ ) is greater than that of inductance ( $L\omega$ ) and the impedance ( $Z = \sqrt{R^2 + (L\omega - \frac{1}{C\omega})^2}$ ) will be more than resistance. Similarly for all the frequencies greater than resonant frequency, the inductive reactance is greater than that of capacitance. Then also the impedance is more than R. Thus as the exiting frequency of the circuit deviate from resonant frequency towards both sides, the impedance increases and thus the current reduces.

The range of frequencies for which the current is greater than or equal to 70.70 % of maximum value is known as band width of the circuit. For these range of frequencies, the power in the circuit will be more than or equal to half of the maximum power.

The Q factor of a circuit is defined as the ratio of energy stored per cycle to average energy dissipated per cycle. It is also known as selectivity; the ability of the circuit to pick a single frequency from a range of frequencies. Thus as the bandwidth increases, the selectivity become poor and vice versa. The Q factor of a circuit can be obtained from the ratio of resonant frequency and bandwidth [2].

The resonant frequency is a function of the capacitance and inductance present in that circuit while the Q factor/Bandwidth is a function of all the three components. Thus by doing some simple mathematical calculations, we can extract the circuit parameters of the antenna from their resonant frequency and bandwidth. These values of circuit parameters can be used to explain the resonance mechanism. These techniques are explained in the following session.

## **1.2 Extraction of circuit components**

This session explains how the distributed components corresponding to the resonant frequency are extracted from the reflection coefficient of the antenna. From the reflection coefficient, we can retrieve the resonant frequency and bandwidth of the antenna. Using these values and the well known equations of resonance, we can find out the value of inductance, capacitance and resistance. The algorithms included in the extraction of parameters of the circuit with necessary explanations are given below.

- **Step1:** Calculate the Bandwidth **BW** and the resonant frequency **F<sub>r</sub>** from reflection coefficient
- **Step2:** Calculate the resistance R of the circuit at resonance by solving the equation  $\frac{R-Z_0}{R+Z_0} = 10^{(S_{11}/20)}$ ; where the return loss is measured at resonant frequency and  $Z_0=50 \Omega$  is the characteristic impedance of the transmission line used to guide the energy into antenna. At resonance the circuit only offers Resistance; the reactance will cancel each other.
- **Step3:** Calculate Q by the relation  $Q = \frac{F_r}{BW}$ .
- **Step4:** Calculate capacitance L by the formula  $L = \frac{RQ}{2\pi F_r}$

- **Step5:** Calculate inductance C by the formula  $C = \frac{1}{2\pi QRf_r}$

Step 4 and 5 are derived from the equation of Q factor given by  $Q = \frac{1}{R} \sqrt{\frac{L}{C}} = \frac{1}{C\omega R} = L\omega R$ . These conditions also satisfy the well-known equation of resonance given by  $f_r = \frac{1}{2\pi\sqrt{LC}}$ .

### 1.3 Circuit components as a function of Dimensional parameters

As explained in the previous step, it is possible to extract the distributed parameters from the  $S_{11}$  curve. From this idea it is also possible to develop the equations for calculating the values of distributed components from the dimensional parameters itself.

- **Step1:** Perform the component extraction explained in previous session (1.2 of Appendix-I) for all the dimensional variation and plot the curve between dimensional parameter versus distributed parameters.
- **Step2:** Analyze all the graphs obtained and by curve fitting those, it is possible to obtain a relation between distributed components and each of the dimensional factors.
- **Step3:** Combining all the relation that obtained from step-2, calculate the offset value (Constant).
- **Step4:** Generalize the relation obtained after step-3 for all substrate by incorporating effective dielectric constant.

### 1.4 Extraction of circuit components of single band dipole

The extraction of single bands dipole antenna discussed in Chapter 3 of the thesis and the development of relation between dimensional factors and



distributed parameters are explained in this session. The calculations are performed by the guidelines explained in session 1.2 and 1.3 of this appendix.

The structure of the single band antenna is shown in Fig. App1.2. Antenna has only four number of dimensional parameters namely  $L_1$ ,  $W_1$ ,  $L_2$  and  $W_2$ .

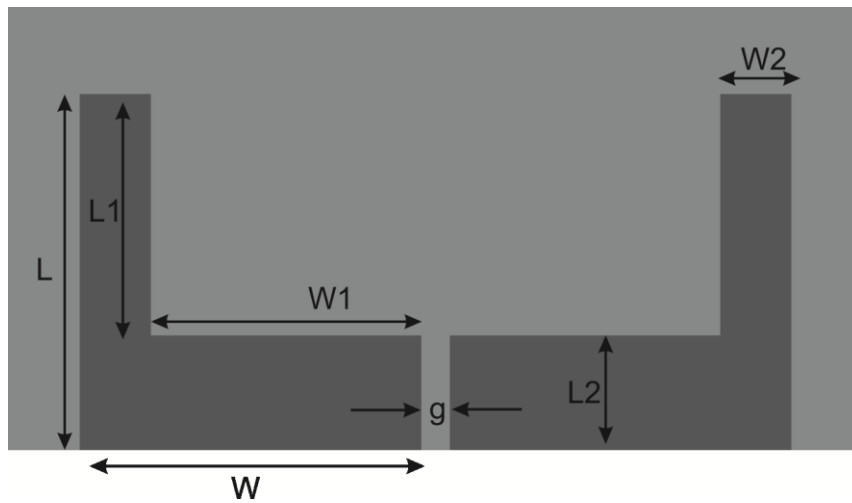


**Fig.App1.2.** Structure of single band Antenna

The variations of reflection co-efficient of the antenna with all these dimensional factors are shown in Fig. App1.3. The variation of reflection co efficient of the antenna with parameter  $L_1$  is shown in the Fig.App1.3.(a). The resonant frequency of the antenna shows a lower shift with parameter  $L_1$ . The variation of reflection co efficient with  $W_1$  is shown in Fig.App1.3.(b). Here also the resonant frequency shows a lower shift with  $W_1$ . Interpretation of variation in  $S_{11}$  curve of the antenna with  $L_2$  is shown in Fig.App1.3.(c). The resonant frequency is found to be abnormally increasing with increase in  $L_2$ . Reason for this up shift is explained in session3.3.1 of Chapter.3. The variation in return loss of the antenna with  $W_2$  is shown in Fig.App1.3.(d). From the figure it is clear that the resonant frequency shift to lower side with  $W_2$ .

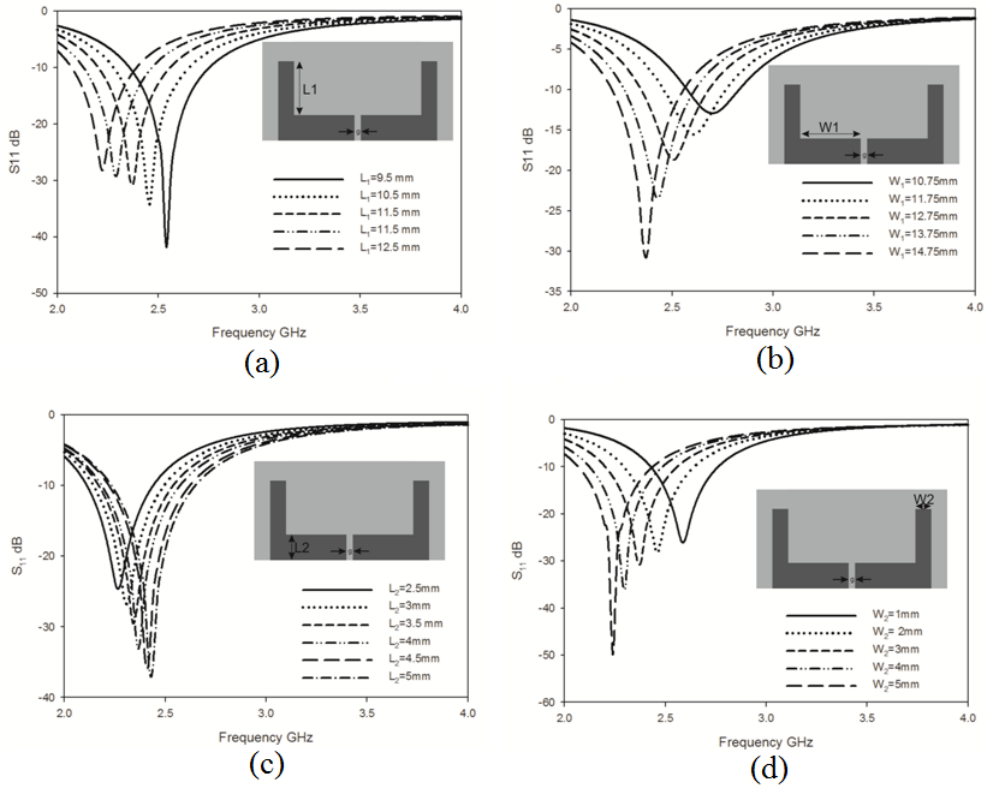


**Fig.App1.3.** Parametric analysis of single band Antenna

The variation of distributed capacitance and inductance corresponding to the each of the dimensional parameters are shown in Fig.App.1.4. The variation in distributed capacitance and inductance of the antenna with  $L_1$  is shown in Fig.App.1.4 (a). Both the reactive components shows an increases with increase in  $L_1$ . As a result the resonant frequency will comes to lower side without affecting the percentage bandwidth considerably. The variation in inductance and capacitance of the antenna with the parameter  $W_1$  is shown in Fig.App.1.4 (b). From the figure it is clear that the capacitance decreases with  $W_1$  while the inductance increases with it. As a result, the resonant frequency will comes lower side with an increase in percentage bandwidth. The changes in distributed

components with parameter  $L_2$  is shown in Fig.App.1.4(c). Both the parameters tend to lower with  $L_2$ . This will results in an increase in resonant frequency without creating vast changes in the bandwidth. Since the change inductance and capacitance is very feeble, the change in frequency will be very low. The variation in distributed parameters with  $W_2$  is shown in Fig.App.1.4(d). From the figure it is clear that as  $W_2$  increases, the capacitance increases while the inductance decreases. This will results in a lower shift in resonant frequency with a decrease in percentage bandwidth. The selectivity will also increases with  $W_2$ .

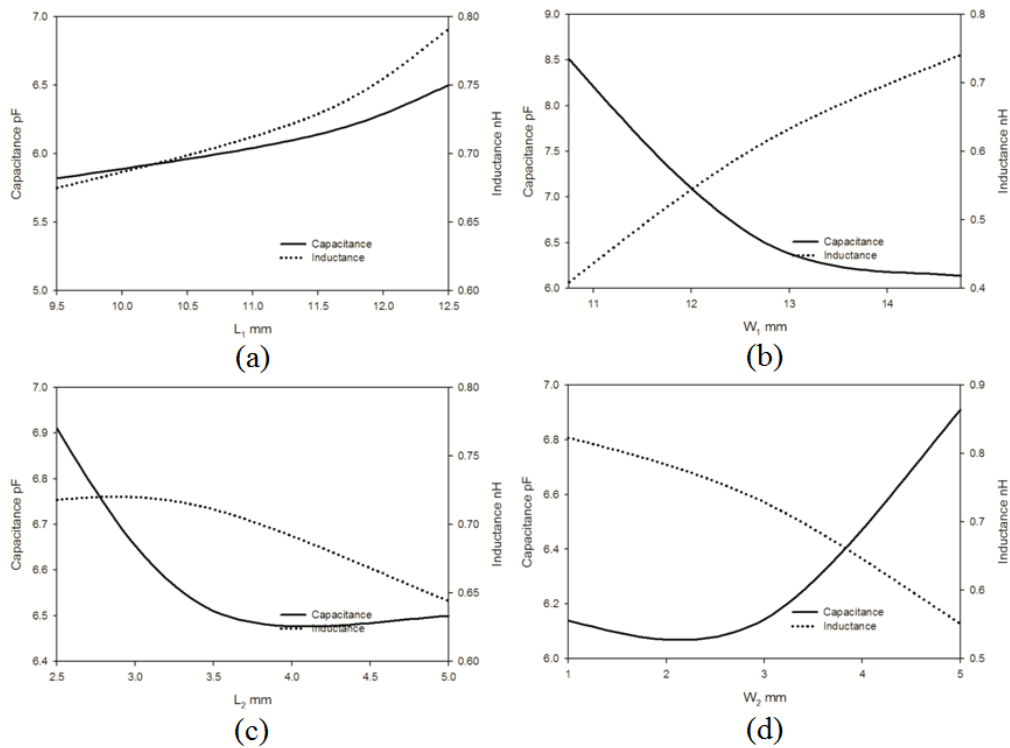


Fig.App1.4. Parametric analysis of single band Antenna.

## 1.5 General expression for capacitance and inductance in terms of dimension

By curve fitting these graphs, the relation between capacitance and inductance in terms of  $L_1$ ,  $W_1$ ,  $L_2$ ,  $W_2$  are obtained as shown below.

Capacitance and inductance in terms of  $L_1$

$$C_{L1} = 11.5833 + L_1(-1.24 + 0.0667L_1)$$

$$L_{L1} = 1.6931 + L_1(-0.218 + 0.0116L_1)$$

Capacitance and inductance in terms of  $W_1$

$$C_{W1} = 47.5829 + W_1(-5.85 + 0.2063W_1)$$

$$L_{W1} = -2.0213 + W_1(0.3304 - 0.0097W_1)$$

Capacitance and inductance in terms of  $L_2$

$$C_{L2} = 6.7251 + \frac{1}{L_2} \left( -0.199 - \frac{10.9163}{L_2} + \frac{31.4243}{L_2^2} \right)$$

$$L_{L2} = 0.6037 + L_2(0.0834 - 0.0151L_2)$$

Capacitance and inductance in terms of  $W_2$

$$C_{W2} = 7.58 + W_2(-0.7655 + 0.0955W_2)$$

$$L_{W2} = 0.431 + W_2(0.1304 - 0.0104W_2)$$

All these equations are combined together to get the expression for the capacitance and inductance in terms of all the dimensions.

$$C = 54.640 + L_1(-1.24 + 0.0667L_1) + W_1(-5.85 + 0.2063W_1) + W_2(-0.7655 + 0.0955W_2) + \frac{1}{L_2} \left( -0.199 - \frac{10.9163}{L_2} + \frac{31.4243}{L_2^2} \right)$$

$$\begin{aligned}
 L &= -1.3036 + L_1(-0.218 + 0.0116L_1) \\
 &+ W_1(0.3304 - 0.0097W_1) \\
 &+ L_2(0.0834 - 0.0151L_2) + W_2(0.1304 - 0.0104W_2)
 \end{aligned}$$

The next step included in the generalization of these equations for different substrates with different dielectric constants. This is done by converting all the dimensional parameters in terms of guided wavelength. The generalized expressions by incorporating effective dielectric constant in the above expression are as follows.

$$\begin{aligned}
 C &= 20.271266 + 0.379\sqrt{\epsilon_{eff}}(L_1(-1.24 + 0.0667\sqrt{\epsilon_{eff}}L_1) \\
 &+ W_1(-5.85 + 0.2063\sqrt{\epsilon_{eff}}W_1) \\
 &+ W_2(-0.7655 + 0.0955\sqrt{\epsilon_{eff}}W_2)) + \frac{1}{L_2\sqrt{\epsilon_{eff}}}(-0.199 \\
 &- \frac{10.9163}{L_2\sqrt{\epsilon_{eff}}} + \frac{31.4243}{L_2^2\epsilon_{eff}}
 \end{aligned}$$

$$\begin{aligned}
 L &= -0.4735 + 0.364\sqrt{\epsilon_{eff}}(L_1(-0.218 + 0.0116\sqrt{\epsilon_{eff}}L_1) \\
 &+ W_1(0.3304 - 0.0097\sqrt{\epsilon_{eff}}W_1) \\
 &+ L_2(0.0834 \pm 0.0151\sqrt{\epsilon_{eff}}L_2) \\
 &+ W_2(0.1304 - 0.0104\sqrt{\epsilon_{eff}}W_2))
 \end{aligned}$$

To validate these expressions, we have to select different dimensions in different substrates. The dimensional parameters of different antennas in different substrates, their calculated distributed capacitances and inductances, calculated resonant frequencies and bandwidth etc are given in Table. App.1. Obtained bandwidth and resonant frequency from HFSS simulation are also included in the table for comparison.

**Table. App1.1.** Validation of developed expressions of single band antenna

$\epsilon_r$	$L_1$	$W_1$	$L_2$	$W_2$	C Pf	L nH	$F_c$ (GHz)		BW (MHz)	
							Calculated	HFSS	Calculated	HFSS
2.2	14.9	15.25	4.55	3.9	6.092581	0.725759	2.39	2.4	435	457
4.4	11.5	11.75	3.5	3	6.130001	0.729623	2.38	2.38	430	460
6.15	10	10.21	3.04	2.6	6.150069	0.731342	2.37	2.38	431	455
10.2	7.95	8.15	2.43	2.1	6.075814	0.723608	2.40	2.42	436	442

From the table it is evident that both the calculated and simulated antenna parameters matches very well.

## References

- [3] Constantine A Balanis "Antenna theory analysis and design" John Wiley and Sons II<sup>nd</sup> edition
- [4] A Sudhakar "Circuits and networks analysis and synthesis" Tata McGraw Hill II<sup>nd</sup> edition



*The theoretical analysis of the antennas discussed in chapter 3 and 4 are done using Finite Difference Time Domain method. Absorbing Boundary Condition based FDTD analysis is briefly discussed in this part of the thesis.*

## **1. Introduction**

Finite Difference Time Domain (FDTD) method which is proposed by Yee in 1966 [1] is widely used in many areas of science and technology. FDTD is techniques that will discrete the computational domain in to both time and space, and gives us the time and frequency domain information of the electromagnetic problem of interest. FDTD provides a direct solution of time dependant Maxwell's equation for electric and magnetic field intensities in a finite, piecewise homogenous media. Due to the lack of analytical preprocessing and modeling, FDTD is a potential tool for planar antenna problems. Moreover, this analysis approach can be used to include the effect of finite ground plane and substrate parameters which is very important in the present investigation. Specifically, certain characteristic strengths of FDTD attract the investigators to apply this algorithm in the antenna design and analysis. The features of FDTD are

1. It is a direct implementation of Maxwell's curl equations. Therefore, analytical processing of Maxwell's equations is almost negligible.
2. Can model complex geometries and feed and other structures and any type of materials of importance to electromagnetic technology, including conductors, dielectrics, dispersive and non linear medium.
3. It is able to excite the antenna using narrow pulse which results in broadband calculations.
4. FDTD is accurate and the availability of time domain and frequency domain data leads to a deep physical insight to the radiation mechanism.

## 2. Discretization in FDTD

Yee divided the computation domain into time and space grids. A complete FDTD Yee cell is shown in Fig.App2.1. In the figure both the Electric and magnetic field vectors are shown in such a way that the E field vectors are lying along the midpoints of the edges and the H field along the center of face of the Yee cell.

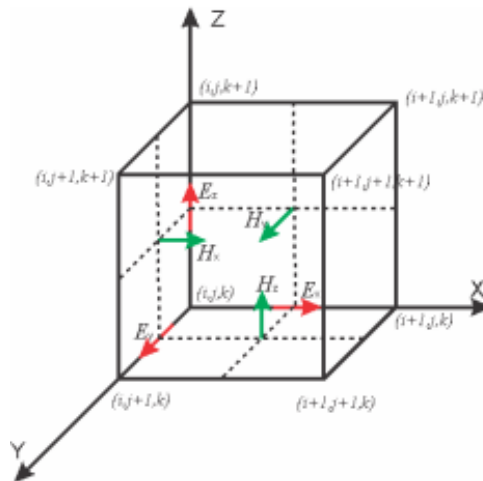


**Fig.App2.1.** Basic Yee Cell



The grid coordinates  $(i, j, k)$  are defined as

$$(i, j, k) = (i\Delta x, j\Delta y, k\Delta z)$$

where  $\Delta x, \Delta y, \Delta z$  are the grid separations.

Any function ‘F’ of space and time is written in terms of grid separation and time steps as

$$F^n(i, j, k) = F(i\Delta x, j\Delta y, k\Delta z, n\Delta t)$$

where  $\Delta t$  is the time increment,  $n$  is the time index.

The spatial and temporal derivatives of  $F^n(i, j, k)$  are written using central finite difference approximations as follows.

$$\frac{\partial F^n(i, j, k)}{\partial x} = \frac{F^n(i + 1/2, j, k) - F^n(i - 1/2, j, k)}{\Delta x}$$
$$\frac{\partial F^n(i, j, k)}{\partial t} = \frac{F^{n+1/2}(i, j, k) - F^{n-1/2}(i, j, k)}{\Delta t}$$

The starting point of the FDTD algorithm is the differential form of Maxwell's curl equations. For an isotropic medium it can be written as follows.

$$\nabla \times E = -\mu \frac{\partial H}{\partial t}$$
$$\nabla \times H = \sigma E + \epsilon \frac{\partial E}{\partial t}$$

In Cartesian coordinates the curl equations can be written as

$$\frac{\partial H_x}{\partial t} = \frac{1}{\mu} \left( \frac{\partial E_y}{\partial z} - \frac{\partial E_z}{\partial y} \right)$$
$$\frac{\partial H_y}{\partial t} = \frac{1}{\mu} \left( \frac{\partial E_z}{\partial x} - \frac{\partial E_x}{\partial z} \right)$$

$$\begin{aligned}\frac{\partial H_z}{\partial t} &= \frac{1}{\mu} \left( \frac{\partial E_x}{\partial y} - \frac{\partial E_y}{\partial x} \right) \\ \frac{\partial E_x}{\partial t} &= \frac{1}{\epsilon} \left( \frac{\partial E_z}{\partial y} - \frac{\partial E_y}{\partial z} - \sigma E_x \right) \\ \frac{\partial E_y}{\partial t} &= \frac{1}{\epsilon} \left( \frac{\partial E_x}{\partial z} - \frac{\partial E_z}{\partial x} - \sigma E_y \right) \\ \frac{\partial E_z}{\partial t} &= \frac{1}{\epsilon} \left( \frac{\partial E_y}{\partial x} - \frac{\partial E_x}{\partial y} - \sigma E_z \right)\end{aligned}$$

Above written six relations can converted into finite difference equations and are given below.

$$\begin{aligned}H_x^{n+1/2}(i, j + 1/2, k + 1/2) &= H_x^{n-1/2}(i, j + 1/2, k + 1/2) \\ &+ \left( \frac{\Delta t}{\mu \Delta z} \right) \left( E_y^n(i, j + 1/2, k + 1) - E_y^n(i, j + 1/2, k) \right) \\ &- \left( \frac{\Delta t}{\mu \Delta y} \right) \left( E_z^n(i, j + 1, k + 1/2) - E_z^n(i, j, k + 1/2) \right)\end{aligned}$$

$$\begin{aligned}H_y^{n+1/2}(i + 1/2, j, k + 1/2) &= H_y^{n-1/2}(i + 1/2, j, k + 1/2) \\ &+ \left( \frac{\Delta t}{\mu \Delta x} \right) \left( E_z^n(i + 1, j, k + 1/2) - E_z^n(i, j, k + 1/2) \right) \\ &- \left( \frac{\Delta t}{\mu \Delta z} \right) \left( E_x^n(i + 1/2, j, k + 1) - E_x^n(i + 1/2, j, k) \right)\end{aligned}$$

$$\begin{aligned}
 H_z^{n+1/2}(i+1/2, j+1/2, k) & \\
 &= H_z^{n-1/2}(i+1/2, j+1/2, k) \\
 &+ \left(\frac{\Delta t}{\mu\Delta y}\right) (E_x^n(i+1/2, j+1, k) - E_x^n(i+1/2, j, k)) \\
 &- \left(\frac{\Delta t}{\mu\Delta x}\right) (E_y^n(i+1, j+1/2, k) - E_y^n(i, j+1/2, k))
 \end{aligned}$$

$$\begin{aligned}
 E_x^{n+1}(i+1/2, j, k) & \\
 &= E_x^n(i+1/2, j, k) \\
 &+ \left(\frac{\Delta t}{\epsilon\Delta y}\right) (H_z^{n+1/2}(i+1/2, j+1/2, k) \\
 &- H_z^{n+1/2}(i+1/2, j-1/2, k)) \\
 &- \left(\frac{\Delta t}{\epsilon\Delta z}\right) (H_y^{n+1/2}(i+1/2, j, k+1/2) \\
 &- H_y^{n+1/2}(i+1/2, j, k-1/2))
 \end{aligned}$$

$$\begin{aligned}
 E_y^{n+1}(i, j+1/2, k) & \\
 &= E_y^n(i, j+1/2, k) \\
 &+ \left(\frac{\Delta t}{\epsilon\Delta z}\right) (H_x^{n+1/2}(i, j+1/2, k+1/2) \\
 &- H_x^{n+1/2}(i, j+1/2, k-1/2)) \\
 &- \left(\frac{\Delta t}{\epsilon\Delta x}\right) (H_z^{n+1/2}(i+1/2, j+1/2, k) \\
 &- H_z^{n+1/2}(i-1/2, j+1/2, k))
 \end{aligned}$$

$$\begin{aligned}
E_z^{n+1}(i, j, k + 1/2) &= E_z^n(i, j, k + 1/2) \\
&+ \left(\frac{\Delta t}{\epsilon \Delta x}\right) \left(H_y^{n+1/2}(i + 1/2, j, k + 1/2) \right. \\
&- H_y^{n+1/2}(i - 1/2, j, k + 1/2)) \\
&- \left(\frac{\Delta t}{\epsilon \Delta y}\right) \left(H_x^{n+1/2}(i, j + 1/2, k + 1/2) \right. \\
&- H_x^{n+1/2}(i, j - 1/2, k + 1/2))
\end{aligned}$$

H and E are evaluated at alternate half time steps using the above stated equations in such a way that all field components are calculated in each time step  $\Delta t$ . The updated new value of a field component at any layer thus depends upon its value in the previous step and the previous value of the components of the other field at the adjacent spatial points. Table.1. indicates the spatial and time relation of the E and H nodes in the Yee lattice.

		<b>X</b>	<b>Y</b>	<b>Z</b>	<b>t</b>
<b>E Node</b>	$E_x$	$i+1/2$	$j$	$k$	$n$
	$E_y$	$i$	$J+1/2$	$k$	$n$
	$E_z$	$i$	$j$	$k+1/2$	$n$
<b>H Node</b>	$H_x$	$i$	$J+1/2$	$k+1/2$	$n \pm 1/2$
	$H_y$	$i+1/2$	$j$	$k+1/2$	$n \pm 1/2$
	$H_z$	$i+1/2$	$J+1/2$	$k$	$n \pm 1/2$

The discretization in space and time and the leap-frog time integration employed in the FDTD method proposed by Yee is shown in Fig.App2. 2 and Fig.App2.3 respectively.

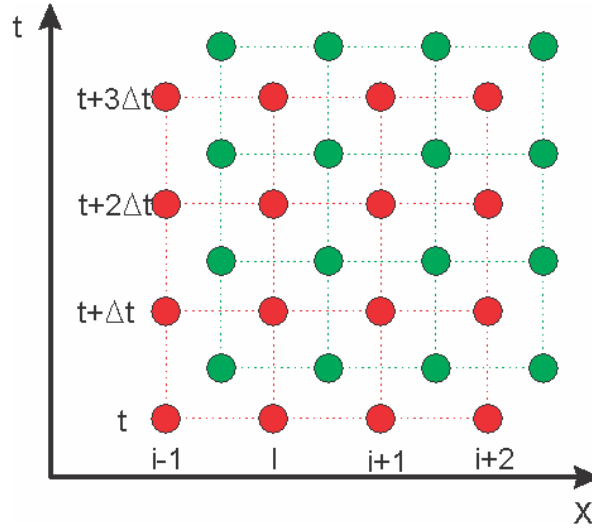


**Fig.App2. 2.** Descretization of space and time

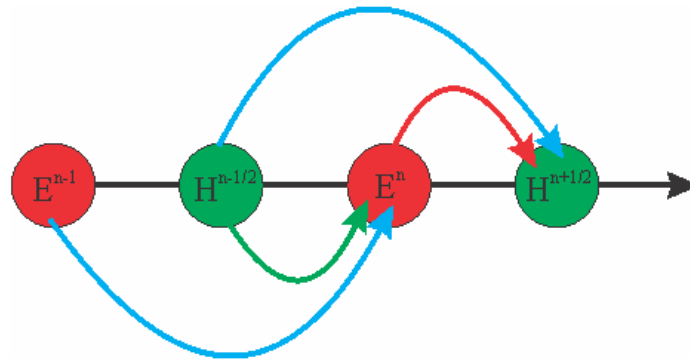


**Fig.App2. 3.** Leap frog time integration

Yee's algorithm is modified and simplified by Sheen for easy programming [2]. Thus the programming implementations of the equations are as follows.

$$H_{x,i,j,k}^{n+1/2} = H_{x,i,j,k}^{n-1/2} + \left(\frac{\Delta t}{\mu\Delta z}\right)(E_{y,i,j,k}^n - E_{y,i,j,k-1}^n) - \left(\frac{\Delta t}{\mu\Delta y}\right)(E_{z,i,j,k}^n - E_{z,i,j-1,k}^n)$$

$$H_{y,i,j,k}^{n+1/2} = H_{y,i,j,k}^{n-1/2} + \left(\frac{\Delta t}{\mu\Delta x}\right)(E_{z,i,j,k}^n - E_{z,i-1,j,k}^n) - \left(\frac{\Delta t}{\mu\Delta z}\right)(E_{x,i,j,k}^n - E_{x,i,j,k-1}^n)$$

$$H_{z,i,j,k}^{n+1/2} = H_{z,i,j,k}^{n-1/2} + \left(\frac{\Delta t}{\mu\Delta y}\right)(E_{x,i,j,k}^n - E_{x,i,j-1,k}^n) - \left(\frac{\Delta t}{\mu\Delta x}\right)(E_{y,i,j,k}^n - E_{y,i-1,j,k}^n)$$

$$E_{x,i,j,k}^{n+1} = E_{x,i,j,k}^n + \left(\frac{\Delta t}{\epsilon\Delta y}\right)(H_{z,i,j+1,k}^{n+1/2} - H_{z,i,j,k}^{n+1/2}) - \left(\frac{\Delta t}{\epsilon\Delta z}\right)(H_{y,i,j,k+1}^{n+1/2} - H_{y,i,j,k}^{n+1/2})$$

$$E_{y,i,j,k}^{n+1} = E_{y,i,j,k}^n + \left(\frac{\Delta t}{\epsilon\Delta z}\right)(H_{x,i,j,k+1}^{n+1/2} - H_{x,i,j,k}^{n+1/2}) - \left(\frac{\Delta t}{\epsilon\Delta x}\right)(H_{z,i+1,j,k}^{n+1/2} - H_{z,i,j,k}^{n+1/2})$$

$$E_{z,i,j,k}^{n+1} = E_{z,i,j,k}^n + \left(\frac{\Delta t}{\epsilon\Delta x}\right)(H_{y,i+1,j,k}^{n+1/2} - H_{y,i,j,k}^{n+1/2}) - \left(\frac{\Delta t}{\epsilon\Delta y}\right)(H_{x,i,j+1,k}^{n+1/2} - H_{x,i,j,k}^{n+1/2})$$

This simplification allows the value of each field component to be stored in a three-dimensional array, with the array indices corresponding to the spatial indices.

### 3. Boundary conditions

Most of the electromagnetic problems have to deal with different types of materials with different conducting and dielectric properties. One of the most commonly used boundaries is Perfect Electric Conductor (PEC). Another important boundary is Dielectric interface boundary which defines the dielectric properties of the material. Many of the Electromagnetic problems are unbounded or associated with open space regions. In the FDTD implementation of such problems requires exhaustive computational efforts and unlimited computational resources. Due to limited computational resources, the simulation domain requires truncation, which may introduce spurious fields from the truncation points unless appropriate measures are taken. To reduce the reflections from truncation points we use reflectionless boundary condition such as Absorbing Boundary Condition (ABC) and Perfect Matched Layer (PML).

### **3.1 Perfect Electric Conductor (PEC) boundary**

The PEC boundary is used to represent ideal conductors. This type of materials will reflect all incident wave energy back into the computational domain. The boundary conditions at a perfect electric conductor are such that the electric field components tangential to the surface must be zero. Mathematically it can be represented as

$$\vec{n} \times \vec{E} = 0$$

Where  $n$  is a surface normal vector,

From Fig.1 it can be inferred that the Electric field components in each Yee cell is tangential and therefore PEC can simply be defined by setting  $E_{\text{tan}} = 0$ . They will remain nearly zero throughout the iterations. In materials finite conductivity, the update equation for the electric field component is

$$E^n = E^{n-1} \left\{ \frac{1 - \sigma\Delta t/2\varepsilon}{1 + \sigma\Delta t/2\varepsilon} \right\} + \left\{ \frac{1}{1 + \sigma\Delta t/2\varepsilon} \right\} \left( \frac{\Delta t}{\varepsilon} \right) \left[ \nabla \times H^{n-\frac{1}{2}} \right]$$

When conductivity  $\sigma$  is very much greater than unity,  $E^n$  will be approximately equal to  $E^{n-1}$ . PEC boundaries are used in the present investigation to model the metallic strip of the printed strips of the slotline fed antennas.

### **3.2 Dielectric interface boundary**

Planar antennas are usually printed on a dielectric substrate which will create an interface between two media (Air and Dielectric). The discretizations of Maxwell's equation become invalid at such interfaces. This is because in the difference equation only one value of permittivity and permeability is used but at the interface we have to use the resultant of material constants. Using the

equivalent parameter approach introduced by Zhang and Mei [3] the condition at the interface is can be approximated as

$$\varepsilon_{eff} = \frac{\varepsilon_1 + \varepsilon_2}{2}$$

### 3.3 First order Mur's Absorbing Boundary Condition (ABC)

The widely used ABC was devised by Mur in 1981 [4]. This boundary condition is derived from a one-way wave equation. As the angle of incidence increases, the attenuation of wave incident on the Mur ABC degrades. But at the grazing angle, the boundary becomes perfectly reflecting. Hence for most of the simulations using Mur's first order ABC at least 20 cells are required between the boundary and the radiating structure.

Mur's ABC was proposed after the theoretical work by Enquist and Majda [5]. It provides satisfactory absorption for a great variety of problems and is extremely simple to implement. Mur's first order ABC looks back one step in time and one cell into the space location. For the structure considered in the thesis, the pulses from the radiating structures will be normally incident to the outer boundary mesh walls and this leads to simple approximate boundary condition that the tangential electric field at the outer boundary obeys one dimensional wave equation in the direction normal to the mesh wall. For the x normal wall, the one dimensional wave equation can be written as

$$\left( \frac{\partial}{\partial x} - \frac{1}{c} \frac{\partial}{\partial t} \right) E_{tan} = 0$$

By imposing above equation on a wave normally incident on planar surface, ABC for a normal incident wave without reflection can be obtained as

$$\frac{\partial E(x, t)}{\partial x} = \frac{1}{c} \frac{\partial E(x, t)}{\partial t}$$



where  $x = \frac{\Delta x}{2}$  and  $t = (n + \frac{1}{2})\Delta t$

For updating of the electric field at  $x = \frac{\Delta x}{2}$  and  $t = (n + 1)\Delta t$  we can modify the above equation as

$$\frac{E_1^{n+1/2} - E_0^{n+1/2}}{\Delta x} = \frac{1}{c} \frac{E_{1/2}^{n+1} - E_{1/2}^n}{\Delta t}$$

The values at the half grid points and half time steps can be averaged from the above said relations as

$$E_m^{n+1/2} = \frac{E_m^{n+1} + E_m^n}{2}$$
$$E_{m+1/2}^n = \frac{E_{m+1}^n + E_m^n}{2}$$

The explicit finite difference equation of the above said ABC is given below

$$E_0^{n+1} = E_1^n + \left( \frac{c\Delta t - \Delta x}{c\Delta t + \Delta x} \right) (E_1^{n+1} - E_0^n)$$

Where  $E_0$  represents the tangential electric field component on the mesh wall and  $E_1$  represents the tangential electric field component on node inside of the mesh wall. Similar expressions are obtained for the other absorbing boundaries by using the corresponding normal directions for each wall. But while implementing the Mur's first order boundary conditions for finite area radiating structures, it should be noted that boundary walls are far enough from the radiating surface to ensure the normal incidence at the boundary walls. For the oblique incidence case the wave will be reflected from the boundary walls. Since it is a simple method to implement, this is used as the ABC in this thesis.

### 3.4 Bergner's Perfect Matched Layer (PML) ABC

In 1994, Berenger [6] derived a new boundary condition referred to as a Perfectly Matched Layer (PML) which reduces reflections several orders of magnitude below other techniques. It uses a modified set of Maxwell's equations in which fields at the ABC-simulation space interface are split into two components and an artificial anisotropic material is introduced within the ABC. The result is a PML wave impedance perfectly matched to the simulation space and independent of incident angle. Incident waves are attenuated in the direction normal to the layers as they propagate through the artificial medium. Reflection coefficients as low as -80 dB have been demonstrated [7] for both 2-D and 3-D FDTD simulations.

### 4. Numerical dispersion and stability criteria

For stability of the Maxwell's curl equations, the time step  $\Delta t$  and the spatial increments  $\Delta x$ ,  $\Delta y$  and  $\Delta z$  will have to satisfy the following Courant-Friedrichs-Lewy (CFL) Stability criterion.

$$\Delta t \leq \frac{1}{c} \frac{1}{\sqrt{\frac{1}{\Delta x^2} + \frac{1}{\Delta y^2} + \frac{1}{\Delta z^2}}}$$

Where  $c$  is the maximum velocity of light inside the computational volume.

These equations will allow the approximate solution of  $E$  and  $H$  in the volume of the computational domain or mesh. In the present investigation the maximum time step is limited as 99.5% of the value given by the above equation.

The discretization of Maxwell's equations in space and time causes the variation of the phase constant of the propagating wave with frequency. This phenomenon is referred to as numerical dispersion. As an effect of this, for a

fixed cell size different frequency components of a wave propagate at slightly different velocities. This will present in the FDTD algorithm also because FDTD divides the computational domain into small cells.

Velocity depends also on the angle of propagation with respect to the coordinate axis. This is called numerical anisotropy. The grid dispersion error can be reduced by reducing the cell size. Accuracy of computation can be ensured by selecting the grid size as at least 10 cells per wavelength ( $\lambda/10$ ) or less at the highest frequency. In the analysis presented in the thesis the accuracy and stability are ensured by selecting  $\Delta x, \Delta y, \Delta z < \frac{\lambda}{50}$

## **5. Luebbers feed model for fast FDTD convergence**

The impedance and scattering parameters of a structure in wide range of frequencies can be calculated using a transient pulse excitation in FDTD method. But it will take a huge amount of time because the transient pulse will decay after a few thousand time steps. This difficulty is common in the case of circuits having very high quality factor. Using signal processing prediction of voltages and currents at later events from result computed in present and past events, we can reduce the time steps. This will make the FDTD algorithm more complex. If ultimate care not taken, this will create large precision errors.

A simple method to reduce the computation time is to include a source with internal resistance which matches with the characteristic impedance of the transmission line to excite the problem. By employing such kind of source we can obtain accurate results while greatly reduces the number of time steps required for convergence.

## 5.1 Resistive source model

FDTD problems are often excited by a voltage source with internal resistance is zero ohms. These sources are very easy to implement in an FDTD code. The electric field at the mesh edge where the source is located is a function of time. For obtaining wide band calculation results, commonly a Gaussian pulse is used. The Gaussian pulses have greater than zero amplitude only for a very short fraction of time. Once the pulse amplitude drops, the source voltage becomes zero, and thus equivalent to a short circuit. At this condition, any energy returns from the computation domain in to the source will again reflected back to the computation domain itself. The only way the energy re-introduced into the calculation space can be dissipated is through radiation or by absorption by lossy media or lumped loads. This will take additional calculation time for the problem to converge. Using a source with an internal resistance to excite the FDTD calculation provides an additional loss mechanism for the calculations.

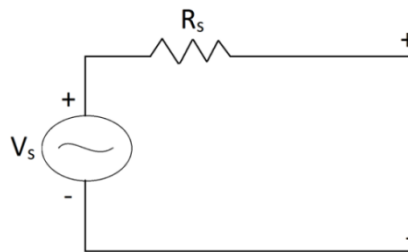


**Fig.App2. 4.** Resistor Feed

Consider that it is desired to excite an FDTD calculation with a voltage source that corresponds to an electric field  $E$  in the  $x$  direction at a certain mesh location  $i_s\Delta x, j_s\Delta y, k_s\Delta z$  described by usual Yee notation. The corresponding equivalent circuit for a voltage source which includes an internal source resistance  $R_s$  is illustrated in Fig. App2. 4. If the source resistance  $R_s$  is set to zero then the usual FDTD electric field at the source location is simply given by

$$E_s^n(i_s, j_s, k_s) = \frac{V_s(n\Delta t)}{\Delta z}$$

$V_s$  is any function of time, here a Gaussian pulse.

To calculate the terminal voltage of Fig.4 and to determine the value of source electric field  $E_s^n(i_s, j_s, k_s)$  we have to determine the current delivered from the source. This can be done by Ampere's circuital law, taking the line integral of the magnetic field around the electric field source location. The current through the source is then given by

$$I_s^{n-\frac{1}{2}} = \Delta x \left[ H_x^{n-\frac{1}{2}}(i_s, j_{s-1}, k_s) - H_x^{n-\frac{1}{2}}(i_s, j_s, k_s) \right] \\ + \Delta y \left[ H_y^{n-1/2}(i_s, j_s, k_s) - H_y^{n-1/2}(i_{s-1}, j_s, k_s) \right]$$

By applying Ohm's law to the circuit given in Fig.4, the electric source field is given by

$$E_s^n(i_s, j_s, k_s) = \frac{V_s(n\Delta t)}{\Delta z} + \frac{R_s I_s^{n-1/2}}{\Delta z}$$

If  $R_s=0$ , in this equation will result in a hard voltage source with field depend only on time and voltage function type. The value of the internal resistance does not appear to be critical. A reasonable choice for  $R_s$  is to use the value of the characteristic impedance of the transmission line. In the thesis  $R_s$  is selected as 50  $\Omega$ .

## **5.2 Staircase transition for Slotline/ Coplanar strip feed**

The microstrip excitation presented by Luebber's [9] approach is a stair cased FDTD mesh transition from electric field sources location to the full width of the microstrip transmission line. Compared to the hard voltage source excitation this approach provides accurate results with reduced computational time. For

implementing the stair cased transition in slotlines, the slot is discretized in order to incorporate more than one Yee cell. A gap feed model can be obtained by applying the excitation field between the two PEC plane in the source end. The staircased mesh transition used in the thesis is shown in Fig.App2. 5

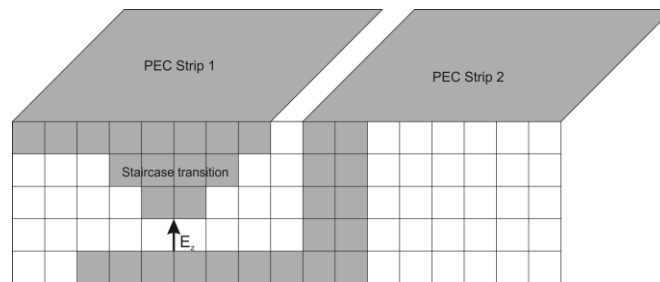


**Fig.App2. 5.** Stair case transition for slotlines

## 6. Excitation Functions

The FDTD problems can be excited using a variety of functions such as Gaussian pulse, sinusoidal function, modulated forms of these functions etc. In this thesis we used Gaussian pulse for obtaining the impedance characteristics of the structure for a wide range of frequency. Sinusoidal functions are also used here for obtaining the field parameters in a single frequency.

### 6.1 Gaussian Pulse

A Gaussian pulse can be expressed as,

$$E(t) = e^{-(t-t_0)^2/T^2}$$

Where  $t$  is the present time,  $t_0$  is the time at which the amplitude is unity (Here the maximum amplitude is 1) and  $T$  determines the pulse width. The pulse width determines the frequency up to which the simulation is accurate. As the pulse width is narrow, broad band simulation can be attained.

## 6.2 Sinusoidal Function

A sinusoidal function is given by

$$E(t) = E_0 \sin(\omega t)$$

Where  $E_0$  determines the amplitude,  $t$  is the current instant of time and  $\omega = 2\pi f$  is the angular frequency in radians / second, where  $f$  is the frequency in Hertz.

## 7. Flowchart of FDTD calculations

The methods for computing the antenna parameters discussed in this thesis is depicted in the self explaining flow chart given in Fig.APP2. 6.

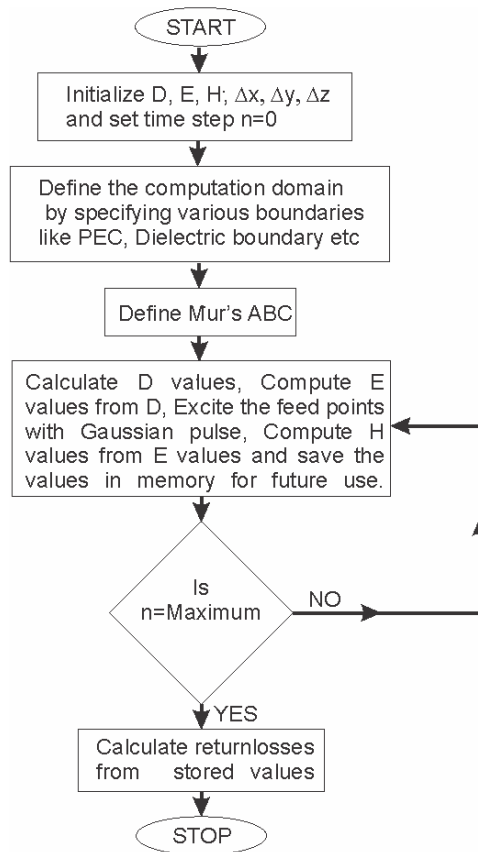


Fig.App2. 6. Flow chart for FDTD algorithm

## 8. Return loss calculation

After maximum time step reached, we have to calculate the return loss parameter of the antenna at its input end. For this calculation we require both incident and reflected waveforms. But after computation we get the sum of these two. To obtain the value of reflected wave form, we have to subtract input wave for from the obtained value. Again these two values are in time domain. To obtain frequency domain parameter we have to apply the famous Fast Fourier Transform (FFT) to these values. The return loss can be calculated as

$$\text{Return loss in dB} = 20 \log_{10} \frac{\text{FFT(Reflected waveform)}}{\text{FFT(Incident waveform)}}$$

## References

- [1] K. S. Yee, "Numerical solution of initial boundary value problems involving Maxwell's equations in isotropic media," *IEEE Transactions on Antennas and Propagation*, AP-14, 4, pp. 302-307, 1966.
- [2] David.M.Sheen, Sami.M.Ali, Mohamed D.Abouzahra and Jin Au Kong, "Application of the Three-Dimensional Finite- Difference Time-Domain method to the analysis of planar Microstrip circuits, "*IEEE Trans. Microwave Theory Tech.*, vol.38, no.7, pp.849-857, July 1990.
- [3] X. Zhang and K. K. Mei, "Time domain finite difference approach to the calculation of the frequency dependent characteristics of microstrip discontinuities," *IEEE Trans. Microwave Theory Tech.*, vol. 36, pp. 1775-1787, Dec. 1988.
- [4] Mur G, Absorbing boundary conditions for the Finite Difference Approximation of the Time domain Electromagnetic field equations, *IEEE Transactions EMC-23*, 1981, pp. 377-382.



- [5] Enquist and Majada, Absorbing Boundary Conditions for the Numerical simulation of waves, *Mathematics of computation*, Vol. 31, 1977, pp. 629-651.
- [6] J.P. Berenger, A perfectly matched layer for the absorption of EM waves, *J. Computational Physics*, Vol. 114, 1994, pp. 185-200
- [7] Sullivan Dennis M, *Electromagnetic simulation using the FDTD method*, IEEE press series on RF and Microwave Technology, USA
- [8] R.J Leubbers and H.S Langdon., "A simple feed Model that reduces Time steps Needed for FDTD Antenna and Microstrip Calculations" *IEEE Trans. Antennas and Propagation*. Vol.44, No.7, July 1996, pp.1000-1005.

## LIST OF PUBLICATIONS OF THE AUTHOR



### International Journals

1. **Sreejith M. Nair**, Shameena V.A, R. Dinesh, and P. Mohanan, "Compact Semicircular Directive Dipole Antenna for UWB Applications", **IEE Electronics Letters**, Vol.47, No.23, November 10, 2011.
2. **Sreejith M. Nair**, Shameena V.A, Nijas C.M, C.K.Aanandan, K.Vasudevan and P. Mohanan, "Compact Slot line fed Enhanced Gain Dipole Antenna for 5.2 GHz/5.8 GHz Applications", **International Journal of RF&Microwave Computer-Aided Engineering** Vol.23, Issue 1, pp.40-46, January 2013.
3. **Sreejith M. Nair**, Shameena V.A, Nijas C.M, C.K. Aanandan, K.Vasudevan and P. Mohanan, "Compact Slot line fed Dual Band Dipole Antenna for 2.4/5.2 GHz WLAN Applications", **International Journal of RF&Microwave Computer-Aided Engineering** Vol.22, Issue.5, pp.581-587, September 2012,
4. **Sreejith M. Nair**, Shameena V.A, Nijas C.M, C.K.Aanandan, K.Vasudevan and P. Mohanan "Novel Chipless RF Identification Technology for On-touch Data Transfer Applications", **Microwave and Optical Technology letters** Vol. 54, No. 10, pp. 2325-2327, October 2012.
5. **Sreejith M. Nair**, Shameena V.A, Sreenath S and P.Mohanan" Slotline fed Ultra Compact Antenna for Wide Band Applications", **Microwave and Optical Technology letters**, Vol.55, Issue 3, pp.526-529, March 2013.
6. D. Laila, R. Sujith, **M. N. Sreejith**, C.K.Aanandan, K.Vasudevan and P. Mohanan "Mobile antenna with reduced radiation hazardstowards human

head”, **Progress in Electromagnetic Research Letters** Vol. 17, pp. 39-46, 2010.

## **Conferences**

---

1. Laila. D, R. Sujith, **Sreejith M. Nair**, C.K.Aanandan, K.Vasudevan and P. Mohanan ”Modified CPW fed monopole antenna with a radiation pattern suitable for mobile handset” 2011 **International conference on Communication and Signal Processing** (ICCSP 2011), Calicut, India.

## Resume of the Author

### **SREEJITH. M. NAIR**

Part Time Research Scholar  
Department of Electronics,  
CUSAT

Assistant Professor,  
Department of Electronics,  
Govt. College Chittur,  
Palakkad, Kerala.

Mob: +91-9745682616  
Email: sreejithnair@gmail.com

### **Objective:**

To pursue research activities in the field of Printed antennas, Computational Electromagnetics, and Microwave imaging, RFID etc. and to perform my duties with dedication and integrity.

### **Education:**

- ◆ Ph. D. in Microwave Electronics  
Cochin University of Science and Technology (Currently Doing)
- ◆ M.Sc Electronics  
Specialization: Microwave Electronics  
Cochin University of Science and Technology (2008)  
Score: CGPA 9.71, First class with Distinction and First Rank.
- ◆ B.Sc Electronics with Computer Hardware  
BPC College Piravom, Ernakulam , Mahatma Gandhi university(2006)  
Score: 89.1% First class with Distinction and First Rank

### **Awards Obtained:**

- ◆ First Rank Holder of B. Sc Electronics, MG University Kottayam (2006)
- ◆ First Rank Holder of M. Sc Electronics, CUSAT (2008)
- ◆ UGC NET with JRF in December-2007 and June-2008

**Research Experience:**

Worked as a part time Research scholar in Centre for Research in Electro Magnetics and Antennas, Dept. of Electronics, Cochin University of Science and Technology from 22<sup>nd</sup> October 2008 to till date

**Work Experience:**

1. Worked as Assistant Professor in Electronics at The Cochin College, Cochin-2 from 22-01-2009 to 10-10-2011.
2. Working as Assistant Professor in Electronics at Govt. College, Chittur, Palakkad from 11-10-2011.

**Publications:**

International Journal : 6

National Conference : 1

**Computer Proficiency:**

1. C, C++, MATLAB, Assembly Level Programming,
2. Antenna Designing software like Ansoft HFSS, CST Microwave Studio.

**Personal:**

DoB : 28-05-1986  
Sex : Male  
Nationality : Indian  
Marital Status : Single  
Permanent Address : Mangattu House  
J. N. Road, Chottanikkara PO, Ernakulam - 682312,  
Kerala  
Mob : 9745682616

## INDEX

### A

Absorbing Boundary 291, 298, 300  
Anechoic chamber 49, 50, 53  
Ansoft 39, 40,  
Antenna 1-310  
Asymmetric 11, 77, 232,

### B

BALUN 18, 77, 110-116  
Bandwidth 7-14, 52, 53, 58, 86  
Beam maxima 51, 108, 132, 167, 224  
Bore Sight 53, 88, 164, 176, 198,  
Broadband 306

### C

Capacitance 85, 96, 288 etc  
Cavity 45, 57  
CFL Criteria 302  
Coaxial 52, 113  
Compact 5, 9, 11, 77, 94  
Computed 103, 128, 146, 168  
Coplanar 5, 10, 17, 77, 79 etc  
CPS 17, 77, 79, 90, 110  
CPW 10, 79  
Cross polarization 12  
Cross Polar Level 90, 108, 133, 173 etc  
Current distribution 40, 83, 92 etc

### D

Design equations 103, 128, 168, 190 etc  
Dielectric constant 6, 13, 44, 78, 82 etc  
Dipole 17, 77, 85, 94, etc  
Directive 90, 132, 149, 165  
Directivity 18, 94, 136, 194, 213  
Distributed 19, 85, 96, 100, 118 etc

### E

Efficiency 7, 11, 13, 39, 54, 109 etc  
EIRP 68, 70, 213, 271  
Electromagnetic 1, 2, 4, 41 etc  
Elliptical 246  
Energy 50, 54, 77, 88, 91  
Enhanced gain 17 177, 123, 247, 272  
Evolution 18, 94, 116, 149, 179

### F

FDTD 18, 56, 138-145, 203,  
291  
FFT 65, 308  
Fidelity 66, 213, 270  
Fourier Transform 58, 65, 70, 80, 267, 308  
Fringing field 83, 92, 102

### G

Gain 18, 53, 109, 136, 149  
Gaussian 62, 64, 138, 304, 306  
Galerkin 43, 80  
Group Delay 61, 263

### H

Horn 2, 51, 88, 106  
HP8510C 39, 47, 48

### I

Impedance Matching 1, 4, 95  
Inductance 85, 96, 288 etc  
Input Impedance 51, 56, 84  
ISM Band 6, 105, 172  
Isotropic 42, 68, 271

### L

Leap frog 296, 297  
Leubbers 309, 303

### M

Magnetic field 57, 291, 305  
 Microstrip 6, 8, 56, 78  
 MoM 57  
 Monopole 8, 15, 75

## **N**

Network analyzers 39, 45, 49, 51, 66  
 Numerical 41, 56, 203

## **O**

Optimization 39, 117, 232  
 Omnidirectional 197, 225

## **P**

Parametric Analysis 83, 96, 117 etc  
 PEC 78, 112, 299  
 Phase 47, 61, 62  
 Polarization 12, 60, 89, 91, 131, 164 etc

## **Q**

Q Factor 9, 85, 100, 152, 179, 281

## **R**

Radiation 7-9, 11, 40, 47, 51, 53, 54 etc  
 Radiation pattern 9, 14, 39-41, 49, 51, 53, 89 etc  
 Reflection coefficient 82, 83-88, 95-103, 110

Resistance 54, 159, 281  
 Return loss 39, 49, 52, 106, 152, 308

## **S**

S<sub>11</sub> 40, 47, 52, 55, 104, 139, etc  
 Semi Circular 19, 213, 231, 270 etc  
 Slotline 10, 11, 17, 77, 79, 81 etc  
 Surface current 52, 57, 80, 91, 108, 112, 200 etc  
 Symmetric 17, 65, 77, 82, 94, 136

## **T**

Transfer function 60, 65, 264-268  
 Transmission line 1, 11, 13, 18, 56, 78, 80, 94  
 Turn Table 49, 51

## **U**

Ultra compact 231, 275, 277  
 UWB 6, 9, 14, 16, 19, 59, 63, 66, 213 etc

## **W**

Wheeler cap 54, 55

## **Y**

Yee Cell 292, 296, 299, 306